OSTEOARTICULAR-IMMUNOLOGICAL INTERPLAY IN RESPONSE TO DISEASE AND THERAPY

EDITED BY: Lisa Deloch, Michal Tomcik and Maria Filkova
PUBLISHED IN: Frontiers in Immunology

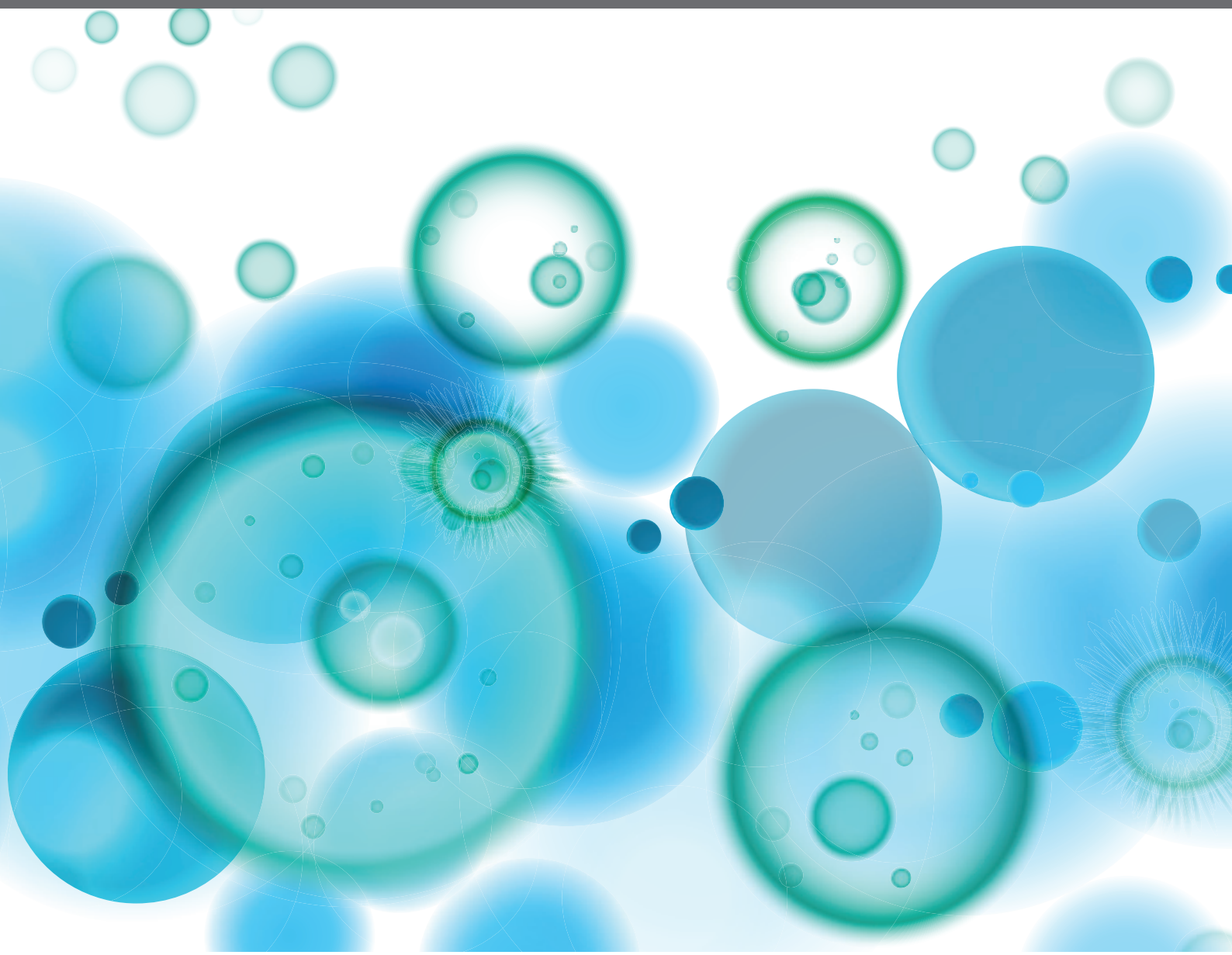

frontiers Research Topics

frontiers

ISSN 1664-8714
ISBN 978-2-83250-580-9
DOI 10.3389/978-2-83250-580-9

About Frontiers

Frontiers is more than just an open-access publisher of scholarly articles: it is a pioneering approach to the world of academia, radically improving the way scholarly research is managed. The grand vision of Frontiers is a world where all people have an equal opportunity to seek, share and generate knowledge. Frontiers provides immediate and permanent online open access to all its publications, but this alone is not enough to realize our grand goals.

Frontiers Journal Series

The Frontiers Journal Series is a multi-tier and interdisciplinary set of open-access, online journals, promising a paradigm shift from the current review, selection and dissemination processes in academic publishing. All Frontiers journals are driven by researchers for researchers; therefore, they constitute a service to the scholarly community. At the same time, the Frontiers Journal Series operates on a revolutionary invention, the tiered publishing system, initially addressing specific communities of scholars, and gradually climbing up to broader public understanding, thus serving the interests of the lay society, too.

Dedication to Quality

Each Frontiers article is a landmark of the highest quality, thanks to genuinely collaborative interactions between authors and review editors, who include some of the world's best academicians. Research must be certified by peers before entering a stream of knowledge that may eventually reach the public - and shape society; therefore, Frontiers only applies the most rigorous and unbiased reviews.
Frontiers revolutionizes research publishing by freely delivering the most outstanding research, evaluated with no bias from both the academic and social point of view. By applying the most advanced information technologies, Frontiers is catapulting scholarly publishing into a new generation.

What are Frontiers Research Topics?

Frontiers Research Topics are very popular trademarks of the Frontiers Journals Series: they are collections of at least ten articles, all centered on a particular subject. With their unique mix of varied contributions from Original Research to Review Articles, Frontiers Research Topics unify the most influential researchers, the latest key findings and historical advances in a hot research area! Find out more on how to host your own Frontiers Research Topic or contribute to one as an author by contacting the Frontiers Editorial Office: frontiersin.org/about/contact

OSTEOARTICULAR-IMMUNOLOGICAL INTERPLAY IN RESPONSE TO DISEASE AND THERAPY

Topic Editors:
Lisa Deloch, Universitätsklinikum Erlangen, Germany
Michal Tomcik, Institute of Rheumatology, Prague, Czechia
Maria Filkova, Institute of Rheumatology, Prague, Czechia

Dr. Tomcik receives research funding from Arxx Therapeutics. The other Topic Editors declare no competing interests.

Citation: Deloch, L., Tomcik, M., Filkova, M., eds. (2022). Osteoarticular-immunological Interplay in Response to Disease and Therapy. Lausanne: Frontiers Media SA. doi: 10.3389/978-2-83250-580-9

Table of Contents

frontiers | Frontiers in Immunology

TYPE Editorial
PUBLISHED 11 October 2022
DOI 10.3389/fimmu.2022.1052196

OPEN ACCESS

EDITED AND REVIEWED BY
Teun J. De Vries,
VU Amsterdam, Netherlands

*CORRESPONDENCE
Maria Filkova
filkova@revma.cz

SPECIALTY SECTION
This article was submitted to Autoimmune and Autoinflammatory Disorders : Autoimmune Disorders, a section of the journal Frontiers in Immunology

RECEIVED 23 September 2022
ACCEPTED 28 September 2022
PUBLISHED 11 October 2022

CITATION
Deloch L, Filkova M and Tomcik M (2022) Editorial: Osteoarticular-immunological interplay in response to disease and therapy. *Front. Immunol.* 13:1052196. doi: 10.3389/fimmu.2022.1052196

Editorial: Osteoarticular-immunological interplay in response to disease and therapy

Lisa Deloch[1,2], Maria Filkova[3]* and Michal Tomcik[3]

[1]Department of Radiation Oncology, Universitätsklinikum Erlangen, Friedrich-Alexander-Universität Erlangen-Nürnberg, Erlangen, Germany, [2]Translational Radiobiology, Department of Radiation Oncology, Universitätsklinikum Erlangen, Friedrich-Alexander-Universität Erlangen-Nürnberg, Erlangen, Germany, [3]Institute of Rheumatology, Department of Rheumatology, 1st Faculty of Medicine, Charles University, Prague, Czechia

KEYWORDS

bone, cartilage, rheumatoid arthritis, osteoarthritis, radiotherapy, osteoclast, T cell, B cell

Editorial on the Research Topic
Osteoarticular-immunological Interplay in Response to Disease and Therapy

Osteoimmunology is defined as an interdisciplinary research area that connects immunology and osteology (1–3). In articular diseases such as rheumatoid arthritis (RA) and osteoarthritis (OA) cells in the synovium, such as synovial fibroblasts, interact with immune cells and the bone to perpetuate the pathogenic mechanisms (4, 5). These cells, therefore, represent additional vital targets to improve therapeutic efficacy.

While the involvement of the immune system has been generally accepted in RA (5–7), this was only recently recognized in OA, where increasing attention has been directed towards systemic inflammation (8), also stressing the importance of the interplay between the synovium, cartilage, and subchondral bone (9). While a plethora of therapeutic modalities are available for the treatment of degenerative diseases of the joint, timely intervention is of the essence to prevent irreversible damage to the bone and joints. A concise understanding of the osteoarticular-immunological interplay is thus essential in providing targeted, additive, and comprehensive treatment options for these patients.

One of the additive treatment options is the so-called low-dose radiotherapy (LDRT) with low doses of ionizing radiation (mostly X-rays) that has analgesic and anti-inflammatory properties (10); however, many of the underlying mechanisms are not completely understood. Donaubauer et al. assessed immune modulations in patients with chronic degenerative and inflammatory diseases in the IMMO-LDRT01 trial (NCT02653079) and found a significant improvement in pain levels, modulations of circulating immune cells (e.g., a decrease in B cells) alongside a reduction in their activation status. Additionally, Eckert et al. examined the effects of LDRT on osteoclast differentiation and bone resorption in the same cohort and found that circulating

monocytes, which were *ex vivo* differentiated into osteoclasts, showed lower numbers of differentiated osteoclasts while apoptotic levels remained low. This decrease in osteoclasts could potentially be due to reduced numbers of nuclei, suggesting an impaired fusion of pre-osteoclasts and a decrease in the Nuclear Factor of Activated T Cells 1 (NFATc1). Likewise, reduced bone resorption was also found in the LDRT group.

One of the biggest drawbacks of LDRT is the lack of placebo-controlled studies, as stated by Weissmann et al. They chose a translational approach and analyzed patient data as well as a pre-clinical model to identify parameters that could be implicated in future patient studies. They found that age and the localization of the affected joint are essential factors in LDRT. Furthermore, pre-clinical data revealed that the potential analgesic effects observed in patients could potentially be determined by an anti-inflammatory response (e.g., a reduction in serum interleukin (IL)-17A levels and a shift from CD8+ to CD4+ T cells in the bone marrow).

Liu et al. used a computational approach to identify potential new therapeutic targets in OA. They looked into five GEO datasets containing normal healthy and OA synovial tissues and identified six genes to be used as potential biomarkers for OA. In particular, they identified Stimulator of Chondrogenesis 1 (SCRG1), a protein-coding gene, as a diagnostic marker of OA, which is up-regulated in OA synovial tissue by hsa-miR-363-3p and regulates immune-related pathways, thus may become a potential new therapeutic target in OA.

To further elucidate the molecular mechanisms, Navrátilová et al. examined the role of B cell associated IL-40 in RA. They found IL-40 to be overexpressed in RA synovial tissue in contrast to the synovial tissue of OA patients, and higher IL-40 levels in the synovial fluid and serum of RA patients. The serum IL-40 levels in RA patients decreased following B cell-depleting therapy. Moreover, both local and systemic levels of IL-40 were associated with levels of autoantibodies, and levels of IL-40 in synovial fluid positively correlated with chemokines and markers of NETosis that unraveled a potential association of IL-40 with neutrophils. Relatedly, IL-40 induced the secretion of chemokines and MMP-13 by synovial fibroblasts *in vitro*.

Another study by Singh et al. demonstrated that transcription factor ETS Proto-Oncogene 2 (Ets2) induced osteoclast-like alterations in RA synovial fibroblasts (RASF). RASF are essential contributors to inflammation and bone destruction in RA *via* a plethora of cytokines and chemokines, including IL-6. While IL-6 contributes to bone loss, the molecular mechanisms of RASF/IL-6-induced bone loss are not completely understood. They found that Ets2 has a fundamental role in IL-6/IL-6 receptor signaling in RASF and thus modulates RASF heterogeneity and bone loss by transforming RASF into osteoclast-like cells.

Moreover, the interplay between Foxp3$^+$ T cells and osteoclasts was the research subject of Dohnke et al. They carried out an extensive characterization of Switching B Cell Complex Subunit SWAP-70 controlled F-actin dynamics and found SWAP70 to be a potential new member of the Foxp3-dependent canonical Treg cell signature. SWAP70-deficient mice failed to efficiently suppress CTLA4/CD80/CD86 mediated bone homeostasis by impairing osteoclastogenesis as well as osteoclast function and thus representing a functional defect of Treg mediated suppressor function.

Similarly, due to a lack of understanding of the molecular processes, the etiology of degenerative joint diseases remains elusive. Ma et al. demonstrated that patients with periodontitis showed a higher risk of developing OA and even severe OA that required knee or hip replacement. Interestingly, OA patients also had a higher risk of developing periodontitis. They suggest that periodontitis following OA might be due to poor oral hygiene as a result of the lack of activity and patient education. A potential explanation for OA following periodontitis could include common underlying inflammatory conditions making certain individuals susceptible to both diseases.

The studies that have been reviewed in this Research Topic show the diversity of osteoarticular-immunological mechanisms as seen in disease and therapy. While more and more factors contributing to this interplay are being unraveled, additional research is needed to connect these findings and to further elucidate the underlying molecular mechanisms. Further research will ultimately facilitate an extensive understanding of the disease onset and progression, and consequently the identification of therapeutic targets for more efficient and personalized treatment options.

Author contributions

All authors listed have made a substantial, direct, and intellectual contribution to the work and approved it for publication.

Funding

Funding for LD by the Bundesministerium für Bildung und Forschung (BMBF; TOGETHER 02NUK073; GREWIS, 02NUK017G and GREWIS-alpha, 02NUK050E), for MF and MT by the Ministry of Health Czech Republic (023728, NU22-05-00226).

Conflict of interest

The authors declare that the research was conducted in the absence of any commercial or financial relationships that could be construed as a potential conflict of interest.

Publisher's note

References

1. Andreev D, Kachler K, Schett G, Bozec A. Rheumatoid arthritis and osteoimmunology: The adverse impact of a deregulated immune system on bone metabolism. *Bone* (2022) 162:116468. doi: 10.1016/j.bone.2022.116468

2. Okamoto K, Nakashima DT, Shinohara M, Negishi-Koga T, Komatsu N, Terashima A, et al. Osteoimmunology: The conceptual framework unifying the immune and skeletal systems. *Physiol Rev* (2017) 97(4):1295–349. doi: 10.1152/physrev.00036.2016

3. Rauner M, Sipos W, Pietschmann P. Osteoimmunology. *Int Arch Allergy Immunol* (2007) 143(1):31–48. doi: 10.1159/000098223

4. Tu J, Huang W, Zhang W, Mei J, Zhu C. Two main cellular components in rheumatoid arthritis: Communication between T cells and fibroblast-like synoviocytes in the joint synovium. *Front Immunol* (2022) 13:922111. doi: 10.3389/fimmu.2022.922111

5. Komatsu N, Takayanagi H. Mechanisms of joint destruction in rheumatoid arthritis - immune cell-fibroblast-bone interactions. *Nat Rev Rheumatol* (2022) 18 (7):415–29. doi: 10.1038/s41584-022-00793-5

6. Auréal M, Machuca-Gayet I, Coury F. Rheumatoid arthritis in the view of osteoimmunology. *Biomolecules Biomolecules* (2020) 11(1):48. doi: 10.3390/biom11010048

7. Jung SM, Kim KW, Yang CW, Park SH, Ju JH. Cytokine-mediated bone destruction in rheumatoid arthritis. *J Immunol Res* (2014) 2014:263625. doi: 10.1155/2014/263625

8. Li Y, Mai Y, Cao P, Wen X, Fan T, Wang X, et al. Relative efficacy and safety of anti-inflammatory biologic agents for osteoarthritis: A conventional and network meta-analysis. *J Clin Med* (2022) 11(14):3958. doi: 10.3390/jcm11143958

9. Motta F, Barone E, Sica A, Selmi C. Inflammaging and osteoarthritis. *Clin Rev Allergy Immunol* (2022). doi: 10.1007/s12016-022-08941-1

10. Lumniczky K, Impens N, Armengol G, Candéias S, Georgakilas AG, Hornhardt S, et al. Low dose ionizing radiation effects on the immune system. *Environ Int* (2021) 149:106212. doi: 10.1016/j.envint.2020.106212

frontiers in Immunology

ORIGINAL RESEARCH
published: 12 October 2021
doi: 10.3389/fimmu.2021.740742

Low Dose Radiation Therapy Induces Long-Lasting Reduction of Pain and Immune Modulations in the Peripheral Blood – Interim Analysis of the IMMO-LDRT01 Trial

Anna-Jasmina Donaubauer[1,2], Ina Becker[1,2], Thomas Weissmann[2], Birgitta M. Fröhlich[1,2], Luis E. Muñoz[3], Thomas Gryc[2], Manuel Denzler[1,2], Oliver J. Ott[2], Rainer Fietkau[2], Udo S. Gaipl[1,2†] and Benjamin Frey[1,2†]*

[1] Translational Radiobiology, Department of Radiation Oncology, Universitätsklinikum Erlangen, Friedrich-Alexander-Universität Erlangen-Nürnberg (FAU), Erlangen, Germany, [2] Department of Radiation Oncology, Universitätsklinikum Erlangen, Friedrich-Alexander-Universität Erlangen-Nürnberg (FAU), Erlangen, Germany, [3] Department of Internal Medicine 3 - Rheumatology and Immunology, Friedrich-Alexander-University Erlangen-Nürnberg (FAU), Universitätsklinikum Erlangen, Erlangen, Germany

The treatment of chronic inflammatory and degenerative diseases by low dose radiation therapy (LDRT) is promising especially for patients who were refractory for classical therapies. LDRT aims to reduce pain of patients and to increase their mobility. Although LDRT has been applied since the late 19th century, the immunological mechanisms remain elusive. Within the prospective IMMO-LDRT01 trial (NCT02653079) the effects of LDRT on the peripheral blood immune status, as well as on pain and life quality of patients have been analyzed. Blood is taken before and after every serial irradiation with a single dose per fraction of 0.5Gy, as well as during follow-up appointments in order to determine a detailed longitudinal immune status by multicolor flow cytometry. Here, we report the results of an interim analysis of 125 patients, representing half the number of patients to be recruited. LDRT significantly improved patients' pain levels and induced distinct systemic immune modulations. While the total number of leukocytes remained unchanged in the peripheral blood, LDRT induced a slight increase of eosinophils, basophils and plasmacytoid dendritic cells and a decrease of B cells. Furthermore, activated immune cells were decreased following LDRT. Especially cells of the monocytic lineage correlated to LDRT-induced improvements of clinical symptoms, qualifying these immune cells as predictive biomarkers for the therapeutic success. We conclude that LDRT improves pain of the patients by inducing systemic immune modulations and that immune biomarkers could be defined for prediction by improved patient stratification in the future.

Keywords: low dose radiation therapy (LDRT), immune status, immunophenotyping, chronic degenerative and inflammatory diseases, subjective pain level, x-rays

OPEN ACCESS

Edited by:
Michal Tomcik, Institute of Rheumatology, Czechia

Reviewed by:
Rostyslav Bilyy, Danylo Halytsky Lviv National Medical University, Ukraine
Katalin Lumniczky, Frédéric Joliot-Curie National Research Institute for Radiobiology and Radiohygiene, Hungary

****Correspondence:***
Udo S. Gaipl
udo.gaipl@uk-erlangen.de

†These authors have contributed equally to this work and share senior authorship

Specialty section:
This article was submitted to Autoimmune and Autoinflammatory Disorders, a section of the journal Frontiers in Immunology

Received: *13 July 2021*
Accepted: *27 September 2021*
Published: *12 October 2021*

Citation:
Donaubauer A-J, Becker I, Weissmann T, Fröhlich BM, Muñoz LE, Gryc T, Denzler M, Ott OJ, Fietkau R, Gaipl US and Frey B (2021) Low Dose Radiation Therapy Induces Long-Lasting Reduction of Pain and Immune Modulations in the Peripheral Blood – Interim Analysis of the IMMO-LDRT01 Trial. Front. Immunol. 12:740742. doi: 10.3389/fimmu.2021.740742

INTRODUCTION

Chronic degenerative and inflammatory diseases, such as osteoarthritis have an increasing prevalence in western countries over the last decades. As the prevalence of these diseases is closely connected to rising mean age in the population, incidence will further increase in the future (1). The term chronic degenerative and inflammatory diseases covers a broad spectrum of conditions ranging from rheumatoid arthritis, which is characterized by steadily progressing inflammatory processes in multiple joints (2), to conditions that are characterized mainly by local, degenerative processes in bone or cartilage tissue, such as the elbow syndrome or osteoarthritis (1). In detail, rheumatoid arthritis is considered as a progressing autoimmune disease that is caused by genetic, as well as environmental factors, such as nutrition, smoking or hormones (3). During the course of the disease, patients experience a severe chronic inflammation of several synovial joints that is followed by a destruction of cartilage and bone (2). For other chronic degenerative diseases on the other hand, such as osteoarthritis, typical risk factors are a high age, obesity or chronic mechanical overload of the joint (4). Those factors lead to a slow degradation of the joint's cartilage and finally even of the bone tissue and a subsequent deformation of the affected joint. In line with inflammatory diseases, an activation of the immune system and inflammatory processes are also a symptom of chronic degenerative diseases in very advanced stages (5). A further common symptom of chronic degenerative and inflammatory diseases is intense pain in the affected joints and a resulting reduction of the joint's mobility that affects patient's quality of life (6).

As chronic degenerative and inflammatory diseases are heterogeneous, the possible treatment options are very broad and depend on the specific diagnosis and stage of disease. As those diseases are progressive, the therapeutic intervention primarily aims to decelerate the destructive and inflammatory processes and to reduce the pain. Depending on the diagnosis, patients can profit from non-pharmacological treatment strategies, such as orthoses, physiotherapy or a weight reduction. Nonetheless, these options often fail to induce a sufficient pain relief. Therefore, pharmacological interventions with non-steroidal anti-inflammatory drugs (NSAIDs), disease-modifying anti-rheumatic drugs (DMARDs), injections or even surgical interventions are considered in advanced stages (6). Even though, there is a plethora of therapeutic options, about 25% of all patients do not respond sufficiently to those interventions or lose their responsiveness over time (7).

Especially for those patients with insufficient therapeutic responses, low dose radiation therapy (LDRT) is a promising alternate therapy. For over 100 years, LDRT is well-known for the pain relieving effects in joint diseases that can last at least for up to one year (8). LDRT is usually applied as a serial, local irradiation with X-Rays, delivered on the affected joint only. The single dose ranges between 0.5 and 1.0 Gray (Gy) and the total dose does usually not exceed six Gy (9, 10). Radiation-induced side effects do play a minor role in LDRT (11).

Even though the analgesic effects of LDRT are well known, the molecular mechanisms are not yet characterized in detail. As pain is often closely connected to inflammatory processes, a modulation of the inflammatory reaction is very likely a central mechanism of action of LDRT. Indeed, numerous preclinical studies focus on the immunological modes of action of LDRT. In general, it was found that LDRT downregulates preexisting inflammatory and bone degrading processes. Up to today, various immune-modulating mechanisms have been found in preclinical models that support this hypothesis. In leukocytes, LDRT increases the apoptosis rate and reduces the adhesion of the immune cells to the endothelium. Moreover, the secretion of pro-inflammatory cytokines such as IL-6 and TNF-α, as well as chemokines is downregulated and the secretion of anti-inflammatory cytokines, such as TGF-β is enhanced. Especially macrophages seem to be modulated by LDRT, as they reduce the secretion of reactive oxygen species and enhance the clearance of apoptotic cells. In summary, an anti-inflammatory microenvironment is formed by LDRT in the affected tissue (12–16). In line with those immunological alterations, LDRT also impacts positively on the bone metabolism, as bone degradation is decelerated and the formation of new bone is enhanced and therefore degenerative processes are ameliorated (17).

All of the immune-modulating effects described above have been examined in preclinical models or *in vitro* studies. On the other hand, a plethora of patient studies are being conducted on the effectiveness of LDRT (18). However, those studies focus primarily on clinical parameters and the analgesic effects (19, 20), rather than unraveling the underlying immunological modes of action.

In order to prospectively examine the immunological mechanisms of LDRT for the first time in a clinical trial, the IMMO-LDRT01 study was initiated in 2015. In this prospective, observatory trial, patients suffering from various chronic degenerative and inflammatory diseases have been enrolled. During the course of the study, these patients are examined for pain-related factors, but additionally a detailed immune status of the peripheral blood is analyzed. Peripheral blood can be drawn easily and be repeated without an additional risk for the patients compared with repeated biopsies tissue and thereby allows a detailed and longitudinal immune monitoring for future definition of prognostic and predictive signatures (21). Thereby, the immunological modulations of LDRT before and after the therapy has been determined for the first time *in vivo* in patients. Here we present an interims analysis with 125 of 250 patients of the IMMO-LDRT01 trial. Our findings prove that LDRT does not only significantly improve clinical symptoms and pain, but also modulates peripheral immune cell numbers, as well as the activation state of distinct immune cells. Certain modulations correlate to the therapeutic outcome and might therefore be valuable in the future for defining predictive and prognostic biomarkers for LDRT.

MATERIAL AND METHODS

Study Design

The IMMO-LDRT01 trial (NCT02653079) was initiated in 2015. This prospective, observatory study aims to unravel the immunological mechanisms underlying LDRT, as well as

proving the pain-relieving effects. Informed consent was obtained from all subjects involved in the study.

After enrollment, patients undergo a serial irradiation with six fractions of a single dose per fraction of 0.5 Gy delivered over three weeks with at least 48 hours between the fractions. If the patient is not subjectively satisfied with the therapeutic outcome, a second radiation series is applied three months later according to the same scheme as before. Radiation therapy is applied using an orthovoltage technique. In detail, an X-ray device (from Xstrahl LTD, Suwanee, GA, US) was used with 180kV and 10mA, a 0.2 mm Cu filter and a focus skin distance of 50 cm. Three months after the completion of LDRT a follow-up visit is performed. **Figure 1** depicts the study design of the trial.

As immunological modulations by LDRT are examined in this trial, a detailed immune status was analyzed from peripheral blood. Therefore, patients underwent blood withdrawals at indicated time points before and after every irradiation series, as well as for the follow-up appointment (**Figure 1**). In addition, the patients filled out a detailed questionnaire on their pain level, health status and quality of life at the same time points. In detail, the first examination time point was on the day the first radiation series started and the second time point was on the day of the last radiotherapy session of the first series (three weeks later). Time point 3 was three months later on the day the second series started and time point 4 was again three weeks later when the last fraction was applied. The final examination was performed after additional three months, when the patients received their follow-up care.

The study was conducted according to the guidelines of the Declaration of Helsinki, and approved by the Institutional Review Board of the Friedrich-Alexander Universität Erlangen-Nürnberg (protocol code: 289_15B; date of approval: 12.11.2015).

Informed consent was obtained from all subjects involved in the study. Written informed consent has been obtained from the patients to publish this paper.

Patient Cohort

For this planned interim analyses, 125 out of planned 250 patients suffering from chronic degenerative and inflammatory diseases have been enrolled. All patients received alternative treatments before being referred to the Department of Radiation Oncology of the Universitätsklinikum Erlangen for LDRT. The detailed patient characteristics are listed in **Table 1**.

Immunophenotyping of Peripheral Blood

In order to determine a detailed immune status from peripheral blood, immunophenotyping was performed. Therefore, whole blood samples were analyzed within three hours after the blood withdrawal by multi-color flow cytometry. Immunophenotyping (IPT) was executed as described in our previously published IPT protocols (22–24). **Figure 2** depicts the gating strategy for the IPT used in this study with all the determined immune cell subtypes and the respective surface molecules that are measured for their identification. A Gallios flow cytometer (Beckman Coulter) in the standard filter configuration was used for data acquisition. The Kaluza Flow Analysis Software (Beckman Coulter), as well as Microsoft Excel were used to calculate immune cell numbers.

Determination of Pain and Quality of Life

In order to quantify the pain-relieving effects of LDRT patients filled out a detailed questionnaire on their pain level in different

TABLE 1 | Patient characteristics.

Factor	Category	n
Total number		125
Age at start	Mean	58
	Range	41-83
Gender	Male	32 (25.6%)
	Female	93 (74.4%)
BMI	Normal (≥ 25)	28 (22.4%)
	Overweight (25-30)	35 (28%)
	Obese (≤ 30)	42 (33.6%)
	N/A	20 (16%)
Number of series	1 series	32 (25.6%)
	2 series	77 (61.6%)
	Drop-out	16 (12.8%)
Indication	Calcaneodynia	45 (36%)
	Osteoarthritis	16 (12.8%)
	Arthritis	10 (8%)
	Elbow syndrome	12 (9.6%)
	Shoulder syndrome	6 (4.8%)
	Achillodynia	9 (7.2%)
	Multiple indications	4 (3.2%)
	Other	23 (18.4%)

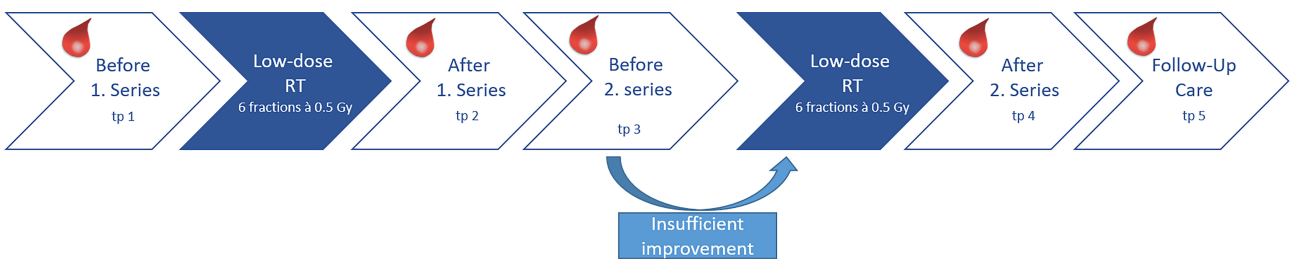

FIGURE 1 | Study design of the prospective IMMO-LDRT01 trial. Examinations are performed before and after the first series of irradiation (tp 1 and 2), before and after the second series of irradiation (tp 3 and 4), as well as for the follow-up appointment three months later (tp 5). The blood drops indicate the time points of the blood withdrawals. Patients fill out questionnaires on life quality and pain levels at the same time points.

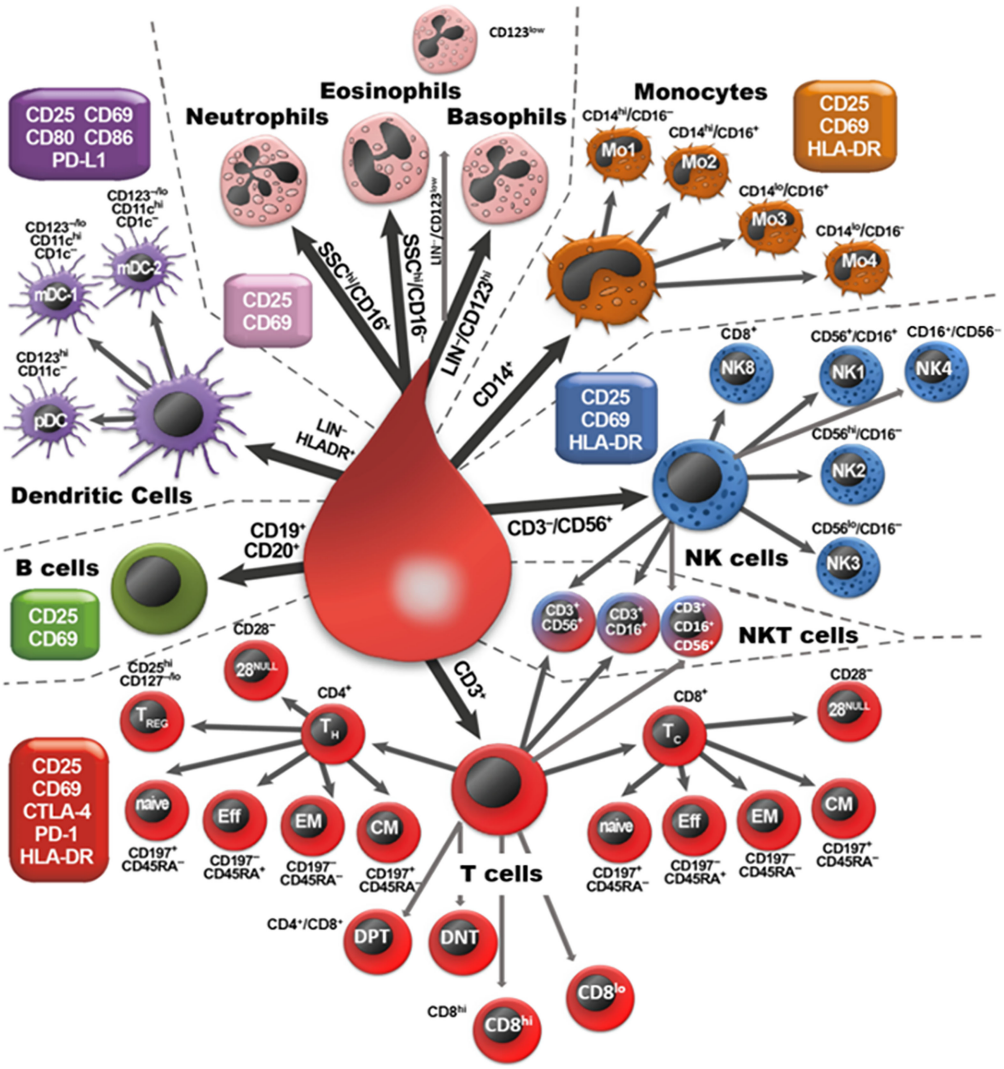

FIGURE 2 | Overview of the analyzed immune cell subpopulations. The scheme presents all nine main immune cell types (neutrophilic, eosinophilic and basophilic granulocytes, monocytes, NK cells, NKT cells, T cells, B cells and DCs) that were identified by the expression of their specific pan marker (big arrows). Those main immune cells were subdivided by analyzing the expression of further surface markers (next to each cell). Finally, all cells are analyzed for the expression of specific activation markers (CD25, CD69, CD80, CD86, PD-L1, HLA-DR, CTLA-4, PD-1), as indicated in the boxes.

daily situations and times, health status, as well as their quality of life. The pain level (and the morning stiffness) were scored on a visual analog scale (VAS) ranging from 10 = worst pain imaginable to 0 = no pain. As most patients experienced a pain reduction that lasted until the follow-up appointment, patients were asked to score their pain level again retrospectively at least six months after the follow-up appointment, in order to determine long-lasting therapeutic effects.

Statistical Analysis

Microsoft Excel was used for data management and GraphPad Prism 9 and IBM SPSS Statistics 24 were used for the statistical analysis.

The Wilcoxon test was applied to evaluate the differences in the scoring of the retrospective pain level, the absolute immune cell numbers and the activation status of the immune cells. A p-value of < 0.05 was considered statistically significant.

A Spearman's rank order correlation was performed to analyze the relationship between the pain level and the study time points, as well as the relationship between the immune cell numbers and the pain level. A p-value of < 0.05 was considered as statistically significant. Afterwards, a simple linear regression was performed. For the graphical illustration the mean values of the pain levels (**Figure 3**) and the immune cell numbers (**Figure 6**) were plotted.

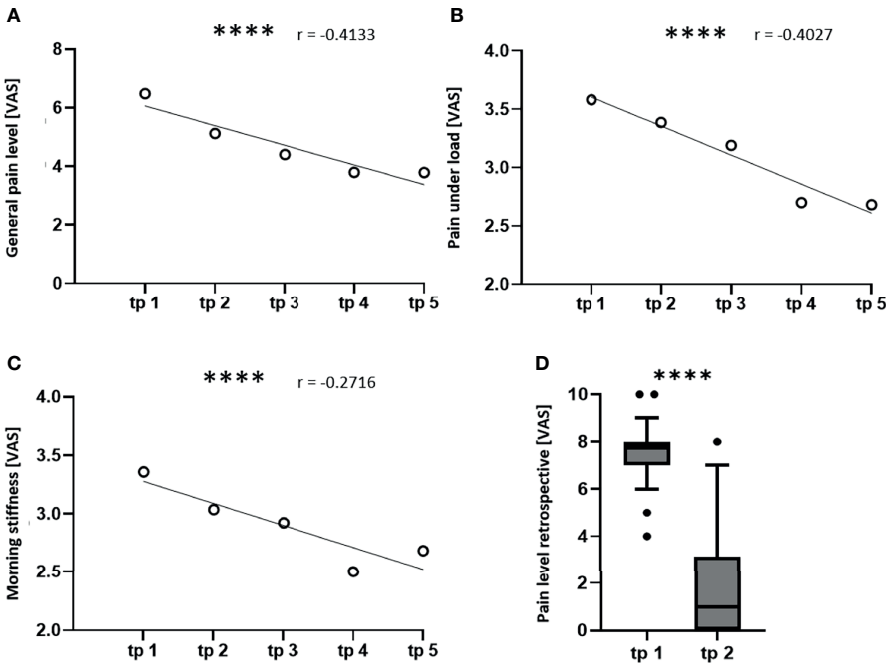

FIGURE 3 | LDRT induces a significant pain reduction. The patients scored their pain level on a visual analogue scale (VAS) ranging from 0 (no pain) to 10 (worst pain imaginable) at the indicated time points (tp). A Spearman correlation and a simple linear regression were performed in order to correlate the pain levels of all patients to the time points **(A–C)**. For the graphical illustration, the mean values of the pain levels were calculated for all five tp. **(A)** shows the correlation of the mean general pain level, **(B)** shows the correlation of the pain under load and **(C)** shows the correlation of the morning stiffness to the study tp (n = 100; ****p < 0.0001). **(D)** shows a box plot for the retrospective determination of the pain level before therapy and at least six months after therapy. A Wilcoxon test was used for the statistical analysis in graph **(D)** (n = 125; ****p < 0.0001).

RESULTS

LDRT Induces Long-Lasting Analgesic Effects

In order to prove and quantify the pain-relieving effects of LDRT, the patients filled out a questionnaire on their subjective pain level, as well as their health status and quality of life. A more detailed understanding of the pain level was generated by asking for the quality of pain or the pain level in different situations, such as the pain at rest, the pain at night or the morning stiffness. Indeed, differences in the pain level in these different situations were detected. The most prominent findings on the pain level are summarized in **Figure 3**.

The general pain level (**Figure 3A**) shows a strong negative correlation (r = -0.4133) to the study time points. This means that the pain level is reduced during the course of the study from average 6.5 to 3.8 points on VAS after the second series of irradiation (tp 4). Afterwards the pain level stagnates at the time point of the follow-up appointment (tp 5). In addition, the pain level under load (B) is also correlating negatively (r = -0.4027) to the study time points. Here, a reduction of the pain from average 3.6 to 2.7 points on VAS at time point four was observed. Again, the pain level stagnates at the follow-up appointment. Further, the morning stiffness correlates negatively (r = -0.2716) to the time points, showing a reduction from average 3.4 to 2.5 points on VAS with a minimum pain level after the second irradiation series. The detailed statistical parameters, such as the mean, the SD, the SEM and the 95% CI are depicted in **Table 2**. Finally, also the retrospective scoring of the pain level proves that LDRT induces a long-lasting analgesic effect, as the patients report a significant pain reduction even six months after the last irradiation series from about 8 to 1 point on VAS. This indicates that patients score their initial pain level even higher retrospectively. Also, they report a further reduction of their symptoms as they score their current pain level at least six months after therapy with around 1 point on VAS.

LDRT Modulates Numbers of Distinct Immune Cells of the Peripheral Blood

A detailed immunophenotyping of the peripheral blood was performed before and after every serial irradiation, as well as for the follow-up appointment (see also **Figure 1**). As analyses of modulations of cellular immune components of the peripheral blood have never been performed in clinical trials with patients receiving LDRT, we first examined which immune cell populations are modulated by a serial irradiation with a total dose of 3 Gy (**Figure 4**).

First, we detected the number of leukocytes remained stable after the first series of irradiation (**Figure 4A**). Nonetheless, we

TABLE 2 | Statistical parameters for the pain levels.

Pain parameter	Time point	Mean	SD	SEM	95% CI
General pain level	tp 1	6,8	2,0	0,3	± 0,5
General pain level	tp 2	5,1	2,1	0,3	± 0,5
General pain level	tp 3	4,4	2,3	0,4	± 0,7
General pain level	tp 4	3,8	2,6	0,4	± 0,8
General pain level	tp 5	3,8	2,6	0,5	± 1,0
Pain under load	tp 1	3,6	0,6	0,1	± 0,2
Pain under load	tp 2	3,4	0,7	0,1	± 0,2
Pain under load	tp 3	3,2	0,7	0,1	± 0,2
Pain under load	tp 4	2,7	0,8	0,1	± 0,3
Pain under load	tp 5	2,7	1,0	0,2	± 0,4
Morning stiffness	tp 1	3,4	1,0	0,1	± 0,3
Morning stiffness	tp 2	3,0	1,0	0,1	± 0,3
Morning stiffness	tp 3	2,9	1,1	0,2	± 0,3
Morning stiffness	tp 4	2,5	1,1	0,2	± 0,3
Morning stiffness	tp 5	2,7	1,2	0,2	± 0,5

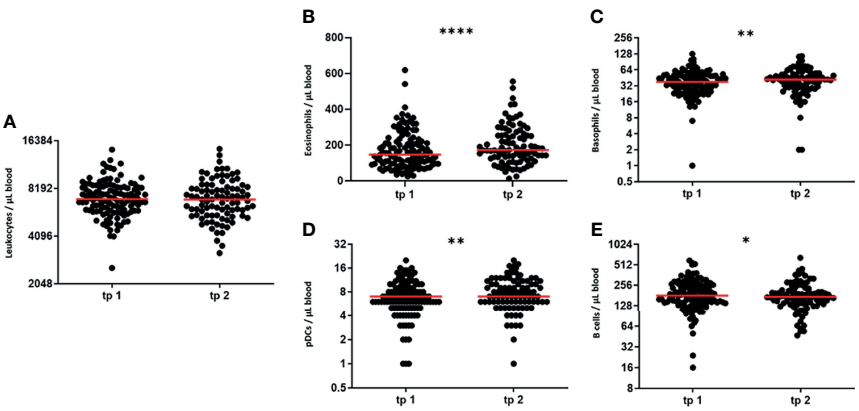

FIGURE 4 | LDRT modulates numbers of certain peripheral immune cells. In order to determine peripheral blood immune cell numbers, immunophenotyping was performed with patient's blood. Blood withdrawals were performed before (tp 1) and after serial irradiation (tp 2). The absolute immune cell numbers were determined by flow cytometry. The Wilcoxon test was used for the statistical analysis. In the figure the immune cell numbers of the blood leukocytes **(A)**, the eosinophilic and basophilic granulocytes **(B, C)**, the plasmacytoid dendritic cells **(D)** and the B cells **(E)** are presented. (n = 125; *p < 0.05; **p < 0.01 ***p < 0.0001).

detected slight, but significant modulations in the numbers of 4 out of all examined key immune cell subtypes. Cells of the innate immune system, namely eosinophilic and basophilic granulocytes and plasmacytoid dendritic cells are significantly upregulated after the first serial irradiation (**Figure 4B–D**). Cells of the adaptive immune system on the other hand, namely the B cells, display a slight, but significant decrease of their cell numbers after irradiation (**Figure 4E**). The detailed parameters (Mean, SD, SEM and 95% CI) are depicted in **Table 3**.

LDRT Decreases the Numbers of Activated Immune Cells

As not only the absolute numbers of immune cells in the periphery are an indicator of a patient's current immune status, activation markers on the immune cells were monitored in addition.

Indeed, not only modulations of cell numbers, but also a downregulation of different activated immune cell subtypes were found. **Figure 5** depicts those modulations.

A significant downregulation of the activation status was detected for the peripheral blood monocytes. These cells show a downregulation of CD25, which is part of the IL-2 cytokine receptor (**Figure 5A**). Moreover, also HLA-DR that is involved in antigen presentation, is downregulated on monocytes after the first series of irradiation (**Figure 5B**). A reduced active state was also determined for T Helper cells after irradiation. In detail, T Helper cells downregulated their expression of the activation marker PD1 (**Figure 5C**). The detailed parameters for the regulation of the activation markers are displayed in **Table 3**. In summary, these findings indicate that LDRT affects patient's immune status by modulating absolute immune cell numbers (**Figure 4**), as well as the activation state of certain immune cell subtypes (**Figure 5**).

Cells of the Monocytic Lineage Predict the Therapeutic Outcome

The data generated from the immunophenotyping is not only valuable to prove and unravel the underlying immunological

TABLE 3 | Statistical parameters for the modulation of the immune cells & activation markers.

Immune cell type	Time point	Mean	SD	SEM	95% CI
Leukocytes	tp 1	7258	1849	168,8	± 330,8
Leukocytes	tp 2	7217	2117	219,5	± 430,2
Eosinophils	tp 1	171	105	9,6	± 18,8
Eosinophils	tp 2	200	108	11,2	± 22,0
Basophils	tp 1	41	20	1,8	± 3,6
Basophils	tp 2	44	21	2,2	± 4,3
pDCs	tp 1	7	4	0,3	± 0,6
pDCs	tp 2	8	4	0,4	± 0,8
B cells	tp 1	204	101	9,3	± 18,2
B cells	tp 2	191	95	9,9	± 19,4
CD25+ monocytes	tp 1	2,4	1,9	0,2	± 0,4
CD25+ monocytes	tp 2	1,8	1,1	0,1	± 0,2
HLA-DR+ monocytes	tp 1	86,0	12,0	1,1	± 2,2
HLA-DR monocytes	tp 2	84,0	11,0	1,1	± 2,2
PD1+ TH cells	tp 1	15,3	10,8	1,0	± 1,9
PD1+ TH cells	tp 2	14,0	9,3	1,0	± 1,9

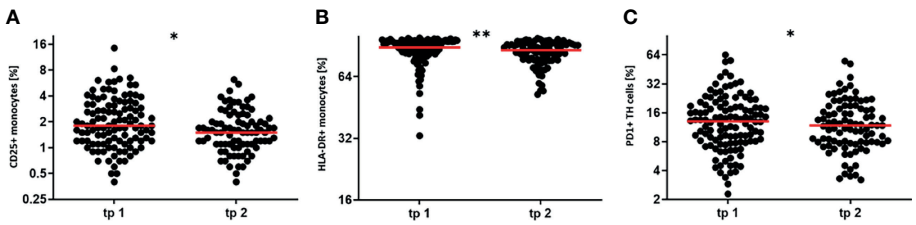

FIGURE 5 | LDRT decreases the percentage of activated immune cells. The activation state of immune cells in the peripheral blood was determined by measuring the expression of distinct activation markers. Blood withdrawals were performed before (tp1) and after the serial irradiation (tp2). The expression levels of common activation markers were determined by flow cytometry. The Wilcoxon test was used for the statistical analysis. In the figure the percentage of CD25 positive and HLA-DR positive monocytes **(A, B)**, as well as the percentage of PD1 positive T Helper cells **(C)** is presented. (n = 125; *p < 0.05; **p < 0.01).

effects of LDRT, but to define therapeutic and prognostic biomarkers that might predict the therapeutic outcome. Therefore, correlations of the pain level scores and the data of patient's immune status were performed in order to identify immune biological factors that correlate with the therapeutic outcome. In fact, three immune cell subtypes correlated strongly to pain-related factors. All of these cell types belong to the monocytic lineage of blood leukocytes (**Figure 6** and **Table 4**).

The numbers of mDCs show a significant negative correlation to the general pain level (r = -0.2123). This means that with increasing numbers of mDCs in peripheral blood, patients report a reduced pain level (**Figure 6A**). Additionally, the numbers of mDCs correlate negatively (r = -0.2729) to the morning stiffness, meaning that the morning stiffness is reduced when slightly higher levels of mDCs are found in the peripheral blood (**Figure 6B**). Not only dendritic cells predict the therapeutic outcome, but also type 1 monocytes (CD14high/CD16-), as well as type 3 monocytes (CD14low/CD16+) correlate negatively (r = -0.2441 and r = -0.2710, respectively) to the morning stiffness. This means that increasing morning stiffness comes along with reduced levels of monocytes. These findings might qualify cells of the monocytic lineage as potential biomarkers for predicting the therapeutic outcome of LDRT.

DISCUSSION

LDRT is well known for its pain-relieving effects in chronic degenerative and inflammatory diseases (25, 26). Indeed, the findings of the IMMO-LDRT01 trial strongly support this. In detail, the general pain level decreased during the course of the diseases, as well as the pain under load. Especially the reduction of pain under load is valuable for the patients, as thereby the mobility and the quality of life can be increased again. Morning stiffness is a common symptom in chronic degenerative diseases, especially in osteoarthritis and rheumatoid arthritis. Also, this symptom is significantly reduced in the patients after LDRT. As, there is still a significant pain reduction at tp 5 (three months after the last irradiation series), patients were asked to score their pain level again retrospectively at least 6 months after the last irradiation series. Even at this time point, patients still reported about a long-lasting pain reduction. As the majority of the patients was not responding sufficiently to previous therapies,

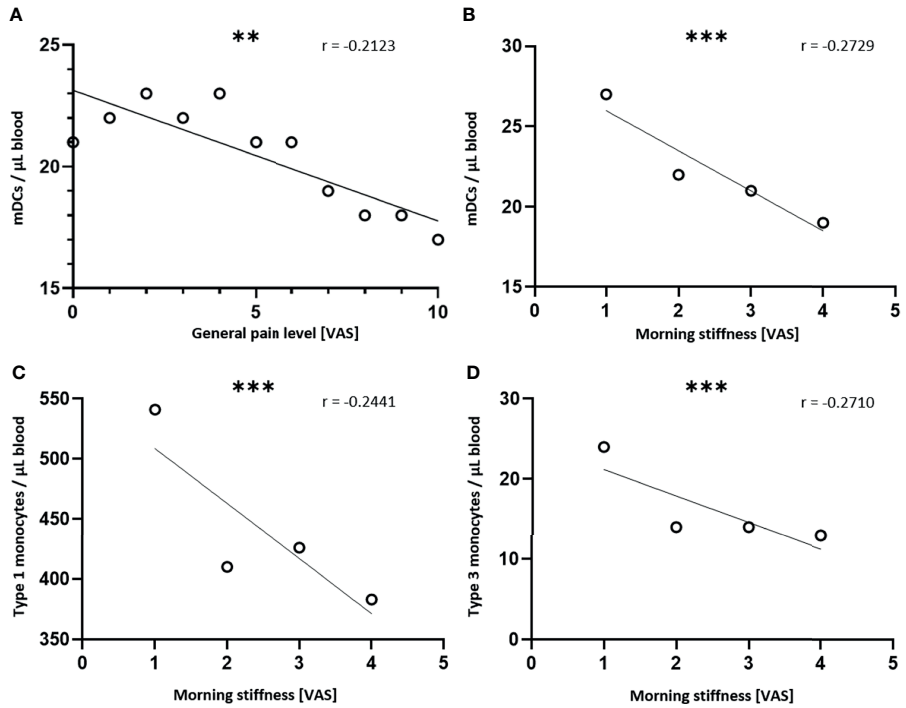

FIGURE 6 | Cells of the monocytic lineage predict the therapeutic outcome. Absolute immune cell numbers were determined by flow cytometry before and after every serial irradiation, as well as for the follow-up appointment. At the same time points, the patients scored their subjective pain level in different situations on a VAS. A Spearman correlation was performed to assess the relationship between the immunological variables and the pain related variables. A simple linear regression was performed afterwards. For the graphical illustration, the mean values of the immune cell numbers were calculated and plotted. In **(A)**, the mean numbers of myeloid DCs (mDCs) are correlated to the general pain level and in **(B)** those numbers are correlated to the morning stiffness. In **(C)** the mean number of type 1 monocytes and in **(D)** the mean number of type 3 monocytes are correlated to the morning stiffness (n = 100; **p < 0.001; ***p < 0.001).

TABLE 4 | Statistical parameters for the modulation of the cells of the monocytic lineage.

Immune cell type	Pain level	Mean	SD	SEM	95% CI
mDCs	General Pain level 10	17	6	2,0	± 4,0
mDCs	General Pain level 9	18	6	1,8	± 3,6
mDCs	General Pain level 8	18	6	1,4	± 2,7
mDCs	General Pain level 7	19	6	1,1	± 2,2
mDCs	General Pain level 6	22	10	1,8	± 3,5
mDCs	General Pain level 5	22	10	1,8	± 3,6
mDCs	General Pain level 4	23	13	3,5	± 6,8
mDCs	General Pain level 3	22	8	1,9	± 3,7
mDCs	General Pain level 2	23	9	1,5	± 3,0
mDCs	General Pain level 1	22	6	1,6	± 3,2
mDCs	General Pain level 0	21	3	1,6	± 3,2
mDCs	Morning stiffness 4	19	7	0,7	± 1,5
mDCs	Morning stiffness 3	21	17	2,5	± 5,0
mDCs	Morning stiffness 2	22	9	1,5	± 2,9
mDCs	Morning stiffness 1	27	10	1,8	± 3,4
Type 1 monocytes	Morning stiffness 4	383	119	13,0	± 25,5
Type 1 monocytes	Morning stiffness 3	425	329	48,0	± 94,0
Type 1 monocytes	Morning stiffness 2	410	135	22,5	± 44,1
Type 1 monocytes	Morning stiffness 1	541	229	41,8	± 81,8
Type 3 monocytes	Morning stiffness 4	13	9	1,0	± 1,9
Type 3 monocytes	Morning stiffness 3	14	12	1,7	± 3,4
Type 3 monocytes	Morning stiffness 2	14	8	1,3	± 2,5
Type 3 monocytes	Morning stiffness 1	24	13	2,4	± 4,7

this finding is even more impressive and supports the effectiveness of this therapy. For future studies these findings indicate that longer follow-up times are necessary to display the whole therapeutic effectiveness of LDRT (18).

Even though the pain-relieving effects of LDRT have already been well described in numerous patient studies, the underlying immunological mechanisms have to date not yet been analyzed in patient trials in a prospective manner. In the IMMO-LDRT01 trial, we show for the first time that LDRT has not only immunomodulatory effects in preclinical models and *in vitro* systems, but that it induces systemic modulations of immune cells of the peripheral blood in patients with chronic inflammatory and degenerative diseases. In detail, LDRT differentially modulates absolute cell numbers of circulating immune cells. Nonetheless, the numbers of the general leukocyte count remained stable after LDRT. This indicates that low dose radiation is not just affecting all circulating immune cells, rather than regulating specific immune cell types. Also, in the context of radiation protection, this fact is valuable, as it is indicating that low doses of X-Rays are not very harmful to healthy tissue.

For the immune cell subtypes, LDRT was found to upregulate the numbers of eosinophils and basophils, as well as the number of pDCs in peripheral blood. pDCs are connectors of the innate and the adaptive immune system as they activate cells of both branches of the immune system (27). Nonetheless, the function of pDCs is not only the activation of immune cells, but also the induction of immunological tolerance, especially T cell tolerance (28). Hence, an upregulation of those cells could be a sign of mitigated inflammatory processes. In line with that, we detected a significant downregulation of the numbers of circulating B cells. These cells of the adaptive immune system have a key role in antigen presentation and humoral immunity and therefore in the progression of immune responses (29). In addition, LDRT does not only regulate the absolute number of peripheral blood immune cells, but is affecting the activation state especially of monocytes and T Helper cells. After a first series of LDRT, monocytes reduced their expression of CD25, that is a common activation marker on leukocytes, as well as their expression of HLA-DR that is a key receptor for antigen presentation. Even though monocytes are mainly HLA-DR positive by definition (30), a downregulation of the expression is often characterized in immunosuppressive situations (31, 32). T cells are essential in mediating immune responses (33) and PD1 expression on T cells is a sign of previously being activated (34). A reduction of activated monocytes and T cells after LDRT is further supporting the hypothesis that LDRT is forming a rather anti-inflammatory milieu. The detected changes are minor but highly significant. This fact is remarkable as LDRT is delivered only locally to the affected joint but induces systemic immunomodulatory effects that can also be detected in peripheral blood. Since the here presented patient collective is rather heterogeneous, for example regarding the age or the indications of the patients, a certain heterogeneity in the immune status is expected. More prominent immunological modulations that are induced by LDRT are expected when patient subgroups are analyzed. Factors, such as gender, and age have a great impact on the immune status and might impact on the here presented data (35, 36). Additionally, all of the underlying indications are based on different biological and immunological mechanisms that might lead to changes in the peripheral blood immune status. In the explorative IMMO-LDRT01 trial we aimed to analyze for the first time peripheral blood immune alterations of patients that routinely do receive LDRT and the indications (displayed in **Table 1**) reflect the clinical routine. In the future, we will analyze patient subgroups defined by the respective disease. However, for this, more patients will have to be included. Additionally, we are currently preparing a prospective trial focusing on patients with arthritis.

The application of the immunophenotyping in clinical trials allows the longitudinal screening of numerous immunological parameters. These analyses are not only valuable to unravel the immunological modes of action of LDRT, but also to define predictive and prognostic biomarkers for LDRT. Therefore, we correlated pain related factors to the immunological data. Indeed, we found that cells of the monocytic lineage show a strong, negative correlation to the general pain level, as well as to the morning stiffness. The later symptom is often found in chronic degenerative and inflammatory diseases, particularly in osteoarthritis and rheumatoid arthritis (37, 38). As pain in arthritis and osteoarthritis is closely connected to the chronic inflammatory processes, a correlation of pain-related symptoms with immunological modulations is obvious (39). The cell numbers of mDCs correlate negatively to the general pain level and the morning stiffness. DCs represent a heterogeneous population of antigen presenting cells. Primarily, mDCs have a key role in initiating adaptive immune responses, but they are also key for tolerance induction and maintenance. Especially in chronic inflammation, that is a key feature in chronic degenerative and inflammatory diseases, mDCs can shift their phenotype towards a regulatory cell type. This shift is often triggered by signals delivered through anti-inflammatory cytokines, such as IL-10 and TGF-β (40). Just like mDCs, monocytes are as well a very heterogeneous cell population. Therefore, we determine three different monocytes subsets in the immunophenotyping panels. The classical monocytes (type 1 monocytes) that make up 90% of all blood monocytes, as well as the non-classical monocytes (type 3 monocytes) correlate negatively to the morning stiffness as well. Classical monocytes can differentiate into monocyte-derived DCs (moDCs), as well as macrophages, whereas non-classical monocytes are not likely to differentiate into moDCs (41). In general, monocytes can activate different branches of the immune system, such as TH1 or TH2 mediated immunity, but also bear tolerogenic functions by the activation of Treg cells that leads to an amelioration of pre-existing inflammatory processes. Which of these different mechanisms is initiated, is strongly depended on the immunological micro-milieu and cytokine signals (42). In order to analyze further how monocytes modulate the inflammation and pain sensation after LDRT, further functional analyses on the monocyte phenotype need to be performed in the future.

DATA AVAILABILITY STATEMENT

The raw data supporting the conclusions of this article will be made available by the authors, without undue reservation.

ETHICS STATEMENT

The studies involving human participants were reviewed and approved by Institutional Review Board of the Friedrich-Alexander Universität Erlangen-Nürnberg (protocol code: 289_15B, date of approval: 12.11.2015). The patients/participants provided their written informed consent to participate in this study.

AUTHOR CONTRIBUTIONS

Conceptualization, UG, RF, OO, and BF. Methodology, A-JD, IB, TG, and TW. Software, A-JD, IB, BMF, and MD. Formal analysis, A-JD, BMF, MD, and LM. Investigation, A-JD and TW. Writing—original draft preparation, A-JD. Writing—review and editing, IB and UG. Visualization, A-JD. Supervision, UG and BF. Project administration, BF. Funding acquisition, UG and BF. All authors contributed to the article and approved the submitted version.

FUNDING

This work is funded by the Bundesministerium für Bildung und Forschung (GREWIS and GREWIS-alpha, 02NUK017G und 02NUK050E).

ACKNOWLEDGMENTS

We acknowledge the support by the German Research Foundation and the Friedrich-Alexander-Universität Erlangen-Nürnberg within the funding program Open Access Publishing.

REFERENCES

1. Lane NE, Shidara K, Wise BL. Osteoarthritis Year in Review 2016: Clinical. *Osteoarthritis Cartilage* (2017) 25:209–15. doi: 10.1016/j.joca.2016.09.025
2. Feldmann MB, Maini FM. Rheumatoid Arthritis. *Cell* (1996) 85:307–10. doi: 10.1016/S0092-8674(00)81109-5
3. McInnes IB, Schett G. The Pathogenesis of Rheumatoid Arthritis. *N Engl J Med* (2011) 365:2205–19. doi: 10.1056/NEJMra1004965
4. Mandl LA. Osteoarthritis Year in Review 2018: Clinical. *Osteoarthritis Cartilage* (2019) 27:359–64. doi: 10.1016/j.joca.2018.11.001
5. Goldring MB, Otero M. Inflammation in Osteoarthritis. *Curr Opin Rheumatol* (2011) 23:471–8. doi: 10.1097/BOR.0b013e328349c2b1
6. Hermann W, Lambova S, Muller-Ladner U. Current Treatment Options for Osteoarthritis. *Curr Rheumatol Rev* (2018) 14:108–16. doi: 10.2174/1573397113666170829155149
7. Sherrer Y. Abatacept in Biologic-Naive Patients and TNF Inadequate Responders: Clinical Data in Focus. *Curr Med Res Opin* (2008) 24:2283–94. doi: 10.1185/03007990802223129
8. Schmid-Monnard. Über Heilung Des Gelenkrheumatismus Durch Röntgenstrahlung Bei Kindern. *Fortschr auf dem Gebiet der Röntgenstrahlung* (1898) 1:209.
9. Ott OJ, Hertel S, Gaipl US, Frey B, Schmidt M, Fietkau R. Benign Painful Shoulder Syndrome: Initial Results of a Single-Center Prospective Randomized Radiotherapy Dose-Optimization Trial. *Strahlenther Onkol* (2012) 188:1108–13. doi: 10.1007/s00066-012-0237-6
10. Ott OJ, Niewald M, Weitmann HD, Jacob I, Adamietz IA, Schaefer U, et al. German Cooperative Group on Radiotherapy for Benign, D. DEGRO Guidelines for the Radiotherapy of non-Malignant Disorders. Part II: Painful Degenerative Skeletal Disorders. *Strahlenther Onkol* (2015) 191:1–6. doi: 10.1007/s00066-014-0757-3
11. Torres Royo L, Antelo Redondo G, Arquez Pianetta M, Arenas Prat M. Low-Dose Radiation Therapy for Benign Pathologies. *Rep Pract Oncol Radiother* (2020) 25:250–4. doi: 10.1016/j.rpor.2020.02.004
12. Roedel F, Kley N, Beuscher HU, Hildebrandt G, Keilholz L, Kern P, et al. Anti-Inflammatory Effect of Low-Dose X-Irradiation and the Involvement of a TGF-Beta1-Induced Down-Regulation of Leukocyte/Endothelial Cell Adhesion. *Int J Radiat Biol* (2002) 78:711–9. doi: 10.1080/09553000210137671
13. Kern PM, Keilholz L, Forster C, Hallmann R, Herrmann M, Seegenschmiedt MH. Low-Dose Radiotherapy Selectively Reduces Adhesion of Peripheral Blood Mononuclear Cells to Endothelium In Vitro. *Radiother Oncol* (2000) 54:273–82. doi: 10.1016/S0167-8140(00)00141-9
14. Schaue D, Marples B, Trott KR. The Effects of Low-Dose X-Irradiation on the Oxidative Burst in Stimulated Macrophages. *Int J Radiat Biol* (2002) 78:567–76. doi: 10.1080/09553000210126457
15. Kern P, Keilholz L, Forster C, Seegenschmiedt MH, Sauer R, Herrmann M. In Vitro Apoptosis in Peripheral Blood Mononuclear Cells Induced by Low-Dose Radiotherapy Displays a Discontinuous Dose-Dependence. *Int J Radiat Biol* (1999) 75:995–1003. doi: 10.1080/095530099139755
16. Wunderlich R, Ernst A, Rodel F, Fietkau R, Ott O, Lauber K, et al. Low and Moderate Doses of Ionizing Radiation Up to 2 Gy Modulate Transmigration and Chemotaxis of Activated Macrophages, Provoke an Anti-Inflammatory Cytokine Milieu, But Do Not Impact Upon Viability and Phagocytic Function. *Clin Exp Immunol* (2015) 179:50–61. doi: 10.1111/cei.12344
17. Deloch L, Derer A, Hueber AJ, Herrmann M, Schett GA, Wolfelschneider J, et al. Low-Dose Radiotherapy Ameliorates Advanced Arthritis in hTNF-Alpha Tg Mice by Particularly Positively Impacting on Bone Metabolism. *Front Immunol* (2018) 9:1834. doi: 10.3389/fimmu.2018.01834
18. Ott OJ, Micke O, Mucke R, Niewald M, Rodel F, Schafer U, et al. Low-Dose Radiotherapy: Mayday, Mayday. We've Been Hit! *Strahlenther Onkol* (2019) 195:285–8. doi: 10.1007/s00066-018-1412-1
19. Hautmann MG, Hipp M, Neumaier U, Steger F, Brockmann S, Treutwein M, et al. Radiotherapy for Osteoarthritis of the Ankle and Tarsal Joints-Analysis of 66 Joints. *Strahlenther Onkol* (2020) 196:569–75. doi: 10.1007/s00066-019-01551-5
20. Donaubauer AJ, Zhou JG, Ott OJ, Putz F, Fietkau R, Keilholz L, et al. Low Dose Radiation Therapy, Particularly With 0.5 Gy, Improves Pain in Degenerative Joint Disease of the Fingers: Results of a Retrospective Analysis. *Int J Mol Sci* (2020) 21:5854–67. doi: 10.3390/ijms21165854
21. Zhou JG, Donaubauer AJ, Frey B, Becker I, Rutzner S, Eckstein M, et al. Prospective Development and Validation of a Liquid Immune Profile-Based Signature (LIPS) to Predict Response of Patients With Recurrent/Metastatic Cancer to Immune Checkpoint Inhibitors. *J Immunother Cancer* (2021) 9. doi: 10.1136/jitc-2020-001845
22. Ruhle PF, Fietkau R, Gaipl US, Frey B. Development of a Modular Assay for Detailed Immunophenotyping of Peripheral Human Whole Blood Samples by Multicolor Flow Cytometry. *Int J Mol Sci* (2016) 17:1316–45. doi: 10.3390/ijms17081316
23. Donaubauer AJ, Ruhle PF, Becker I, Fietkau R, Gaipl US, Frey B. One-Tube Multicolor Flow Cytometry Assay (OTMA) for Comprehensive Immunophenotyping of Peripheral Blood. *Methods Mol Biol* (2019) 1904:189–212. doi: 10.1007/978-1-4939-8958-4_8

24. Donaubauer AJ, Becker I, Ruhle PF, Fietkau R, Gaipl US, Frey B. Analysis of the Immune Status From Peripheral Whole Blood With a Single-Tube Multicolor Flow Cytometry Assay. *Methods Enzymol* (2020) 632:389–415. doi: 10.1016/bs.mie.2019.03.003
25. Rogers S, Eberle B, Vogt DR, Meier E, Moser L, Gomez Ordonez S, et al. Prospective Evaluation of Changes in Pain Levels, Quality of Life and Functionality After Low Dose Radiotherapy for Epicondylitis, Plantar Fasciitis, and Finger Osteoarthritis. *Front Med (Lausanne)* (2020) 7:195. doi: 10.3389/fmed.2020.00195
26. Abdus-Salam AA, Olabumuyi AA, Jimoh MA, Folorunso SA, Orekoya AA. The Role of Radiation Treatment in the Management of Inflammatory Musculoskeletal Conditions: A Revisit. *Radiat Oncol J* (2020) 38:151–61. doi: 10.3857/roj.2020.00178
27. Koucky V, Boucek J, Fialova A. Immunology of Plasmacytoid Dendritic Cells in Solid Tumors: A Brief Review. *Cancers (Basel)* (2019) 11:470–84. doi: 10.3390/cancers11040470
28. Mitchell D, Chintala S, Dey M. Plasmacytoid Dendritic Cell in Immunity and Cancer. *J Neuroimmunol* (2018) 322:63–73. doi: 10.1016/j.jneuroim.2018.06.012
29. LeBien TW, Tedder TFB. Lymphocytes: How They Develop and Function. *Blood* (2008) 112:1570–80. doi: 10.1182/blood-2008-02-078071
30. Bunbury A, Potolicchio I, Maitra R, Santambrogio L. Functional Analysis of Monocyte MHC Class II Compartments. *FASEB J* (2009) 23:164–71. doi: 10.1096/fj.08-109439
31. Mengos AE, Gastineau DA, Gustafson MP. The CD14(+)HLA-DR(lo/neg) Monocyte: An Immunosuppressive Phenotype That Restrains Responses to Cancer Immunotherapy. *Front Immunol* (2019) 10:1147. doi: 10.3389/fimmu.2019.01147
32. Lima DS, Lemes RPG, Matos DM. Immunosuppressive Monocytes (CD14 (+)/HLA-DR(low/-)) Increase in Childhood Precursor B-Cell Acute Lymphoblastic Leukemia After Induction Chemotherapy. *Med Oncol* (2018) 35:36. doi: 10.1007/s12032-018-1092-9
33. Kumar BV, Connors TJ, Farber DL. Human T Cell Development, Localization, and Function Throughout Life. *Immunity* (2018) 48:202–13. doi: 10.1016/j.immuni.2018.01.007
34. Riley JL. PD-1 Signaling in Primary T Cells. *Immunol Rev* (2009) 229:114–25. doi: 10.1111/j.1600-065X.2009.00767.x
35. Muller L, Di Benedetto S, Pawelec G. The Immune System and Its Dysregulation With Aging. *Subcell Biochem* (2019) 91:21–43. doi: 10.1007/978-981-13-3681-2_2
36. Moulton VR. Sex Hormones in Acquired Immunity and Autoimmune Disease. *Front Immunol* (2018) 9:2279. doi: 10.3389/fimmu.2018.02279
37. Zhang W, Doherty M, Peat G, Bierma-Zeinstra MA, Arden NK, Bresnihan B, et al. EULAR Evidence-Based Recommendations for the Diagnosis of Knee Osteoarthritis. *Ann Rheum Dis* (2010) 69:483–9. doi: 10.1136/ard.2009.113100
38. Orange DE, Blachere NE, DiCarlo EF, Mirza S, Pannellini T, Jiang CS, et al. Rheumatoid Arthritis Morning Stiffness Is Associated With Synovial Fibrin and Neutrophils. *Arthritis Rheumatol* (2020) 72:557–64. doi: 10.1002/art.41141
39. Harth M, Nielson WR. Pain and Affective Distress in Arthritis: Relationship to Immunity and Inflammation. *Expert Rev Clin Immunol* (2019) 15:541–52. doi: 10.1080/1744666X.2019.1573675
40. Chistiakov DA, Sobenin IA, Orekhov AN, Bobryshev YV. Myeloid Dendritic Cells: Development, Functions, and Role in Atherosclerotic Inflammation. *Immunobiology* (2015) 220:833–44. doi: 10.1016/j.imbio.2014.12.010
41. Boyette LB, Macedo C, Hadi K, Elinoff BD, Walters JT, Ramaswami B, et al. Phenotype, Function, and Differentiation Potential of Human Monocyte Subsets. *PloS One* (2017) 12:e0176460. doi: 10.1371/journal.pone.0176460
42. Roberts CA, Dickinson AK, Taams LS. The Interplay Between Monocytes/Macrophages and CD4(+) T Cell Subsets in Rheumatoid Arthritis. *Front Immunol* (2015) 6:571. doi: 10.3389/fimmu.2015.00571

Conflict of Interest: The authors declare that the research was conducted in the absence of any commercial or financial relationships that could be construed as a potential conflict of interest.

The reviewer KL declared a past co-authorship with authors UG and BF to the handling editor.

Publisher's Note: All claims expressed in this article are solely those of the authors and do not necessarily represent those of their affiliated organizations, or those of the publisher, the editors and the reviewers. Any product that may be evaluated in this article, or claim that may be made by its manufacturer, is not guaranteed or endorsed by the publisher.

frontiers in Immunology

ORIGINAL RESEARCH
published: 21 October 2021
doi: 10.3389/fimmu.2021.745523

IL-40: A New B Cell-Associated Cytokine Up-Regulated in Rheumatoid Arthritis Decreases Following the Rituximab Therapy and Correlates With Disease Activity, Autoantibodies, and NETosis

Adela Navrátilová[1,2†], Lucie Andrés Cerezo[1,2†], Hana Hulejová[1], Viktor Bečvář[1], Michal Tomčík[1,2], Martin Komarc[3], David Veigl[4], Dana Tegzová[1,2], Jakub Závada[1,2], Marta Olejárová[1,2], Karel Pavelka[1,2], Jiří Vencovský[1,2] and Ladislav Šenolt[1,2]*

[1] Department of Experimental Rheumatology, Institute of Rheumatology, Prague, Czechia, [2] Department of Rheumatology, First Faculty of Medicine, Charles University, Prague, Czechia, [3] Department of Methodology, Faculty of Physical Education and Sport, Charles University, Prague, Czechia, [4] First Orthopaedic Clinic, 1st Faculty of Medicine, Charles University, Prague, Czechia

OPEN ACCESS

Edited by:
Maria I. Bokarewa, University of Gothenburg, Sweden

Reviewed by:
Deepika Sharma, University of Chicago, United States
Oliver Michael Steinmetz, Universität Hamburg, Germany

***Correspondence:**
Adela Navrátilová
navratilova@revma.cz

†These authors have contributed equally to this work and share first authorship

Specialty section:
This article was submitted to Autoimmune and Autoinflammatory Disorders, a section of the journal Frontiers in Immunology

Received: *22 July 2021*
Accepted: *24 September 2021*
Published: *21 October 2021*

Citation:
Navrátilová A, Andrés Cerezo L, Hulejová H, Bečvář V, Tomčík M, Komarc M, Veigl D, Tegzová D, Závada J, Olejárová M, Pavelka K, Vencovský J and Šenolt L (2021) IL-40: A New B Cell-Associated Cytokine Up-Regulated in Rheumatoid Arthritis Decreases Following the Rituximab Therapy and Correlates With Disease Activity, Autoantibodies, and NETosis. Front. Immunol. 12:745523. doi: 10.3389/fimmu.2021.745523

Background: Interleukin 40 (IL-40) is a newly identified B cell-associated cytokine implicated in humoral immune responses and B cell homeostasis. As B cells play a pivotal role in autoimmunity, we investigated the function of IL-40 in rheumatoid arthritis (RA).

Methods: IL-40 expression was determined in the synovial tissue from RA and osteoarthritis (OA) patients. IL-40 was analysed in the serum/synovial fluid of patients with RA (n=50), systemic lupus erythematosus (SLE, n=69), OA (n=44), and healthy controls (HC, n=50). We assessed the changes of IL-40 levels in RA patients following the B cell depletion by rituximab (n=29) or after the TNF inhibition by adalimumab (n=25). We examined the relationship between IL-40, disease activity, autoantibodies, cytokines, and NETosis markers. Effect of IL-40 on synovial fibroblasts was determined.

Results: IL-40 was overexpressed in RA synovial tissue, particularly by synovial lining and infiltrating immune cells. The levels of IL-40 were up-regulated in the synovial fluid of RA versus OA patients ($p<0.0001$). Similarly, IL-40 was increased in the serum of RA patients compared to HC, OA, or SLE ($p<0.0001$ for all) and decreased after 16 and 24 weeks ($p<0.01$ and $p<0.01$) following rituximab treatment. No significant effect of adalimumab on IL-40 was observed. IL-40 levels in RA patients correlated with rheumatoid factor-IgM and anti-cyclic citrullinated peptides (anti-CCP) in the serum ($p<0.0001$ and $p<0.01$), as well as in the synovial fluid ($p<0.0001$ and $p<0.001$). Synovial fluid IL-40 was also associated with disease activity score DAS28 ($p<0.05$), synovial fluid leukocyte count ($p<0.01$), neutrophil attractants IL-8 ($p<0.01$), MIP-1α ($p<0.01$), and markers of neutrophil extracellular traps externalization (NETosis) such as proteinase 3 ($p<0.0001$) and neutrophil elastase

(p<0.0001). Synovial fibroblasts exposed to IL-40 increased the secretion of IL-8 (p<0.01), MCP-1 (p<0.05), and MMP-13 (p<0.01) compared to the unstimulated cells.

Conclusions: We show the up-regulation of IL-40 in RA and its decrease following B cell depleting therapy. The association of IL-40 with autoantibodies, chemokines, and markers of NETosis may imply its potential involvement in RA development. Moreover, IL-40 up-regulates the secretion of chemokines and MMP-13 in synovial fibroblasts, indicating its role in the regulation of inflammation and tissue destruction in RA.

Keywords: interleukin-40, rheumatoid arthritis, autoantibodies, disease activity, B cells, NETosis

INTRODUCTION

Rheumatoid arthritis (RA) is a common chronic autoimmune disease characterized by persistent synovitis with various extra-articular manifestations (1). The pathogenic process of RA is localised particularly in the synovial joint infiltrated by immune cells, which together with synovial fibroblasts release inflammatory mediators and matrix-degrading enzymes, contributing to bone erosion and cartilage destruction (2). For decades, RA has been widely accepted as a T cell-driven autoimmune disease. Emerging evidence emphasized the significance of B cells in the pathogenesis of RA beyond antibody production (3). As documented in the experimental models of arthritis, cytokines secreted by B cells may be involved in the induction and promotion of arthritis (4, 5). Recently, B cell depleting agents have proved highly effective in RA treatment (6). Nevertheless, elimination of B cells often results in a decline of autoantibody levels in RA (7), but does not always correlate with the clinical response to therapy (7, 8). It is apparent that autoantibody-independent mechanisms of B cells are implicated in the progression of RA (9). Therefore, identification of new B cell-associated biomarkers embedded in the pathogenesis of RA would be beneficial.

Interleukin 40 (IL-40) is recently identified as a B cell-associated cytokine, which is related to immune response mechanisms and B cell homeostasis (10). This cytokine was originally described by Catalan-Dibene et al. in 2017 as a small (27 kDa) secreted protein encoded by the *C17orf99* gene (chromosome 17 open reading frame 99) (10). Based on its unique structural properties, IL-40 fell into the category of the few so-called "orphan" cytokines (11), which do not share homologies with any of the established cytokine families. To date, there have been only few studies regarding the *C17orf99* gene or its product IL-40 protein. It is well established that C17orf99 or IL-40 are expressed only in mammals and are particularly enhanced in fetal liver, bone marrow, and activated B cells (10–13). As demonstrated in IL-40 knockout mice, IL-40 is associated with lactation and affects the production of IgA and, thereby, the composition of the intestinal microbiome in mice (10). Moreover, IL-40 knockout mice exhibited abnormalities in B cell populations, indicating the role of IL-40 in B cell development (10). Under *in vitro* conditions, IL-40 is expressed by human B cells upon activation by anti-CD40 mAb, anti-IgM, and IL-4, and its expression is further potentiated by transforming growth factor (TGF)-β1 (10). Furthermore, IL-40 was detected in several cell lines of human diffuse large B cell lymphoma (10), and its differential expression among the lymphoma subtypes was reported (14, 15). Very recently, C17orf99 was found down-regulated in the co-culture of human respiratory epithelial cells with macrophages upon treatment with anti-inflammatory cytokine IL-38 (16), suggesting the role of IL-40 in inflammation. The only evidence linking IL-40 to autoimmune inflammation was reported back in 2012 by Zingaretti et al., who identified *C17orf99* as one of the four autoantigens discriminating autoimmune hepatitis from healthy individuals (17).

Altogether, the implication of IL-40 in the B cell homeostasis and in the regulation of immune mechanisms makes it a suitable candidate player in the pathogenesis of autoimmune diseases. Thus, we aimed to analyse the expression of IL-40 in patients with RA, its association with disease-specific parameters, and its immunomodulatory capacity *in vitro*.

Abbreviations: anti-CCP, Anti-cyclic citrullinated peptides; BSA, Bovine serum albumin; bDMARDs; biological disease-modifying antirheumatic drugs; c17ORF99, Chromosome 17 open reading frame 99; CRP, C-reactive protein; csDMARDS, Conventional synthetic disease-modifying antirheumatic drugs; ctrl, Unstimulated cells; DAPI, 4',6-diamidin-2-fenylindol; DAS28, Disease activity score in 28 joints using the erythrocyte sedimentation rate; DMEM, Dulbecco's Modified Eagle Medium; ELISA, Enzyme-linked immunosorbent assay; ESR, Erythrocyte sedimentation rate; FBS, Fetal bovine serum; FGF, Fibroblast growth factors; GCs, Glucocorticoids; G-CSF, Granulocyte colony stimulating factor; GM-CSF, Granulocyte-macrophage colony-stimulating factor; HC, Healthy control; IFN-γ, Interferon gamma; Ig, Immunoglobulin; IL, Interleukin; IP-10, Interferon gamma-induced protein 10; IQR, Interquartile range; LPS, Lipopolysaccharide; MCP-1, Monocyte chemoattractant protein 1; MIP, Macrophage inflammatory protein; MMP, Metalloproteinase; MPO, Myeloperoxidase; NE, Neutrophil elastase; NETosis, process of externalization of neutrophil extracellular traps; NETs, Neutrophil extracellular traps; ns, non-significant; OA, Osteoarthritis; PDGF, Platelet Derived Growth Factor; PR3, Proteinase 3; RA, Rheumatoid arthritis; RANTES, Regulated on activation; normal T cell expressed and secreted; RF, Rheumatoid factor; RT, Room temperature; RTX, Rituximab; SD, Standard deviation; SJC, Swollen joint count; SLE, Systemic lupus erythematosus; TGF, Transforming growth factor; TJC, tender joint count; TNF, Tumor necrosis factor; TNFi, TNF inhibitors; VEGF, Vascular endothelial growth factor.

MATERIALS AND METHODS

Patients

This study included three cohorts of patients with RA. Cohort 1 involved patients with active RA with knee effusion (total of 50

patients (31 women and 19 men) with a mean (SD) age of 55 (13) years and a disease duration of 14 (12) years. A total of 68% RA patients were IgM rheumatoid factor (RF-IgM) positive and 58% anti-CCP positive. Cohort 2 included patients with RA indicated for the treatment with rituximab (MabThera, Roche): a total of 29 patients (26 women and 3 men) with a mean (SD) age of 49 (14) years and a disease duration of 14 (10) years. In cohort 2, 72% of patients were IgM rheumatoid factor (RF-IgM) positive, 69% anti-CCP positive, and 82% of patients received anti-Tumor necrosis factor (TNF) therapy prior to the administration of rituximab. Rituximab, a chimeric monoclonal anti-human CD20 antibody, which primarily causes B cell depletion, was administrated as a 1000 mg intravenous infusion at baseline and on day 14. Cohort 3 involved patients with RA indicated for the treatment with the TNF inhibitor (TNFi) adalimumab (Humira, Abbott Laboratories): a total of 25 patients (22 women and 3 men) with a mean (SD) age of 50 (13) years and a disease duration of 7 (7) years. A total of 68% RA patients were RF-IgM positive and 72% anti-CCP positive. Adalimumab was administrated subcutaneously at a standard dose of 40 mg every other week. In all patients, RA was diagnosed according to the 2010 American College of Rheumatology (ACR)/European League Against Rheumatism (EULAR) criteria (18). The control groups comprised of 44 patients with knee OA (33 women and 11 men) with a mean (SD) age of 67 (12) years and a disease duration of 7 (6) years, and 50 healthy controls (HC) (37 women and 13 men) with a mean (SD) age of 52 (14) years. Demographic and clinical characteristics of the study subjects are shown in **Table 1**. In addition, a cohort of 69 patients with systemic lupus erythematosus (SLE) (62 women and 7 men) with a mean (SD) age of 43 (16) years and a disease duration of 2 (8) years, fulfilling the 2012 Systemic Lupus International Collaborating Clinics Classification Criteria (19), was included in the study as it represents an autoimmune rheumatic disease where B cells carry out a central role in the pathogenesis. Written informed consent was obtained from all patients and healthy individuals participating in the study. This study was approved by the Ethics Board of the Institute of Rheumatology in Prague.

Laboratory Measurements

In cohort 1, paired blood and synovial fluid samples were collected at the time of clinically indicated knee arthrocentesis in 50 RA and 44 knee OA patients. In cohorts 2 and 3, only peripheral blood samples were obtained from 29 RA patients who received rituximab therapy (cohort 2) at baseline and at weeks 16 and 24 and from 25 patients receiving adalimumab (cohort 3) at baseline and at weeks 12 and 52. All samples were immediately processed, aliquoted, and stored at -80°C until use. Prior to analysis, the synovial fluid samples were treated with hyaluronidase (Hylase Dessau; Riemser Arzneimittel, Greifswald, Germany) for 30 minutes at 37°C. The disease severity was assessed by the disease activity score in 28 joints using the erythrocyte sedimentation rate (DAS28-ESR). Levels of C-reactive protein (CRP) were analysed by turbidimetry using an Olympus Biochemical Analyzer (Olympus CO Ltd., Tokyo, Japan), and anti-CCP and RF-IgM levels were determined using standard enzyme-linked immune sorbent assay (ELISA) kits (Test Line s.r.o., Czech Republic). CD19+ B cells were assessed by flow cytometry as previously described (20).

Measurement of Cytokines

Levels of IL-40 in the serum and synovial fluid were analysed by commercially available ELISA kits, according to the

TABLE 1 | Characteristics of patients with rheumatoid arthritis (RA), osteoarthritis (OA), systemic lupus erythematosus (SLE) and healthy controls (HC).

Characteristics	RA			OA	SLE	HC
	Cohort 1 (Knee joint effusion)	Cohort 2 (RTX therapy)	Cohort 3 (TNFi therapy)			
Number of patients	50	29	25	44	69	50
Gender (F/M)	31/19	26/3	22/3	33/11	62/7	37/13
Age (years)	54.0 (46.0-65.0)	50.0 (39.5-58.0)	52.0 (40.5-59.5)	67.0 (58.0-77.0)	43.0 (29.0-55.0)	55.0 (41.5-62.5)
Disease duration (years)	10.0 (6.0-19.0)	13.2 (5.7-23.1)	5.0 (3.0-11.5)	6.5 (2.0-10.8)	1.0 (0.0-2.0)	–
CRP (mg/l)	17.5 (5.2-39.5)	23.7 (8.4-31.6)	13.1 (7.6-39.4)	2.5 (1.4-5.4)	1.9 (0.9-22.3)	1.3 (0.6-2.5)
ESR (mm/h)	29.5 (17.8-53.0)	50.0 (27.5-68.5)	33.0 (20.0-62.5)	9.5 (6.0-19.2)	–	–
DAS28 score (ESR)	5.3 (4.1-6.5)	6.5 (5.7-7.5)	6.4 (5.8-7.0)	–	–	–
RF positivity, n (%)	34 (68%)	21 (72%)	17 (68%)	–	–	–
anti-CCP positivity, n (%)	29 (58%)	20 (69%)	18 (72%)	–	–	–
Current medication(csDMARDs/GCs)	36/26	22/26	25/12	–	–	–
bDMARDs	20*	29**	25	–	–	–

Anti-CCP, anti-cyclic citrullinated peptide antibody; CRP, C-reactive protein; DAS28 score, disease activity score; csDMARDs, conventional synthetic disease-modifying antirheumatic drugs; bDMARDs, biological disease-modifying antirheumatic drugs; ESR, erythrocyte sedimentation rate; F, female; GCs, glucocorticoids; HC, healthy controls; M, male; OA, osteoarthritis; RA, rheumatoid arthritis; RF, rheumatoid factor; RTX, rituximab; SLE, systemic lupus erythematosus; TNFi, tumour necrosis factor inhibitor. Data are expressed as median (IQR).

**Out of 20 patients, 15 were treated with anti-TNF therapy, 4 with anti-CD20 therapy, and 1 with anti-IL-6 therapy. **Out of 29 patients treated with rituximab, 24 received anti-TNF therapy prior to the administration of rituximab.*

manufacturer's protocol (MyBioSource, San Diego, USA). The detection limit of the assay is 0.1 ng/ml. The levels of neutrophil extracellular traps externalization process (NETosis) associated markers proteinase 3 (PR3) and neutrophil elastase (NE) were analysed by commercially available kits (Biovendor, Brno, Czech Republic, and Abcam, Cambridge, UK). The analyses were performed using a SUNRISE ELISA reader (Tecan, Salzburg, Austria) at 450 nm. A panel of cytokines, chemokines, and growth factors (FGF, eotaxin, G-CSF, GM-CSF, IFN-γ, IL-1β, IL-1ra, IL-2, IL-4, IL-5, IL-6, IL-7, IL-8, IL-9, IL-10, IL-12 (p70), IL-13, IL-15, IL-17a, IP-10, MCP-1, MIP-1α, MIP-1β, PDGF-BB, RANTES, TNF-α, VEGF) was quantified using commercially available Bio-Plex Pro TM human Cytokine 27-plex Assay (BIO-RAD, California, USA) according to the manufacturer's protocol. The analysis was performed using the luminex BIO-PLEX 200 System (Bio-Rad, California, USA).

Immunohistochemistry

Samples of synovial tissue were obtained from five patients with RA (5 females, with a mean (SD) age of 67 (7) years) from one knee joint, two elbow joints, and two small hand joints. The control group comprised of synovial tissue from four patients with OA (2 females and 2 males, with a mean (SD) age of 63 (8) years) from three knee joints and one hip joint. All synovial tissue samples were obtained during joint surgery, embedded in paraffin, and cut into 5-µm-thick sections. Subsequently, the sections were deparaffinised and rehydrated. Endogenous peroxidase activity was inhibited by adding DAKO Dual Endogenous Enzyme Block (Agilent, Santa Clara, CA, USA) for 10 min, and non-specific hydrophobic binding activity was prevented by adding 2% bovine serum albumin (BSA, Thermo Fisher Scientific, Waltham, Massachusetts, USA) diluted in PBS. In order to detect IL-40 in the synovial tissue, the slides were immunoprobed with primary rabbit polyclonal C17orf99 antibody (Sinobiological, Eschborn, Germany) diluted 1:500 in 2% BSA in PBS, and were incubated overnight at 4°C. Isotype IgG Universal Negative Control for IS-Series Rabbit Primary Antibodies (Agilent, Santa Clara, CA, USA) was used as a negative control. After rinsing with PBS buffer, HRP conjugated polyclonal goat anti-rabbit secondary antibody (Agilent, Santa Clara, CA, USA) diluted 1:200 in 2% BSA in PBS was added for 1h at room temperature (RT). Liquid DAB + Substrate (Dako Cytomation, Glostrup, Denmark) was used as a chromogen. The slides were counterstained with Mayer's Haematoxylin solution. Evaluation of results was performed using an Olympus BX53 microscope with DP80 Digital Microscope Camera and CellSens Standard V1.18imaging software (Olympus, Philadelphia, PA, USA).

Immunofluorescence

Synovial tissue samples from patients with RA (3 females and 1 male, with a mean (SD) age of 62 (16) years) were obtained and processed as described above. At first, the 5-µm-thick slides were immunoprobed with rabbit polyclonal C17orf99 antibody (Sinobiological, Eschborn, Germany) diluted 1:700 in 2% BSA in PBS overnight at 4°C. Then, goat anti-rabbit IgG H&L Alexa Fluor 488 (Abcam, Cambridge, UK) diluted 1:200 in 2% BSA in PBS was added as a secondary antibody for 1h at RT. Consequently, slides were incubated with primary antibodies against CD68 (1:100), CD3 (1:100), CD20 (1:50), CD1a (1:100) all from Abcam (Cambridge, UK) and against myeloperoxidase (MPO,1:200; Invitrogen, Carlsbad, CA, USA) overnight at 4°C. After incubation, goat anti-mouse IgM mu chain Alexa Fluor 647 (Abcam, Cambridge, UK) diluted 1:200 in 2% BSA in PBS was added for 1h at RT. DAPI (Thermo Fisher Scientific, Waltham, Massachusetts, USA) was used to stain the cell nuclei. Evaluation of results was performed using a BX53 microscope with DP80 Digital Microscope Camera and CellSens Standard 3.1 imaging software (Olympus, Philadelphia, PA, USA).

Cell Cultures and *In Vitro* Experiments

RA synovial fibroblasts were obtained from biopsies from RA patients (n=9) as previously described (21), and were cultured in DMEM medium (Gibco-Thermo Fisher, Waltham, MA, USA) supplemented with 10% fetal bovine serum (FBS) at 37°C in a 5% CO_2 humidified atmosphere. Cells between passages 4 and 8 were seeded on 6-well plates (1.0×10^5 cells/well) and stimulated with IL-40 (C17ORF99 Recombinant Protein, N-terminal 10 x His-tagged and C-terminal Myc-tagged, produced in E.coli, low endotoxin, sterile filtered from Aviva Systems Biology, San Diego, CA, USA) at concentrations of 100, 200 and 250 ng/ml or with lipopolysaccharide (LPS, 100 ng/ml, LPS from E. coli O26:B6, Sigma-Aldrich, St. Louis, MO, USA) for 24 hours, cell culture supernatants were collected after 24 hours and stored at -80°C. The range of IL-40 concentrations used for *in vitro* experiments was selected based on physiological concentrations detected in the serum and in the synovial fluid of RA patients.

Statistical Analysis

The data are presented as median and interquartile range (IQR) if not stated otherwise. Normality of data across analysed groups was tested by Kolmogorov-Smirnov test with 5% level of statistical significance. For analysis of differences between groups, Mann-Whitney U-test for non-paired data was performed. Wilcoxon matched-pairs signed rank test was applied for the *in vitro* data. Bivariate relationships between variables under study were determined by Spearman's correlation coefficient. Multivariate regression analysis was used to predict levels of IL-40 in the serum and synovial fluid by a set of predictors. The predictors for both dependent variables (serum IL-40 and synovial fluid IL-40) were selected based on significant bivariate associations. Highly collinear predictors were excluded from the analysis, and only the best predictor (with the highest correlation with dependent variable) was retained in the regression model. Longitudinal observations of IL40 were examined using two-way (cohorts 2 and 3 by time) repeated-measures analysis of variance (RM-ANOVA) to assess the inter-group differences, followed by one-way RM-ANOVA with least significant difference (LSD) post-hoc tests conducted within each group. P values less than 0.05 were considered statistically significant (*$p<0.05$, **$p<0.01$, ***$p<0.001$,

****p<0.0001). GraphPad Prism 6 (GraphPad Software, La Jolla, CA, USA) and IBM SPSS 25.0® (Chicago, IL, USA) were used to perform the analysis.

RESULTS

Increased Expression of IL-40 in the RA Synovial Tissue

IL-40 was detected in both RA and OA synovial tissue (**Figure 1**). The IL-40 expression was significantly enhanced in RA compared to OA synovial tissue, particularly within the inflammatory infiltrate (**Figure 1**). Moreover, the hyperplastic lining layer of the RA synovial tissue showed significant positivity for IL-40. Moderate expression of IL-40 was detected in the endothelial cells in RA synovium. In contrast, OA synovium had negligible IL-40 expression with only sparse staining positivity within the tissue (**Figure 1**). Further analysis of RA synovium using double-immunofluorescence staining demonstrated co-localization of IL-40 with macrophages (CD68), B cells (CD20), T cells (CD3), and neutrophils (MPO) (**Figure 2**).

Levels of IL-40 Are Up-Regulated in the Synovial Fluid and Serum of RA Patients (Cohort 1)

IL-40 is significantly up-regulated in the synovial fluid of RA in contrast to OA patients [33.2 (6.6-68.9) vs. 0.7 (0.1-2.4) ng/ml; p<0.0001] (**Figure 3A**). Also, serum IL-40 is increased in RA patients compared to OA, HC or SLE [5.4 (12.0-22.2) vs. 1.4 (0.6-3.1), 1.4 (1.0-1.9) or 1.5 (0.7-2.7) ng/ml, respectively; p<0.0001 for all], (**Figure 3B**). Interestingly, IL-40 is markedly enhanced at local sites of inflammation in the RA synovial fluid compared to RA serum [33.2 (6.6-68.9) vs. 5.4 (2.0-22.2) ng/ml; p<0.0001]. The opposite phenomenon is present in OA, where systemic levels of IL-40 are higher compared to the synovial fluid IL-40 [1.4 (1.0-1.9) vs. 0.7 (0.1-2.4) ng/ml; p<0.0001]. Levels of IL-40 in the serum or the synovial fluid were not affected by sex or

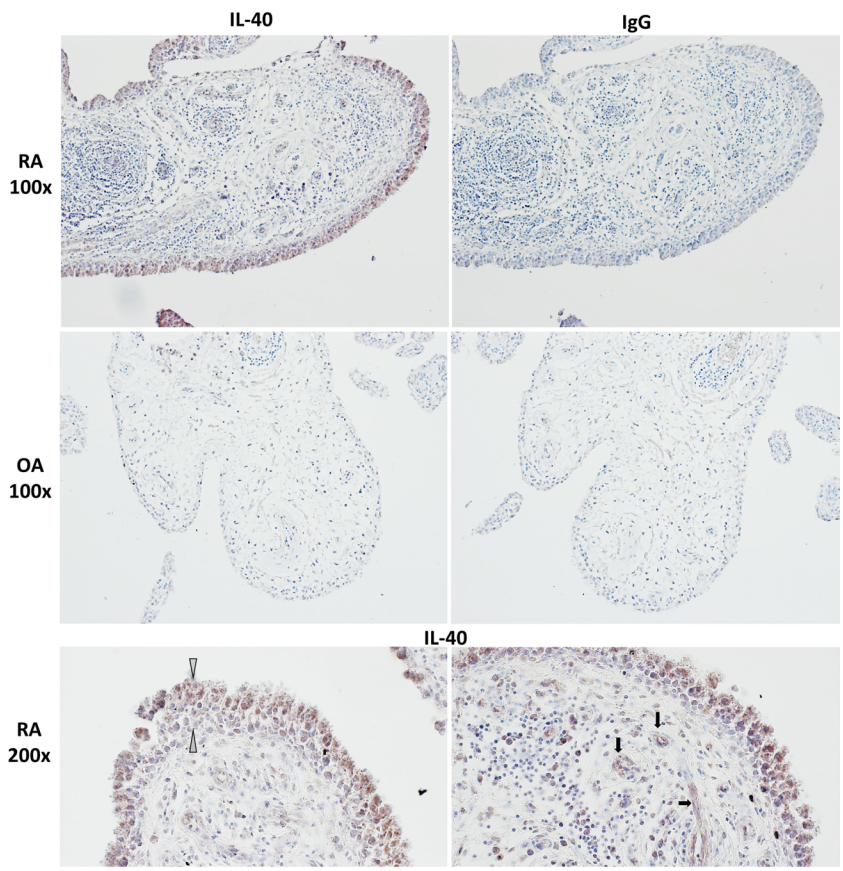

FIGURE 1 | IL-40 in the synovial membrane of patients with rheumatoid arthritis (RA) and osteoarthritis (OA). Intensive IL-40 positivity was observed in RA, especially in the hyperplastic lining layer and within the inflammatory infiltrates of the RA synovium. Moderate expression of IL-40 was detected in the endothelial cells. IL-40 expression was quite sparse with only few IL-40 positive immune cells within the OA synovial tissue. Rabbit IgG was used as an isotype control. The white arrows point to the hyperplastic lining layer, and the black arrows point to capillaries. Representative images of immunohistochemistry staining are shown at × 100 magnification, detailed view at × 200 magnification (RA, n = 5; OA, n = 4).

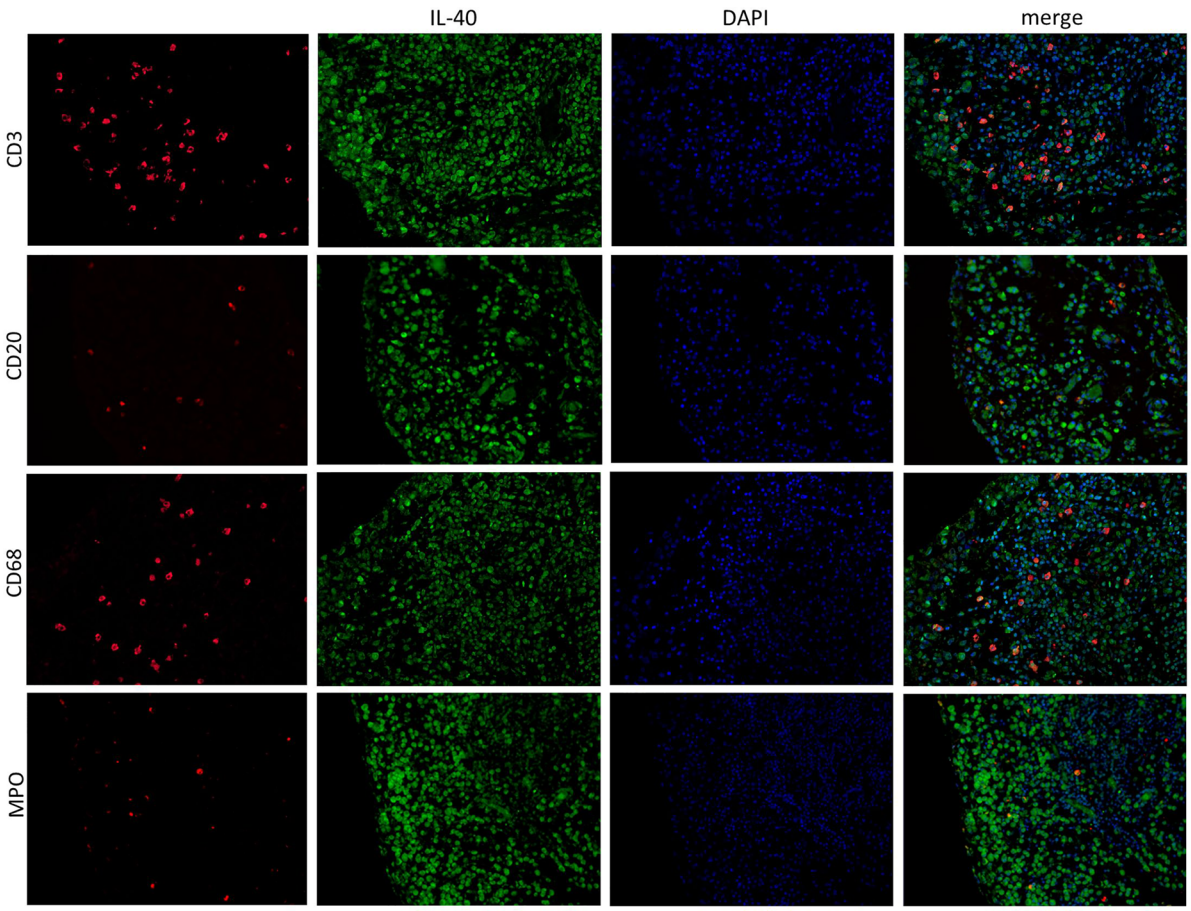

FIGURE 2 | IL-40 is expressed by immune cells in the synovial membrane of patients with rheumatoid arthritis (RA). In addition to the synovial lining, IL-40 positivity (green) was observed in infiltrating cells of RA synovial tissue, demonstrated by specific marker staining (red) for T lymphocytes (CD3), B lymphocytes (CD20), macrophages (CD68), and neutrophil myeloperoxidase (MPO). Nuclei were stained by DAPI (blue). Representative images of immunofluorescence staining are shown at × 200 magnification (RA, n = 4). DAPI, 4',6-diamidino-2-phenylindole.

treatment with conventional synthetic disease-modifying antirheumatic drugs (csDMARDs) or glucocorticoids (GCs) (**Supplementary File 1**). No association of IL-40 levels with age was found. Moreover, the levels of IL-40 are markedly up-regulated in double-positive (RF+/anti-CCP+) compared to double-negative (RF-/anti-CCP-) patients with RA in the synovial fluid [66.6 (41.5-93.1) vs. 9.9 (3.7-24.0) ng/ml; $p<0.0001$], as well as in the serum [10.9 (4.2-96.0) vs. 3.3 (1.6-6.6) ng/ml; $p<0.001$]. Additional data regarding the relation of IL-40 levels to the autoantibody positivity are summarized in **Supplementary File 2**.

IL-40 Is Associated With RA Disease Activity and Levels of Autoantibodies (Cohort 1)

There is a significant association between the levels of IL-40 in serum and synovial fluid in both RA and OA patients ($r=0.705$, $p<0.0001$ and $r=0.791$, $p<0.0001$, respectively). Levels of IL-40 in the synovial fluid of RA patients positively correlated with ESR ($r=0.440$, $p=0.003$), disease activity DAS28-ESR ($r=0.346$, $p=0.025$) and synovial fluid leukocyte count ($r=0.443$, $p=0.002$). A weak correlation was observed between synovial fluid IL-40 and the number of swollen joints ($r=0.284$, $p=0.049$). Serum IL-40 was weakly associated to ESR ($r=0.318$, $p=0.038$) but not to DAS28-ESR ($r=0.194$, $p=0.218$) in RA patients.

Levels of IL-40 significantly correlated with the levels of anti-CCP and RF-IgM autoantibodies in the serum ($r=0.423$, $p<0.01$ and $r=0.631$, $p<0.0001$, respectively) and in the synovial fluid ($r=0.548$, $p<0.001$ and $r=0.684$, $p<0.0001$, respectively). Bivariate associations of serum and synovial fluid IL-40 with major clinical and laboratory parameters are summarized in **Table 2**. All the selected parameters (IgM, anti-CCP, and ESR) remained significantly associated with IL-40 in the synovial fluid, while only IgM and anti-CCP with IL-40 in the serum in a multivariate regression model. IgM had the strongest association with IL-40 in both synovial fluid and serum (standardized $\beta = 0.45$ and 0.38, respectively), even after adjusting for other variables in the model (**Table 3**).

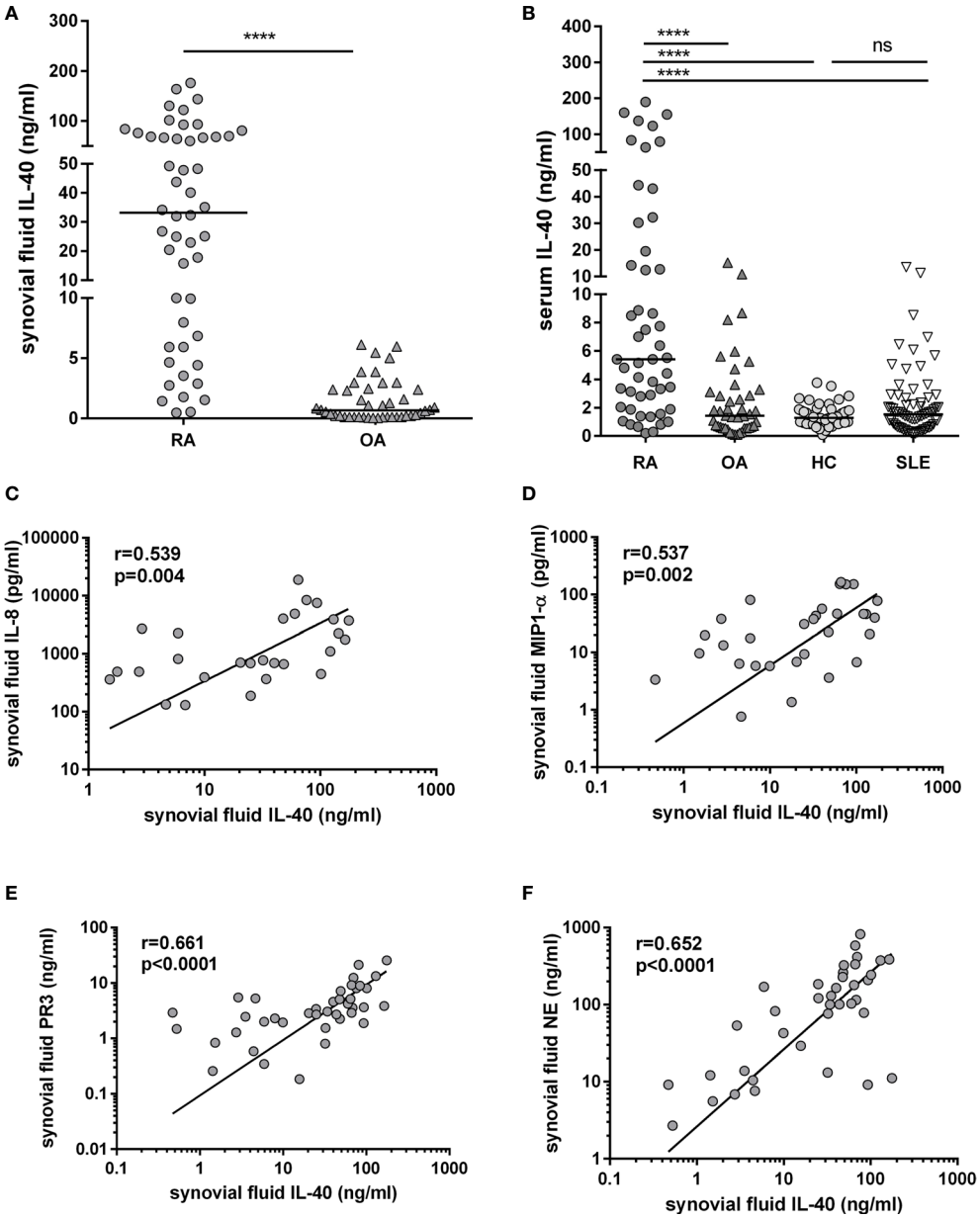

FIGURE 3 | Up-regulation of IL-40 in patients with rheumatoid arthritis (RA) and its association with the levels of chemokines and markers of NETosis. Levels of IL-40 in synovial fluid are significantly higher in RA patients compared to osteoarthritis (OA) **(A)**. Levels of IL-40 in serum are elevated in RA patients compared to OA patients, healthy controls (HC), and patients with systemic lupus erythematosus (SLE) **(B)**. Synovial fluid IL-40 significantly correlated with the levels of chemokines IL-8 **(C)** and MIP1-α **(D)** and with the markers of NETosis such as proteinase 3 (PR3) and neutrophil elastase NE **(E, F)** in the synovial fluid of patients with RA. ****$p < 0.0001$; ns, nonsignificant. The horizontal line represents the median. The association of IL-40 with chemokines was analysed using Spearman correlation.

Synovial Fluid IL-40 Correlates With the Count and Activation of Neutrophils and With Markers of NETosis (Cohort 1)

In patients with RA, synovial fluid IL-40 significantly correlates with the number of synovial fluid neutrophils (r=0.375, p=0.017) and with the synovial fluid levels of chemokines IL-8 (r=0.539, p=0.004) and MIP-1α (r=0.537, p=0.002), (**Figures 3C, D**). Given the association of IL-40 with the neutrophil attractant and activator IL-8, we sought to analyse the relation between IL-40 and markers of NETosis. We found that synovial fluid IL-40 strongly correlates with the levels of proteinase 3 (PR3) (r=0.661, p<0.0001) and neutrophil elastase (NE) (r=0.652, p<0.0001) (**Figures 3E, F**). No relation was found between serum IL-40 and any of the studied cytokines, chemokines or NETosis markers (data now shown).

TABLE 2 | Bivariate correlations of IL-40 levels with clinical and laboratory parameters in patients with RA (cohort 1).

		Serum	Synovial fluid
Laboratory parameters	**CRP**	0.021	0.190
	ESR	0.318*	0.440**
	RF-IgM	0.631****	0.684****
	anti-CCP	0.423**	0.548***
	SF- leukocyte count	0.089	0.443**
Clinical parameters	**DAS28 (ESR)**	0.194	0.346*
	SJC	0.106	0.284*
	TJC	0.009	-0.016

*Data were analysed using Spearman correlation and are presented as correlation coefficient r. *p < 0.05, **p < 0.01, ***p < 0.001, ****p < 0.0001. anti-CCP, anti-cyclic citrullinated peptide antibody; CRP, C-reactive protein; DAS, disease activity score; ESR, erythrocyte sedimentation rate; IgM, immunoglobulin M; RF, rheumatoid factor; SF, synovial fluid; SJC, swollen joint count; TJC, tender joint count.*

B Cell Depletion Therapy, but Not TNF Inhibition, Significantly Reduced the Serum Levels of IL-40 in RA Patients (Cohorts 2 and 3)

To assess the role of B cell homeostasis on IL-40 production, we measured the serum levels of IL-40 prior to and after rituximab administration in patients with RA (cohort 2). Levels of circulating IL-40 significantly decreased in the majority of patients after 16 weeks [3.5 (1.2-9.6) vs. 1.4 (0.1-3.8) ng/ml, p = 0.003] and 24 weeks [3.5 (1.2-9.6) vs. 1.4 (0.5-4.4) ng/ml, p = 0.007] following rituximab treatment (**Figure 4A**). In parallel with that, significant depletion of peripheral B cells was achieved after 16 weeks [0.1 (0.1-0.3) vs. 0.001 (0.0-0.006) G/l, p < 0.0001] and 24 weeks of the therapy [0.1 (0.1-0.3) vs. 0.004 (0.001-0.03) G/l, p < 0.0001]. Rituximab treatment also resulted in a significant decrease in disease activity as represented by DAS28 (ESR) in week 16 [6.5 (5.7-7.5) vs. 5.0 (4.4-6.0), p < 0.0001] and week 24 [6.5 (5.7-7.5) vs. 5.0 (3.6-5.8), p < 0.0001], **Figure 4B**. No association was observed between the levels of IL-40 and B cell count at baseline or following the treatment (data not shown).

Furthermore, no significant changes in the serum levels of IL-40 were observed in cohort 3 treated with TNFi adalimumab after 12 weeks [2.2 (0.8-8.7) vs. 1.8 (0.8-7.7) ng/ml, p = ns] and 52 weeks [2.2 (0.8-8.7) vs. 1.7 (1.2-4.2) ng/ml, p = ns] of the therapy (**Figure 4C**). Nevertheless, disease activity [DAS28 (ESR)] was significantly reduced in week 12 [6.4 (5.7-7.0) vs. 4.0 (2.9-4.4), p < 0.0001] and week 52 [6.4 (5.7-7.0) vs. 3.3 (2.3-4.4), p < 0.0001] following adalimumab therapy (**Figure 4D**). The inter-group analysis confirmed a significant difference in the change of serum IL-40 levels between cohort 2 and cohort 3 over the studied period of time (p = 0.004).

IL-40 Stimulates the Expression of Pro-Inflammatory Cytokines/Chemokines and MMP-13 in RA Synovial Fibroblasts

RA synovial fibroblasts exposed to IL-40 up-regulated the secretion of IL-8 into the supernatants in a dose-dependent manner [250 ng/ml: 34.1 (11.8-62.7) pg/ml, p = 0.004; 200 ng/ml: 16.61 (9.9-51.8) pg/ml, p = 0.049; 100 ng/ml: 18.4 (7.1-41.7) pg/ml, p = ns, compared to the unstimulated control: 15.0 (2.6-24.9) pg/ml] (**Figure 5A**). Similarly, MCP-1 secretion by synovial fibroblasts significantly increased upon stimulation by IL-40 [250 ng/ml: 548.0 (368.6-686.1) pg/ml, p=0.042; 200 ng/ml: 486.5 (375.8-707.2) pg/ml, p = 0.016; 100 ng/ml: 425.8 (315.2-581.0) pg/ml, p = ns, compared to the unstimulated control: 402.7 (285.2-614.5) pg/ml] (**Figure 5B**). No significant changes in the levels of IL-6, RANTES or IFNγ were observed upon treatment with IL-40 (data not shown). The levels of the other cytokines/chemokines or growth factors included in the 27-plex assay were under the detection limit of the assay (the 27 analysed cytokines are listed in Methods).

In addition, we observed a significant effect of IL-40 on the secretion of metalloproteinase MMP-13 [250 ng/ml: 224.0 (40.5-637.5) pg/ml, p=0.008; 200 ng/ml: 223.0 (73.8-819.0) pg/ml, p = 0.008; 100 ng/ml: 79.0 (19.5-445.5) pg/ml, p = ns, compared to the unstimulated control: 89.0 (14.5-433.5) pg/ml] (**Figure 5C**). Stimulation of RA synovial fibroblasts by IL-40 did not affect the release of MMP-1 and MMP-3 (data not shown).

DISCUSSION

We are the first to demonstrate the implication of the new cytokine IL-40 in the pathogenesis of RA. We show local and

TABLE 3 | Multivariate regression analysis predicting IL-40 levels in the serum and synovial fluid of RA patients based on laboratory parameters (cohort 1).

Variables	Serum		Synovial fluid	
	β (95% CI)	P-value	β (95% CI)	P-value
IgM	0.376 (0.026-0.184)	**0.011**	0.450 (0.057-0.183)	**0.0001**
anti-CCP	0.332 (0.009-0.076)	**0.014**	0.302 (0.011-0.064)	**0.007**
ESR	-0.147 (-0.895-0.265)	0.280	0.234 (0.021-0.941)	**0.041**

Dependent variable: IL-40; β-standardized regression coefficient; CI, confidence interval.
anti-CCP, anti-cyclic citrullinated peptide antibody; ESR, erythrocyte sedimentation rate; IgM, immunoglobulin M. Statistically significant differences (p<0.05) are marked in bold.

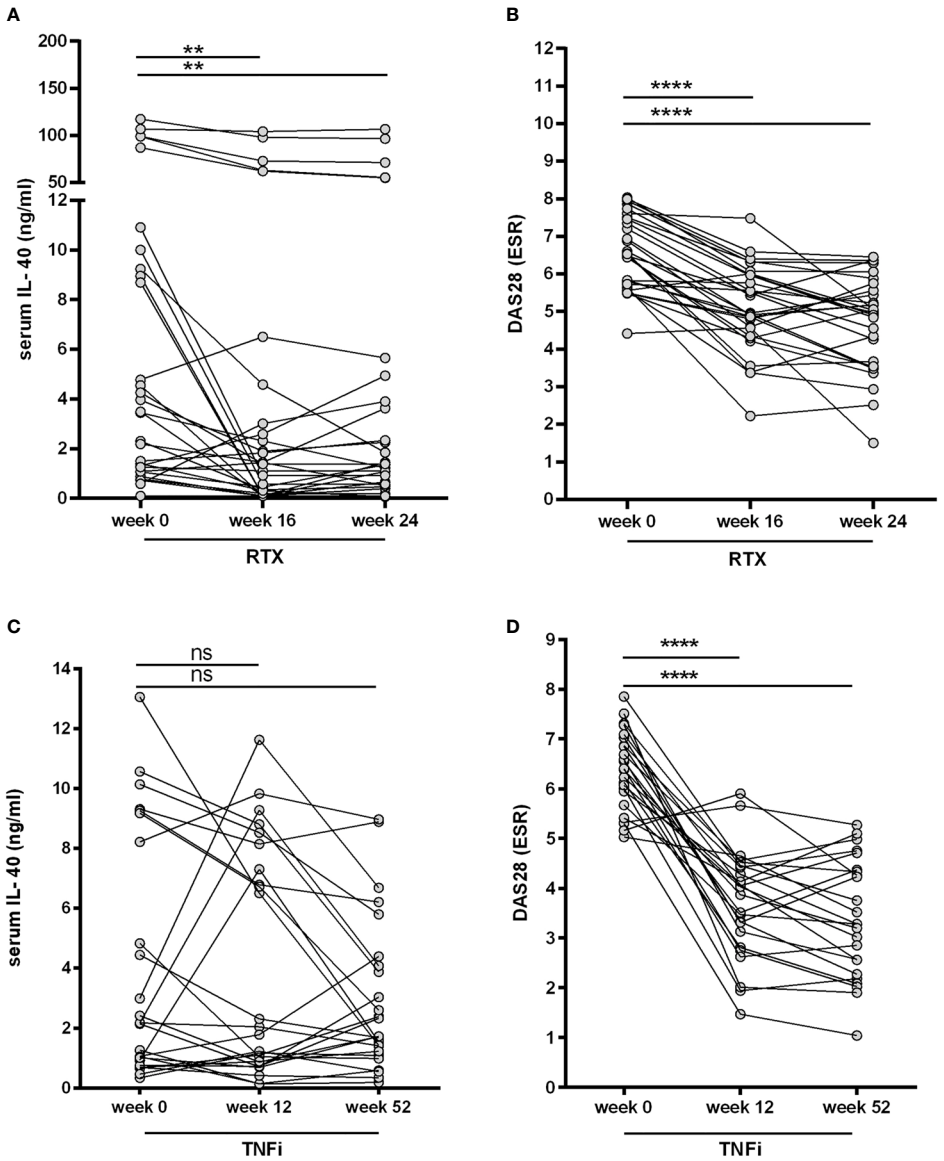

FIGURE 4 | Effect of biological therapies on the serum IL-40 in patients with rheumatoid arthritis (RA). A decrease in IL-40 serum levels **(A)** was observed after the first series of rituximab (RTX) at weeks 16 and 24 and was associated with a drop in the disease activity (DAS28) **(B)**. No significant changes of IL-40 serum levels following therapy with TNF inhibitors (TNFi) after 12 and 52 weeks were detected **(C)**, even though disease activity (DAS28) markedly declined **(D)**. **p < 0.01; ****p < 0.0001; ns, nonsignificant.

systemic up-regulation of IL-40 in patients with RA and its association with disease activity, levels of autoantibodies, chemokines, and markers of NETosis. We also provide evidence that extracellular IL-40 enhances the secretion of chemokines and matrix-degrading enzyme MMP-13 in synovial fibroblasts.

IL-40 is a recently discovered B cell-associated cytokine related to immune response and B cell homeostasis (10, 17). Here we demonstrated that IL-40 is accumulated in the synovial tissue of RA patients. We observed intensive IL-40 staining within the hyperplastic synovial lining layer, indicating its expression by activated synovial fibroblasts. Also, immune cells infiltrating the RA synovial tissue tested positive for IL-40. According to Catalan-Dibene et al., IL-40 expression is associated with B cells (10); however, our data on synovial tissue indicate that besides B cells, other immune cells such as macrophages, T cells and neutrophils are involved in IL-40 expression in RA. This possibility is supported by our analysis of serum IL-40 in RA patients treated with B cell depleting agent rituximab. We showed that high levels of IL-40 decreased following rituximab therapy in 70% of patients, whereas the remaining 30% showed unchanged or even increased levels of serum IL-40. Indeed, no significant association of IL-40 levels with the number of B cell at baseline or following the therapy was

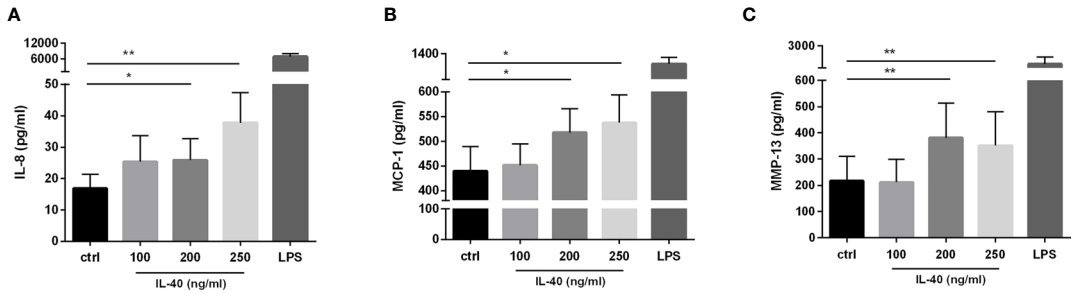

FIGURE 5 | IL-40 dose-dependently induced the secretion of pro-inflammatory cytokines/chemokines and MMP-13 in RA synovial fibroblasts (n=9). RA synovial fibroblasts significantly up-regulate the secretion of interleukin (IL)-8 **(A)**, monocyte chemoattractant protein (MCP)-1 **(B)**, and matrix-metalloproteinase (MMP)-13 **(C)** when treated by IL-40 at concentrations of 200-250 ng/ml. Fibroblasts were stimulated for 24h prior to protein analysis. Data are represented as mean ± SEM. *$p < 0.05$, **$p < 0.01$ compared to unstimulated fibroblasts (ctrl).

found. Since the B cell depletion was accompanied by a decline in disease activity, dysregulation of other immune cells might have occurred and contributed to the changes in the IL-40 levels following the treatment. Altogether, these data suggest that IL-40 is produced by multiple cell types in RA. Of note, serum levels of IL-40 do not seem to be significantly affected by the treatment with TNF inhibitor adalimumab. Targeting specific upstream events, such a B cells activation, rather than TNF itself, may be responsible for reducing IL-40, which indicates that IL-40 may be related to specific mechanisms in the pathogenesis of RA linked to B cells and their regulatory effects.

Furthermore, IL-40 was elevated in the paired samples of serum and synovial fluid of RA patients compared to OA. In addition to that, we assessed IL-40 in the serum of patients with SLE, a systemic autoimmune rheumatic disease characterised by abnormalities and hyperactivity of B cells (22). Surprisingly, the serum levels of IL-40 in SLE were comparable to the ones in OA and healthy controls, suggesting no specific association of IL-40 with neither B cells nor the systemic nature of the disease. These findings imply that the enhanced systemic levels of IL-40 in RA may be related to the local inflammation and originate from the inflamed joints rather than from systemic inflammation. In support of this claim, levels of IL-40 in the RA synovial fluid are about six times higher than those in the serum and are strongly associated with each other. In addition, IL-40 correlates with several indicators of local inflammation such as synovial fluid leukocyte count, but also with the disease activity score, or the number of swollen joints, but not with CRP. In light of these findings, it should also be stressed that only a negligible amount of IL-40 was detected in the OA synovial fluid, and the levels of IL-40 in the OA serum were comparable to the ones found in healthy individuals. This observation further reinforces the hypothesis that IL-40 diffuses from the RA joints to the blood circulation and reflects the intensity of the local inflammation.

We also demonstrated that IL-40 is significantly associated with the levels of RF-IgM and anti-CCP autoantibodies and thereby with the activation of B cells, which is in agreement with previously reported data (10). Of particular interest is the correlation of IL-40 with anti-CCP, a finding which outlines a possible implication of IL-40 in the process of citrullination and autoimmune reaction in RA. It is well established that the anti-CCP production in RA is fuelled by citrullinated antigens released during the formation of neutrophil extracellular traps - NETosis (23) and that anti-CCP antibodies play an important role in the early phases of RA development (24). In this regard, we showed that synovial fluid IL-40 correlates with the number of neutrophils in the synovial fluid and with the synovial fluid levels of IL-8, a neutrophil chemoattractant and potent inducer of NETosis (25). Consistently, IL-40 co-localized with MPO, one of common neutrophil markers, in the RA synovial tissue. In addition, the strong correlation of synovial fluid IL-40 with the levels of proteinase 3 and neutrophil elastase further highlight the link of IL-40 to neutrophils and NETosis. Moreover, our unpublished preliminary data indicate that IL-40 is released by RA neutrophils undergoing NETosis. A question which therefore arises is whether the high concentration of IL-40 in the synovial fluid may be a result of the crosstalk between the activated B cells and neutrophils in RA joint. In addition to all that, *in vitro* data show that RA synovial fibroblasts enhanced the IL-8 secretion upon IL-40 stimulation. Given the abundance of IL-40 in the RA synovial fluid, we can speculate that IL-40 stimulates fibroblasts in the synovial lining layer to produce IL-8, which in turn, can activate synovial fluid neutrophils and thereby fuel the autoimmune reaction in RA joints. Moreover, IL-40 up-regulates the secretion of pro-inflammatory chemokine MCP-1 by synovial fibroblasts. MCP-1 has recently been demonstrated to act on synovial fibroblasts to promote their aggressive phenotype (26). Thus, it is tempting to assume that IL-40 may be implicated in the development of synovial hyperplasia. Noteworthy is the association of synovial fluid IL-40 with the levels of MIP-1α, which not only functions as multifunctional chemokine and neutrophil attractant (27) but, according to Jordan et al., also represents a potent regulator of bone resorption in arthritis (28). In the context of bone remodelling, the correlation of IL-40 with anti-CCP and IL-8 should be emphasized, as IL-8 is involved in the anti-CCP-driven osteoclast activation and bone loss (29, 30). Last but not least, we revealed that IL-40 acts on the RA synovial fibroblasts to up-regulate the secretion of MMP-13, a key molecule in the cartilage degradation network (31). These data imply that IL-40 may play

a particular role in the RA joint damage, a subject that requires further investigation.

Some limitations of the study should be taken into account. The relationship between the IL-40 expression in the synovial tissue and fluid could not be assessed since the tissue samples were obtained from a group of patients different from those who underwent synovial fluid aspiration. Furthermore, the correlation between IL-40 and increased NETosis observed in the synovial fluid could not be further explored in patients following biological therapies, as there are no synovial fluid samples available after the treatment.

Notwithstanding these limitations, this study shows for the first time an implication of IL-40 in the pathogenesis of RA. In fact, these novel findings may pave the way for placing IL-40 into the portfolio of molecules involved in the immune reaction and tissue remodelling control in RA. Also, this work may inspire further studies on IL-40 in other autoimmune diseases.

CONCLUSION

Taken together, our results show that IL-40 is elevated in RA and decreases following the B cell depleting therapy. Moreover, IL-40 correlates with disease activity, autoantibodies, chemokines, and markers of NETosis, indicating its potential implication in RA development. In addition, IL-40 up-regulates chemokines and MMP-13 in synovial fibroblasts, which implies its potential role in inflammation and tissue destruction in RA.

DATA AVAILABILITY STATEMENT

The raw data supporting the conclusions of this article will be made available by the authors, without undue reservation.

ETHICS STATEMENT

The studies involving human participants were reviewed and approved by Institutional Ethics Committee of Institute of Rheumatology, Prague, Czech Republic. The patients/participants provided their written informed consent to participate in this study.

AUTHOR CONTRIBUTIONS

LAC and LŠ were responsible for the study concept and design. LŠ, MT, DT, MO, and JZ recruited the patients and collected the clinical data. HH, VB, and AN carried out the ELISAs and analysed the data. DV performed the biopsies of synovial tissues. VB, AN, and LAC performed the immunohistochemistry and immunofluorescence experiments. AN and LAC performed the *in vitro* experiments. MK, MT, and LAC carried out the statistical analysis. LAC, AN, and LŠ were responsible for data interpretation and manuscript preparation. JV, LŠ, MT and KP revised the manuscript and gave their final approval of the version to be published. All authors contributed to the article and approved the submitted version.

FUNDING

This study was funded by Research Project AZV-NU21-05-00276 of the Agency for Healthcare Research of the Czech Republic and by Research Project No. 023728 of the Ministry of Health of the Czech Republic, Charles University project SVV 260 523, and BBMRI-CZ LM2018125.

ACKNOWLEDGMENTS

We would like to thank Xiao Švec for language editing of our manuscript.

SUPPLEMENTARY MATERIAL

The Supplementary Material for this article can be found online at: https://www.frontiersin.org/articles/10.3389/fimmu.2021.745523/full#supplementary-material

REFERENCES

1. Smolen JS, Aletaha D, McInnes IB. Rheumatoid Arthritis. *Lancet* (2016) 388:2023–38. doi: 10.1016/S0140-6736(16)30173-8
2. McInnes IB, Schett G. Cytokines in the Pathogenesis of Rheumatoid Arthritis. *Nat Rev Immunol* (2007) 7:429–42. doi: 10.1038/nri2094
3. Bugatti S, Vitolo B, Caporali R, Montecucco C, Manzo A. B Cells in Rheumatoid Arthritis: From Pathogenic Players to Disease Biomarkers. *BioMed Res Int* (2014) 2014:681678. doi: 10.1155/2014/681678
4. Hamel KM, Cao Y, Olalekan SA, Finnegan A. B Cell-Specific Expression of Inducible Costimulator Ligand Is Necessary for the Induction of Arthritis in Mice. *Arthritis Rheumatol* (2014) 66:60–7. doi: 10.1002/art.38207
5. Olalekan SA, Cao Y, Hamel KM, Finnegan A. B Cells Expressing IFN-γ Suppress Treg-Cell Differentiation and Promote Autoimmune Experimental Arthritis. *Eur J Immunol* (2015) 45:988–98. doi: 10.1002/eji.201445036
6. Lopez-Olivo MA, Amezaga Urruela M, McGahan L, Pollono EN, Suarez-Almazor ME. Rituximab for Rheumatoid Arthritis. *Cochrane Database Syst Rev* (2015) 20:1:CD007356. doi: 10.1002/14651858.CD007356.pub2
7. Cambridge G, Leandro MJ, Edwards JCW, Ehrenstein MR, Salden M, Bodman-Smith M, et al. Serologic Changes Following B Lymphocyte Depletion Therapy for Rheumatoid Arthritis. *Arthritis Rheum* (2003) 48:2146–54. doi: 10.1002/art.11181
8. Cambridge G, Perry HC, Nogueira L, Serre G, Parsons HM, de la Torre I, et al. The Effect of B Cell Depletion Therapy on Serological Evidence of B Cell and Plasmablast Activation in Patients With Rheumatoid Arthritis Over Multiple Cycles of Rituximab Treatment. *J Autoimmun* (2014) 50:67–76. doi: 10.1016/j.jaut.2013.12.002
9. Fillatreau S. B Cells and Their Cytokine Activities Implications in Human Diseases. *Clin Immunol* (2018) 186:26–31. doi: 10.1016/j.clim.2017.07.020
10. Catalan-Dibene J, Vazquez MI, Luu VP, Nuccio S-P, Karimzadeh A, Kastenschmidt JM, et al. Identification of IL-40, a Novel B Cell–Associated Cytokine. *J Immunol* (2017) 199:3326–35. doi: 10.4049/jimmunol.1700534

11. Catalan-Dibene J, McIntyre LL, Zlotnik A. Interleukin 30 to Interleukin 40. *J Interferon Cytokine Res* (2018) 38:423–39. doi: 10.1089/jir.2018.0089
12. Lee J, Hever A, Willhite D, Zlotnik A, Hevezi P. Effects of RNA Degradation on Gene Expression Analysis of Human Postmortem Tissues. *FASEB J* (2005) 19:1356–8. doi: 10.1096/fj.04-3552fje
13. Roth RB, Hevezi P, Lee J, Willhite D, Lechner SM, Foster AC, et al. Gene Expression Analyses Reveal Molecular Relationships Among 20 Regions of the Human CNS. *Neurogenetics* (2006) 7:67–80. doi: 10.1007/s10048-006-0032-6
14. Liu Z, Meng J, Li X, Zhu F, Liu T, Wu G, et al. Identification of Hub Genes and Key Pathways Associated With Two Subtypes of Diffuse Large B Cell Lymphoma Based on Gene Expression Profiling. *via Integrated Bioinf BioMed Res Int* (2018) 2018:3574534. doi: 10.1155/2018/3574534
15. Zhou H, Xu-Monette ZY, Xiao L, Strati P, Hagemeister FB, He Y, et al. Prognostic Factors, Therapeutic Approaches, and Distinct Immunobiologic Features in Patients With Primary Mediastinal Large B Cell Lymphoma on Long-Term Follow-Up. *Blood Cancer J* (2020) 10:49. doi: 10.1038/s41408-020-0312-7
16. Gao X, Chan PKS, Lui GCY, Hui DSC, Chu IM, Sun X, et al. Interleukin-38 Ameliorates Poly(I:C) Induced Lung Inflammation: Therapeutic Implications in Respiratory Viral Infections. *Cell Death Dis* (2021) 12:53. doi: 10.1038/s41419-020-03283-2
17. Zingaretti C, Arigò M, Cardaci A, Moro M, Crosti M, Sinisi A, et al. Identification of New Autoantigens by Protein Array Indicates a Role for IL4 Neutralization in Autoimmune Hepatitis. *Mol Cell Proteomics* (2012) 11:1885–97. doi: 10.1074/mcp.M112.018713
18. Aletaha D, Neogi T, Silman AJ, Funovits J, Felson DT, Bingham CO, et al. 2010 Rheumatoid Arthritis Classification Criteria: An American College of Rheumatology/European League Against Rheumatism Collaborative Initiative. *Ann Rheum Dis* (2010) 69:1580–8. doi: 10.1136/ard.2010.138461
19. Petri M, Orbai A-M, Alarcón GS, Gordon C, Merrill JT, Fortin PR, et al. Derivation and Validation of Systemic Lupus International Collaborating Clinics Classification Criteria for Systemic Lupus Erythematosus. *Arthritis Rheum* (2012) 64:2677–86. doi: 10.1002/art.34473
20. Šenolt L, Kryštůfková O, Hulejová H, Kuklová M, Filková M, Cerezo LA, et al. The Level of Serum Visfatin (PBEF) Is Associated With Total Number of B Cells in Patients With Rheumatoid Arthritis and Decreases Following B Cell Depletion Therapy. *Cytokine* (2011) 55:116–21. doi: 10.1016/j.cyto.2011.04.004
21. Senolt L, Housa D, Vernerova Z, Jirasek T, Svobodova R, Veigl D, et al. Resistin in Rheumatoid Arthritis Synovial Tissue, Synovial Fluid and Serum. *Ann Rheum Dis* (2007) 66:458–63. doi: 10.1136/ard.2006.054734
22. Feng Y, Yang M, Wu H, Lu Q. The Pathological Role of B Cells in Systemic Lupus Erythematosus: From Basic Research to Clinical. *Autoimmunity* (2020) 53:56–64. doi: 10.1080/08916934.2019
23. Khandpur R, Carmona-Rivera C, Vivekanandan-Giri A, Gizinski A, Yalavarthi S, Knight JS, et al. NETs Are a Source of Citrullinated Autoantigens and Stimulate Inflammatory Responses in Rheumatoid Arthritis. *Sci Transl Med* (2013) 5:178ra40. doi: 10.1126/scitranslmed.3005580
24. Rantapää-Dahlqvist S, De Jong BAW, Berglin E, Hallmans G, Wadell G, Stenlund H, et al. Antibodies Against Cyclic Citrullinated Peptide and IgA Rheumatoid Factor Predict the Development of Rheumatoid Arthritis. *Arthritis Rheum* (2003) 48:2741–9. doi: 10.1002/art.11223
25. An Z, Li J, Yu J, Wang X, Gao H, Zhang W, et al. Neutrophil Extracellular Traps Induced by IL-8 Aggravate Atherosclerosis *via* Activation NF-κb Signaling in Macrophages. *Cell Cycle* (2019) 18:2928–38. doi: 10.1080/15384101.2019
26. Tong X, Zeng H, Gu P, Wang K, Zhang H, Lin X. Monocyte Chemoattractant Protein−1 Promotes the Proliferation, Migration and Differentiation Potential of Fibroblast−Like Synoviocytes *via* the PI3K/P38 Cellular Signaling Pathway. *Mol Med Rep* (2020) 21:1623–32. doi: 10.3892/mmr.2020.10969
27. Lee SC, Brummet ME, Shahabuddin S, Woodworth TG, Georas SN, Leiferman KM, et al. Cutaneous Injection of Human Subjects With Macrophage Inflammatory Protein-1 Alpha Induces Significant Recruitment of Neutrophils and Monocytes. *J Immunol* (2000) 164:3392–401. doi: 10.4049/jimmunol.164.6.3392
28. Jordan LA, Erlandsson MC, Fenner BF, Davies R, Harvey AK, Choy EH, et al. Inhibition of CCL3 Abrogated Precursor Cell Fusion and Bone Erosions in Human Osteoclast Cultures and Murine Collagen-Induced Arthritis. *Rheumatol (Oxford)* (2018) 57:2042–52. doi: 10.1093/rheumatology/key196
29. Krishnamurthy A, Joshua V, Haj Hensvold A, Jin T, Sun M, Vivar N, et al. Identification of a Novel Chemokine-Dependent Molecular Mechanism Underlying Rheumatoid Arthritis-Associated Autoantibody-Mediated Bone Loss. *Ann Rheum Dis* (2016) 75:721–9. doi: 10.1136/annrheumdis-2015-208093
30. Wigerblad G, Bas DB, Fernades-Cerqueira C, Krishnamurthy A, Nandakumar KS, Rogoz K, et al. Autoantibodies to Citrullinated Proteins Induce Joint Pain Independent of Inflammation *via* a Chemokine-Dependent Mechanism. *Ann Rheum Dis* (2016) 75:730–8. doi: 10.1136/annrheumdis-2015-208094
31. Li H, Wang D, Yuan Y, Min J. New Insights on the MMP-13 Regulatory Network in the Pathogenesis of Early Osteoarthritis. *Arthritis Res Ther* (2017) 19:248. doi: 10.1186/s13075-017-1454-2

Conflict of Interest: The authors declare that the research was conducted in the absence of any commercial or financial relationships that could be construed as a potential conflict of interest.

Publisher's Note: All claims expressed in this article are solely those of the authors and do not necessarily represent those of their affiliated organizations, or those of the publisher, the editors and the reviewers. Any product that may be evaluated in this article, or claim that may be made by its manufacturer, is not guaranteed or endorsed by the publisher.

frontiers in Immunology

ORIGINAL RESEARCH
published: 02 November 2021
doi: 10.3389/fimmu.2021.746503

Ets-2 Propagates IL-6 Trans-Signaling Mediated Osteoclast-Like Changes in Human Rheumatoid Arthritis Synovial Fibroblast

Anil K. Singh[1], Mahamudul Haque[1], Bhanupriya Madarampalli[1], Yuanyuan Shi[2], Benjamin J. Wildman[3], Abdul Basit[1], Sadik A. Khuder[4], Bhagwat Prasad[1], Quamarul Hassan[3], Madhu M. Ouseph[5] and Salahuddin Ahmed[1,6]**

[1] Department of Pharmaceutical Sciences, Washington State University College of Pharmacy, Spokane, WA, United States, [2] Department of Pharmaceutics, University of Washington School of Medicine, Seattle, WA, United States, [3] Department of Oral and Maxillofacial Surgery, School of Dentistry, University of Alabama at Birmingham, Birmingham, AL, United States, [4] Department of Medicine and Public Health, University of Toledo, Toledo, OH, United States, [5] Department of Pathology and Laboratory Medicine, Weill Cornell Medical College, New York, NY, United States, [6] Division of Rheumatology, University of Washington School of Medicine, Seattle, WA, United States

Rheumatoid arthritis synovial fibroblasts (RASFs) contribute to synovial inflammation and bone destruction by producing a pleiotropic cytokine interleukin-6 (IL-6). However, the molecular mechanisms through which IL-6 propels RASFs to contribute to bone loss are not fully understood. In the present study, we investigated the effect of IL-6 and IL-6 receptor (IL-6/IL-6R)-induced trans-signaling in human RASFs. IL-6 trans-signaling caused a significant increase in tartrate-resistant acid phosphatase (TRAP)-positive staining in RASFs and enhanced pit formation by ~3-fold in the osteogenic surface *in vitro*. IL-6/IL-6R caused dose-dependent increase in expression and nuclear translocation of transcription factor Ets2, which correlated with the expression of osteoclast-specific signature proteins RANKL, cathepsin B (CTSB), and cathepsin K (CTSK) in RASFs. Chromatin immunoprecipitation (ChIP) analysis of *CTSB* and *CTSK* promoters showed direct Ets2 binding and transcriptional activation upon IL-6/IL-6R stimulation. Knockdown of Ets2 significantly inhibited IL-6/IL-6R-induced RANKL, CTSB, and CTSK expression and TRAP staining in RASFs and suppressed markers of RASF invasive phenotype such as Thy1 and podoplanin (PDPN). Mass spectrometry analysis of the secretome identified 113 proteins produced by RASFs uniquely in response to IL-6/IL-6R that bioinformatically predicted its impact on metabolic reprogramming towards an osteoclast-like phenotype. These findings identified the role of Ets2 in IL-6 trans-signaling induced molecular reprogramming of RASFs to osteoclast-like cells and may contribute to RASF heterogeneity.

Keywords: osteoclast, interleukin-6, synovial fibroblasts, rheumatoid arthritis, reprogramming

OPEN ACCESS

Edited by:
Lisa Deloch, Universitätsklinikum Erlangen, Germany

Reviewed by:
Denise Eckert, GSI Helmholtz Center for Heavy Ion Research, Germany
Darja Andreev, University of Erlangen-Nuremberg, Germany

***Correspondence:**
Salahuddin Ahmed
salah.ahmed@wsu.edu
Anil K. Singh
anil.singh@wsu.edu

Specialty section:
This article was submitted to Autoimmune and Autoinflammatory Disorders, a section of the journal Frontiers in Immunology

Received: *23 July 2021*
Accepted: *06 October 2021*
Published: *02 November 2021*

Citation:
Singh AK, Haque M, Madarampalli B, Shi Y, Wildman BJ, Basit A, Khuder SA, Prasad B, Hassan Q, Ouseph MM and Ahmed S (2021) Ets-2 Propagates IL-6 Trans-Signaling Mediated Osteoclast-Like Changes in Human Rheumatoid Arthritis Synovial Fibroblast. Front. Immunol. 12:746503. doi: 10.3389/fimmu.2021.746503

INTRODUCTION

Rheumatoid arthritis (RA) is a chronic autoimmune disease characterized by synovial inflammation, hyperplasia, and pannus formation, leading to progressive joint destruction. RA synovial fibroblasts (RASFs) contribute to bone and cartilage degradation by producing numerous inflammatory cytokines and matrix metalloproteinases (1, 2). High osteoclast-like activity in the joints is a major contributing factor to bone deformities and progressive bone loss in RA patients (3, 4). Previous studies suggest that SFs could be converted to osteoblast-like cells by induced cellular reprogramming (5). Using a heterogenous cell population commonly present in RA synovial tissue, Takayangi et al. (6, 7) reported that RASFs could be differentiated into osteoclast-like cells by chronic stimulation with a low dose of macrophage colony stimulating factor (M-CSF) and receptor activator nuclear factor-κB ligand (RANKL), suggesting the role of SFs in modulating bone health by tilting balance towards osteolytic function. Interleukin-6 (IL-6) is a proinflammatory cytokine produced by RASFs that contributes to osteoclastogenesis (8) by further activating RANKL expression (9), and, as we show herein, predisposes RASFs to osteoclast-like signaling and/or differentiation. However, the mechanism by which IL-6 independently activates the signaling pathways and/or crosstalks with M-CSF and RANKL in RASFs to stimulate and maintain the osteoclast-like reprogramming in the synovial microenvironment remains unclear.

Osteoclasts are traditionally formed by the fusion of mononuclear cells (monocytes) that stay in a multinuclear state. It is mainly a $CD14^+$ mononuclear subtype that can differentiate into osteoclasts (10, 11). The formation of osteoclasts depends on RANKL signaling *via* the RANK receptor, whereas osteoprotegerin (OPG), also known as TNFRSF11B, is a decoy ligand for RANK produced by various cells and an endogenous inhibitor for RANKL binding to the RANK receptor (12, 13). When RANKL signaling predominates OPG signaling, it induces differentiation of osteoclast precursor cells to mature osteoclasts (13). Exogenous M-CSF makes cells resistant to apoptosis and, thereby, promotes osteoclast proliferation (14–16). Since SFs express M-CSF, RANK, and OPG, these cells possess the predeterminants to undergo metabolic reprogramming to osteoclast-like cells and may independently contribute or accelerate the bone resorption in the diseased joints.

Current understanding of IL-6 biology suggests that it contributes to bone destruction by accelerating osteoclastogenesis in RA (17), with IL-6 trans-signaling contributing to bone formation and osteoclastogenesis (18). However, there are several gaps in this understanding, such as the potential role of IL-6 in forcing a phenotypic switch in RASFs to osteoclast-like cells, the key signaling mediators involved in this process, and if the effect of IL-6 trans-signaling on metabolic reprogramming is independent or in crosstalk with M-CSF/RANKL signaling. The present study was undertaken to identify the novel mediators influenced by IL-6 signaling to accelerate the phenotypic conversion of RASFs to osteoclast-like cells and to elucidate the effects of Ets2 transcription factor in bone destruction in RA.

MATERIALS AND METHODS

Detailed information about antibodies and reagents, Western immunoblotting, ELISA, and *in vitro* scratch test are provided in the *Materials and Methods* section of the **Supplementary Information (SI)**.

Isolation and Culture of Human Nondiseased SFs and RASFs

The deidentified nondiseased (NL) and RA synovial tissues (RASTs) were procured under a protocol approved by the Washington State University IRB (IRB#14696) from the Cooperative Human Tissue Network (Columbus, OH) and National Disease Research Interchange (Philadelphia, PA). STs from RA patients were obtained from joint surgery or synovectomy according to an Institutional Review Board (IRB)-approved protocol and in compliance with the Declaration of Helsinki. NLSTs were obtained from autopsy or amputation. Disease RA tissue was digested in dispase, collagenase, and DNase before being seeded in 72 cm^2 flasks.

Cells were grown in RPMI 1640 medium supplemented with 15% fetal bovine serum (FBS, Invitrogen, Waltham, MA, USA), 5,000 U/ml penicillin, 5 mg/ml streptomycin from Sigma (St. Louis, MO, USA), and 10 μg/ml gentamicin (Invitrogen, Waltham, MA, USA). Upon confluency (>85%), cells were passaged with brief trypsinization. Experiments were done using cells passed at least four to five times to ensure a pure fibroblast population. Similarly, we also established primary human synovial fibroblasts from nondiseased (NLSFs) tissues under an IRB-approved protocol.

Cell Culture and Stimulation

Human primary NLSF and RASF cells were maintained in RPMI 1640 culture media, with 10% FBS and antibiotics. For chronic exposure of cytokines ranging 12 days of exposure, 2 ng/ml M-CSF+10 ng/ml RANKL were used with or without a combination of 100 ng/ml IL-6 along with 100 ng/ml IL-6Rα. For acute exposure, cells were starved overnight in plain RPMI 1640, followed by stimulation cytokines. Acute treatment of cytokines ranging between 30 min and 4 h using 25 ng/ml MCSF+50 ng/ml RANKL was used with or without combination 100 ng/ml IL-6 along with 100 ng/ml IL-6R experiments. For chronic exposure of cells, RPMI 1640 with 10% FBS in combination with cytokines was changed every 3 days. On day 11 of differentiation, media without FBS was replenished for an additional 24 h before termination of the experiment. Supernatant and whole-cell extracts were prepared accordingly for further experiments. Likewise, we isolated bone marrow cells from 8-week-old C57BL/6 and allowed them to differentiate using 25 ng/ml M-CSF+10 ng/ml RANKL for 14 days with or without 100 ng/ml IL-6 or 100 ng/ml IL-6+100 ng/ml IL-6R (IL-6/IL-6R) for bone marrow macrophage-derived osteoclast studies. Human PBMCs were obtained from a commercial source (Zen-Bio, Inc., Research Triangle, NC, USA).

For the inhibitor experiments, overnight-starved RASF cells were subjected to 2 h pretreatment with 5 μM tofacitinib or 3 μg/

ml anti-IL-6 antibody followed by M-CSF+RANKL and/or IL-6/IL-6R stimulation for 30 min for Western blotting. TRAP staining was performed on RASFs based on manufacturer instructions from PMC-AK04F-COS (CosmoBio, Carlsbad, CA, USA).

Chromatin Immunoprecipitation Assay

Chromatin immunoprecipitation (ChIP) was performed for Ets2 as described previously (19). Human RASFs from three different donors were subjected to differentiation by M-CSF+RANKL with or without IL-6+IL-6R combination for 12 days. Detailed protocol is provided in the *SI Materials and Methods*. The list of primer pairs used for the ChIP assay has been provided in *SI* (**Supplementary Table S1**).

Untargeted Proteomics of RASFs

The untargeted proteomics analysis was conducted on an Orbitrap Fusion Lumos mass spectrometer (Thermo Fisher Scientific, Waltham, MA, USA) equipped with a Nano-Acquity UPLC system (Waters, Milford, MA, United States) and in-house developed nanospray ionization source at the University of Washington Proteomics Center, Seattle, WA. A detailed method is provided in the *SI Material and Methods* file. Candidates from IL-6+IL-6R treatment cohorts were also subjected to Metascape and or Ingenuity Pathways Analysis-based (IPA-Qiagen, Hilden, Germany) gene ontology prediction. The mass spectrometry proteomics data have been deposited to the ProteomeXchange Consortium *via* the PRIDE partner repository with the dataset identifier PXD028374.

In Vitro Pit Formation Assay

Human RASFs (2×10^4) were seeded in calcium phosphate-coated 24-well plates (CSR-BRA-24KIT, CosmoBio, Carlsbad, CA, USA) and allowed to reach ~85% confluency. Cells were differentiated under 2 ng/ml M-CSF+10 ng/ml RANKL with and without combination of 100 ng/ml IL-6+100 ng/ml IL-6R for 12 days. Every 3 days, media were replaced with fresh cytokines. After 12 days of differentiation, plates were washed with 10% sodium hypochlorite for 45 min, followed by an extensive wash using deionized water. Plates were air-dried, followed by staining with 1% toluidine blue staining for an additional 5 min. Plates were rewashed and air-dried. Each well of toluidine blue stain plates were photographed using a Zeiss microscope. Pit areas (three independent pits from each triplicate well) were calculated using ImageJ software (NIH, Bethesda, MD, United States). The total cumulative pit area was divided by the whole field and reported as a percentage of pit area per field.

Statistical Analysis

Statistical analysis of multiple comparisons between control *versus* treatment group means was performed using a one-way ANOVA followed by Dunnett's test or using Tukey's multiple comparison test when comparing multiple treatment groups to each other. All tests assumed normal distribution where $p < 0.05$ was considered significant.

RESULTS

IL-6 Trans-Signaling Enhances Osteoclast-Like Features in Human RASFs *In Vitro*

To understand the development of TRAP-positive RASFs that indicate osteoclast-like phenotype, human RASFs treated under different conditions for 12 days were washed with ice-cold PBS, fixed immediately, and stained using a TRAP substrate. Analysis of the stained area showed that IL-6/IL-6R increased the number of TRAP-positive cells in cultured conditions more than M-CSF/RANKL, the known drivers of osteoclastogenesis (**Figures 1A, B**). To confirm this observation, we differentiated bone marrow-derived macrophage (BMDM) using M-CSF/RANKL or treated in combination with IL-6 for 14 days. Upon differentiation, IL-6 markedly increased in the number of TRAP-positive BMDMs compared with M-CSF/RANKL treatment (**Supplementary Figure S1**). To confirm this phenotypic switch of RASFs to osteoclast-like cells also influenced their function, we performed the *in vitro* pit formation assay using calcium phosphate-coated plates. Evaluation of the pit areas showed that RASFs treated with chronic IL-6/IL-6R caused a significantly higher erosion of calcium phosphate from the plates independent of the osteoclastic cytokines M-CSF/RANKL (**Figure 1C**). Quantitative analysis showed that the percentage of pit area formed were significantly increased by ~2-fold in IL-6/IL-6R-treated samples compared with M-CSF/RANKL, and no further increase in the percentage of pit area formed was observed with M-CSF/RANKL plus IL-6/IL-6R treatment (**Figure 1D**; $p < 0.01$; $n = 3$), suggesting that IL-6 trans-signaling can independently be a major factor in RASF-induced bone loss. Furthermore, our FACS analysis identified the lack of CD14+ cell population in RASF culture preparations used in the study, suggesting the pure synovial fibroblast lineage of the cells used (**Supplementary Figure S2**).

Ets2 Mediates IL-6 Trans-Signaling Induced RASF Reprogramming to Osteoclast-Like Cells

Human RASFs grown for 12 days under the differentiation with M-CSF/RANKL and/or IL-6/IL-6R were evaluated for osteoclast-specific proteins. Western blot analysis of osteoclast-specific signature proteins confirms upregulation of cathepsin K, cathepsin B, p-STAT-3, RANKL, OPG, and RANKL expression by both M-CSF/RANKL and IL-6/IL-6R treatment (**Figures 2A, B**). Interestingly, while M-CSF/RANKL were able to preferentially activate traditional osteoclast markers such as OSCAR, OPG, and RANKL, IL-6/IL-6R was unique in inducing Ets2 transcription factor, in addition to p-STAT3 activation, to induce cathepsins K and B expression in human RASFs (**Figure 2A**). Furthermore, IL-6 trans-signaling in RASF-induced dose-dependent Ets2 expression by 70%–85% ($p < 0.01$; $n = 4$) and consequently induced cathepsins K and B expression by ~70% and 100%–125%, respectively, compared with untreated RASFs (**Figures 2C, D**; $p < 0.05$ or $p < 0.01$; $n = 3$). To compare these changes to a classical osteoclast model, primary human PBMC-derived macrophages were differentiated into osteoclasts by M-CSF/RANKL or IL-6/IL-6R

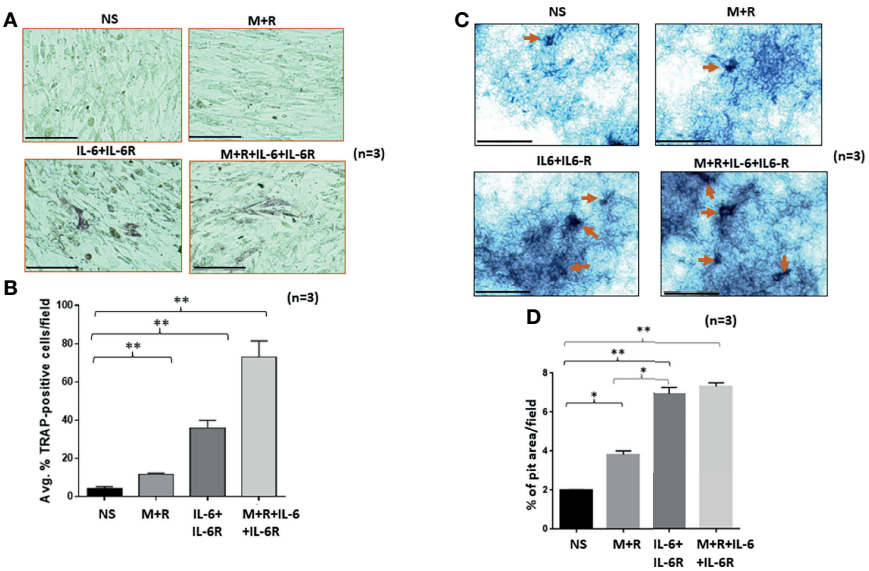

FIGURE 1 | Human RASFs in the presence of IL-6/IL-6R exhibit enhanced TRAP-positive staining and transform to an invasive phenotype. **(A)** RASFs grown with M-CSF (2 ng/ml)+ RANKL (10 ng/ml) (M+R) alone or with IL-6 and IL-6R (100 ng/ml each) for 12 days show an increased number of TRAP-positive RASFs compared with M-CSF/RANKL-differentiated and nonstimulated (NS) cell population. **(B)** IL-6+IL-6R treatment found to be almost 40% TRAP-positive cells which is more synergetic in combination with MCSF+RANKL where 70% of RASF cells are TRAP positive. **(C)** RASFs grown on calcium phosphate plates with M-CSF+ANKL alone or with IL-6+IL-6R for 12 days shows the increased pit formation on calcium phosphate-coated plates. **(D)** An average of three independent field quantifications of pits formed by RASFs from $n = 3$ patient donor samples reveal a threefold increase in the number of pits formed in calcium phosphate-coated plates when RASFs were stimulated with IL-6/IL-6R alone or in combination with M-CSF/RANKL as compared with nonstimulated RASFs, presented as mean ± SEM. $^{*}p < 0.05$; $^{**}p < 0.01$. Bar scale for images acquired is 150 μm.

for 12 days. Western blot analysis showed that IL-6/IL-6R induced the expression of cathepsin B, Ets2, and p-STAT-3 (Ser^{705}) that were independent of and comparable with M-CSF/RANKL treatment (**Figure 2E**). Furthermore, BMDM in response to M-CSF/RANKL and IL-6/IL-6R combination showed the marked upregulation of osteoclast-specific cathepsin K, cathepsin B, MITF, and Ets2 expression when compared with M-CSF/RANKL alone treatment (**Figure 2F**). Western blot analysis of joint homogenates prepared from naïve and AIA rats showed a marked increase in the expression of Ets2 along with other bone resorption markers including cathepsin K, cathepsin B, and RANKL (**Figure 2G**), suggesting a potential role of Ets2 in bone resorption in RA.

Untargeted Proteomics Analysis of the Secretome Reveals RASF Metabolic Reprogramming in Response to Chronic IL-6/IL-6R Exposure

To characterize the composition of the secretory proteins in response to IL-6/IL-6R stimulation and determine if that reflects the signature of osteoclast-like proteins, the conditioned media obtained from human RASFs untreated or treated with M-CSF/RANKL, IL-6/IL-6R, or the combination of M-CSF/RANKL and IL-6/IL-6R (All) were used for the untargeted proteomic analysis using MS. Initial data analysis identified roughly 107 common secreted proteins from RASFs under various treatments; these are presented with differential spectral count in the heatmap (**Figure 3A**). Further analysis of proteomic data identified 113 proteins unique to the secretome of RASFs treated with IL-6/IL-6R, in contrast to only 73 proteins specific for M-CSF/RANKL stimulation (**Figure 3B**). An additional 27 proteins were identified in both M-CSF/RANKL- and IL-6/IL-6R-stimulated supernatants. Western blot analysis on the concentrated supernatants from these differentiated RASFs confirmed increased production of cathepsin B, cathepsin K, and RANKL in IL-6/IL-6R-activated secretome (**Figure 3C**). Overall, gene signatures of all secretome in response to M-CSF+RANKL, IL-6+IL-6R, and M-CSF+RANKL+IL-6+IL-6R are listed in **Supplementary Table S2**; followed by Gene Ontology studies of M-CSF+RANKL, IL-6+IL-6R, and MCSF+RANKL+IL-6+IL-6R which are also described in **Supplementary Figure S3**. Focusing on the 113 proteins secreted explicitly by IL-6/IL-6R treatment of RASFs, we performed a Gene Ontology study using Metascape and Ingenuity Pathway Analysis (**Figures 3D, E**), revealing the metabolic changes in RASFs. Metascape analysis of the proteomics data identified the metabolic reprogramming of the RASFs as evident from the changes in metabolic pathway-related candidates such as *carboxylic acid metabolism*, *oxidation*, *glycolysis*, *phagocytosis*, *stem cell differentiation*, and *ammonia metabolism* (**Figure 3D**). In addition, the Ingenuity Pathway Analysis predicted the impact on tryptophan, isoleucine, and valine pathways, hematopoiesis from pluripotent stem cells, hepatic fibrosis, retinoid X receptor activation, endocytosis, and the complement system by IL-6/IL-6R treatment

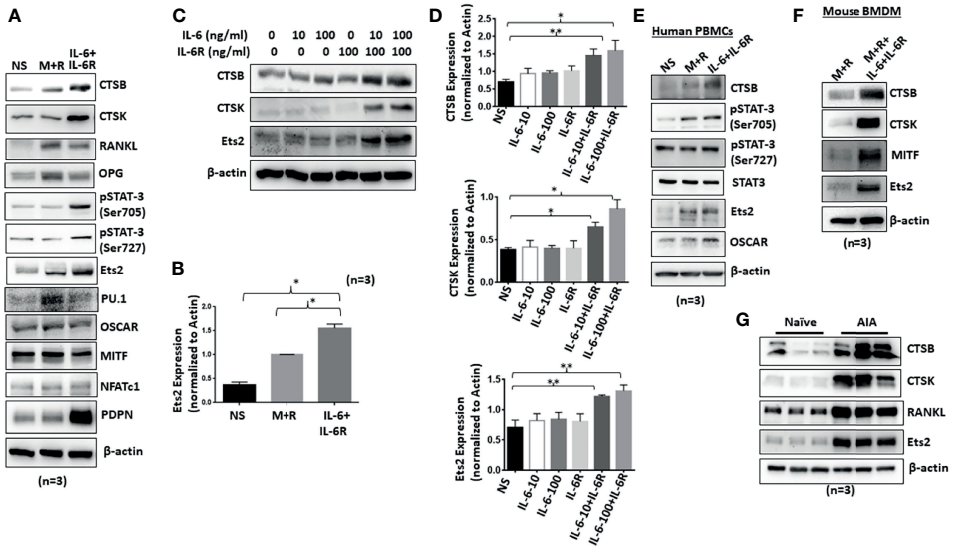

FIGURE 2 | Chronic exposure of IL-6/IL-6R induces cathepsin K, cathepsin B, and Ets2 expression in RASFs. **(A)** Western blot analysis of whole cell extracts prepared from human RASFs grown in the presence of IL-6+IL-6R for 12 days shows upregulation of endogenous CTSB, CTSK, RANKL, and Ets2. **(B)** Quantitative analysis of Ets2 expression reveals significant upregulation of Ets2 expression in response to IL-6+IL-6R treatment for 12 days. **(C, D)** CTSK, CTSB, and Ets2 were upregulated specifically in the presence of both IL-6 and IL-6R in human RASFs. **(E)** Human PBMC-derived osteoclast progenitor cells were stimulated with either M-CSF+RANKL or IL-6+IL-6R for 12 days. Western blot analysis of whole cell extracts prepared from these cells showed increased expression of CTSB and Ets2 in response to IL-6 trans-signaling. **(F)** CTSB, CTSK, and Ets2 expression was upregulated in mouse BMDMs in response to M-CSF+RANKL or IL-6+IL-6R. **(G)** Joint homogenates prepared from adjuvant-induced arthritis (AIA) rats show significant upregulation of CTSB, CTSK, RANKL, and Ets2 expression.**$p < 0.01$ while *$p < 0.05$.

(**Figure 3E**). Details of the top 10 molecular networks predicted by IPA in response to IL-6/IL-6R treatment are mentioned in **Supplementary Table S3**.

IL-6 Trans-Signaling Crosstalk With M-CSF/RANKL and Independent Activation of MAPK Pathway in Human RASFs *In Vitro*

IL-6/IL-6R-initiated trans-signaling activates the JAK/STAT pathway (20), whereas M-CSF/RANKL drives MAPK-dependent signaling for cell survival and differentiation (21). To understand how early signaling events play a role in RASF reprogramming, we stimulated cells with M-CSF/RANKL and/or IL-6/IL-6R for 30 min. Western blot analysis of the cell lysates showed that IL-6/IL-6R selectively induced the activation of p-JAK1 ($Tyr^{1022/1023}$), p-JAK1 ($Tyr^{1007/1008}$), p-STAT3 (Tyr^{705}), and p-STAT3 (Ser^{727}), without activating NF-κBp65 in RASFs (**Figure 4A**). Interestingly, IL-6/IL-6R induced the expression of p-Akt, a potent cell survival and proliferation marker protein. While M-CSF/RANKL combination was ineffective in activating the JAK/STAT3 pathway itself, the combination partially suppressed IL-6/IL-6R-induced activation of JAK/STAT3 and Akt pathways (**Figure 4A**). Pretreatment of RASFs with tofacitinib or anti-IL-6 antibody showed not only the reduction in JAK/STAT signaling but also suppressed IL-6/IL-6R-induced activation of p-Akt in human RASFs (**Figure 4A**). Interestingly, anti-IL-6 antibody was more effective in reducing the phosphorylation of JAK1 while tofacitinib seems to be more effective on suppressing the phosphorylation of JAK2.

To understand if IL-6 trans-signaling influences M-CSF/RANKL-induced MAPK activation, we analyzed the same samples for proteins upstream of the MAPK pathway (IRAK1/IRAK4/TAK1) in RASF signaling (22). Western blot analysis showed that IL-6/IL-6R markedly induced phosphorylation of p-IRAK4 (Thr^{345}/Ser^{346}) and p-TAK1 ($Thr^{184/187}$) expression alone or in combination with M-CSF/RANKL in RASFs, which was not effectively inhibited by tofacitinib or anti-IL-6R antibody (**Figure 4B**), suggesting that IL-6/IL-6R and M-CSF/RANKL activation of the MAPK pathways are independent of its JAK-STAT signaling and may remain activated even with IL-6-targeted treatments. Quantitative analysis of TAK1 phosphorylation and STAT3 phosphorylation suggesting TAK1 is unaffected by IL-6 inhibitors (**Figures 4C, D**).

Ets2 Translocates to the Nucleus in Response to IL-6 Trans-Signaling and Activates the Cathepsin Promoters

We hypothesized that Ets2 activity and binding in osteoclast-specific *CTSK* and *CTSB* gene promoters are mechanistically linked to the differentiation of human RASFs to an osteoclast-like phenotype. To address this hypothesis, we first verified Ets2 nuclear translocation in response to M-CSF/RANKL and/or IL-6/IL-6R combination in the nuclear extract prepared as previously described (23). We observed that M-CSF/RANKL increased the nuclear translocation of Ets2 by twofold ($p < 0.05$; $n = 3$) compared with the untreated samples (**Figure 5A**). Interestingly, IL-6/IL-6R increased Ets2 nuclear content by almost threefold, which was

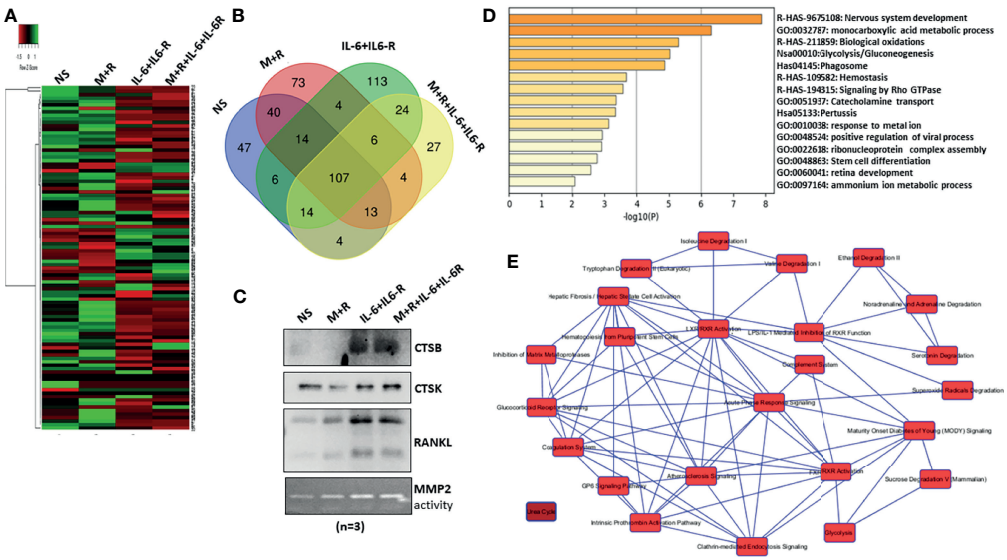

FIGURE 3 | MS-MS analysis of conditioned media identified uniquely expressed protein by IL-6/IL-6R treatment in human RASFs *in vitro*. **(A)** Conditioned media from four RASF donor cells treated with M-CSF/RANKL, IL-6/IL-6R, and M-CSF/RANKL plus IL-6/IL-6R (All) for 12 days were subjected to untargeted proteomics, which revealed 107 common proteins with differential expression. **(B)** Venn diagram shows the number of common and unique secretory proteins identified through untargeted proteomics in RASFs. **(C)** Increased secretion of CTSB, CTSK, and RANKL by transformed RASFs was confirmed through Western blotting of the conditioned media from the treated RASFs. **(D)** Cellular pathway changes brought about by chronic exposure of IL-6+IL-6 R in RASFs were analyzed using Metascape Gene Ontology studies, and **(E)** network analysis using ingenuity pathway analysis which predicted metabolic reprogramming in RASFs.

higher than M-CSF/RANKL-stimulated samples and did not increase further in M-CSF/RANKL and IL-6/IL-6R combination (All) treatment (**Figure 5A**; $p < 0.01$; $n = 3$). Ets2 nuclear localization loading control tubulin and lamin B shown in **Supplementary Figure S4**. Aligned to this finding, pretreatment of RASFs with tofacitinib significantly inhibited the combination-triggered nuclear translocation of Ets2 to the level seen in unstimulated samples (**Figure 5A**; $p < 0.01$; $n = 3$), suggesting that JAK/STAT is a pivotal pathway to interfere in this process. We further utilized bioinformatic and ChIP-seq analysis to determine the core-binding motif (GGAA/T) for Ets2 and the transcriptionally active regions in *CTSK* and *CTSB* gene promoters. We observed

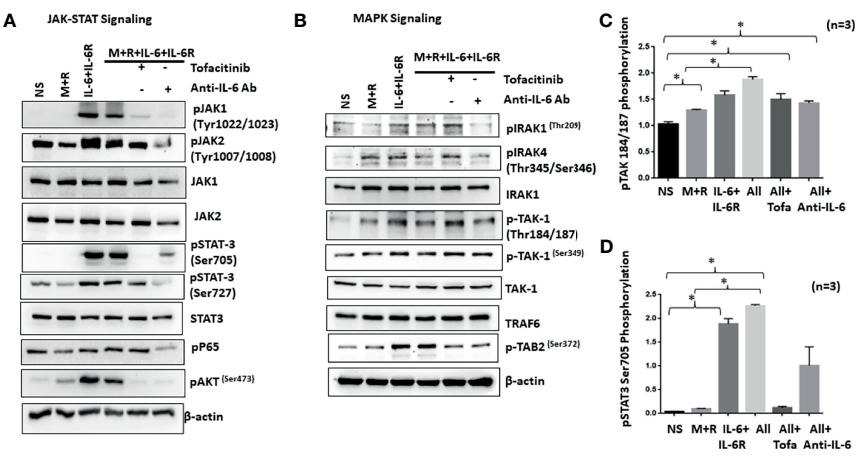

FIGURE 4 | IL-6+IL-6R activates MAPK pathway in addition to canonical JAK-STAT signaling pathway. **(A)** Stimulation of RASFs with M+R (M-CSF+RANK), IL-6 +IL-6R, and M+R+IL-6+IL-6R (All) activated the canonical JAK-STAT signaling pathway, evidenced by the increased phosphorylation of JAK1, JAK2, STAT3, and AKT, which was abrogated by tofacitinib and anti-IL-6 antibody treatment. **(B)** M-CSF+RANK, known to engage the MAPK signaling pathway, show cooperativity with IL-6+IL-6R and M+R+IL-6+IL-6R (All)-induced JAK-STAT signaling. Activation of key MAPK proteins by phosphorylation such as TAK1 seems unaffected by tofacitinib or anti-IL-6 antibody pretreatment. **(C, D)** Quantitative analysis of TAK1 phosphorylation at Thr184/187 and phospho-STAT3 Ser 705 shows M+R+IL-6 +IL-6R (All) samples are unaffected for phosphorylation of TAK1 in presence of inhibitors. *p < 0.05.

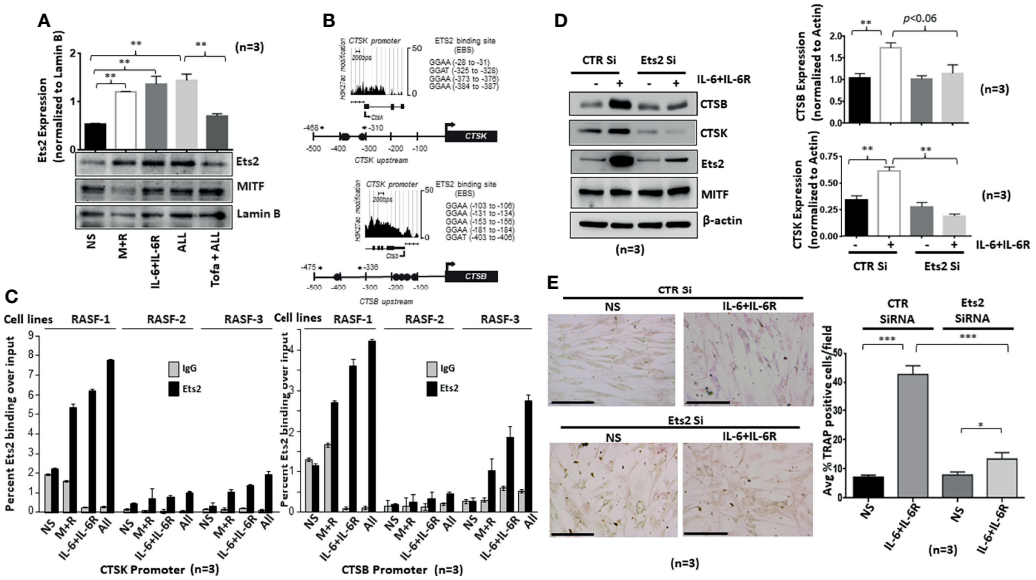

FIGURE 5 | IL-6/IL-6R-induced nuclear translocation of Ets2 and binds to the promoters of *CTSK* and *CTSB* genes to promote osteoclastogenesis in RASFs. **(A)** Ets2 translocates to the nucleus of RASFs within 4 h of IL-6+IL-6R stimulation alone or in combination with M-CSF+RANKL, which was inhibited by tofacitinib. **(B)** Bioinformatic and ChIP-seq analysis on tracks generated by GSE31621 identified the core-binding motif (GGAA/T) for Ets2 and the transcriptionally active regions in the promoters of *CTSK* and *CTSB* genes. **(C)** Chromatin immunoprecipitation using anti-Ets2 antibodies enriched CTSK and CTSB promoters from three independent human RASF donor cells upon stimulation with IL-6+IL-6R and M+R+IL-6+IL-6R (All). **(D)** Ets2 knockdown along with control (CTR), using siRNA, in RASFs treated with IL-6+IL-6R for 12 days resulted in the downregulation of endogenous CTSB and CTSK expression. Bar scale for images acquired is 150 μm. **(E)** Knockdown of Ets2 in RASFs obliterated the IL-6+IL-6R-induced TRAP-positive staining. *p < 0.05, **p < 0.05-p < 0.01, and ***p < 0.001.

four Ets2-binding sites in *CTSK* and five in *CTSB* within −500 bps upstream of respective promoters (**Figures 5B, C**). ChIP-seq analysis of previously published GSE31621 datasets further demonstrated that the genomic regions around −500 bps upstream of both the *CTSK* and *CTSB* gene are highly occupied with histone H3K27 acetylation (H3K27ac) modifications (**Figure 5B**). These high levels of the active chromatin marks around Ets2 binding indicate that Ets2 is directly involved in activating *CTSK* and *CTSB* gene expression and promoting differentiation. To further define the involvement of Ets2, we performed ChIP assay in RASFs treated with M-CSF/RANKL, IL-6/IL-6R, or M-CSF/RANKL and IL-6/IL-6R combination for 12 days. The results of the ChIP analysis showed that Ets2-immunoprecipitated DNA showed a significant increase in the occupancy of Ets2 protein in the *CTSK* promoter after treatment with M-CSF/RANKL, IL-6/IL-6R, and their combination when compared with control IgG (**Figure 5C**; $n = 3$). We also found similar enrichment in the *CTSB* promoter. Taken together, our promoter analysis and ChIP assay findings indicate that Ets2 binding is implicated in the osteoclast-like differentiation of RASFs. Furthermore, we performed the repeated knockdown of Ets2 on every 4th day for 12 days in IL-6/IL-6R-treated RASFs, followed by Western blot analysis to observe a reduced expression of IL-6/IL-6R-induced cathepsin B and cathepsin K, which confirms Ets2 transactivation of cathepsin genes (**Figure 5D**; $p < 0.01$, $n = 3$). Our observation of no change in expression of osteoclastic transcription factor MITF suggests that it is not directly involved in IL-6/IL-6R-induced reprogramming of RASFs to osteoclast-like phenotype. Interestingly, the reduced TRAP staining of RASFs on 12 days of IL-6/IL-6R treatment upon Ets2 knockdown further validated its role in the osteoclast-like phenotype of RASFs (**Figure 5E**).

RASFs Are Predetermined to Be Responsive to IL-6 Trans-Signaling Mediated Differentiation

Synovial tissue-derived RASFs possess a unique capability to dedifferentiate and have recently been identified as synovial mesenchymal stem cells (SMCs) (24). To understand how human RASFs respond to IL-6/IL-6R-induced osteoclast-like phenotype and functions compared with nondiseased human SFs (NLSFs), we treated both cell types with IL-6/IL-6R for 5 or 10 days in culture. Western blot analysis of the cell lysates showed selectively higher expression of osteoclast-specific markers (cathepsin K, cathepsin B, RANKL, and Ets2) by RASFs compared with the NLSFs, with no difference in p-STAT3 activation between two groups (**Figure 6A**). To our surprise, we observed a temporal decrease in the endogenous levels of gp130 and JAK1 in both NLSFs and RASFs treated with IL-6/IL-6R. When probed for the stem cell markers, RASF lysates showed markedly higher basal expression level of KLF4, Nanog, Oct4, and Sox-2, along with consistently higher response of these markers to IL-6/IL-6R stimulation compared with NLSFs (**Figure 6B**; $p < 0.05$). This suggests that RASFs are more susceptible than NLSFs to cytokine-driven metabolic reprogramming. Knockdown of Ets2 in RASFs stimulated with

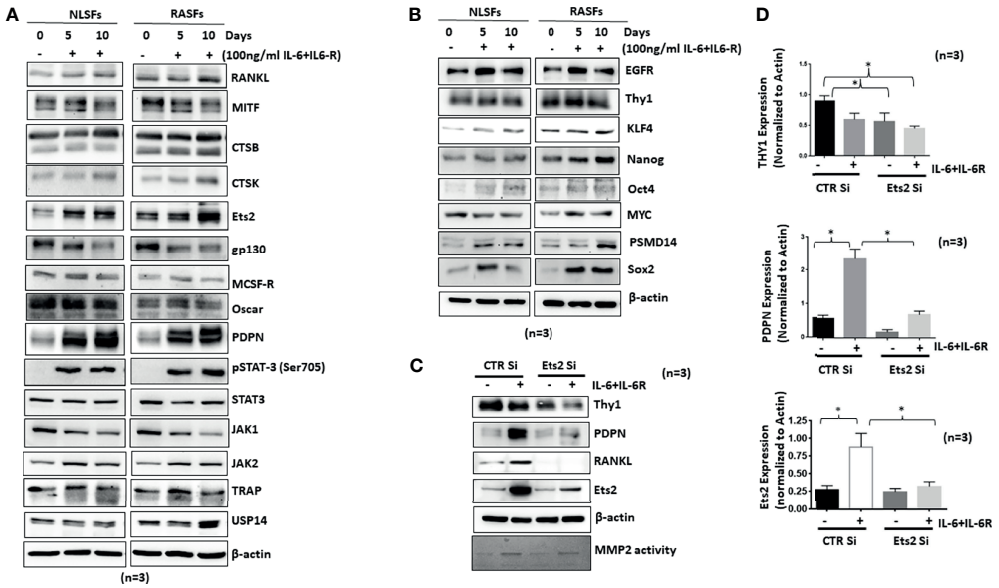

FIGURE 6 | IL-6+IL-6R trans-signaling activates both NLSFs and RASFs to an aggressive and invasive phenotype mediated by Ets2. **(A)** NLSFs and RASFs were differentiated in the presence of IL-6+IL-6R for 5 and 10 days followed by preparation of whole cell extracts that were then probed for osteoclast-specific markers. IL-6 trans-signaling was activated in both NLSFs and RASFs that led to the increased expression of Ets2 which in turn increased the expression of RANKL, CTSK, CTSB, and PDPN. **(B)** IL-6+IL-6R stimulation upregulated the expression of differentiation marker proteins Sox2, Oct4, KLF4, and Nanog higher in RASFs as compared with NLSFs. **(C)** IL-6+IL-6R-induced heterogeneity markers in RASFs, Thy1, and PDPN were downregulated in the absence of Ets2. **(D)** Quantitation of Thy1, PDPN, and Ets2 in 12-day differentiated RASFs confirms more then 80% knockdown of Ets2 as well as significant reduction in PDPN and Thy1 expression. *p < 0.05.

IL-6/IL-6R revealed that Ets2 might play a critical role in its invasive phenotype or osteoclast-like phenotype reprogramming by targeting Thy1, podoplanin, and RANKL expression (**Figures 6C, D**). Although IL-6/IL-6R did not induce the expression of Thy1, the knockdown of Ets2 abrogated the expression of Thy1 in untreated and IL-6/IL-6R-treated samples, suggesting its involvement in RASF heterogeneity beyond the regulatory role of IL-6 trans-signaling.

DISCUSSION

The present study revealed a novel mechanism of IL-6/IL-6R-driven metabolic reprogramming of RASFs to osteoclast-like cells that could contribute to bone destruction in RA. This reprogramming of RASFs to an osteoclastic phenotype is the first study to identify the role of transcription factor Ets2 in IL-6/IL-6R-induced cathepsins K and B and its therapeutic relevance in limiting the bone loss mediated by aggressive and invasive RASFs. We also identified the stem cell markers that were uniquely higher in RASFs when compared with the NLSFs that suggest increased plasticity in activated RASFs to switch their phenotype and function in the synovial microenvironment. These findings shed light on a noncanonical pathway that IL-6/IL-6R exploits to exacerbate bone destruction, highlighting an opportunity to examine the current IL-6 signaling and trans-signaling inhibitors used in the clinics for their efficacy in suppressing the pathological effects of IL-6 mediated through Ets2. Since Ets2 is a transcription factor, it may have some influence on global transcriptomics of RASFs, which may also contribute to the metabolic reprogramming of RASFs as osteoclast-like cells.

IL-6 is a pleiotropic cytokine that supports B-cell proliferation (20) and directly stimulates CRP production from hepatocytes (21). IL-6 drives the chronic inflammation in RA synovial microenvironment and exerts its function through classical and trans-signaling (25, 26). IL-6 trans-signaling is mediated by the binding of IL-6 to the soluble IL-6 receptor (sIL-6R) and signal transduction *via* membrane-bound gp130 to the JAK-STAT pathway. Apart from its role in inflammation, IL-6 signaling is implicated in osteoclastogenesis in RA. The levels of IL-6 and IL-6R in the synovial fluid from RA patients are higher and known to induce osteoclastogenesis in the synovial microenvironment (27). Studies have demonstrated the role of IL-6 trans-signaling in osteoclastogenesis in both osteoclast progenitors and bone marrow-derived cells depending on the presence of IL-6R (28, 29). Both IL-6 and sIL-6R concentrations increase in RA patients' sera and synovial fluid and correlate with the disease activity (26). We observed IL-6/IL-6R-induced osteoclast-specific TRAP staining, *in vitro* pit formation, cathepsins K and B expression in cultured human RASFs similar to that induced by M-CSF/RANKL, indicating their transformation to osteoclast-like cells. Interestingly, IL-6/IL-6R-driven osteoclastic-like features in RASFs were primarily dependent on Ets2, since its knockdown abolished the production of IL-6/IL-6R-induced bone resorption mediators by RASFs. Previously,

Ets2 was shown to be inducible by inflammatory cytokines such as TNF-α and involved in osteoblast reprogramming (30, 31); however, there are no prior publications demonstrating how IL-6 signaling utilizes Ets2 to enhance transcriptional activation of *CTSK* and *CTSB* promoter to cause bone resorption executed by RASFs. These findings provide a rationale for targeting Ets2 transcription factor for reducing bone resorption in RA pathogenesis.

Furthermore, a comprehensive proteomic analysis of the conditioned media from the transformed RASFs revealed 113 proteins secreted exclusively in response to chronic IL-6/IL-6R stimulation, including cathepsins K and B. Further Gene Ontology analysis of this data suggests RASFs undergo a massive metabolic reprogramming that transforms these cells into multipotent stem cell phenotype. It has been previously reported that RASFs are metabolically altered cells with high glycolysis rates which maintain their hyperproliferative rate and aggressive phenotype in the inflamed synovial microenvironment (32–36). Our preliminary findings confirm IL-6/IL-6R trans-signaling engages the metabolic pathways such as glycolysis and the catabolic pathway for sucrose and amino acids (tryptophan, isoleucine, valine) to propel metabolic reprogramming of RASFs. However, we primarily focused our work on examining the functional reprogramming in the influence of chronic IL-6 and predicted pathways obtained from Metascape and IPA analyses of proteomics data may further be subjected to in-depth study for better understanding of the role of IL-6 trans-signaling and Ets2 in metabolic reprogramming of synovial fibroblasts. Oshita et al. reported that mesenchymal stem cells (MSCs) constitutively express osteoprotegerin (OPG) protein (11, 16, 37). Surprisingly, OPG is expressed by RASFs (38) constitutively as well as under stimulation (data not shown), which aligns well with the report by Li et al. (24) classifying RASFs as MSCs. Our data further show that in addition to the activation of JAK-STAT pathway, IL-6/IL-6R simultaneously activated the MAPK signaling pathway in RASFs, as revealed by the increased phosphorylation of IRAK1, IRAK4, and TAK1 proteins. However, the inability of IL-6 inhibitors to target this noncanonical pathway leaves an opportunity for IL-6 to continuously activate the MAPK pathway and potentially contribute to the chronic bone loss in RA. These findings overlap with our observation that Ets2 is central to IL-6/IL-6R-driven bone resorption, partly by activating RASFs to contribute to this process through metabolic reprogramming that coincided with a transition to osteoclast-like phenotype and functions.

Delineating the fundamental role of Ets2 in this pathological process of RASF transformation to osteoclast-like cells could establish Ets2 as a potential therapeutic target in RA. Our ChIP assay using anti-Ets2 antibody revealed the recruitment of Ets2 on the promoters of *CTSK* and *CTSB*, suggesting the direct role of Ets2 in osteoclastic-like changes in RASFs. Interestingly, increased Ets2 expression has been demonstrated in the synovia of some RA patients (39), and the expression of extracellular MMPs has been reported to be driven by Ets2 (40) in invasion and metastasis as well as stem cell self-renewal process (41, 42). However, there is very little published data on the role of Ets2 in RA pathogenesis, and in light of our findings, it warrants further investigation as a potential therapeutic target for the treatment of RA. Given the limitation of tofacitinib and anti-IL-6 Ab to inhibit IL-6-induced trans-signaling through TAK1 suggests that inhibiting Ets2 may have pronounced benefit that is potentially elicited by the suppression of MAPK and JAK/STAT signaling in human RASFs. Our results suggest that RASFs undergo accelerated reprogramming due to IL-6-induced expression of differentiation markers such as Sox2, KLF, OPG, and Nanog, and the hyperinvasive fibroblast marker Thy1, which were inhibited by silencing Ets2. Overall, our findings provide novel evidence for the central role of Ets2 in IL-6 trans-signaling induced cellular reprograming of RASFs to osteoclast-like cells and its contribution to RASF heterogeneity and bone destruction in RA.

Despite being the most ubiquitous stromal cell type in the synovium, RASFs have proven to be difficult to characterize for their molecular functions and repertoire. Recent studies have made progress in identification of different RASF subsets that play unique role in various bone remodeling processes that lead to pannus outgrowth and joint deformities (43–45). Of particular note, RASF subsets that express podoplanin, fibroblast activation protein-α, and CD90/Thy1 are bound to alter extracellular matrix by producing MMP activity, enhance RANKL expression, and stimulate osteoclast differentiation and activation (46–48). Our study provides evidence that in addition to the contribution of RASF to bone destruction, these cells can actively transform functionally into osteoclast-like cells to propagate these processes using Ets2 as a novel mediator. Further *in vivo* studies evaluating the role of Ets2 in functional reprogramming of RASFs to osteoclast-like cells may have therapeutic value in the treatment of RA.

DATA AVAILABILITY STATEMENT

The original contributions presented in the study are publicly available. This data can be found here: https://www.ebi.ac.uk/pride/ under the accession number PXD028374.

ETHICS STATEMENT

The animal study was reviewed and approved by Washington State University IACUC Committee.

AUTHOR CONTRIBUTIONS

AS and SA designed this study and participated in drafting the manuscript. AS, MH, and BM performed experiments and analyzed the data. BW and QH performed ChIP analysis and data interpretation. YS, AB, and BP performed and analyzed the proteomics data. MO performed the quantitative analysis of stained slides. SK performed statistical analysis. All authors contributed to the article and approved the submitted version.

FUNDING

Research reported in this publication was supported by National Institute of Arthritis and Musculoskeletal and Skin Diseases of the National Institutes of Health under award number R01 AR072615 (SA) and the Arthritis National Research Foundation under grant award 849781 (AKS).

ACKNOWLEDGMENTS

The authors thank the National Disease Research Interchange and the Cooperative Human Tissue Network for providing RA synovial tissue. The authors thank Dr. David A Fox, University of Michigan, Ann Arbor for providing some RASF cell lines generated in his lab. The authors also thank Paul Panipinto for his help in FACS experiments and Ms. Ruby J. Siegel for critical reading of the manuscript.

SUPPLEMENTARY MATERIAL

The Supplementary Material for this article can be found online at: https://www.frontiersin.org/articles/10.3389/fimmu.2021.746503/full#supplementary-material

REFERENCES

1. Okada Y, Nagase H, Harris EDJr. A Metalloproteinase From Human Rheumatoid Synovial Fibroblasts That Digests Connective Tissue Matrix Components. Purification and Characterization. *J Biol Chem* (1986) 261 (30):14245–55. doi: 10.1016/S0021-9258(18)67011-5
2. Henderson B, Edwards JCW, Pettipher ER. *Mechanisms and Models in Rheumatoid Arthritis*. London; San Diego: London; San Diego: Academic Press (1995).
3. Gravallese EM. Bone Destruction in Arthritis. *Ann Rheumatic Dis* (2002) 61 Suppl 2:ii84–6. doi: 10.1136/ard.61.suppl_2.ii84
4. Schett G, Hayer S, Zwerina J, Redlich K, Smolen JS. Mechanisms of Disease: The Link Between RANKL and Arthritic Bone Disease. *Nat Clin Pract* (2005) 1(1):47–54. doi: 10.1038/ncprheum0036
5. Yamamoto K, Kishida T, Nakai K, Sato Y, Kotani S, Nishizawa Y, et al. Direct Phenotypic Conversion of Human Fibroblasts Into Functional Osteoblasts Triggered by a Blockade of the Transforming Growth Factor-β Signal. *Sci Rep* (2018) 8(1):8463–11. doi: 10.1038/s41598-018-26745-2
6. Takayanagi H. Osteoimmunology: Shared Mechanisms and Crosstalk Between the Immune and Bone Systems. *Nat Rev Immunol* (2007) 7 (4):292–304. doi: 10.1038/nri2062
7. Takayanagi H, Iizuka H, Juji T, Nakagawa T, Yamamoto A, Miyazaki T, et al. Involvement of Receptor Activator of Nuclear Factor κb Ligand/Osteoclast Differentiation Factor in Osteoclastogenesis From Synoviocytes in Rheumatoid Arthritis. *Arthritis Rheumatism* (2000) 43(2):259–69. doi: 10.1002/1529-0131(200002)43:2<259::aid-anr4>3.0.co;2-w
8. Amarasekara DS, Yun H, Kim S, Lee N, Kim H, Rho J, et al. Regulation of Osteoclast Differentiation by Cytokine Networks. *Immune Netw* (2018) 18(1): e8–8. doi: 10.4110/in.2018.18.e8
9. Hashizume M, Hayakawa N, Mihara M. IL-6 Trans-Signalling Directly Induces RANKL on Fibroblast-Like Synovial Cells and is Involved in RANKL Induction by TNF-Alpha and IL-17. *Rheumatol (Oxford England)* (2008) 47(11):1635–40. doi: 10.1093/rheumatology/ken363
10. Flanagan M. Human Osteoclasts Derive From CD14-Positive Monocytes. *Br J Haematol* (1999) 106(1):167–70. doi: 10.1046/j.1365-2141.1999.01491.x
11. Shalhoub V, Elliott G, Chiu L, Manoukian R, Manoukian M, Hawkins N, et al. Characterization of Osteoclast Precursors in Human Blood. *Br J Haematol* (2000) 111(2):501–12. doi: 10.1111/j.1365-2141.2000.02379.x
12. Oliver JL, Alexander MP, Norrod AG, Mullins IM, Mullins DW. Differential Expression and Tumor Necrosis Factor-Mediated Regulation of TNFRSF11b/osteoprotegerin Production by Human Melanomas. *Pigment Cell Melanoma Res* (2013) 26(4):571–79. doi: 10.1111/pcmr.12091
13. Kapasa ER, Giannoudis PV, Jia X, Hatton PV, Yang XB. The Effect of RANKL/OPG Balance on Reducing Implant Complications. *J Funct Biomater* (2017) 8(4):42. doi: 10.3390/jfb8040042
14. Quinn JMW, Elliott J, Gillespie MT, Martin TJ. A Combination of Osteoclast Differentiation Factor and Macrophage-Colony Stimulating Factor Is Sufficient for Both Human and Mouse Osteoclast Formation *in Vitro*. *Endocrinol (Philadelphia)* (1998) 139(10):4424–27. doi: 10.1210/endo.139.10.6331
15. Hofbauer LC, Khosla S, Dunstan CR, et al. The Roles of Osteoprotegerin and Osteoprotegerin Ligand in the Paracrine Regulation of Bone Resorption. *J Bone Mineral Res* (2000) 15(1):2–12. doi: 10.1359/jbmr.2000.15.1.2
16. Lacey DL, Timms E, Tan HL, Kelley MJ, Dunstan CR, Burgess T, et al. Osteoprotegerin Ligand Is a Cytokine That Regulates Osteoclast Differentiation and Activation. *Cell (Cambridge)* (1998) 93(2):165–76. doi: 10.1016/s0092-8674(00)81569-x
17. Nathalie F, Sheila R, Anne MD, Ernesto C. Interleukin-6 and Its Soluble Receptor Cause a Marked Induction of Collagenase 3 Expression in Rat Osteoblast Cultures. *J Biol Chem* (1997) 272(18):12144–50. doi: 10.1074/jbc.272.18.12144
18. McGregor NE, Murat M, Elango J, Poulton IJ, Walker EC, Crimeen-Irwin B, et al. IL-6 Exhibits Both Cis- and Trans-Signaling in Osteocytes and Osteoblasts, But Only Trans-Signaling Promotes Bone Formation and Osteoclastogenesis. *J Biol Chem* (2019) 294(19):7850–63. doi: 10.1074/jbc.RA119.008074
19. Singh AK, Fechtner S, Chourasia M, Sicalo J, Ahmed S. Critical Role of IL-1α in IL-1β-Induced Inflammatory Responses: Cooperation With NF-κbp65 in Transcriptional Regulation. *FASEB J* (2019) 33(2):2526–36. doi: 10.1096/fj.201801513R
20. Kojima H, Inoue T, Kunimoto H, Nakajima K. IL-6-STAT3 Signaling and Premature Senescence. *JAK-STAT* (2013) 2(4):e25763–e63. doi: 10.4161/jkst.25763
21. Anesi A, Generali L, Sandoni L, Pozzi S, Grande A. From Osteoclast Differentiation to Osteonecrosis of the Jaw: Molecular and Clinical Insights. *Int J Mol Sci* (2019) 20(19):4925. doi: 10.3390/ijms20194925
22. Singh AK, Umar S, Riegsecker S, Chourasia M, Ahmed S. Regulation of Transforming Growth Factor Beta-Activated Kinase Activation by Epigallocatechin-3-Gallate in Rheumatoid Arthritis Synovial Fibroblasts: Suppression of K(63) -Linked Autoubiquitination of Tumor Necrosis Factor Receptor-Associated Factor 6. *Arthritis Rheumatol* (2016) 68(2):347–58. doi: 10.1002/art.39447
23. Singh AK, Haque M, O'Sullivan K, Chourasia M, Ouseph MM, Ahmed S. Suppression of Monosodium Urate Crystal-Induced Inflammation by Inhibiting TGF-Beta-Activated Kinase 1-Dependent Signaling: Role of the Ubiquitin Proteasome System. *Cell Mol Immunol* (2021) 18(1):162–70. doi: 10.1038/s41423-019-0284-3
24. Li F, Tang Y, Song B, Yu M, Li Q, Zhang C, et al. Nomenclature Clarification: Synovial Fibroblasts and Synovial Mesenchymal Stem Cells. *Stem Cell Res Ther* (2019) 10(1):260–60. doi: 10.1186/s13287-019-1359-x
25. Baran P, Hansen S, Waetzig GH, Akbarzadeh M, Lamertz L, Huber HJ, et al. The Balance of Interleukin (IL)-6, IL-6.Soluble IL-6 Receptor (sIL-6R), and IL-6.sIL-6R.Sgp130 Complexes Allows Simultaneous Classic and Trans-Signaling. *J Biol Chem* (2018) 293(18):6762–75. doi: 10.1074/jbc.RA117.001163
26. Lacroix M, Rousseau F, Guilhot F, Malinge P, Magistrelli G, Herren S, et al. Novel Insights Into Interleukin 6 (IL-6) Cis- and Trans-Signaling Pathways by Differentially Manipulating the Assembly of the IL-6 Signaling Complex. *J Biol Chem* (2015) 290(45):26943–53. doi: 10.1074/jbc.M115.682138

27. Kotake S, Sato K, Kim KJ, Takahashi N, Udagawa N, Nakamura I, et al. Interleukin-6 and Soluble Interleukin-6 Receptors in the Synovial Fluids From Rheumatoid Arthritis Patients are Responsible for Osteoclast-Like Cell Formation. *J Bone Miner Res* (1996) 11(1):88–95. doi: 10.1002/jbmr.5650110113
28. Udagawa N, Takahashi N, Katagiri T, Tamuta T, Wada S, Findlay DM, et al. Interleukin (IL)-6 Induction of Osteoclast Differentiation Depends on IL-6 Receptors Expressed on Osteoblastic Cells But Not on Osteoclast Progenitors. *J Exp Med* (1995) 182(5):1461–8. doi: 10.1084/jem.182.5.1461
29. Kotake S, Udagawa N, Takahashi N, Matsuzaki K, Itoh K, Ishiyama S, et al. IL-17 in Synovial Fluids From Patients With Rheumatoid Arthritis is a Potent Stimulator of Osteoclastogenesis. *J Clin Invest* (1999) 103(9):1345–52. doi: 10.1172/JCI5703
30. Raouf A, Seth A. Ets Transcription Factors and Targets in Osteogenesis. *Oncogene* (2000) 19(55):6455–63. doi: 10.1038/sj.onc.1204037
31. Zhang Q, Badell IR, Schwarz EM, Boulukos KE, Yao Z, Boyce BF, et al. Tumor Necrosis Factor Prevents Alendronate-Induced Osteoclast Apoptosis *In Vivo* by Stimulating Bcl-xL Expression Through Ets-2. *Arthritis Rheumatism* (2005) 52(9):2708–18. doi: 10.1002/art.21236
32. Fearon U, Hanlon MM, Wade SM, Fletcher JM. Altered Metabolic Pathways Regulate Synovial Inflammation in Rheumatoid Arthritis. *Clin Exp Immunol* (2019) 197(2):170–80. doi: 10.1111/cei.13228
33. Falconer J, Murphy AN, Young SP, Clark AR, Tiziani S, Guma M, et al. Synovial Cell Metabolism and Chronic Inflammation in Rheumatoid Arthritis. *Arthritis Rheumatol (Hoboken NJ)* (2018) 70(7):984–99. doi: 10.1002/art.40504
34. Turner JD, Filer A. The Role of the Synovial Fibroblast in Rheumatoid Arthritis Pathogenesis. *Curr Opin Rheumatol* (2015) 27(2):175–82. doi: 10.1097/BOR.0000000000000148
35. Bottini N, Firestein GS. Duality of Fibroblast-Like Synoviocytes in RA: Passive Responders and Imprinted Aggressors. *Nat Rev Rheumatol* (2013) 9(1):24–33. doi: 10.1038/nrrheum.2012.190
36. Lefevre S, Knedla A, Tennie C, Kampmann A, Wunrau C, Dinser R, et al. Synovial Fibroblasts Spread Rheumatoid Arthritis to Unaffected Joints. *Nat Med* (2009) 15(12):1414–20. doi: 10.1038/nm.2050
37. Oshita K, Yamaoka K, Udagawa N, Fukuyo S, Sonomoto K, Maeshima K, et al. Human Mesenchymal Stem Cells Inhibit Osteoclastogenesis Through Osteoprotegerin Production. *Arthritis Rheumatism* (2011) 63(6):1658–67. doi: 10.1002/art.30309
38. Ziolkowska M, Kurowska M, Radzikowska A, Luszczykiewicz G, Wiland P, Dziewczopolski W, et al. High Levels of Osteoprotegerin and Soluble Receptor Activator of Nuclear Factor κb Ligand in Serum of Rheumatoid Arthritis Patients and Their Normalization After Anti–Tumor Necrosis Factor α Treatment. *Arthritis Rheumatism* (2002) 46(7):1744–53. doi: 10.1002/art.10388
39. Kasperkovitz PV, Timmer TCG, Smeets TJ, Verbeet NL, Paul PT, Baarsen LGMV, et al. Fibroblast-Like Synoviocytes Derived From Patients With Rheumatoid Arthritis Show the Imprint of Synovial Tissue Heterogeneity - Evidence of a Link Between an Increased Myofibroblast-Like Phenotype and High-Inflammation Synovitis. *Arthritis Rheumatism* (2005) 52(2):430–41. doi: 10.1002/art.20811
40. Singh S, Barrett J, Sakata K, Tozer RG, Singh G. ETS Proteins and MMPs: Partners in Invasion and Metastasis. *Curr Drug Targets* (2002) 3(5):359. doi: 10.2174/1389450023347489
41. Wen F, Tynan JA, Cecena G, Williams R, Múnera J, Mavrothalassitis G, et al. Ets2 is Required for Trophoblast Stem Cell Self-Renewal. *Dev Biol* (2007) 312 (1):284–99. doi: 10.1016/j.ydbio.2007.09.024
42. Pitarresi JR, Liu X, Sharma SM, Cuitiño MC, Kladney RD, Mace TA, et al. Stromal ETS2 Regulates Chemokine Production and Immune Cell Recruitment During Acinar-To-Ductal Metaplasia. *Neoplasia* (2016) 18 (9):541–52. doi: 10.1016/j.neo.2016.07.006
43. Miura Y, Ota S, Peterlin M, McDevitt G, Kanazawa S. A Subpopulation of Synovial Fibroblasts Leads to Osteochondrogenesis in a Mouse Model of Chronic Inflammatory Rheumatoid Arthritis. *JBMR Plus* (2019) 3(6):e10132. doi: 10.1002/jbm4.10132
44. Nygaard G, Firestein GS. Restoring Synovial Homeostasis in Rheumatoid Arthritis by Targeting Fibroblast-Like Synoviocytes. *Nat Rev Rheumatol* (2020) 16(6):316–33. doi: 10.1038/s41584-020-0413-5
45. Wehmeyer C, Pap T, Buckley CD, Naylor AJ. The Role of Stromal Cells in Inflammatory Bone Loss. *Clin Exp Immunol* (2017) 189(1):1–11. doi: 10.1111/cei.12979
46. Croft AP, Campos J, Jansen K, Turner JD, Marshall J, Attar M, et al. Distinct Fibroblast Subsets Drive Inflammation and Damage in Arthritis. *Nature* (2019) 570(7760):246–51. doi: 10.1038/s41586-019-1263-7
47. Stephenson W, Donlin LT, Butler A, Rozo C, Bracken B, Rashidfarrokhi A, et al. Single-Cell RNA-Seq of Rheumatoid Arthritis Synovial Tissue Using Low-Cost Microfluidic Instrumentation. *Nat Commun* (2018) 9(1):791. doi: 10.1038/s41467-017-02659-x
48. Zhang F, Wei K, Slowikowski K, Foneeka CY, Rao DA, Kelly S, et al. Defining Inflammatory Cell States in Rheumatoid Arthritis Joint Synovial Tissues by Integrating Single-Cell Transcriptomics and Mass Cytometry. *Nat Immunol* (2019) 20(7):928–42. doi: 10.1038/s41590-019-0378-1

Conflict of Interest: The authors declare that the research was conducted in the absence of any commercial or financial relationships that could be construed as a potential conflict of interest.

Publisher's Note: All claims expressed in this article are solely those of the authors and do not necessarily represent those of their affiliated organizations, or those of the publisher, the editors and the reviewers. Any product that may be evaluated in this article, or claim that may be made by its manufacturer, is not guaranteed or endorsed by the publisher.

frontiers in Immunology

CORRECTION
published: 26 November 2021
doi: 10.3389/fimmu.2021.808756

Corrigendum: Ets-2 Propagates IL-6 Trans-Signaling Mediated Osteoclast-Like Changes in Human Rheumatoid Arthritis Synovial Fibroblast

Anil K. Singh[1], Mahamudul Haque[1], Bhanupriya Madarampalli[1], Yuanyuan Shi[2], Benjamin J. Wildman[3], Abdul Basit[1], Sadik A. Khuder[4], Bhagwat Prasad[1], Quamarul Hassan[3], Madhu M. Ouseph[5] and Salahuddin Ahmed[1,6]**

[1] Department of Pharmaceutical Sciences, Washington State University College of Pharmacy, Spokane, WA, United States, [2] University of Washington School of Medicine, Seattle, WA, United States, [3] Department of Oral and Maxillofacial Surgery, School of Dentistry, University of Alabama at Birmingham, AL, United States, [4] Department of Medicine and Public Health, University of Toledo, Toledo, OH, United States, [5] Department of Pathology and Laboratory Medicine, Weill Cornell Medical College, New York, NY, United States, [6] Division of Rheumatology, University of Washington School of Medicine, Seattle, WA, United States

OPEN ACCESS

Approved by:
Frontiers Editorial Office,
Frontiers Media SA, Switzerland

***Correspondence:**
Salahuddin Ahmed
salah.ahmed@wsu.edu
Anil K. Singh
anil.singh@wsu.edu

Specialty section:
This article was submitted to Autoimmune and Autoinflammatory Disorders, a section of the journal Frontiers in Immunology

Received: 03 November 2021
Accepted: 12 November 2021
Published: 26 November 2021

Citation:
Singh AK, Haque M, Madarampalli B, Shi Y, Wildman BJ, Basit A, Khuder SA, Prasad B, Hassan Q, Ouseph MM and Ahmed S (2021) Corrigendum: Ets-2 Propagates IL-6 Trans-Signaling Mediated Osteoclast-Like Changes in Human Rheumatoid Arthritis Synovial Fibroblast. Front. Immunol. 12:808756. doi: 10.3389/fimmu.2021.808756

Keywords: osteoclast, interleukin-6, synovial fibroblasts, rheumatoid arthritis, reprogramming

A Corrigendum on

Ets-2 Propagates IL-6 Trans-Signaling Mediated Osteoclast-Like Changes in Human Rheumatoid Arthritis Synovial Fibroblast

By Singh AK, Haque M, Madarampalli B, Shi Y, Wildman BJ, Basit A, Khuder SA, Prasad B, Hassan Q, Ouseph MM and Ahmed S (2021). Front. Immunol. 12:746503. doi: 10.3389/fimmu.2021.746503

In the published article, there was a mistake in the order of the listed authors. The correct authors list appears below:

"*Anil K. Singh, Mahamudul Haque, Bhanupriya Madarampalli, Yuanyuan Shi, Benjamin J. Wildman, Abdul Basit, Sadik A. Khuder, Bhagwat Prasad, Quamarul Hassan, Madhu M. Ouseph and Salahuddin Ahmed*".

The authors apologize for this error and state that this does not change the scientific conclusions of the article in any way. The original article has been updated.

frontiers in Immunology

ORIGINAL RESEARCH
published: 03 January 2022
doi: 10.3389/fimmu.2021.777792

Low-Dose Radiotherapy Leads to a Systemic Anti-Inflammatory Shift in the Pre-Clinical K/BxN Serum Transfer Model and Reduces Osteoarthritic Pain in Patients

Thomas Weissmann[1], *Michael Rückert*[1,2], *Jian-Guo Zhou*[1,2,3], *Michaela Seeling*[4], *Sebastian Lettmaier*[1], *Anna-Jasmina Donaubauer*[1,2], *Falk Nimmerjahn*[4], *Oliver J. Ott*[1], *Markus Hecht*[1], *Florian Putz*[1], *Rainer Fietkau*[1], *Benjamin Frey*[1,2], *Udo S. Gaipl*[1,2]* *and Lisa Deloch*[1,2]

[1] *Department of Radiation Oncology, Universitätsklinikum Erlangen, Friedrich-Alexander-Universität Erlangen-Nürnberg, Erlangen, Germany,* [2] *Translational Radiobiology, Department of Radiation Oncology, Universitätsklinikum Erlangen, Friedrich-Alexander-Universität Erlangen-Nürnberg, Erlangen, Germany,* [3] *Department of Oncology, The second affiliated Hospital of Zunyi Medical University, Zunyi, China,* [4] *Department of Biology, Institute of Genetics, Friedrich-Alexander-Universitätsklinikum Erlangen, Friedrich-Alexander-Universität Erlangen-Nürnberg, Erlangen, Germany*

OPEN ACCESS

Edited by:
Steven O'Reilly,
STipe Therapeutics, Denmark

Reviewed by:
Franz Rödel,
University Hospital Frankfurt, Germany
Xiaoxiang Chen,
Shanghai JiaoTong University, China

***Correspondence:**
Udo S. Gaipl
udo.gaipl@uk-erlangen.de

Specialty section:
This article was submitted to Autoimmune and Autoinflammatory Disorders, a section of the journal Frontiers in Immunology

Received: *15 September 2021*
Accepted: *07 December 2021*
Published: *03 January 2022*

Citation:
Weissmann T, Rückert M, Zhou J-G, Seeling M, Lettmaier S, Donaubauer A-J, Nimmerjahn F, Ott OJ, Hecht M, Putz F, Fietkau R, Frey B, Gaipl US and Deloch L (2022) Low-Dose Radiotherapy Leads to a Systemic Anti-Inflammatory Shift in the Pre-Clinical K/BxN Serum Transfer Model and Reduces Osteoarthritic Pain in Patients. Front. Immunol. 12:777792. doi: 10.3389/fimmu.2021.777792

Osteoarthritis (OA) is the leading degenerative joint disease in the western world and leads, if left untreated, to a progressive deterioration of joint functionality, ultimately reducing quality of life. Recent data has shown, that especially OA of the ankle and foot are among the most frequently affected regions. Current research in OA points towards a complex involvement of various cell and tissue types, often accompanied by inflammation. Low-dose radiotherapy (LDRT) is widely used for the treatment of degenerative and inflammatory diseases. While the reported analgesic effects are well known, the underlying molecular mechanisms are only poorly understood. We therefore correlated a clinical approach, looking at pain reduction in 196 patients treated with LDRT with a pre-clinical approach, utilizing the K/BxN serum transfer mouse model using flow cytometry and multiplex ELISA for analysis. While an improvement of symptoms in the majority of patients was found, patients suffering from symptoms within the tarsi transversa show a significantly lower level of improvement. Further, a significant impact of therapy success was detected depending on whether only one or both feet were affected. Further, patients of younger age showed a significantly better outcome than older ones while needing fewer treatment series. When looking on a cellular level within the mouse model, a systemic alteration of immune cells namely a shift from CD8+ to CD4+ T cells and reduced numbers of DCs was observed. A general reduction of inflammatory cytokines was detected, with significant alterations in IL-4 and IL-17 levels, all of which could potentially be responsible for the highly effective clinical improvement in patients. Taken together our data indicate that LDRT can be regarded as a highly effective treatment option for patients suffering from OA of the foot and ankle, in terms of analgesic effects, especially in younger patients. Furthermore, the observed effects are mediated by an interplay of cellular and soluble

immune factors, as observed in the K/BxN serum transfer model. With this interdisciplinary approach we aim to encourage the usage of LDRT as an additive treatment strategy not only as a last resort, but also earlier in the course of disease.

Keywords: low-dose radiotherapy, osteoarthritis, rheumatoid arthritis, mouse model, foot, pain, X-rays, K/BxN serum transfer

INTRODUCTION

Osteoarthritis (OA) as the leading degenerative joint disease leads, during the course of the disease, to a reduction in functionality, consequently resulting in reduced quality of life. OA in general accounts for approximately 15% off all musculoskeletal consultations in primary care (1). The high prevalence of OA affects 10% of men and 18% of women over 60 years of age (2, 3) thus posing a true socioeconomic burden consuming up to 1.0 – 2.5% of the gross domestic product in the western world due to treatment costs and loss of productivity (4). While the disease seems to undergo a slow but steady progression, its initial occurrence seems to be accompanied by multiple genetic, biological and biomechanical risk factors such as female gender, higher age, obesity, mechanical strain, idiopathic reasons and suffered injuries. While former pathogenesis was understood as a simple mechanical cartilage degradation, the evolved scientific insights describe OA as a complex interaction of different types of tissue and cells. Here, a diverse spectrum of matrix proteases underlying a vast number of pathways is involved, causing changes in cartilage volume, proteoglycan content, cartilage vascularization and cartilage perfusion leading to an involvement and inflammation of the whole joint resulting in a steady deterioration (5, 6).

While the occurrence of OA is, in theory, possible for every joint, recent data substantiate OA of the ankle and foot to be among the most frequent in the lower limbs (7). OA of the foot is most often reported as being mostly found in the metatarsophalangeal joint and the mid foot and less often in the hind foot or ankle. Different studies indicate a higher incidence of OA in abnormal structural status of the foot like toe length abnormalities, wider bone structure, long sesamoids, flat feet or higher arches of the foot (8). Patients with OA of the feet suffer from a variety of symptoms including pain, stiffness, swelling, as well as limited range of motion resulting in a decreased physical function. End-stage OA of the foot can lead to severe deformities that ultimately substantially reduce the mobility of patients.

Treatment strategies for OA of the foot and ankle pose a true challenge due to the complex structure of the entire organ. Therefore, treatment should always be adapted to individual characteristics recommending conservative treatment approaches in early stages and more invasive procedures in advanced stages. Conservative approaches include basic strategies like weight-loss approaches as well as physical therapy and the utilization of ortheses. Drug medication includes a broad variety of substance groups like non-steroidal anti-inflammatory drugs (NSAIDs) and biologics, applied solely or in combinations. Further approaches include the intraarticular injection of glucocorticoids, hyaluronic acid or radiosynoviorthesis (9). Surgery should be regarded as an ultima ratio approach for advanced or end-stage disease. On the other hand, radiotherapy (RT) for benign diseases holds the potential of filling the gap between conservative and more invasive treatment approaches.

Low-dose radiotherapy (LDRT) with X-rays for different degenerative and inflammatory diseases such as enthesiopathies and OA has successfully been applied for decades and is further gaining acceptance by orthopedic specialists and general physicians due to the satisfying results achieved (10–15). Especially patients that are refractory to classical treatment options may benefit from LDRT, as the therapy induces long-lasting pain-relieving effects. Several pre-clinical and clinical studies provide evidence for the effect of LDRT on the immune system and modulation of inflammation (16, 17).

Further effects include osteoimmunological mechanisms affecting bone formation and resorption activity of osteoclasts (18–20), the inflammatory phenotype of macrophages (21–23) or the adhesion of infiltrating immune cells to endothelial cells (24–26) that are most likely responsible for the pain relieving and anti-inflammatory effects (14, 27, 28). Although these progressive scientific insights have significantly diluted criticisms like the major effect being caused by placebo-effects, the underlying molecular mechanisms still need to undergo extensive fundamental research to make the transition from preclinical data to clinical outcome more comprehensible. Placebo-controlled studies are still needed and patient samples cannot always be taken easily from the affected regions. We therefore examined the corresponding regions in a K/BxN serum transfer mouse model in order to investigate LDRT-induced effects at a molecular level. While this mouse model is generally looked at as a model for inflammatory arthritides (29), it also shares similarities with OA, such as a fibrotic synovium releasing inflammatory cytokines (e.g. Interleukin (IL)-1 and tumor necrosis factor-α (TNF-α) (30), activated macrophages and inflammation (5, 31, 32). Additionally, this mouse model also shows signs of cartilage and bone remodeling as well as destruction, signs, that can also be found in OA joints (33) and is a useful tool in order to examine arthritic pain (29, 34). Further, as summarized in (33, 35, 36) there is no ideal murine model that can be regarded as the "gold standard" in OA, as all of the model systems lack some of the properties observed in patients. Additionally, we were able to show in previous studies, that an underlying inflammatory condition is needed for LDRT to be able to modulate inflammation that results in the observed beneficial effects (18, 19). In the present patient study we mainly focused on the analgesic effects of LDRT that,

according to our hypothesis, are mediated *via* a modulation of inflammation. We thus opted for the approach to use the K/BxN serum transfer mouse model as an inflammatory model with pathological changes in the joints for pain related processes.

Despite the rising prevalence of OA due to the higher age of the general population, OA of the foot and ankle is rather seldom subject to intensified clinical research. RT of the ankle and foot has been reported only very sporadically presenting only a very limited number of patients (37).

In addition, further pre-clinical research that helps to discover the underlying mechanisms involved in anti-inflammatory and analgesic effects of LDRT is needed. In the present study, we therefore combined clinical and pre-clinical data in order to better understand the underlying mechanisms of LDRT.

MATERIAL AND METHODS

Patient Cohort

Between November 2004 and February 2019, 196 (47 men, 149 woman) patients with OA of the foot and ankle, received LDRT at the Department of Radiation Oncology of the Universitätsklinikum Erlangen. The patients were referred by their treating orthopedic specialist. All patients had received several therapies before undergoing LDRT, as an alternative treatment modality. The majority of the patients did not undergo full clinical, rheumatologic diagnostics directly before therapy. In general, patients have been referred to our clinic with a history of chronic degenerative joint disease of the foot and ankle. The categorization of different localizations was carried out by marking the origin of pain before undergoing LDRT. At time of LDRT, the median age of the patients was 65.9 years with a median age of 66.4 for women and 63.7 for men. As pre-clinical studies indicate stronger anti-inflammatory effects with a single dose of 0.5 Gy, most patients underwent LDRT with 0.5 Gy. 177 patients underwent LDRT with a single dose of 0.5 (total dose 3 Gy) and 19 patients underwent LDRT with a single dose of 1.0 Gy (total dose 6 Gy). Furthermore, 24 patients received one series of LDRT, 165 patients received two series and 6 patients underwent three series of LDRT. Only one patient underwent four consecutive series of LDRT. **Table 1** provides a summary of these patient characteristics.

Written informed consent was obtained from all patients before LDRT. In addition, patients provided informed consent for the retrospective analysis of their data, as well as the publication of the data in a pseudonymized manner (ethical approval Ref.169_21 Bc, FootRetroRad trial).

TABLE 1 | Overview of patient characteristics.

Patient characteristics	Cohort (N = 196)
Gender (Number of patients/[%] total cohort)	
Male	47/24%
Female	149/76%
Age (Mean ± SD)	
All patients	65.9 ± 14.5
Male	63.7 ± 12.6
Female	66.4 ± 15.1
Number of series (Number of patients/[%] total cohort)	
1	24/12%
2	165/84%
3	6/3%
4	1/0.5%
Applied single dose (Number of patients/[%] total cohort)	
0.5 Gy	177/90%
1.0 Gy	19/10%
Localization (Number of patients/[%] total cohort)	
Metatarsophalangeal	49/25%
Tarsophalangeal	51/26%
Tarsi transversa	40/20%
Lower ankle	21/11%
Upper ankle	35/18.5%
Affected side (Number of patients/[%] total cohort)	
Right	83/42%
Left	73/37%
Both	40/20%

Treatment

Patients

All patients underwent LDRT applied with an orthovoltage technique. LDRT was applied using a Stabilipan machine (180kev, 20 mA, 0,2mm Cu filter, focus skin distance 40 cm) until September 2016. Afterwards a X-Strahl machine was used (180 keV, 10mA, 0,2mm Cu filter, focus skin distance 50 cm). No qualitative differences can be expected concerning radiation quality. The single fields applied for both machines ranged from 6 x 8cm to 10 x 8cm and 10 x 15cm, according to the field needed for the joint. The fields were positioned directly on the affected joint with a determination of the dosage at the middle of the joint. One radiotherapy series consisted of six single fractions (single dose: 0.5 Gy or 1.0 Gy) delivered over three weeks with an interfractional radiation-free interval of at least two days (total dose: 3 Gy or 6 Gy). Patients not showing an improvement of their pain or not being subjectively satisfied six weeks after the end of the first series underwent a consecutive second series 12 weeks following the first. The application of further series occurred only on an individual basis.

Mice

Similar to the patient treatment, mice received 0.5 Gy as a locally applied single dose using orthovoltage technique with a X-Strahl orthovolt X-ray machine (180 keV, 10mA, 1mm copper filter) as previously described in (19).

Measurement of Therapeutic Outcome

The data on patients outcome was collected prospectively exclusively for clinical routine and afterward analyzed retrospectively. The retrospective use of the patient`s data is covered by an approval by the Ethics Committee of the Friedrich-Alexander-Universität Erlangen-Nürnberg (Ref.169_21 Bc, FootRetroRad trial). The study was performed in accordance with the 1964 Declaration of Helsinki and its later amendments. The outcome in the present study was measured by quantifying the subjective pain reduction in terms of percentage of improvement with reference to their initial pain status before LDRT. The interrogation of patients was performed directly after the last radiotherapy session and during the follow-up appointments 8 to

12 weeks later, as well as six months after LDRT. Joints of the foot were discriminated as such: metatarsophalangeal, tarsometatarsal, tarsi-transversa, and the upper and lower ankle joint. The discrimination occurred according to diagnosis of the orthopedic specialist and clinical examination and marking before radiotherapy. Analyses were performed with the subjective rating obtained at the last session of RT, three months post RT and six months post RT, if available.

K/BxN Mouse Model and Arthritis Scoring

Mice were maintained in a SPF facility under sterile atmosphere at the animal facility of the Universitätsklinikum Erlangen. The animal procedures have been approved by the "Regierung of Unterfranken" and were conducted in accordance with the guidelines of the Federation of European Laboratory Animal Science Associations (FELASA; Approval numbers: 55.2-DMS-2532-2-114 from 13 November 2015 and 10 December 2015; TS-3/14 from 21 February 2014). Pooled serum from transgenic K/BxN mice (29, 38) was kindly provided by F.Nimmerjahn. 200µl serum was injected intraperitoneally into 10 week old female C57Bl/6 mice (Janvier, Le Genest-Saint-Isle, France). Arthritis scoring was carried out in a blinded manner with a score system ranging from 0 (no swelling) to 3 (massive swelling) as described previously (38).

Flow Cytometry Analysis

For multicolor flow cytometry analysis whole blood and bone marrow (BM) of the mice was collected. Erythrocytes in 100µl whole blood were lysed using a TQ-Prep Workstation (Beckmann Coulter, Brea, CA, USA), for analysis of BM, $1x10^5$ cells/stain were used. Cells (lysed blood cells and BM) were resuspended in 50µl Fc-block solution (eBioscience, San Diego, CA, USA) and incubated for 10min at room temperature. Staining for antibody panels was then carried out at 4°C for 30min as described previously (39). Cells were analyzed using a CytoFLEX S flow cytometer and data was analyzed with the help of the Kaluza analysis software (both: Beckman Coulter, Brea, CA, USA).

MSD® Multi-Spot Assay System

Multiplex ELISA was carried out with Meso Scale Discovery® system (MSD®; Rockville, MD, USA) according to the manufacturer's recommendation. For this experiment, the Proinflammatory Panel 1 (mouse) Kit V-Plex® Assay (including detection of IFN-γ, IL1-β, IL-2, IL-4, IL-5, IL-6, KC/GRO, IL-10, IL12p70, TNF-α) as well as the TH17 Panel 1 (mouse) Kit (MIP-3α, IL-22, IL-23, IL-17C, IL-31, IL-21, IL-16, IL-17A, IL17E/IL-25) were used. For analysis, serum samples were diluted 1:2 for the Proinflammatory and 1:4 for the TH17 Panel, with the provided buffer respectively, as recommended by the manufacturer. Subsequent analysis was carried out using MSD® Discovery Workbench®.

Statistical Analysis

Patient Studies

The Wilcoxon ($\alpha = 0.05$) test was used to evaluate the difference between groups on the best improvement during therapy using ggplot2 (version 3.3.5) ($p<0.05$). Univariate and multivariate logistic regression was used to evaluate the association of clinical factors and the best improvement. A correlation analysis of the factors in each group was performed by ggcorrplot (version 0.1.3). Data management was performed using the IBM SPSS software for MS Windows (SPSS Inc Chicago, IL, USA, version 21). All analyses were carried out using R version 3.6.1 (R Foundation for Statistical Computing) and related packages. P-values ≤ 0.05 were considered statistically significant.

Pre-Clinical Studies

Data is presented as either Mean ± SEM or Median + IQR. Samples were tested for normal distribution and variance equality and subsequently analyzed using two-tailed Mann-Whitney-U test in comparison to untreated controls. Generation of graphs as well as statistical analysis was done using GraphPad Prism Software (Version 8.3.0; GraphPad software, Inc., San Diego, CA, USA). P-values ≤ 0.05 were considered to be statistically significant.

RESULTS

LDRT Improves Pain Levels in Patients

The patients scored their subjective pain reduction directly after the last RT session and, if available, after three and six months post treatment. In order to depict the therapeutic success, the best therapeutic response independent of the time point of data collection and the cumulative dose is presented in **Figure 1A**.

The majority of the patients (75%; 148/196 patients) reported a subjective improvement exceeding the clinical benchmark of 20% which was considered as a therapeutic success. An improvement between 20-40% was observed in 11% (22/196) of all patients. Over 15% (30/196) of the patients reported halving of subjective pain reporting improvement of 40-60% whereas 12% (25/196) even reported improvement of around 60-80%. The biggest group of the patient cohort of about 37% (71/196) of the patients even scored near complete and complete response reporting improvement of 80-100%. Only two patients reported a worsening of symptoms.

LDRT Treatment Success Is Partially Dependent on Localization

Several different confounding factors like age, gender, number of radiation series, location of arthritis, laterality as well as the single dose were examined for their effect on the therapeutic success. For this reason, a univariate and multivariate analysis was carried out. As a cut off, an improvement of 20% was set for the statistical analysis with the best response (independent of the time point of data collection directly after LDRT as well as after 3 month or 6 months post treatment) used for measurement. No correlation between gender and number of series, as well as the applied single dose was observed. A significant impact was found for localization of the OA (see **Figure 1B**) as well as for the age (≥50 years vs. <50 years). Due to these results more in depth investigations were carried out. Results of the univariate and multivariate analysis are depicted in **Table 2**.

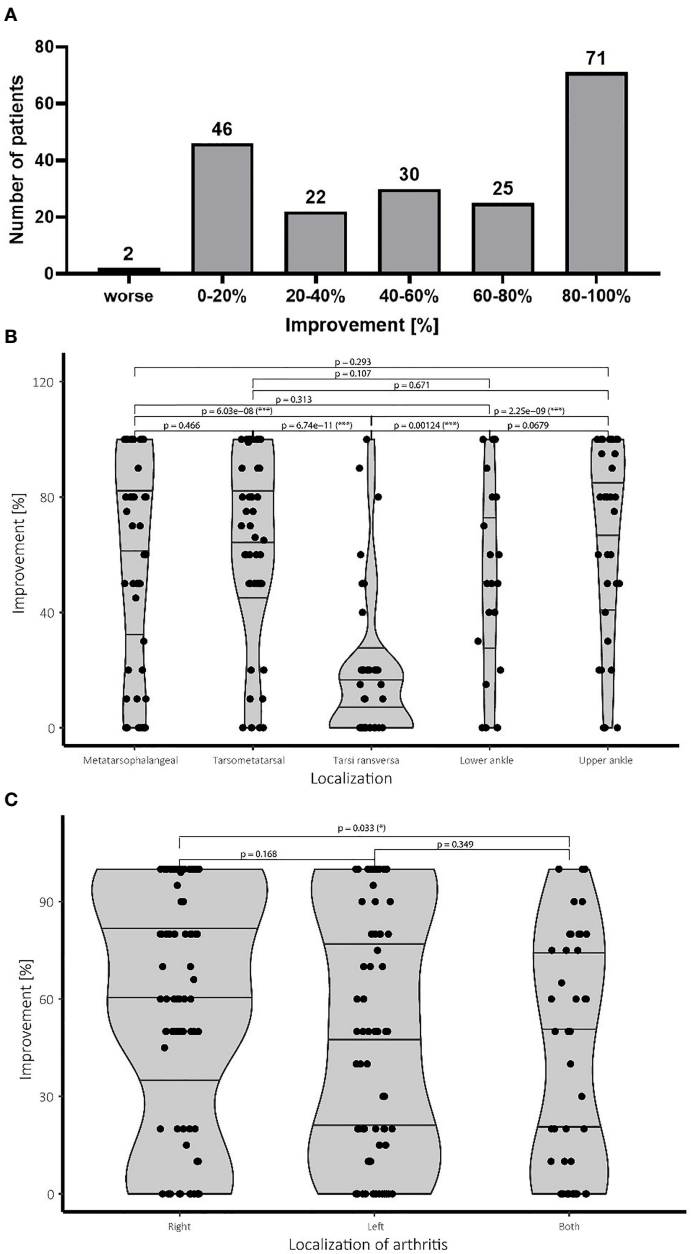

FIGURE 1 | Pain improvement and treatment success following LDRT. **(A)** Patients scored the subjective improvement of their pain level in percentage of improvement in regard of their initial pain level before therapy. The pain levels were determined after the last LDRT session, as well as 12 and 24 weeks after LDRT, if available. The figure depicts the best therapeutic response of the patients independent of the time point and the single and cumulative dose. Patients reporting improvement up to 20% were considered as stable disease. **(B)** Affection of the tarsi transversa region is associated with significantly worse outcome compared to all other localisations. All other treatment groups show a more favorable treatment outcome. **(C)** While treatment response for an affection of the right side is significantly better, affection of the left side does not show worse treatment result than an involvement of both feet. N=196 patients.

Patients with affection of the joints of the tarsi transversa show significantly worse treatment response than any other group with the majority of the patients reporting lower levels of improvement. No statistical difference between the other groups concerning treatment success was observed. Despite not being statistically significant the lower ankle seems to show a slight tendency towards a worse treatment result than the upper ankle. Meanwhile an affection of the midfoot at the tarsometatarsal joint shows similar treatment results compared to the forefoot represented by the metatarsophalangeal joints. Summarizing LDRT in the treatment of OA of the tarsi transversa does not seem to be equally effective compared to other localizations of the

TABLE 2 | Overview of the results of the univariate and multivariate analysis.

Parameter	Univariate regression			Multivariate regression		
	RR	95% CI	p-value	RR	95% CI	p-value
Gender (male vs. female)	0.619	0.22 – 1.323	0.204	0.893	0.763 – 1.076	0.244
Number of series	0.890	0.386 – 2.010	0.779	1.031	0.851 – 1.249	0.757
Single dose (1.0 vs. 0.5 Gy)	0.668	0.086 – 7.038	0.715	0.962	0.547 – 1.629	0.888
Location (tarsi transversa)	1.087	0.858 – 1.389	0.495	1.020	0.965 – 1.077	0.483
Location (both feet vs. right or left)	0.536	0.251 – 1.179	0.111	0.827	0.670 – 1.014	0.075
Age (≥50 years vs. < 50 years)	5.654	1.541 – 23.052	**0.010**	1.991	1.261 – 3.380	**0.006**

RR, relative risk; CI, confidence interval.
Bold values indicate statistically relevant values.

foot, but should still be considered due to the complete remission achieved in some patients in our cohort as can be seen in **Figure 1B**.

LDRT Treatment Is Dependent on Laterality

Regarding the side of the affection, significantly worse results were observed for patients suffering from bilateral affection compared to patients suffering only of OA in the right foot. No difference in improvement between the left and right leg as well as the left side and both sides was observed. Therefore, a clearly worse prognosis for affection of both feet cannot be given, although a slightly worse treatment response cannot be ruled out either (**Figure 1C**).

An Increased Number of Series Does Not Significantly Improve Therapy Outcome

While most patients in our cohort received 2 series of LDRT, Some patients demanded further treatment series. Patients receiving a single series of LDRT report a high median of over 60% of improvement compared to pre-therapeutic base line, while also showing a very broad spread between 15% and 100%. Patients undergoing a second or even a third series show a very similar median of improvement compared with patients with two series showing a median improvement of 55% and patients with a third series showing a median improvement of 57% (**Figure 2A**). Despite not being significant, patients undergoing a third series show a small tendency towards a better median and a broader spread towards higher levels of improvement. Only one patient underwent a fourth series.

A Single Dose of 1.0 Gy Shows No Significant Therapeutic Improvement Over a Single Dose of 0.5 Gy

Neither in the univariate nor in the multivariate analysis nor in the Wilcoxon test significant differences were observed by comparing treatments with a single dose of 1.0 Gy with those of 0.5 Gy. While the 1.0 Gy group shows a slightly higher median, the interquartile distance shows no convincing tendency towards better results of improvement. Despite the lack of a discernible difference, the results (see **Figure 2B**) are still limited by the small number of patients undergoing LDRT with a single dosage of 1.0 Gy.

For a summarizing overview a heat map was created to investigate the impact of confounding factors and the best improvement by logistic regression. Confounding factors include gender, number of radiation series, age, type of arthritis and side of involvement. **Figure 2C** summarizes and visualizes these correlations.

Locally Applied LDRT With 0.5 Gy Shows Systemic Effects in the Bone Marrow of the K/BxN Serum Transfer Mouse Model

As these studies are performed retrospectively and researchers are often confronted with the worries of these effects being a placebo effect, we aimed to look into the molecular effects behind the analgesic properties of LDRT by using a pre-clinical model system. K/BxN serum transfer mice were locally irradiated with a local single dose of 0.5 Gy [**Figures 3**, **4**, and as previously described in (19)]. While assessment of clinical score in the mice pointed towards a similar response as in patients (e.g. incline in disease progression in untreated and stable or declining disease in 5/7 of the treated animals 1 week after LDRT; **Figures 3A, B**), histomorphological effects of the LDRT treatment displayed a slight reduction in the inflammatory area alongside a slight tendency of increased cartilage area (**Figures 3C, D**). When analyzing bone marrow cells, derived from the long bones of the hindfeet of mock and LDRT treated animals, we found that distinct immune cells were significantly systemically altered in LDRT-treated mice (**Figures 4D–I**).

Among the most affected cell types were dendritic cells (DCs) that were found to be significantly reduced in the irradiated leg of treated animals (**Figure 4D**). In the case of T cells, a general significant reduction of total T cell numbers in both legs (treated and protected) of the irradiated animals (**Figure 4G**) was detected. Notably, T cell subsets shifted from the rather inflammatory CD8+ T cells, that were found to be significantly reduced in both legs of the LDRT-treated animals (**Figure 4I**) to CD4+ T cells that, depending on the subtype, can have rather anti-inflammatory effects, and that were found to be significantly increased in both legs, respectively (**Figure 4H**).

LDRT With 0.5 Gy Only Slightly Modulates Immune Cell Subsets and Their Activation Status in the Peripheral Blood of K/BxN Serum Transfer Mice

We then wanted to elucidate whether the effects observed in both legs of the LDRT treated mice could be explained through a

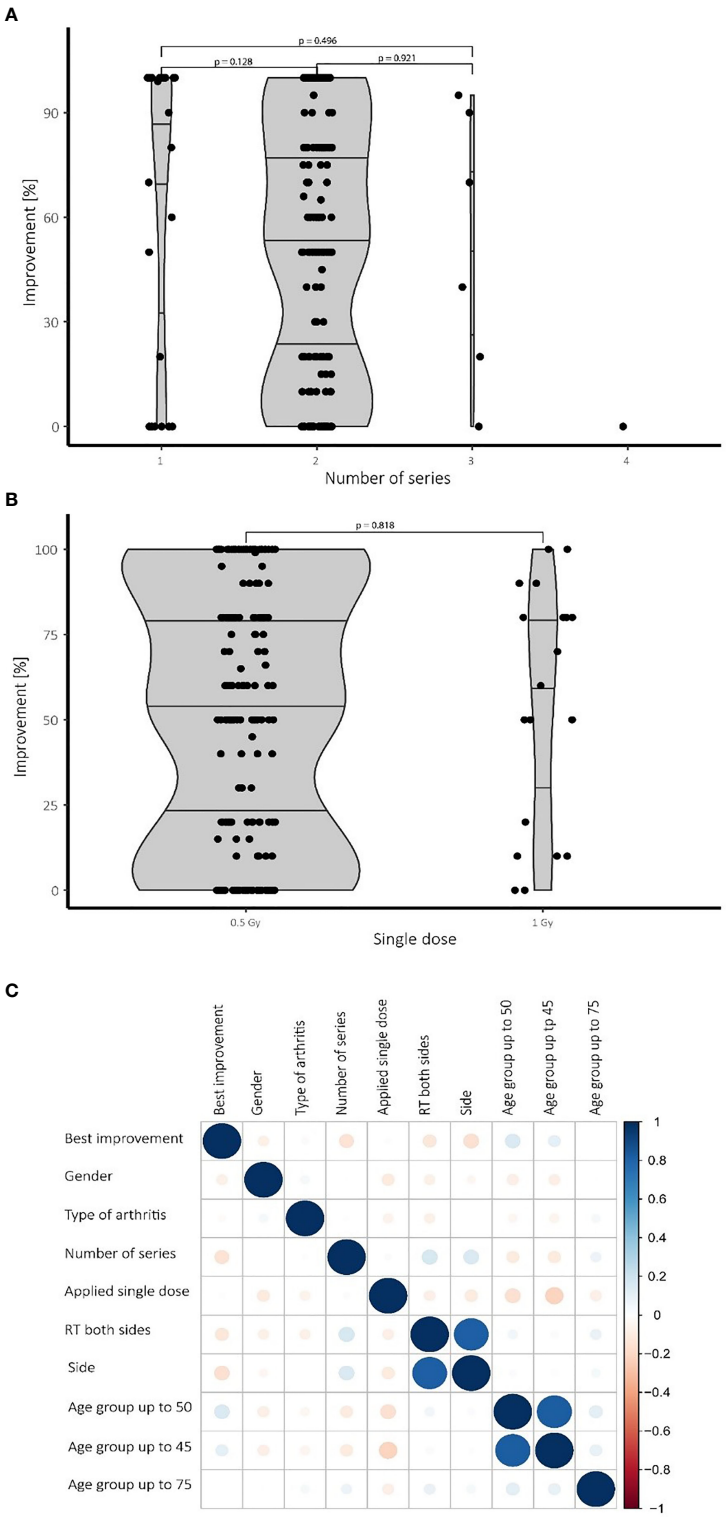

FIGURE 2 | Therapeutic success depending on the number of series and applied single doses also depending on confounding factors. **(A)** While most patients received two series of LDRT, no significant differences in treatment effects have been observed for a higher number of series. **(B)** No significant difference in treatment outcome was observed comparing the 0.5 Gy and the 1.0 Gy group. **(C)** Heat map visualizing various confounding factors: Blue color symbolizes positive correlations while red dots represent negative connections. The size of the dots is proportional to the strength of the correlation. Younger patients (up to 50 years), for example, tend to show a better improvement and need fewer series than older patients. N=196 patients.

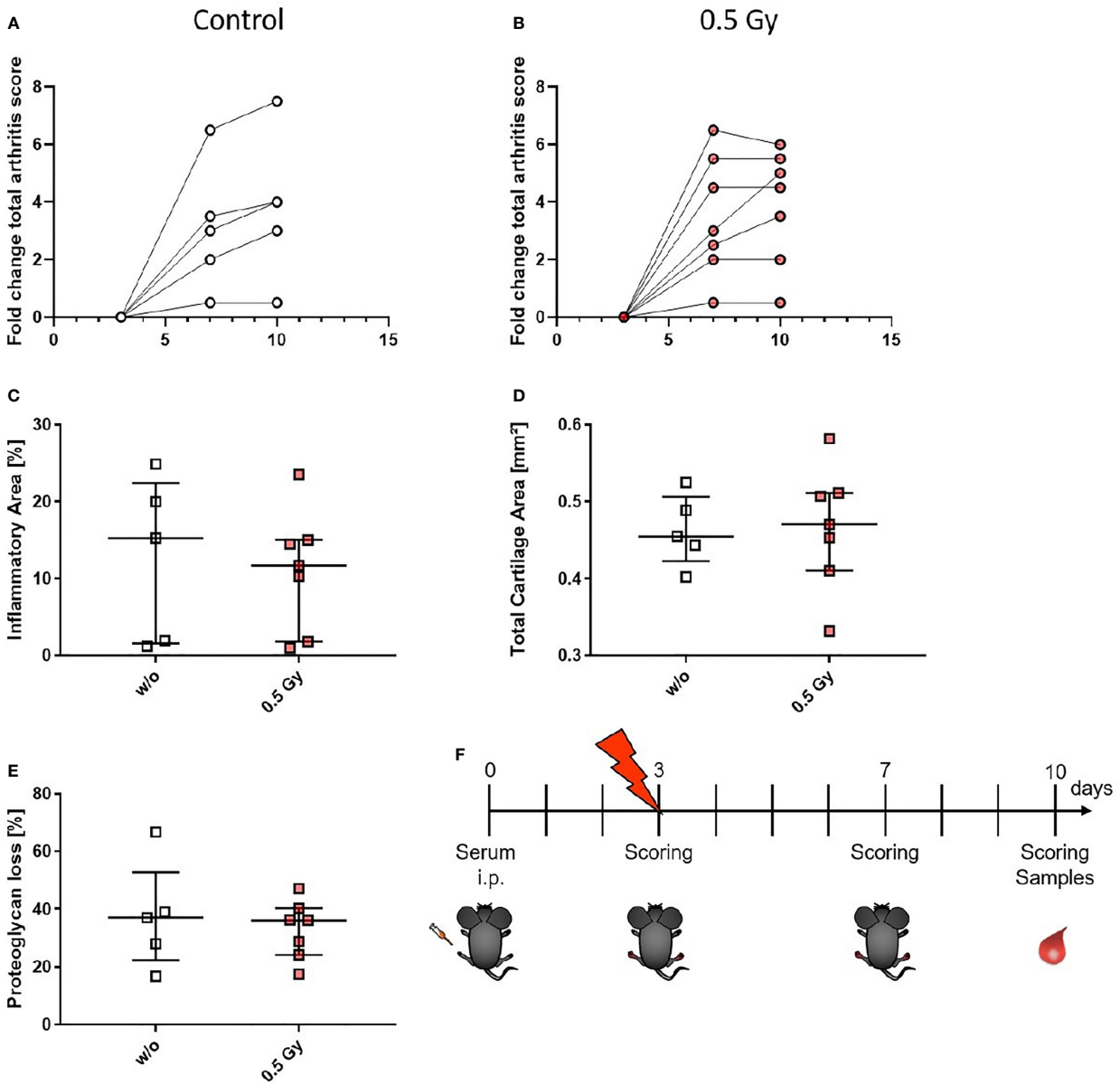

FIGURE 3 | LDRT with 0.5 Gy stabilizes the arthritis score and slightly reduces the inflammatory area in K/BxN serum transfer mice. Age and sex matched mice were injected intraperitoneal (i.p.) with 200µl of K/BxN serum and either locally irradiated with 0.5 Gy X-rays or mock treated on day 3 after the injection (nw/o=5; n0.5Gy=7). Over the entire experimental procedure, arthritis score was assessed **(A, B)**. 7 days after the irradiation hind legs of treated and untreated animals were collected, decalcified, paraffin embedded and cut into 1µm thin slices. Histomorphological evaluation was carried out using the OsteoMeasure™ system (OsteoMetrics, Decatur, GA, USA) after staining with hematoxylin eosin for inflammatory areas **(C)** and toluidinblue for cartilage areas **(D)** and proteoglycan loss **(E)**. **(F)** Shows timeline of pre-clinical experiments: Female C57Bl/6 mice were injected i.p. on d0. On d3 after the injection, mice were scored and randomly distributed into two groups. While one group received mock treatment, the other received 0.5 Gy of locally applied X-rays. Both groups were scored again on d7 and d10. On d10 mice were sacrificed and samples (whole blood, serum, bone marrow and hind feet) were collected. Data is presented as Median+IQR.

generally systemic response, and therefore examined the peripheral blood of the animals *via* flow cytometry (see **Figure 5**). Monocytes/macrophages (**Figure 5B**) and NK cells (**Figure 5C**) tended to be lower in LDRT treated animals in comparison to mock treated ones. In addition, similar to the findings in the BM (**Figure 4**), T cell numbers in LDRT treated animals were reduced (**Figure 5D**), while no shift from CD8+ (**Figure 5F**) to CD4+ T cells (**Figure 5E**) could be observed in the peripheral blood, as both T cell subsets were found to be generally decreased after LDRT.

Notably, we found slightly increased numbers of exhausted CD8+ PD-1+ T cells in LDRT treated animals (**Figure 5H**), while

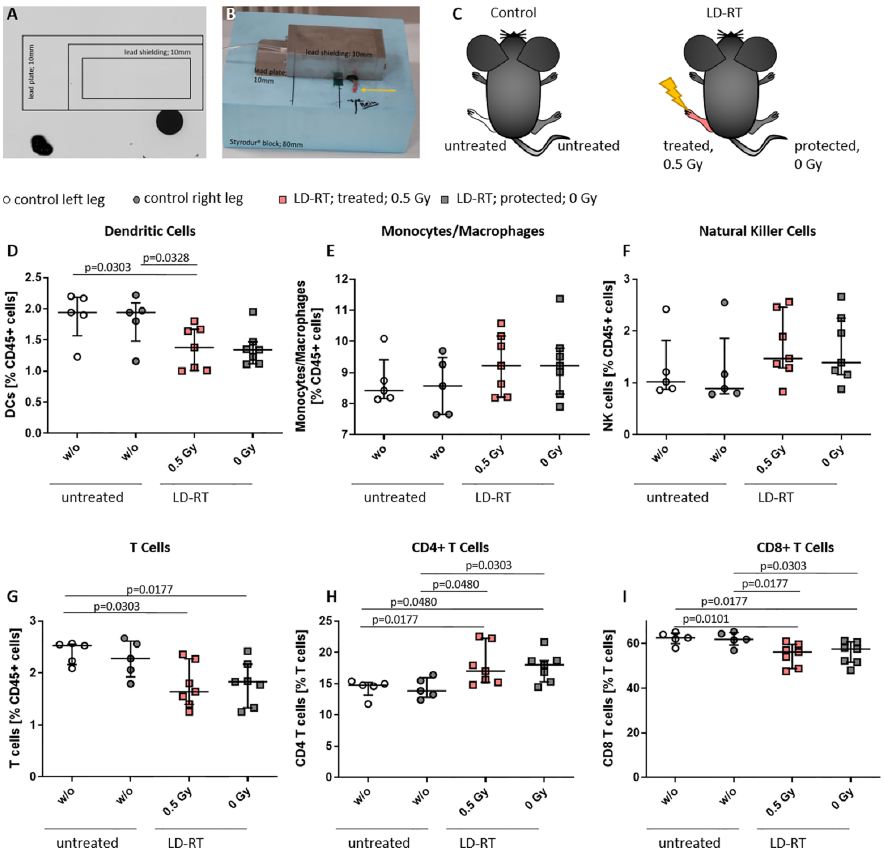

FIGURE 4 | Locally applied LDRT with 0.5 Gy systemically alters distinct immune cell subsets in the bone marrow of treated and protected legs of K/BxN serum transfer mice. Age- and sex-matched mice were injected i.p. with 200µl of K/BxN serum and either locally irradiated with 0.5 Gy X-rays or mock treated on day 3 after the injection (nw/o=5; n0.5Gy=7) **(A–C)**. 7 days after the irradiation, bone marrow was collected and flow cytometry analysis was carried out for the indicated immune cell subtypes **(D–I)**. The figure shows different immune cell subsets as found in the left or right hind leg of mock treated (control left/right leg) and irradiated animals (treated 0.5 Gy or protected 0 Gy) **(C)**, respectively. Data is presented as Median + IQR, statistical analysis was carried out using Mann-Whitney U test, statistical significances are indicated above.

the numbers of exhausted CD4+ PD-1+ T cells were found to slightly decrease after LDRT (**Figure 5G**).

Locally Applied LDRT Results in an Anti-Inflammatory Cytokine Milieu in K/BxN Serum Transfer Mice

As alterations in immune cell subsets in both, bone marrow and peripheral blood, were observed following LDRT, we then looked into serum levels of various cytokines to examine whether altered immune cell subsets could be due to altered cytokine milieu (**Figure 6**). Most of the examined cytokines were generally found to be slightly altered after LDRT (decrease: Interleukin (IL)-1β, IL-2, IL-10, IL-17C, IL-22, Interferon (IFN)-γ, Tumor necrosis factor (TNF)-α; increase: IL-4, IL-6, IL12p70, IL-17E/IL-25 KC, MIP-3α; no alteration: IL-5) when being compared to serum levels of mock treated control animals. However, significantly increased serum levels were found for IL-4 (**Figure 6C**) and IL-6 (**Figure 6E**), while IL-17A levels were found to be significantly decreased (**Figure 6H**) after LDRT.

DISCUSSION

The use of LDRT has often been offered as an alternative treatment option in the treatment of OA and other degenerative joint diseases if first line treatments have failed. This is due to the positive results achieved and the vast body of data attesting to its efficacy (40–43). In the treatment application orthovoltage as well as megavoltage radiotherapy techniques have been used successfully. Despite recent prospective data showing disappointing results, several limitations of these studies like the short-term follow-up of only 3 months, low patient numbers, poor patient selection, reduced treatment volume and too optimistic prognosis assessment for the evaluation of treatment success have to be taken into account (44–47). Data investigating the effect of LDRT on osteoarthritis of the foot have been published before (37, 40). The presented data of our analyses investigates a larger number of patients, and performs detailed correlation of localization and treatment success. As a further difference to previous studies, the present cohort of patients has

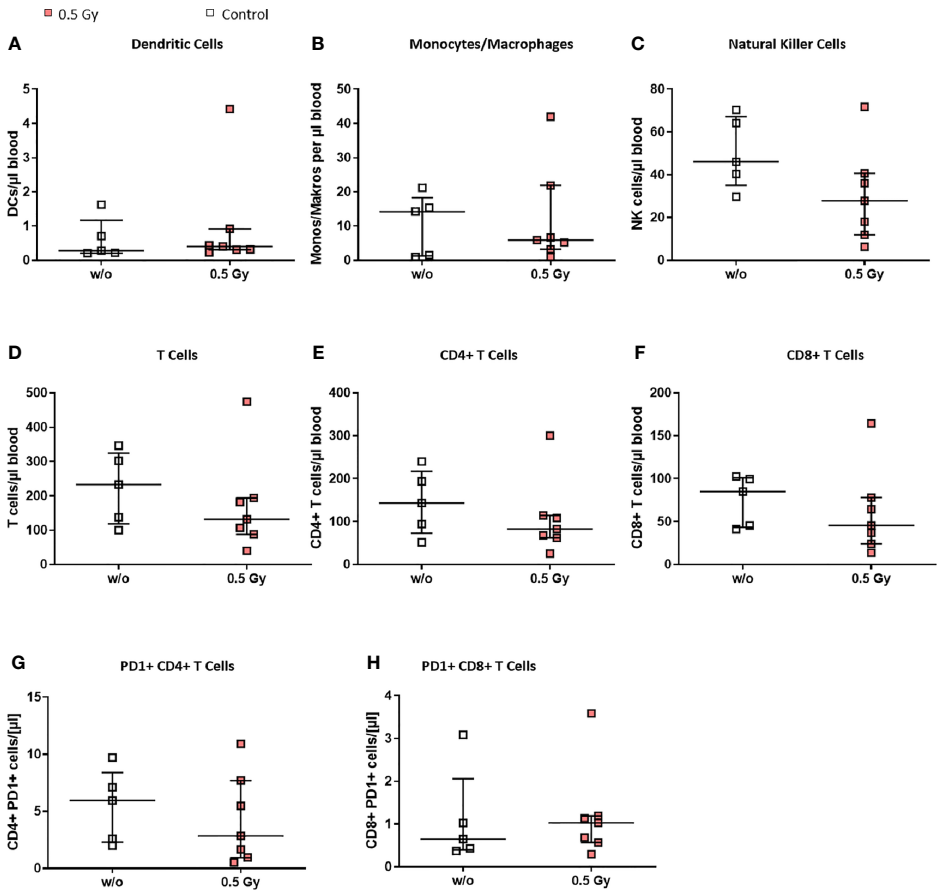

FIGURE 5 | LDRT with 0.5 Gy induces slight changes of immune cells in the peripheral blood of K/BxN serum transfer mice. Age and sex matched mice were injected i.p. with 200µl of K/BxN serum and either locally irradiated with 0.5 Gy X-rays or mock treated on day 3 after the injection (nw/o=5; n0.5Gy=7). 7 days after, the whole blood of all animals was collected, erythrocytes were lysed and flow cytometry analysis for immune cell subtypes **(A–H)** was carried out. Depicted are different immune cell subsets as found in the whole blood of mock treated (w/o) and irradiated animals (0.5 Gy), respectively. Data is presented as Median + IQR, statistical analysis was carried out using Mann-Whitney U test.

homogenously undergone orthovoltage therapy. The analysis of 196 patients confirms the convincing data of LDRT in the treatment of osteoarthritis of the ankle and foot with a majority of patients reporting improvement right after radiation. With only 1% (2/196) of the patients reporting a worsening of symptom burden following radiation and only 25% (48/196) patients reporting improvement <20%, the rate of non-responders has to be regarded as low. Regarding the fact that LDRT is commonly applied for patients that are refractory to classical treatment strategies, this finding is even more promising.

Investigating the success of treatment depending on localization, clearly worse treatment results can be expected for patients suffering from OA of the tarsi transversa. Despite this exact localization not being overrepresented in our cohort and in general thought to be rather uncommon, the involvement seems to be associated with a worse prognosis. While the genuine reasons remain unknown due to the retrospective approach of the present study one possible explanation could be related to previously experienced injuries. While the joint is not only of significant importance during the stance phase but also of utmost importance for pivoting movements, injuries can involve high as well as low energy forces. Mechanism of injury usually involves twisting force to the plantar flexed foot requiring carful diagnosis and high-quality radiographs (48). The high rates of up to 40% of misdiagnosis could therefore lead to long term chronic impairment (48). Another explanation could be due to the joint of the tarsi transversa showing the highest maximum joint reaction forces among all joints of the foot, potentially hindering recovery (49).

While a large number of investigations using classifications of forefoot, midfoot and hindfoot have been carried out, very few data is published on the affection of the side of the feet. Our results show no difference in treatment success between the right and the left foot, while patients with symptoms of the right foot seem to respond better to treatment compared to patients suffering symptoms of both feet. One possible explanation could be seen in the fact that in most patients the right foot is the dominant foot and thus more prone to acute inflammatory conditions that are

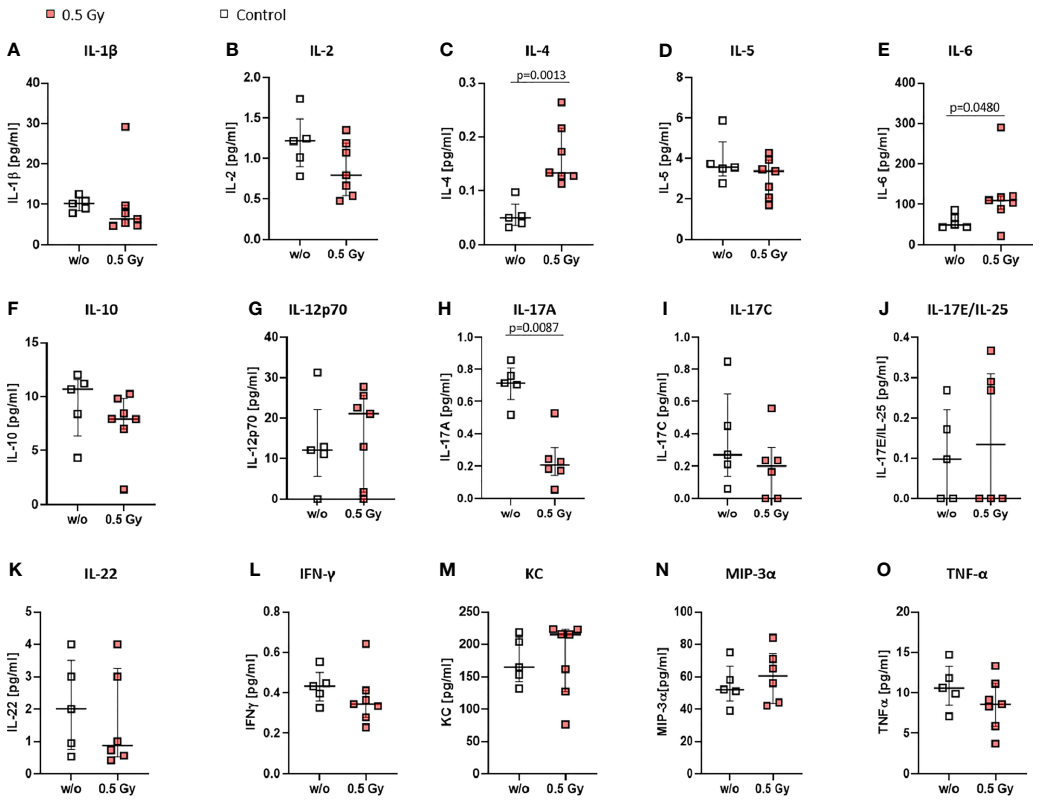

FIGURE 6 | Locally applied LDRT with 0.5 Gy affects pro-inflammatory cytokines in K/BxN serum transfer mice. Age and sex matched mice were injected i.p. with 200µl of K/BxN serum and either locally irradiated with 0.5 Gy X-rays or mock treated on day 3 after the injection (nw/o=5; n0.5Gy=7). On day 7 after the irradiation, serum was collected and analyzed via MSD Multiplex Assay **(A-–O)**. Depicted are serum levels of various cytokines playing a role in inflammatory processes **(A–O)**. Data is presented as Median + IQR, statistical analysis was carried out using Mann-Whitney U test, statistical significances are indicated above.

more addressable by LDRT, while affection of both feet could possibly occur due to more degenerative processes. The lack of significance for the left foot could possibly be due to a combination of inflammatory and degenerative processes.

Regarding the number of applied series, no tendency towards improved results for a higher number of series can be detected in our cohort. While the application of two series is most common, the request for further series, which are applied only on an individual basis and on personal request, implies that patients may experience worsening of symptoms following a good initial response and strive towards recovery of their initial treatment success. Although the application of a third series does not significantly improve treatment outcome the results at least suggest that a recovery after initial worsening seems to be possible. Apart from the very small number of patients in this cohort, our data does not support the application of a fourth series. Despite no side effects being reported in our cohort the benefit of additional LDRT series should be discussed with the patient and balanced against the potential radiation risk (50). While there is a vast body of data showing that a single dose of 0.5 Gy is superior to 1.0 Gy regarding anti-inflammatory effects, our data also does not support the application of a single dose per fraction of 1.0 Gy, despite being often utilized and still embedded in guidelines (19, 51).

While OA is known to be a disease of more advanced age, it is even more impressive and a novel result to see that younger patients show better improvement (**Table 2**). Younger patients might suffer more from inflammatory conditions rather than advanced degenerative conditions which are more addressable by LDRT.

As radiobiological data recommends, we used a single dose of 0.5 Gy for our animal experiments. While in our patient study neither dosage showed superiority over the other, in general, a reduced dosage is always advisable, especially in foresight of potential additional LDRT series, as mentioned above. In previous studies (19) we already showed that in a human TNF-α transgenic mouse model, local irradiation with 0.5 Gy leads to an improvement of inflammatory areas not only in the irradiated but also in distant extremities, while bone erosions were only reduced locally at the site of irradiation. We therefore hypothesize, that there are several mechanisms involving inflammation and bone repair that are responsible for LDRT mediated beneficial effects. This is also visible in the examined patient cohort, as most patients report a reduction in pain levels, while data does not show improvement in all of the joints. We therefore aimed to look into immunological modifications after LDRT in a K/BxN serum transfer mouse model, in order to better understand modulation of inflammation after LDRT which could be related to improved pain perception in patients.

While OA is generally looked at as a non-inflammatory disease, increasing evidence points towards inflammatory processes at the site of bone erosions as well. In that matter, OA patients often show infiltration of the synovial membrane by immune cells such as e.g. macrophages, T cells, B cells natural killer cells (NKs), and DCs, all of these immune cells can also be found in the mouse model (29, 52).

When looking into the BM, we found a significant reduction of DCs in the irradiated legs of locally irradiated mice (see **Figure 4**). While the role of DCs in OA is not yet fully understood, inflammatory DCs are involved in OA inflammation and inhibition of chondrogenesis (53). While significant alterations were found in the BM, no significant differences between LDRT and mock treated animals was found in the blood (**Figure 5**). However, DCs are able to pass on either stimulatory or anti-inflammatory signals to T cells and B cells (54), in the form of cytokines. In the case of T cells, IL-12p70 for the induction of T_H1, IL-4 for T_H2, and IL-17 for T_H17 cells (55), are of special interest. As can be seen in the cytokine profile in the serum of LDRT treated mice, IL-12p70 was found to be slightly, and IL-4 to be significantly increased after LDRT in the serum of the mice (**Figures 6C, G**). This potentially indicates an increased T_H1 and T_H2 response, while IL-17A levels were significantly reduced (**Figure 6H**), suggesting a reduced number or activity of T_H17 cells. While T_H17 cells are predominantly looked at as target cells in RA, there are also indications of T_H17 cells being elevated in OA lesions as well (52). Reduced amounts of IL-17A might thus contribute to an overall anti-inflammatory response in LDRT treated animals.

While total T cell numbers were reduced in the BM (**Figure 4**) and blood (**Figure 5**), a shift from CD8+ in favor of CD4+ T cells was only visible in the BM. While CD8+ T cells have not been found to be key players in OA, they have been found to be able to significantly shape OA pathogenesis (52). A reduction in CD8+ and increase of CD4+ T cells might therefore add to the overall beneficial anti-inflammatory and analgesic effects of LDRT in OA. While these differences were not found in the peripheral blood of treated animals, we did find a slight increase in CD8+ PD-1+ T cells, while CD4+ PD-1+ T cells were decreased (**Figure 5**). T cell exhaustion is characterized by increased amounts of inhibitory surface receptors, one of them being PD-1 (56). This finding thus points towards a potential inhibition of cytotoxic T cells, while the activity of CD4+ T cells is not compromised by LDRT.

In general, differences in immune cell subsets in the peripheral blood were lower than those in the BM. A potential explanation for alterations of immune cell subsets in the periphery is the influence of an altered cytokine milieu. Indeed, we also found alterations in the cytokine milieu in the serum of treated animals (see **Figure 6**). While, in general, pro-inflammatory cytokines were found to be slightly reduced after LDRT with 1x 0.5 Gy, IL-6 (**Figure 6**) on the other hand was found to be significantly increased. IL-6 is generally looked at as a pro-inflammatory cytokine that is involved in a plethora of pathways, one of them being bone metabolism. While it mainly has pro-resorptive and -inflammatory properties, under certain conditions it can also show anti-resorptive effects on bone through e.g. an increase in osteprotegerin, a potent inhibitor of osteoclastogenesis (57). However, further research is needed in elucidating the effects of IL-6 in this specific setting.

Among the most prominent alterations is IL-4 that was found to be significantly upregulated after LDRT (**Figure 6**). IL-4 is involved in the induction of T_H2 cells, enhances IL-10 production in T_H1 cells, as well as polarizes macrophages towards a more anti-inflammatory phenotype. Additionally, it has been found to have antagonistic effects in OA with a special emphasis on chondroprotective effects, which, however, where not visible in the short observation period following LDRT (**Figures 3D, E**). In that matter Wojdasiewicz et al. summarized that it was found to inhibit degradation of proteoglycans through an inhibition of matrixmetalloproteinases (58). Our findings thus suggest a potential beneficial effect of LDRT on cartilage degradation in OA at later timepoints.

Summarizing our study, some limitations have to be addressed: While selecting radiological findings or questionnaires as endpoint seems intuitive for the measurement of the clinical effect, these exact scales haven not proven valid and sensitive for the recording of the efficacy of LDRT in previous studies (44, 45). Nevertheless one point that needs to be addressed in future studies is the severity of OA. Different grades of OA should be correlated to treatment results to increase informative value. After all we are convinced that biomarkers can be a lot more sensitive. While in the present study patients were referred for LDRT mostly by their orthopedic specialist after failing several preceding treatment approaches, the time interval between initial imaging and actual treatment could have varied a lot between patients which is why we chose not to evaluate initial imaging. For future prospective studies if imaging is intended we would recommend imaging right before treatment especially using MRI as this is the best modality to capture anti-inflammatory changes. Despite functionality tests being outside the scope of the present study they could underline the clinical significance to this treatment method in a prospective setting. Including patient logbooks reporting on medication intake and pain perception could further help to distinguish LDRT-mediated effects from medication related improvement in order to reduce bias in data interpretation and need to be subject in prospective trials. Regarding our pre-clinical data, we have to stress, that neither this, nor an alternative available OA model, is able to completely resemble the situation in our patient cohort. Especially, since localization and severity of OA can significantly vary between patients. However, as patient material usually is scarce, the present pre-clinical insights could possibly improve future study designs by indicating potential key factors of the involved biological mechanisms. This enables an optimized usage of patient material in future prospective studies.

In conclusion, LDRT is highly effective in the majority of patients undergoing treatment for OA of the foot and ankle. While clinically acquired data are justifiably predominantly utilizing clinical questionnaires and radiographical signs, the underlying molecular mechanisms have not been investigated sufficiently. Our results clearly show local as well as systemic effects in a mouse model, which could be responsible for the beneficial clinical results achieved by LDRT. One can further conclude, that the observed anti-inflammatory and analgesic effects of LDRT are not mediated by a single pathway, but rather

by the interplay of many individual factors. Nevertheless, further pre-clinical research as well as placebo-controlled patient studies are necessary in order to fully understand the underlying mechanisms Our results should serve as a basis for well-reasoned and carefully planned placebo-controlled patient studies in the future. By improving the understanding of the underlying molecular processes and presenting our convincing clinical results, we hope to encourage more clinicians to rely more on this low risk and cost effective treatment option.

DATA AVAILABILITY STATEMENT

The data presented in this study are available from the corresponding author on reasonable request.

ETHICS STATEMENT

The studies involving human participants were reviewed and approved by Ethics Committee of the Friedrich-Alexander-Universität Erlangen-Nürnberg. Written informed consent was obtained from all patients before LDRT. In addition, patients provided written informed consent for the retrospective analysis of their data, as well as the publication of the data in a pseudonymized manner (ethical approval Ref.169_21 Bc, FootRetroRad trial). The animal procedures have been reviewed and approved by the "Regierung of Unterfranken" and were conducted in accordance with the guidelines of the Federation of European Laboratory Animal Science Associations (FELASA) Approval numbers: 55.2-DMS-2532-2-114 from 13 November 2015 and 10 December 2015; TS-3/14 from 21 February 2014).

AUTHOR CONTRIBUTIONS

TW, LD, and UG designed the study and wrote the manuscript. TW analyzed patient data, LD performed and analyzed pre-clinical data, MR, A-JD, and MS helped performing the experiments. J-GZ performed the statistical analysis of patient data. FN helped with the design of K/BxN model experiments and contributed to writing the manuscript. BF designed the *in vivo* irradiation chamber and performed irradiation of mice. RF contributed to the experimental design and writing of the manuscript. SL, OO, FP, and MH critically revised the manuscript and contributed to writing the article. All authors contributed to the article and approved the submitted version.

FUNDING

This work was funded by the *Bundesministerium für Bildung und Forschung* (BMBF; GREWIS, 02NUK017G, GREWIS-alpha, 02NUK050E; as well as FOR 2886) as well as the German Research Foundation (DFG; Research Training Group GK16660 as well as CRC1181-A07).

ACKNOWLEDGMENTS

The authors would like to thank Willi Stillkrieg for helping with the *in vivo* irradiation set-up and the group of Prof. Falk Nimmerjahn for providing the K/BxN serum. We further acknowledge the support by the German Research Foundation and the Friedrich-Alexander-Universität Erlangen-Nürnberg within the funding program Open Access Publishing.

REFERENCES

1. C. National Collaborating Centre for Chronic. *National Institute for Health and Clinical Excellence: Guidance, Osteoarthritis: National Clinical Guideline for Care and Management in Adults*. Royal College of Physicians of London, London: Royal College of Physicians (UK) Copyright © 2008 (2008).
2. Pereira D, Peleteiro B, Araújo J, Branco J, Santos RA, Ramos E. The Effect of Osteoarthritis Definition on Prevalence and Incidence Estimates: A Systematic Review. *Osteoarthritis Cartilage* (2011) 19:1270–85. doi: 10.1016/j.joca.2011.08.009
3. Woolf AD, Pfleger B. Burden of Major Musculoskeletal Conditions. *Bull World Health Organ* (2003) 81(9):646–56.
4. Hiligsmann M, Cooper C, Arden N, Boers M, Branco JC, Luisa Brandi M, et al. Health Economics in the Field of Osteoarthritis: An Expert's Consensus Paper From the European Society for Clinical and Economic Aspects of Osteoporosis and Osteoarthritis (ESCEO). *Semin Arthritis Rheum* (2013) 43:303–13. doi: 10.1016/j.semarthrit.2013.07.003
5. Glyn-Jones S, Palmer AJ, Agricola R, Price AJ, Vincent TL, Weinans H, et al. Osteoarthritis. *Lancet* (2015) 386:376–87. doi: 10.1016/S0140-6736(14)60802-3
6. Riskowski J, Dufour AB, Hannan MT. Arthritis, Foot Pain and Shoe Wear: Current Musculoskeletal Research on Feet. *Curr Opin Rheumatol* (2011) 23:148–55. doi: 10.1097/BOR.0b013e3283422cf5
7. Paterson KL, Gates L. Clinical Assessment and Management of Foot and Ankle Osteoarthritis: A Review of Current Evidence and Focus on Pharmacological Treatment. *Drugs Aging* (2019) 36:203–11. doi: 10.1007/s40266-019-00639-y
8. Iagnocco A, Rizzo C, Gattamelata A, Vavala C, Ceccarelli F, Cravotto E, et al. Osteoarthritis of the Foot: A Review of the Current State of Knowledge. *Med Ultrason* (2013) 15:35–40. doi: 10.11152/mu.2013.2066.151.ai1ofr2
9. Karavida N, Notopoulos A. Radiation Synovectomy: An Effective Alternative Treatment for Inflamed Small Joints. *Hippokratia* (2010) 14(1):22–7.
10. Prokein B, Holtmann H, Hautmann MG, Rösler HP, Graeber S, Dzierma Y, et al. Radiotherapy of Painful Heel Spur With Two Fractionation Regimens : Results of a Randomized Multicenter Trial After 48 Weeks' Follow-Up. *Strahlenther Onkol* (2017) 193:483–90. doi: 10.1007/s00066-017-1116-y
11. Rudat V, Tontcheva N, Kutz G, Orovwighose TO, Gebhardt E. Long-Term Effect and Prognostic Factors of a Low-Dose Radiotherapy of Painful Plantar Calcaneal Spurs : A Retrospective Unicenter Study. *Strahlenther Onkol* (2021) 197(10):876–84. doi: 10.1007/s00066-020-01741-6
12. Javadinia SA, Nazeminezhad N, Ghahramani-Asl R, Soroosh D, Fazilat-Panah D, PeyroShabany B, et al. Low-Dose Radiation Therapy for Osteoarthritis and Enthesopathies: A Review of Current Data. *Int J Radiat Biol* (2021) 97(10):1352–67. doi: 10.1080/09553002.2021.1956000
13. Donaubauer AJ, Zhou JG, Ott OJ, Putz F, Fietkau R, Keilholz L, et al. Low Dose Radiation Therapy, Particularly With 0.5 Gy, Improves Pain in Degenerative Joint Disease of the Fingers: Results of a Retrospective Analysis. *Int J Mol Sci* (2020) 21(16):5854. doi: 10.3390/ijms21165854
14. Torres Royo L, Antelo Redondo G, Árquez Pianetta M, Arenas Prat M. Low-Dose Radiation Therapy for Benign Pathologies. *Rep Pract Oncol Radiother* (2020) 25:250–4. doi: 10.1016/j.rpor.2020.02.004
15. Cosset JM, Deutsch E. [Low-Dose Irradiation of non-Malignant Diseases: Did We Throw the Baby Out With the Bathwater?]. *Cancer Radiother* (2021) 25:279–82. doi: 10.1016/j.canrad.2020.09.002

16. Lumniczky K, Impens N, Armengol G, Candéias S, Georgakilas AG, Hornhardt S, et al. Low Dose Ionizing Radiation Effects on the Immune System. *Environ Int* (2021) 149:106212. doi: 10.1016/j.envint.2020.106212
17. Rödel F, Frey B, Manda K, Hildebrandt G, Hehlgans S, Keilholz L, et al. Immunomodulatory Properties and Molecular Effects in Inflammatory Diseases of Low-Dose X-Irradiation. *Front Oncol* (2012) 2:120. doi: 10.3389/fonc.2012.00120
18. Deloch L, Rückert M, Fietkau R, Frey B, Gaipl US. Low-Dose Radiotherapy Has No Harmful Effects on Key Cells of Healthy Non-Inflamed Joints. *Int J Mol Sci* (2018) 19(10):3197. doi: 10.3390/ijms19103197
19. Deloch L, Derer A, Hueber AJ, Herrmann M, Schett GA, Wölfelschneider J, et al. Low-Dose Radiotherapy Ameliorates Advanced Arthritis in hTNF-α Tg Mice by Particularly Positively Impacting on Bone Metabolism. *Front Immunol* (2018) 9:1834. doi: 10.3389/fimmu.2018.01834
20. Chen M, Huang Q, Xu W, She C, Xie ZG, Mao YT, et al. Low-Dose X-Ray Irradiation Promotes Osteoblast Proliferation, Differentiation and Fracture Healing. *PloS One* (2014) 9:e104016. doi: 10.1371/journal.pone.0104016
21. Deloch L, Fuchs J, Ruckert M, Fietkau R, Frey B, Gaipl US. Low-Dose Irradiation Differentially Impacts Macrophage Phenotype in Dependence of Fibroblast-Like Synoviocytes and Radiation Dose. *J Immunol Res* (2019) 2019:3161750. doi: 10.1155/2019/3161750
22. Wunderlich R, Ruhle PF, Deloch L, Rodel F, Fietkau R, Gaipl US, et al. Ionizing Radiation Reduces the Capacity of Activated Macrophages to Induce T-Cell Proliferation, But Does Not Trigger Dendritic Cell-Mediated non-Targeted Effects. *Int J Radiat Biol* (2019) 95:33–43. doi: 10.1080/09553002.2018.1490037
23. Frischholz B, Wunderlich R, Rühle PF, Schorn C, Rödel F, Keilholz L, et al. Reduced Secretion of the Inflammatory Cytokine IL-1β by Stimulated Peritoneal Macrophages of Radiosensitive Balb/c Mice After Exposure to 0.5 or 0.7 Gy of Ionizing Radiation. *Autoimmunity* (2013) 46:323–8. doi: 10.3109/08916934.2012.747522
24. Rödel F, Frey B, Capalbo G, Gaipl U, Keilholz L, Voll R, et al. Discontinuous Induction of X-Linked Inhibitor of Apoptosis in EA.hy.926 Endothelial Cells is Linked to NF-κb Activation and Mediates the Anti-Inflammatory Properties of Low-Dose Ionising-Radiation. *Radiother Oncol* (2010) 97:346–51. doi: 10.1016/j.radonc.2010.01.013
25. Rödel F, Keilholz L, Herrmann M, Weiss C, Frey B, Voll R, et al. Activator Protein 1 Shows a Biphasic Induction and Transcriptional Activity After Low Dose X-Irradiation in EA. *hy.926 endothelial Cells Autoimmun* (2009) 42:343–5. doi: 10.1080/08916930902831597
26. Rodel F, Hofmann D, Auer J, Keilholz L, Rollinghoff M, Sauer R, et al. The Anti-Inflammatory Effect of Low-Dose Radiation Therapy Involves a Diminished CCL20 Chemokine Expression and Granulocyte/Endothelial Cell Adhesion. *Strahlenther Onkol* (2008) 184:41–7. doi: 10.1007/s00066-008-1776-8
27. Calabrese EJ, Calabrese V. Reduction of Arthritic Symptoms by Low Dose Radiation Therapy (LD-RT) is Associated With an Anti-Inflammatory Phenotype. *Int J Radiat Biol* (2013) 89:278–86. doi: 10.3109/09553002.2013.752594
28. Arenas M, Sabater S, Hernández V, Rovirosa A, Lara PC, Biete A, et al. Anti-Inflammatory Effects of Low-Dose Radiotherapy. Indications, Dose, and Radiobiological Mechanisms Involved. *Strahlenther Onkol* (2012) 188:975–81. doi: 10.1007/s00066-012-0170-8
29. Christensen AD, Haase C, Cook AD, Hamilton JA. K/BxN Serum-Transfer Arthritis as a Model for Human Inflammatory Arthritis. *Front Immunol* (2016) 7:213. doi: 10.3389/fimmu.2016.00213
30. Fernandes JC, Martel-Pelletier J, Pelletier JP. The Role of Cytokines in Osteoarthritis Pathophysiology. *Biorheology* (2002) 39(1–2):237–46.
31. Bonnet CS, Walsh DA. Osteoarthritis, Angiogenesis and Inflammation. *Rheumatology* (2004) 44:7–16. doi: 10.1093/rheumatology/keh344
32. Jena A, Taneja S, Rana P, Goyal N, Vaish A, Botchu R, et al. Emerging Role of Integrated PET-MRI in Osteoarthritis. *Skeletal Radiol* (2021) 50(12):2349–63. doi: 10.1007/s00256-021-03847-z
33. Little CB, Zaki S. What Constitutes an "Animal Model of Osteoarthritis" – the Need for Consensus? *Osteoarthritis Cartilage* (2012) 20:261–7. doi: 10.1016/j.joca.2012.01.017
34. Christianson CA, Corr M, Yaksh TL, Svensson CI. K/BxN Serum Transfer Arthritis as a Model of Inflammatory Joint Pain. *Methods Mol Biol* (2012) 851:249–60. doi: 10.1007/978-1-61779-561-9_19
35. Bapat S, Hubbard D, Munjal A, Hunter M, Fulzele S. Pros and Cons of Mouse Models for Studying Osteoarthritis. *Clin Transl Med* (2018) 7:36–6. doi: 10.1186/s40169-018-0215-4
36. Kuyinu EL, Narayanan G, Nair LS, Laurencin CT. Animal Models of Osteoarthritis: Classification, Update, and Measurement of Outcomes. *J Orthop Surg Res* (2016) 11:19–9. doi: 10.1186/s13018-016-0346-5
37. Hautmann MG, Hipp M, Neumaier U, Steger F, Brockmann S, Treutwein M, et al. Radiotherapy for Osteoarthritis of the Ankle and Tarsal Joints-Analysis of 66 Joints. *Strahlenther Onkol* (2020) 196:569–75. doi: 10.1007/s00066-019-01551-5
38. Korn MA, Schmitt H, Angermüller S, Chambers D, Seeling M, Lux UT, et al. Siglec-15 on Osteoclasts Is Crucial for Bone Erosion in Serum-Transfer Arthritis. *J Immunol* (2020) 205:2595–605. doi: 10.4049/jimmunol.2000472
39. Rückert M, Deloch L, Frey B, Schlücker E, Fietkau R, Gaipl US. Combinations of Radiotherapy With Vaccination and Immune Checkpoint Inhibition Differently Affect Primary and Abscopal Tumor Growth and the Tumor Microenvironment. *Cancers (Basel)* (2021) 13(4):714. doi: 10.3390/cancers13040714
40. Hautmann MG, Rechner P, Neumaier U, Süß C, Dietl B, Putz FJ, et al. Radiotherapy for Osteoarthritis-an Analysis of 295 Joints Treated With a Linear Accelerator. *Strahlenther Onkol* (2020) 196:715–24. doi: 10.1007/s00066-019-01563-1
41. Kriz J, Seegenschmiedt HM, Bartels A, Micke O, Muecke R, Schaefer U, et al. Updated Strategies in the Treatment of Benign Diseases-a Patterns of Care Study of the German Cooperative Group on Benign Diseases. *Adv Radiat Oncol* (2018) 3:240–4. doi: 10.1016/j.adro.2018.02.008
42. Mücke R, Seegenschmiedt MH, Heyd R, Schäfer U, Prott FJ, Glatzel M, et al. [Radiotherapy in Painful Gonarthrosis. Results of a National Patterns-of-Care Study]. *Strahlenther Onkol* (2010) 186:7–17. doi: 10.1007/s00066-009-1995-7
43. Seegenschmiedt MH, Katalinic A, Makoski H, Haase W, Gademann G, Hassenstein E. Radiation Therapy for Benign Diseases: Patterns of Care Study in Germany. *Int J Radiat Oncol Biol Phys* (2000) 47:195–202. doi: 10.1016/S0360-3016(99)00537-4
44. Mahler EAM, Minten MJ, Leseman-Hoogenboom MM, Poortmans PMP, Leer JWH, Boks SS, et al. Effectiveness of Low-Dose Radiation Therapy on Symptoms in Patients With Knee Osteoarthritis: A Randomised, Double-Blinded, Sham-Controlled Trial. *Ann Rheum Dis* (2019) 78:83–90. doi: 10.1136/annrheumdis-2018-214104
45. Minten MJM, Leseman-Hoogenboom MM, Kloppenburg M, Kortekaas MC, Leer JW, Poortmans PMP, et al. Lack of Beneficial Effects of Low-Dose Radiation Therapy on Hand Osteoarthritis Symptoms and Inflammation: A Randomised, Blinded, Sham-Controlled Trial. *Osteoarthritis Cartilage* (2018) 26:1283–90. doi: 10.1016/j.joca.2018.06.010
46. Montero A, Sabater S, Rödel F, Gaipl US, Ott OJ, Seegenschmiedt MH, et al. Is it Time to Redefine the Role of Low-Dose Radiotherapy for Benign Disease? *Ann Rheum Dis* (2020) 79:e34. doi: 10.1136/annrheumdis-2018-214873
47. Ott OJ, Micke O, Mücke R, Niewald M, Rödel F, Schäfer U, et al. Low-Dose Radiotherapy: Mayday, Mayday. We've Been Hit! *Strahlenther Onkol* (2019) 195:285–8. doi: 10.1007/s00066-018-1412-1
48. Kutaish H, Stern R, Drittenbass L, Assal M. Injuries to the Chopart Joint Complex: A Current Review. *Eur J Orthop Surg Traumatol* (2017) 27:425–31. doi: 10.1007/s00590-017-1958-0
49. Kim Y, Lee KM, Koo S. Joint Moments and Contact Forces in the Foot During Walking. *J Biomech* (2018) 74:79–85. doi: 10.1016/j.jbiomech.2018.04.022
50. Trott KR, Kamprad F. Estimation of Cancer Risks From Radiotherapy of Benign Diseases. *Strahlenther Onkol* (2006) 182:431–6. doi: 10.1007/s00066-006-1542-8
51. Rödel F, Hantschel M, Hildebrandt G, Schultze-Mosgau S, Rödel C, Herrmann M, et al. Dose-Dependent Biphasic Induction and Transcriptional Activity of Nuclear Factor Kappa B (NF-Kappab) in EA.hy.926 Endothelial Cells After Low-Dose X-Irradiation. *Int J Radiat Biol* (2004) 80:115–23. doi: 10.1080/09553000310001654701
52. Li YS, Luo W, Zhu SA, Lei GH. T Cells in Osteoarthritis: Alterations and Beyond. *Front Immunol* (2017) 8:356. doi: 10.3389/fimmu.2017.00356
53. Alahdal M, Zhang H, Huang R, Sun W, Deng Z, Duan L, et al. Potential Efficacy of Dendritic Cell Immunomodulation in the Treatment of Osteoarthritis. *Rheumatol (Oxford)* (2021) 60:507–17. doi: 10.1093/rheumatology/keaa745
54. Rühle PF, Wunderlich R, Deloch L, Fournier C, Maier A, Klein G, et al. Modulation of the Peripheral Immune System After Low-Dose Radon Spa Therapy: Detailed Longitudinal Immune Monitoring of Patients Within the

RAD-ON01 Study. *Autoimmunity* (2017) 50:133–40. doi: 10.1080/08916934.2017.1284819
55. Santos PM, Butterfield LH. Dendritic Cell–Based Cancer Vaccines. *J Immunol* (2018) 200:443–9. doi: 10.4049/jimmunol.1701024
56. Miggelbrink AM, Jackson JD, Lorrey SJ, Srinivasan ES, Waibl Polania J, Wilkinson DS, et al. CD4 T-Cell Exhaustion: Does it Exist and What are its Roles in Cancer? *Clin Cancer Res* (2021) 200(2):443–9. doi: 10.1158/1078-0432.CCR-21-0206
57. Ginaldi L, De Martinis M. Osteoimmunology and Beyond. *Curr Med Chem* (2016) 23:3754–74. doi: 10.2174/0929867323666160907162546
58. Wojdasiewicz P, Poniatowski Ł.A., Szukiewicz D. The Role of Inflammatory and Anti-Inflammatory Cytokines in the Pathogenesis of Osteoarthritis. *Mediators Inflammation* (2014) 2014:561459. doi: 10.1155/2014/561459

Conflict of Interest: MH conflict of interest with Merck Serono (advisory role, speakers' bureau, honoraria, travel expenses, research funding); MSD (advisory role, speakers' bureau, honoraria, travel expenses, research funding); AstraZeneca (research funding); Novartis (research funding); BMS (advisory role, honoraria, speakers' bureau); Teva (travel expenses). RF conflict of interest Astra-Zeneca and MSD as well as honoraria from Merck Serono, Astra-Zeneca, MSD, Novocure and research funding from Fresenius Nutrition, Merck Oncology, MSD, Astra-Zeneca, Novocure and Siemens AG. FP reports grants and speaker fees from Siemens Healthcare GmbH not related to the present work.

The remaining authors declare that the research was conducted in the absence of any commercial or financial relationships that could be construed as a potential conflict of interest.

frontiers in Immunology

CORRECTION
published: 07 February 2022
doi: 10.3389/fimmu.2022.859489

Corrigendum: Low Dose Radiation Therapy Induces Long-Lasting Reduction of Pain and Immune Modulations in the Peripheral Blood - Interim Analysis of the IMMO-LDRT01 Trial

Anna-Jasmina Donaubauer[1,2], Ina Becker[1,2], Thomas Weissmann[2], Birgitta M. Fröhlich[1,2], Luis E. Muñoz[3], Thomas Gryc[2], Manuel Denzler[1,2], Oliver J. Ott[2], Rainer Fietkau[2], Udo S. Gaipl[1,2†] and Benjamin Frey[1,2†]*

[1] Translational Radiobiology, Department of Radiation Oncology, Universitätsklinikum Erlangen, Friedrich-Alexander-Universität Erlangen-Nürnberg (FAU), Erlangen, Germany, [2] Department of Radiation Oncology, Universitätsklinikum Erlangen, Friedrich-Alexander-Universität Erlangen-Nürnberg (FAU), Erlangen, Germany, [3] Department of Internal Medicine 3 -Rheumatology and Immunology, Friedrich-Alexander-University Erlangen-Nürnberg (FAU), Universitätsklinikum Erlangen, Erlangen, Germany

OPEN ACCESS

Edited and Reviewed by:
Michal Tomcik, Institute of Rheumatology, Prague, Czechia

****Correspondence:***
Udo S. Gaipl
udo.gaipl@uk-erlangen.de

[†]These authors have contributed equally to this work and share senior authorship

Specialty section:
This article was submitted to Autoimmune and Autoinflammatory Disorders, a section of the journal Frontiers in Immunology

Received: *21 January 2022*
Accepted: *25 January 2022*
Published: *07 February 2022*

Citation:
Donaubauer A-J, Becker I, Weissmann T, Fröhlich BM, Muñoz LE, Gryc T, Denzler M, Ott OJ, Fietkau R, Gaipl US and Frey B (2022) Corrigendum: Low Dose Radiation Therapy Induces Long-Lasting Reduction of Pain and Immune Modulations in the Peripheral Blood - Interim Analysis of the IMMO-LDRT01 Trial. Front. Immunol. 13:859489. doi: 10.3389/fimmu.2022.859489

Keywords: low dose radiation therapy (LDRT), immune status, immunophenotyping, chronic degenerative and inflammatory diseases, subjective pain level, x-rays

A Corrigendum on

Low Dose Radiation Therapy Induces Long-Lasting Reduction of Pain and Immune Modulations in the Peripheral Blood – Interim Analysis of the IMMO-LDRT01 Trial

By Donaubauer A-J, Becker I, Weissmann T, Fröhlich BM, Muñoz LE, Gryc T, Denzler M, Ott OJ, Fietkau R, Gaipl US and Frey B (2021). Front. Immunol. *12:740742. doi: 10.3389/fimmu.2021.740742*

In the original article, there was an error. The mistake is found in the sentence "While the total number of leukocytes remained unchanged in the peripheral blood, LDRT induced a slight reduction of eosinophils, basophils and plasmacytoid dendritic cells and an increase of B cells." in the abstract of the article.

As it is correctly stated in the results section of the paper, the eosinophils, the basophils and the plasmacytoid dendritic cells increased, while the B cells were decreased.

A correction has been made to the **Abstract**:

"While the total number of leukocytes remained unchanged in the peripheral blood, LDRT induced a slight increase of eosinophils, basophils and plasmacytoid dendritic cells and a decrease of B cells."

The authors apologize for this error and state that this does not change the scientific conclusions of the article in any way. The original article has been updated.

frontiers in Immunology

ORIGINAL RESEARCH
published: 11 March 2022
doi: 10.3389/fimmu.2022.836646

Role of Dynamic Actin Cytoskeleton Remodeling in Foxp3$^+$ Regulatory T Cell Development and Function: Implications for Osteoclastogenesis

Sebastian Dohnke[1,2], Stephanie Moehser[1,2], Alexey Surnov[3†], Thomas Kurth[4], Rolf Jessberger[3], Karsten Kretschmer[2] and Annette I. Garbe[1]*

[1] Osteoimmunology, Center for Regenerative Therapies Dresden (CRTD), Center for Molecular and Cellular Bioengineering (CMCB), Technische Universität Dresden, Dresden, Germany, [2] Molecular and Cellular Immunology/Immune Regulation, Center for Regenerative Therapies Dresden (CRTD), Center for Molecular and Cellular Bioengineering (CMCB), Technische Universität Dresden, Dresden, Germany, [3] Institute of Physiological Chemistry, Medical Faculty Carl Gustav Carus, Technische Universität Dresden, Dresden, Germany, [4] Center for Molecular and Cellular Bioengineering, Technology Platform, Electron Microscopy and Histology Facility, Technische Universität Dresden, Dresden, Germany

OPEN ACCESS

Edited by:
Lisa Deloch, Universitätsklinikum Erlangen, Germany

Reviewed by:
Xiuwei Yang, University of Kentucky, United States
Giacomina Brunetti, University of Bari Aldo Moro, Italy

***Correspondence:**
Annette I. Garbe
Annette.Garbe@tu-dresden.de

†Present Address:
Alexey Surnov, Helmholtz Zentrum München, Munich, Germany

Specialty section:
This article was submitted to Autoimmune and Autoinflammatory Disorders, a section of the journal Frontiers in Immunology

Received: *15 December 2021*
Accepted: *17 February 2022*
Published: *11 March 2022*

Citation:
Dohnke S, Moehser S, Surnov A, Kurth T, Jessberger R, Kretschmer K and Garbe AI (2022) Role of Dynamic Actin Cytoskeleton Remodeling in Foxp3$^+$ Regulatory T Cell Development and Function: Implications for Osteoclastogenesis. Front. Immunol. 13:836646. doi: 10.3389/fimmu.2022.836646

In T cells, processes such as migration and immunological synapse formation are accompanied by the dynamic reorganization of the actin cytoskeleton, which has been suggested to be mediated by regulators of RhoGTPases and by F-actin bundlers. SWAP-70 controls F-actin dynamics in various immune cells, but its role in T cell development and function has remained incompletely understood. CD4$^+$ regulatory T (Treg) cells expressing the transcription factor Foxp3 employ diverse mechanisms to suppress innate and adaptive immunity, which is critical for maintaining immune homeostasis and self-tolerance. Here, we propose *Swap-70* as a novel member of the Foxp3-dependent canonical Treg cell signature. We show that *Swap-70*$^{-/-}$ mice have increased numbers of Foxp3$^+$ Treg cells with an effector/memory-like phenotype that exhibit impaired suppressor function *in vitro*, but maintain overall immune homeostasis *in vivo*. Upon formation of an immunological synapse with antigen presenting cells *in vitro*, cytosolic SWAP-70 protein is selectively recruited to the interface in Treg cells. In this context, *Swap-70*$^{-/-}$ Treg cells fail to downregulate CD80/CD86 on osteoclast precursor cells by trans-endocytosis and to efficiently suppress osteoclastogenesis and osteoclast function. These data provide first evidence for a crucial role of SWAP-70 in Treg cell biology and further highlight the important non-immune function of Foxp3$^+$ Treg cells in bone homeostasis mediated through direct SWAP-70-dependent mechanisms.

Keywords: SWAP-70, Foxp3, actin dynamics, osteoclasts, Treg cell, T cell homeostasis

INTRODUCTION

Foxp3$^+$ regulatory T (Treg) cells are indispensable for the maintenance of immunological self-tolerance and homeostasis. While the majority of Treg cells in the periphery are thymus-derived (thymic Treg cells; tTreg cells), a proportion is generated extrathymically at peripheral sites (peripherally generated Treg cells; pTreg cells) (1–3). Treg cells are able to control immune

responses by suppressing proliferation, activation, differentiation and effector function of various types of immune cells (4–7), whereby they protect the body against autoimmune diseases and excessive inflammation. In addition, there is increasing evidence that Treg cells exert key non-immune functions, including controlling metabolic and regenerative processes, the differentiation of hematopoietic stem cells, and the function of osteoclasts, bone resorbing cells and central mediators of skeletal diseases (8–11). Though it is now generally recognized that the interplay of bone and immune system has a crucial impact on health and disease, the exact function of Treg cells in bone homeostasis remains elusive.

Foxp3$^+$ Treg cells are equipped with multiple mechanisms required to suppress target cells in a cell contact-dependent and/or -independent manner (12). While it has been suggested that Treg cells have the ability to suppress osteoclastogenesis *in vitro*, the mechanisms of suppression are still incompletely understood and controversially discussed: Some reports identified inhibitory cytokines as main players in Treg cell-mediated suppression of osteoclastogenesis (13–15), while other studies proposed cell-cell contact-dependent mechanisms (15–18). Since osteoclasts are derived from hematopoietic precursors, express a variety of immune receptors and are regulated similarly to dendritic cells (DCs) and macrophages, it has been proposed, that osteoclasts play a role in the active regulation of the immune system and can act for example as antigen presenting cells (APCs) (19–21). In this context, it was suggested that, similar to DCs, osteoclast progenitors express on their surface the costimulatory molecules CD80 and CD86, and that Treg cells can control osteoclastogenesis *via* engagement of CD80/CD86 by CTLA-4 (9, 22).

Appropriate Treg cell positioning in the tissue is the prerequisite for effective suppressive capacity *in vivo*. Migration and homing of Foxp3$^+$ Treg cells to their anatomical sites of action, and the *in situ* retention of Treg cells upon immune synapse formation with tissue-resident APCs are driven by dynamic changes in the actin cytoskeleton (23, 24). SWAP-70 has been described as a unique F-actin regulatory protein, which binds and bundles F-actin (25), and has several non-redundant functions in various hematopoietic cells such as polarization (26), endocytosis (27), integrin-mediated adhesion (28, 29), migration (30), and homing (26). In many of these cell types, it was observed that SWAP-70 localizes to sites of active F-actin rearrangement (31–36). *Swap-70*$^{-/-}$ mice exhibit an osteopetrotic phenotype, characterized by increased bone mineral density caused by decreased resorptive activity of osteoclasts defective in F-actin ring formation (31, 35). In addition, earlier studies suggested that *Swap-70* might represent a previously unappreciated member of the Treg cell signature (37). This initial observation prompted us to hypothesize that the control of osteoclast differentiation and function by Treg cells could represent an additional, non-mutually exclusive mechanism underlying the dysregulated bone homeostasis in *Swap-70*$^{-/-}$ mice. Here, we report on the identification of functional defects in *SWAP-70*-deficient Foxp3$^+$ Treg cells and their impact on T cell homeostasis and interaction with osteoclasts.

MATERIALS AND METHODS

Mice

Foxp3^{GFP} mice (38) were crossed to *Swap-70*$^{-/-}$ mice (39) to generate *Swap70*$^{-/-}$ x Foxp3^{GFP} mice. Foxp3$^{RFP/GFP}$ mice expressing the Cre recombinase GFP (GFP-Cre) fusion protein as a Foxp3 BAC transgene and the RFP reporter from an internal ribosome entry site (IRES) downstream of the Foxp3 coding region (Foxp3$^{IRES\text{-}RFP}$) have been previously described (40). Foxp3^{GFP} mice were bred to 2D2 mice (Jackson Laboratory), expressing the transgenic, self-reactive Vα3.2 (2D2) T cell receptor (TCR) specific for myelin oligodendrocyte glycoprotein [MOG, (41)] to generate Foxp3^{GFP} x 2D2-MOG mice. Foxp3^{GFP} x 2D2-MOG mice were then bred with *Swap70*$^{-/-}$ mice to obtain *Swap70*$^{-/-}$ x 2D2 x Foxp3^{GFP} mice. All mice were on C57/BL6 background and were housed and bred either at the animal facility of the CRTD, TU Dresden or the Experimental Center of the Medizinisch-Theoretisches Zentrum, TU Dresden. Animal experiments were performed as approved by the Regierungspräsidium Dresden (AZ 24-9168.24-1/2014-5, 24-9168.24-1/2014-1).

Flow Cytometry and Cell Sorting

Single cell suspensions of thymus, spleen, mesenteric lymph nodes (mesLN) or pooled subcutaneous LN (scLN) (Lnn. mandibularis, Lnn. cervicales superficiales, Lnn. axillares et cubiti, Lnn. inguinales superficiales, and Lnn. subiliaci) were prepared using 70 µm cell strainers (BD Biosciences). DCs were isolated by enzymatic digestion of spleen slices using 0.2 mg/ml Dispase I (Roche), 0.2 mg/ml Collagenase D (Roche) and 25 µg/ml DNase (Qiagen) for 10 min at 37°C and labeled with biotinylated α-CD11c Abs, streptavidin-conjugated microbeads and fluorochromes for enrichment with the AutoMACS Pro magnetic cell separation system. Primary bone marrow-derived macrophages (BMMs) were isolated from long bones of C57BL/6 mice. Bones were rinsed with PBS containing 5% FCS (v/v) and 2 mM EDTA (Thermo Fisher, Invitrogen), followed by lysis of erythrocytes and filtration through a 100 µm mesh. Fluorochrome-conjugated antibodies against CD3 (145-2C11), CD4 (RM4-5), CD8 (53-6.7), CD11b (M1/70), CD11c (HL3), CD25 (PC61, 7D4), CD38 (90), CD44 (IM7), CD45.1 (A20), CD62L (MEL-14), CD69 (H1.2F3), CD80 (16-10-A1), CD86 (GL1), CD103 (M290), CD134/Ox40 (OX-46), cfms (AFS98), ICAM1 (eBioKAT-1), ICOS (7E.17G9), KLRG1 (2F1), Ly6c (HK1.4), Nrp1 (761705), TCRb (H57-597), CTLA-4 (UC10-4F10-11), Helios (22f6), SWAP-70 (polyclonal) were purchased from BD, eBiosciences or Novus Biologicals. For some experiments, cells were labeled with 5 µM eFluor670 cell proliferation dye (eBiosciences). Surface marker expression of CD62L and CD44 was employed to characterize naïve (CD62L$^+$CD44$^-$), effector-memory (CD62L$^-$CD44$^+$) and central memory (CD62L$^+$CD44^{hi}) CD8$^+$ T cell subsets, as well as naïve (CD62L$^+$CD44$^-$) and memory-type (CD62L$^-$CD44$^+$) CD4$^+$ Tcon/Treg cell subsets.

Biotin-conjugated mAbs were additionally labeled with Streptavidin-PE-Cy7 or Streptavidin-ef450 (BD Biosciences, eBiociences). The polyclonal rabbit anti-SWAP-70 antibody

(produced in our lab or purchased from Novus Biologicals) was conjugated with α-chain IgG-AF647 (Thermo Fischer, Invitrogen). Prior to cell sorting, cells were enriched for $CD4^+$ or $CD25^+$ cells using biotinylated mAbs directed against CD4 or CD25, respectively, streptavidin-conjugated microbeads + fluorochromes and the AutoMACS Pro magnetic cell separation system (Miltenyi Biotec). Where indicated, CD3-, CD4- and CD8-depleted splenocytes were used as APCs. For flow cytometric analysis, samples were analyzed on a LSRII or LSR Fortessa. Cell sorting was performed using a FACS Aria II, FACS Aria III or FACS Aria Fusion system (all BD). Cell-cell interactions and/or subcellular localization of Ags detected by fluorochrome-labeled Abs were analyzed by imaging flow cytometry (Amnis Imagestream X Mark II).

T Cell Culture

T cells were cultured in RPMI complete, consisting of RPMI 1680 medium supplemented with 1 mM Sodium pyruvate, 1 mM HEPES, 2 mM Glutamax, 100 U/ml Penicillin, 100 µg/ml Streptomycin, 100 µg/ml Gentamycin, 0.1 mM non-essential amino-acids, 0.55 mM β-mercaptoethanol and 10% FCS (v/v) (all Thermo Fisher, Life Technologies). If not stated otherwise, T cells were cultured in 96-well round-bottom plates (Greiner) at 37°C and 5% CO_2 (Hera Cell 240, Thermo Fisher Scientific) in 200 µl RPMI complete medium. For short-term stimulation, *ex vivo* sorted cells were cultivated for 4 h in the presence of 50 ng/ml phorbol 12-myristate 13-acetate (PMA, Sigma Aldrich) and 200 ng/ml ionomycin (Iono, Calbiochem). Where indicated, 2 µM cyclosporine A (CsA, Sigma Aldrich) was added 1 h prior to stimulation. For polyclonal TCR stimulation, *ex vivo* FACS-purified T cells were cultured in RPMI complete in the presence of Mouse T-Activator CD3/CD28 Dynabeads (Gibco, Thermo Fisher Scientific). For some experiments, 100-1000 U/ml human recombinant IL-2 (Teceleukin, Roche) was added, as indicated. Ag-specific stimulation of 2D2 receptor expressing T cells was performed in the presence of purified DCs (DC: Treg:Tcon cell ratio 1:5:5) and 10 µg/ml MOG_{35-55} peptide (H-Met-Glu-Val-Gly-Trp-Tyr-Arg-Ser-Pro-Phe-Ser-Arg-Val-Val-His-Leu-Tyr-Arg-Asn-Gly-Lys-OH, JPT Peptide Technologies). T cells were cultured for 48 h in 96-well round-bottom plates at 37°C and 5% CO_2 in 200 µl RPMI complete medium.

In Vitro Suppression Assay

The suppressive capacity of $Foxp3^+$ Treg cells was assessed in co-culture with T responder (Tresp) cells. To this end, $CD4^+Foxp3^{GFP-}CD25^-CD44^-CD62L^+$ Tresp cells were FACS-purified and labeled with eFluor670 proliferation dye. $CD4^+Foxp3^{GFP+}CD25^{+/-}$ Treg cells were FACS-purified from CD4 bead-enriched LNs (mesLN, scLN) and spleen. 5 x 10^4 Tresp cells were co-cultured with 2.5 x 10^5 irradiated APCs and Treg cells in different ratios and in the presence of 1 µg/ml soluble α-CD3ϵ. Tresp cell proliferation and CD25 expression was assessed at indicated time points by flow cytometry.

Co-Cultivation of $Foxp3^+$ Treg Cells and Osteoclasts

FACS-purified $CD4^+CD25^+Foxp3^{GFP+}$ Treg cells were TCR-stimulated for 24 h in the presence of 2 α-CD3/CD28-coated beads/cell and 1000 U/ml IL-2 (Teceleukin, Roche) in RPMI complete. BMMs were seeded in minimal essential α-Medium (α-Mem, Merck, Biochrom) supplemented with 20% FCS, 100 U/ml penicillin, 100 µg/ml streptomycin, 2 mM glutamine (all Thermo Fisher, Life Technologies) and 25 ng/ml M-CSF 12 h before activated Treg cells and freshly isolated 20 Gy irradiated anti-CD3/CD4/CD8-depleted splenocytes were transferred to the BMM culture. At day 0, osteoclast differentiation medium (α-Mem with 20% FCS, 100 U/ml penicillin, 100 µg/ml streptomycin, 25 ng/ml M-CSF, 40 ng/ml RANKL) and 5 µg/ml α-CD3ϵ was added. The osteoclast differentiation medium was exchanged at day 2 and 5 and supplemented with fresh α-CD3ϵ. M-CSF was obtained from sterile filtrated L929-M-CSF-conditioned medium (42), human soluble RANKL was produced by recombinant expression in *Pichia pastoris*, kindly provided by B. Hoflack (Biotechnology Center Biotec, Technische Universität Dresden). Cells were stained for tartrate-resistant acid phosphatase (Acid phosphatase, Leukocyte kit, Merck, Sigma Aldrich) at day 6-7 according to the manufacturer's protocol, imaged by light microscopy (Apotome inverse, Zeiss) and analyzed with Cell Profiler V.3.0. For some experiments, the cells were harvested at indicated time points and analyzed by flow cytometry or imaging flow cytometry (Amnis Imagestream X Mark II), respectively.

CTX Elisa

Pre-osteoclast-Treg cell co-culture was seeded on bovine bone slices (#1BON1000, Nordic Bioscience) at different ratios (Treg cell: monocyte ratio: 1:100, 1:10, 1:5; control: without Treg cells). The cell culture supernatants were harvested on day five of the co-culture and carboxy-terminal collagen crosslinks (CTX) concentrations were determined from one sample of each titration step by (CTX-I) ELISA (IDS) and Tecan infinite 200Pro (Tecan i-control V 1.10.4.0 Software) according to the manufacturer's recommendations. Samples were diluted according to the protocol.

Scanning Electron Microscopy

The bone slices were harvested at day 7, fixed in 1% glutaraldehyde in PBS followed by dehydration in a graded ethanol series and critical point drying using the Leica CPD300 drier. Dried samples were mounted on 12 mm aluminium stubs using conductive carbon pads as a substrate and sputter coated with gold (Baltec SCD 050). The samples were analyzed by a table top scanning electron microscope (Hitachi TM 1000) running at 15kV acceleration voltage and using a backscatter electron detector.

Gene Expression Analysis

Total RNA was extracted from 1-5 x 10^5 FACS-purified cells from pooled scLN, mesLN and spleen with the RNeasy Micro kit (all Qiagen) according to the manufacturer's protocol. For quantitative RT-PCR, cDNA was synthesized according to the

manufacturer's recommendations (SuperScript II reverse transcriptase and Oligo-d(T) primers from Invitrogen). The expression levels of mRNA transcripts were determined using the QuantiTect SYBR Green PCR Kit (Qiagen), a Mastercycler ep realplex thermal cycler (Eppendorf) and the following primers: *Cd4:* 5'-CTC ACA GGT CAA AGT ATT GTT G-3'; 5'-GAG AGT CAG CGG AGT TCT C-3'; *CD25:* 5'-ACC ACA GAC TTC CCA CAA CCC ACA-3'; 5'-CGC TCA GGA GGA GGA TGC TGA TGA-3'; *Foxp3* 5'-CCC AGG AAA GAC AGC AAC CTT-3'; 5'-CAA ACA GGC CGC CGT CTG GAG CC-3'; *Il-2*: 5'-CCT GAG CAG GAT GGA GAA TTA CA-3'; 5'-TCC AGA ACA TGC CGC AGA G-3'; *Swap-70*: 5'-ATG TGA GCG AGG ATC TGA AAG-3'; 5'-ATG GTG GAG TAA ATG GCC TG-3'. Expression levels were normalized to *Gapdh* or *HPRT*, as indicated (*Gapdh*: 5'-TGT GAT GGG TGT GAA CCA CGA GAA -3'; 5'-GAG CCC TTC CAC AAT GCC AAA GTT-3'; *HPRT*: 5'-GTC AAC GGG GGA CAT AAA AG-3'; 5'-AGG GCA TAT CCA ACA ACA AAC-3').

Statistical Analysis

Statistical significance was assessed using Prism 6.07. For statistical analysis of two groups, student's t-test was applied. Differences were considered as significant when: * $P \leq 0.05$; ** $P \leq 0.01$; *** $P \leq 0.001$; or **** $P \leq 0.0001$.

RESULTS

Swap-70 Is Constitutively Expressed in Foxp3$^+$ Treg Cells and Up-Regulated Upon TCR-Mediated Stimulation in Initially Naïve Swap-70$^-$ CD4$^+$ Tcon

Consistent with a previous study (37), qPCR analysis of FACS-purified T and B cell populations from pooled peripheral lymphoid organs revealed that *Swap-70* expression in truly naïve CD4$^+$ T cells (CD25$^-$Foxp3^{GFP-}CD62L$^+$CD44$^-$) was at the limit of detection, but significantly increases upon short-term stimulation with PMA/Ionomycin *in vitro*. Notably, *Swap-70* expression was comparable in short-term stimulated and antigen-experienced memory-type CD4$^+$ T cells (CD25$^-$ Foxp3GFP$^-$CD62L$^-$CD44$^+$) (**Figure 1A**, right). As expected, *Il2ra* mRNA was constitutively expressed in naïve and memory-type Treg cells and up-regulated in CD4$^+$ Tcon upon short-term stimulation, while *Foxp3* expression was restricted to Treg cells (**Figure 1A** left, middle). *Swap-70* mRNA was constitutively expressed in naïve and memory-type Foxp3$^+$ Treg cells, with similar expression levels. By comparison, *Swap-70* expression in short-term stimulated Tcon cells accounted for about 24% of the levels detected in Foxp3$^+$ Treg cells. Due to the known high-level constitutive expression of SWAP-70 in the B cell lineage (43), CD19$^+$B220$^+$ B lineage cells were included for comparison. Notably, expression levels of *Swap-70* mRNA in peripheral Foxp3$^+$ Treg cells corresponded to approximately 15% of that of CD19$^+$B220$^+$ B lineage cells (**Figure 1A**, right).

T cell development and Foxp3$^+$ tTreg commitment occurs in the thymus. Taking advantage of Foxp3^{GFP} reporter mice harboring a GFP-Foxp3 fusion protein reporter knock-in allele allowed us to track Foxp3$^+$ thymocytes which are committed to the tTreg cell lineage by flow cytometry (38).

Intracellular (IC) SWAP-70 staining revealed that in the thymus, SWAP-70 protein was highly expressed in Foxp3^{GFP+} CD4 single positive (SP) thymocytes, while its expression was not detectable in Foxp3^{GFP-} CD4SP or CD8SP thymocytes (**Figure 1B** and **Supplementary Figure S1**). In peripheral lymphoid tissues, SWAP-70 protein was neither detectable in naïve, effector-memory and central memory CD8$^+$.

T cells, nor in naïve and memory-type CD4$^+$ Tcon cells, but was exclusively expressed in CD4$^+$Foxp3$^+$ Treg cells. Within the Foxp3$^+$ Treg cell population, memory-type Treg cells exhibited the highest levels of SWAP-70 expression (**Figure 1B** and **Supplementary Figure S1**). While Foxp3^{GFP} expression was readily detectable in both, a fraction of CD4SP thymocytes and of peripheral CD4$^+$ T cells, the two anatomical sites clearly differed in the level of SWAP-70 expression: based on the MFI values of anti-SWAP-70 Ab fluorescence, expression levels of SWAP-70 protein in CD4$^+$Foxp3$^+$ thymocytes were approximately twice as high as in the total CD4$^+$Foxp3$^+$ Treg cell population in the periphery. Normalized MFI values showed that expression levels of SWAP-70 protein in intra- and extrathymic Foxp3$^+$ Treg lineage cells accounted for 4-7% of that of CD19$^+$B220$^+$ B lineage cells (**Figure 1B**).

Swap-70 mRNA Expression Is Controlled by the Nuclear Factor of Activated T cells (NF-AT)

Next, we sought to gain insight into the transcriptional regulation of *Swap-70* in T cells and employed a bioinformatics approach to predict T cell-relevant TF binding sites. Importantly, the Forkhead motif (37) could be identified in close proximity (108 bp), upstream of the transcription start site, implying that *Swap-70* is under the direct control of Foxp3. In addition, the NF-AT consensus sequence and a putative binding site for AP-1 were located 135 bp and 292 bp upstream of the transcription start site, respectively. Furthermore, a zinc finger binding motif, which is a putative binding site for TFs of the zinc finger superfamily, such as Ikaros proteins, was located 974 bp upstream from the transcription start site of *Swap-70* (**Figure 1C**).

To determine whether *Swap-70* is directly regulated by NF-AT, we assessed the impact of cyclosporine A (CsA) treatment on the up-regulation of *Swap-70* in PMA/Ionomycin-stimulated, initially naive CD4$^+$ Tcon and Foxp3$^+$ Treg cells. Our data revealed that PMA/Ionomycin stimulation increased *Swap-70* mRNA levels (3-fold compared to unstimulated) while pretreatment with CsA prevented this effect (**Figure 1D**, left). This response to PMA/Ionomycin stimulation ± CsA is reminiscent of other direct Foxp3 target genes of the Treg signature, such as *Il2ra* [**Figure 1D**, middle, (37, 44)]. In addition, we observed that *Swap-70*$^{-/-}$ Treg cells up-regulated *Il2ra* mRNA upon PMA/Iono stimulation comparable to their

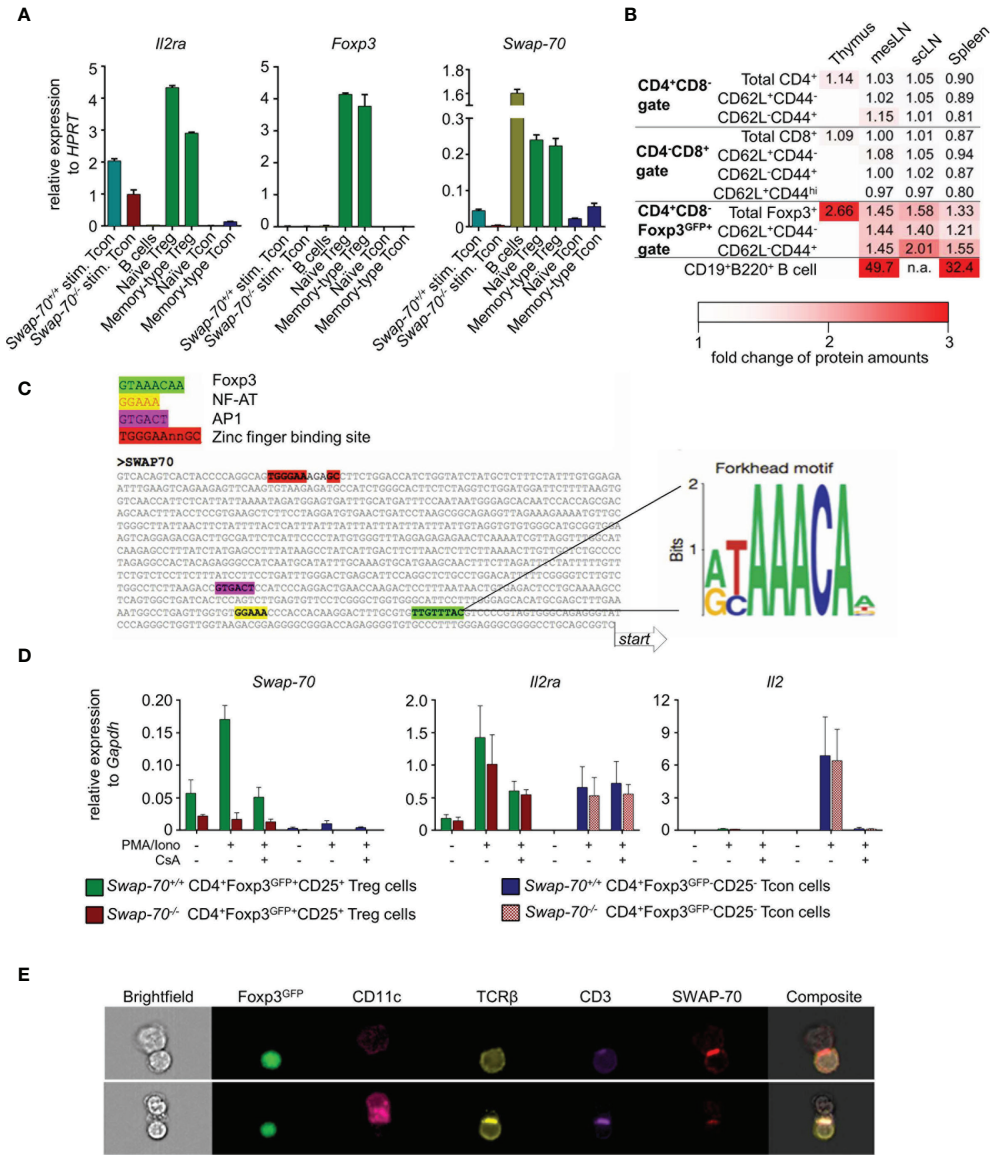

FIGURE 1 | Constitutive SWAP-70 expression in Foxp3$^+$ Treg cells and inducible *Swap-70* expression in short-term stimulated and memory-type CD4$^+$ Tcon cells. **(A)** mRNA expression levels of *IL2ra, Foxp3* and *Swap-70* determined by real-time RT-PCR employing FACS-purified T cell populations (naïve Treg cells, memory-type Treg cells, naïve Tcon cells and memory-type Tcon cells). Where indicated, naïve *Swap-70*$^{+/+}$ and *Swap-70*$^{-/-}$ Tcon were short-term stimulated *in vitro* in the presence of PMA/Ionomycin. Peripheral B cells were used as positive control. Mean values ± S.D. of relative expression determined in a representative experiment (from three independent experiments) are shown for indicated genes. **(B)** Flow cytometric protein level analysis of intracellular (IC) SWAP-70 expression in electronically gated thymic and peripheral (scLN, mesLN, and spleen) T cell subsets. B cells were used as positive control. MFIs of samples from 6 individual mice (n=1 for CD19$^+$B220$^+$ B cells) were normalized to *Swap-70*$^{-/-}$ controls (set to 1). Data are shown as heatmap displaying *Swap-70*$^{+/+}$ to *Swap-70*$^{-/-}$ fold-change values of SWAP-70 expression. See also **Supplementary Figure S1**. **(C)** Identification of putative Foxp3, NF-AT, AP1 and zinc finger binding sites in the promoter region of *Swap-70* by multiple sequence alignment (left). **(D)** mRNA expression levels of *Swap-70, IL2ra* and *Il2* of Treg cells (green, red) and Tcon (blue, purple) cells FACS-purified from *Swap-70*$^{+/+}$ (green, blue) and *Swap-70*$^{-/-}$ mice (red, purple) were cultured for 1h in the absence or presence of cyclosporine A (CsA) prior to a 4h stimulation with PMA/Iono as indicated. Mean values ± S.D. of relative expression (n=4 from 2 independent experiments), determined in triplicate, are shown for indicated genes. **(E)** Representative imaging flow cytometry of co-cultures of FACS-purified Treg cells and Tcon cells expressing the transgenic 2D2 MOG-specific TCR cultured for 48h in the presence of CD11c$^+$ dendritic cells (DCs) (DC: Treg:Tcon cell ratio 1:5:5) and 10 µg/ml MOG peptide. Cell clusters were analyzed for Foxp3^{GFP}, CD11c, TCRβ, CD3 and IC SWAP-70 expression. DC-Treg cell interactions between *Swap-70*$^{+/+}$ DCs and *Swap-70*$^{+/+}$ Treg cells are shown in both rows.

Swap-70$^{+/+}$ counterparts and that CsA completely abrogates *Il2* mRNA transcription in *Swap-70*$^{+/+}$ and *Swap-70*$^{-/-}$ CD4$^+$ Tcon cells (**Figure 1D**, right). In summary, our results identify *Swap-70* as a direct Foxp3/NFAT target and a novel member of the canonical Treg cell signature.

SWAP-70 Is Recruited to the Immunological Synapse of Activated Treg Cells

To address whether SWAP-70 is involved in cytoskeletal rearrangement at the immunological synapse formed between CD4$^+$ Treg/Tcon cells and DCs, we took advantage of 2D2 MOG-specific TCR transgenic Foxp3^{GFP} mice. FACS-purified Foxp3$^+$ Treg cells and CD4$^+$ Tcon cells expressing the transgenic 2D2 TCR were co-cultured in the presence of DCs and MOG peptide. Imaging flow cytometry at day 2 of co-culture revealed that Treg cells could be reliably identified by the expression of TCRβ, CD3 and Foxp3^{GFP} and DCs by CD11c. SWAP-70 was detected in stimulated Foxp3$^+$ Treg cells and DCs, but was barely detectable in stimulated CD4$^+$ Teff cells (**Figure 1E** and data not shown), which is consistent with our qPCR data (**Figure 1A**). Analysis of DC-T cell interactions revealed clustered expression of TCRβ and CD3 at the T cell-APC interface, indicating the formation of the central supramolecular activation cluster (cSMAC) of the immunological synapse. In SWAP-70-proficient Treg cells, SWAP-70 was recruited to the immunological synapse and co-localizes with the cluster. These data provide first direct evidence that, upon TCR : MHC/peptide engagement, cytosolic SWAP-70 protein is selectively recruited to the immunological synapse in primary T cells.

Expression of SWAP-70 During the Instructive Phase of tTreg Cell Development

Considering that Foxp3 expression is not a prerequisite of Treg cell lineage commitment, but rather a consequence thereof (45, 46), we next examined SWAP-70 expression in thymocytes that are still lacking Foxp3 protein expression but are already committed to the tTreg cell lineage. To this end, we employed Foxp3$^{RFP/GFP}$ mice (40), which allow to track developmental stages of thymic Treg cell lineage development based on differential GFP and RFP expression. Early tTreg cell precursors in the instructive phase (stage I) exhibit a Foxp3^{RFP-}Foxp3^{GFP-}CD25$^+$ CD4SP phenotype, Foxp3^{RFP+}Foxp3^{GFP-}CD25$^+$ CD4SP tTreg cells represent precursors in the early consolidation phase (stage II), while Foxp3$^+$ thymocytes at a later developmental stage are Foxp3^{RFP+}Foxp3^{GFP+}CD25^{hi} CD4SP (stage III) (47, 48). Following FACS-purification of CD25$^+$ CD4SP Treg precursor stages according to the differential expression of RFP and GFP (**Figure 2A** and **Supplementary Figure S2A**), cells were stained for expression of IC SWAP-70 and co-expression of IC Helios and Nrp-1 (**Figure 2B** and **Supplementary Figure S2B**). Our analyses revealed high expression levels of Helios, but low expression levels of CD25, Nrp-1 and SWAP-70 during the instructive phase of Treg cell development (stage I). Notably, CD25, Nrp-1 and SWAP-70 were up-regulated in the early consolidation phase (stage II), concomitant with Foxp3$^{IRES-RFP}$, and continuously expressed during the late consolidation phase (stage III), accompanied by Foxp3$^{Cre-GFP}$. MFI values indicated a gradual upregulation of Helios and CD25 during the early and late consolidation phase of tTreg cell lineage commitment (**Figures 2B, C**). Overall, these data show that SWAP-70 expression is not yet detectable in CD25$^-$ CD4SP thymocytes, but is induced concomitantly with CD25, Helios and Nrp-1 in the instructive phase of tTreg cell lineage commitment (stage I) and is progressively up-regulated to high levels during developmental progression and lineage consolidation (stage II and III). The observed kinetics suggests a mechanism of TCR-mediated induction and subsequent Foxp3-mediated amplification/stabilization of SWAP-70 expression during tTreg cell development.

SWAP-70 Expression in Mature Treg Cells Correlates With Expression of CD44, Helios and Nrp-1

There is growing evidence that Helios and Nrp-1 expression is not unequivocally restricted to tTreg cells and that both molecules can be up-regulated upon TCR stimulation in pTreg cells (40, 47, 49, 50). Since our data revealed a correlation between SWAP-70 expression and Helios and Nrp-1 in tTreg cells, we next assessed whether SWAP-70 expression is restricted to the tTreg lineage. For this aim, tTreg and pTreg cells were FACS-purified from scLN of Foxp3$^{RFP/GFP}$ mice (**Figure 2D** and **Supplementary Figure S2C**) and stained for expression of IC SWAP-70, IC Helios and Nrp-1 (**Figure 2E** and **Supplementary Figure S2D**). Similar to Helios and Nrp-1, SWAP-70 expression could not only be detected in tTreg but also to a similar extend in pTreg cells and can therefore not be considered as a tTreg lineage specific marker (**Figures 2E, F**). Consistent with previous reports (49, 51), the vast majority of Foxp3$^+$ CD4SP thymocytes co-expressed high levels of Helios (> 90%), whereas in the periphery Helios expression was restricted to a subset of CD4$^+$Foxp3$^+$ Treg cells (**Figures 2E, F**). Importantly, our data clearly show that SWAP-70 expression correlates with Helios and Nrp-1 expression both in thymus and peripheral lymphoid tissues: high expression levels of SWAP-70 coincided with high Helios and Nrp-1 expression, while CD4$^+$Foxp3$^+$ Treg cells with a Helios^{low}Nrp-1^{low} phenotype were almost negative for SWAP-70 (**Figures 2G, H**). In summary, these results reveal a distinct expression pattern of SWAP-70 within the Foxp3$^+$ Treg cell population and suggest SWAP-70 as a putative marker for Helios^{hi}Nrp-1^{hi} Treg cells.

The Role of SWAP-70 in Immune Homeostasis

To determine the function of SWAP-70 in T cells, we took advantage of the *Swap70*$^{-/-}$ x Foxp3^{GFP} mouse model, that lacks SWAP-70 (39) and carries the Foxp3^{GFP} fluorochrome reporter (38). First, fertility, mortality and cellularity of lymphoid organs were analyzed, to assess whether *SWAP-70*-deficiency affects the

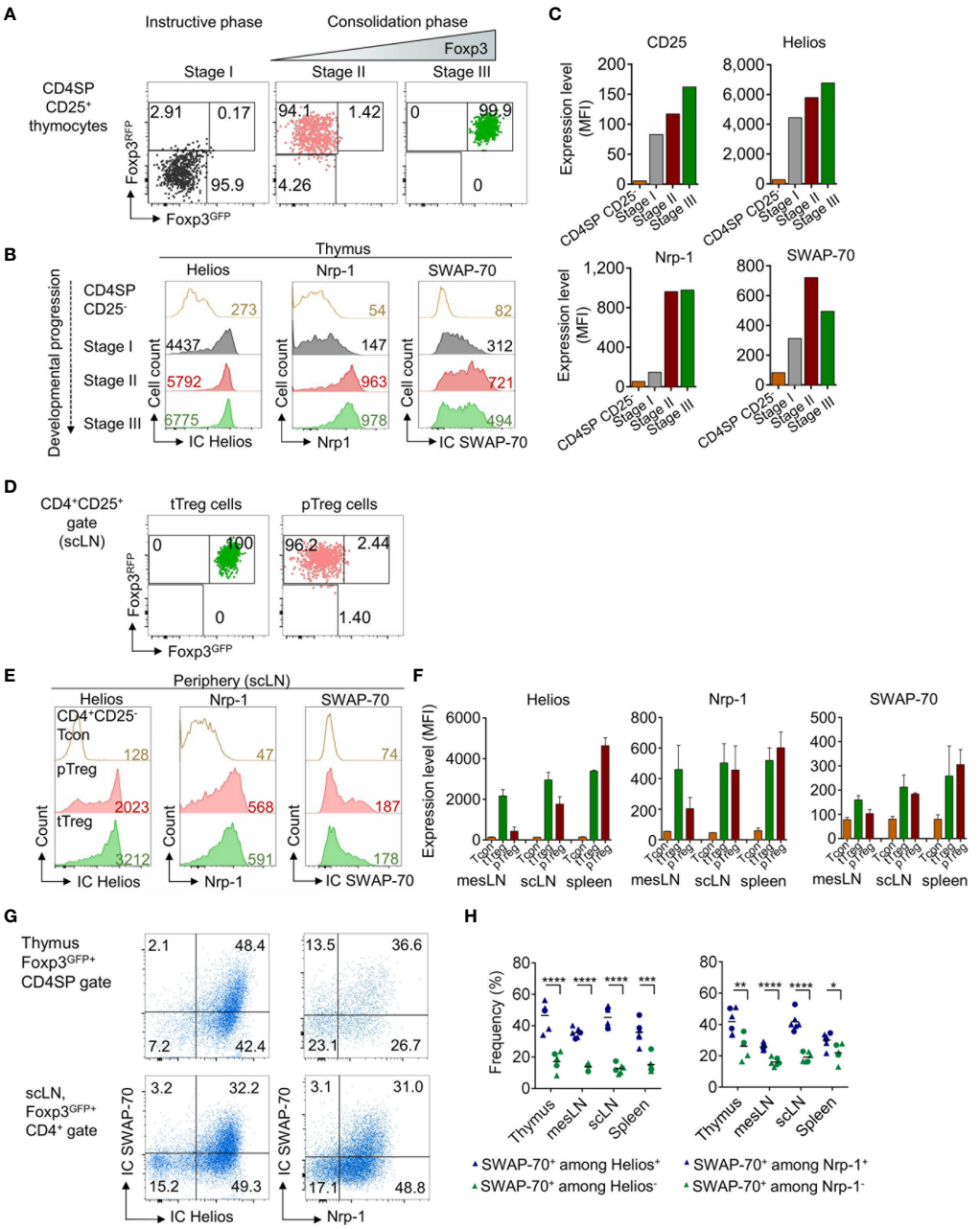

FIGURE 2 | SWAP-70, Helios and Nrp-1 expression during tTreg cell development and in extrathymic Treg cells. **(A)** Postsort analysis of FACS-purified CD4SP CD25$^+$ Treg precursor stages from the thymus of Foxp3$^{RFP/GFP}$ mice showing Foxp3^{GFP} and Foxp3^{RFP} expression. **(B)** IC Helios, Nrp-1 and IC SWAP-70 expression during the instructive phase (Foxp3^{RFP-}Foxp3^{GFP-}CD25$^+$ CD4SP, stage I, grey) and both stages of the consolidation phase (Foxp3^{RFP+}Foxp3^{GFP-} CD25$^+$ CD4SP, stage II, red and Foxp3^{RFP+}Foxp3^{GFP+}CD25^{hi} CD4SP, stage III, green) of tTreg cell lineage commitment. **(C)** Bar charts depict representative expression levels (MFI) of CD25, Helios, Nrp-1 and SWAP-70 in CD4SP CD25$^-$ thymocytes and during Treg cell development (stages I-III). **(D)** Postsort analysis of FACS-purifed tTreg (Foxp3^{RFP+}Foxp3^{GFP+}CD25$^+$CD4$^+$) and pTreg cells (Foxp3^{RFP+}Foxp3^{GFP-}CD25$^+$CD4$^+$) cells isolated from scLN of Foxp3$^{RFP/GFP}$ mice showing Foxp3^{GFP} and Foxp3^{RFP} expression. **(E)** IC Helios, Nrp-1 and IC SWAP-70 expression in CD4$^+$CD25$^-$ Tcon, pTreg and tTreg cells. **(F)** Bar charts depict mean expression levels (MFI) of Helios, Nrp-1 and SWAP-70 in CD4$^+$CD25$^-$ Tcon, pTreg and tTreg cells isolated from different anatomical locations (mesLN, scLN, and spleen). **(G)** Representative flow cytometry of electronically gated Foxp3^{GFP+}CD4SP thymocytes (top) and extrathymic Foxp3^{GFP+}CD4$^+$ Treg cells (scLN, bottom) from Foxp3^{GFP} mice stained for IC SWAP-70 in combination with IC Helios or Nrp-1. **(H)** Graph illustrates frequencies of IC SWAP-70 expressing cells among the respective Foxp3^{GFP+}CD4$^+$CD8$^-$ cell subsets. Symbols and horizontal lines indicate individual mice and mean values, respectively (blue symbols: SWAP-70$^+$ among Helios$^+$ or Nrp-1$^+$ cells, green symbols: SWAP-70$^+$ among Helios$^-$ or Nrp-1$^-$ cells) mean of 6 individual mice shown, circles: 8-9-week-old, triangles 10-13-week-old mice. Numbers in dot plots indicate representative frequencies of gated cells within the respective gate. Numbers in histograms indicate representative MFIs of gated cells. See also See also **Supplementary Figure S2**.

overall fitness of these mice, and whether there are clinical signs of systemic or organ-specific autoimmunity. For this aim, the litter sizes from homozygous *Swap-70*$^{-/-}$ mating trios (2♀ x 1♂) were analyzed and compared with their WT counterparts. The analyzes of 8 WT and 6 *Swap-70*$^{-/-}$ mating trios over a period of 15 months revealed comparable litter sizes and genotype distribution among the litters. The average litter size was 5.7 ± 2.9 pups for WT and 6.3 ± 2.9 pups for *Swap-70*$^{-/-}$ breedings. Large litters of 12-15 pups could occasionally be observed in both groups (**Figure 3A**). Evaluation of 2616 progeny from heterozygous mating trios of the *Swap-70*$^{-/-}$ x Foxp3^{GFP} strain revealed a relatively even distribution of the genotypes (**Figure 3B**): as expected, half of the descendants were heterozygous for the *Swap-70* knockout allele. However, the ratio between *Swap-70*$^{+/+}$ pups and *Swap-70*$^{-/-}$ pups was slightly biased towards the WT (26.9 vs 23.0%). The mortality rate was below 2/100 individual mice and independent of the *Swap-70* genotype (n = 2616 mice, **Figure 3C**). Organ cellularity of thymus and peripheral lymphoid organs (mesLN, scLN, spleen) was similar in *Swap-70*$^{+/+}$ and *Swap-70*$^{-/-}$ mice, implying the absence of severe multi-organ autoimmunity (**Figure 3D**). Overall, mice carrying a heterozygous or homozygous *Swap-70* knockout allele exhibited a largely healthy normal phenotype, bred like their WT counterparts and did not show obvious clinical signs of severe systemic autoimmunity.

Impact of SWAP-70-Deficiency on Thymic and Peripheral T Cell Homeostasis

To assess the impact of SWAP-70-deficiency on T cell development and homeostasis, T cell developmental stages and populations in thymus and periphery were analyzed. Flow cytometric analysis of the CD4CD8 double negative (DN), CD4CD8 double positive (DP), CD4SP and CD8SP and Foxp3$^+$ CD4SP populations revealed that frequencies and cell numbers of these compartments were similar in *Swap-70*$^{-/-}$ and *Swap-70*$^{+/+}$ mice, even though the frequency of total Foxp3$^+$ CD4SP thymocytes was slightly increased in some *Swap-70*$^{-/-}$ mice (**Figure S3A**). Since SWAP-70 expression positively correlated with Helios and Nrp-1 in Treg cells in thymus and periphery (**Figure 2G** and **Supplementary Figures S2B, D**), we extended our analysis to additional Treg cell markers. *Ex vivo* analysis revealed comparable expression levels (MFI) of Foxp3^{GFP} and CD25 in the thymic Foxp3$^+$ CD4SP population of *Swap-70*$^{+/+}$ and *Swap-70*$^{-/-}$ mice (data not shown), while the analysis of CD44 and CD62L provided evidence for an increased frequency of Foxp3$^+$CD62L$^-$CD44$^+$ thymocytes in *Swap-70*$^{-/-}$ mice, accompanied by a reduction of the Foxp3$^+$CD62L$^+$CD44$^-$ population. However, this was not reflected by absolute numbers (**Figures 3E, F** and **Supplementary Figure S3A**). In contrast, the enriched Foxp3$^+$Helios$^+$Nrp-1$^+$ thymocyte compartment detected in *Swap-70*$^{-/-}$ mice was reflected by both, elevated frequencies and cell numbers (**Figures 3E, F** and **Supplementary Figure S3A**). Notably, expression levels of Helios were not affected, while expression of Nrp-1 was clearly increased (**Figure 3F**).

To explore whether the quantitative changes of Treg cell subsets in the thymus of *Swap-70*$^{-/-}$ mice have an impact on the Treg/Teff cell balance in adult *Swap-70*$^{-/-}$ mice, we systematically analyzed the size of the naïve and memory/effector-memory cell compartments of the CD4$^+$ and CD8$^+$ T cell populations in scLN, mesLN, and spleen (**Figures 3G, H** and **Supplementary Figure S3B**). Flow cytometric analysis of the total CD4 and CD8 compartments revealed comparable frequencies and cell numbers in *Swap-70*$^{+/+}$ and *Swap-70*$^{-/-}$ mice (**Supplementary Figure S3B**). Notably, the CD4$^+$Foxp3$^-$CD25$^-$ Tcon cell compartment exhibited a slightly increased frequency of memory-type CD4$^+$ T cells in the scLN of *Swap-70*$^{-/-}$ mice. However, the difference in cell numbers did not meet statistical significance (**Figure 3H** and **Supplementary Figure S3B**). Analysis of the naïve, effector-memory and central memory subsets within the CD8 compartment revealed a comparable distribution (frequencies) and population size (numbers). Albeit not being statistically significant, the CD8$^+$ effector-memory compartment was somewhat increased in some *Swap-70*$^{-/-}$ mice (**Supplementary Figure S3B**). To directly assess the role of SWAP-70 in peripheral Treg cell function, we next aimed to phenotypically characterize the total Foxp3$^+$ Treg cell population in the periphery. Flow cytometric analysis of the CD4$^+$ T cell population revealed an increased frequency of total Foxp3$^+$ Treg cells in the spleen of adult *Swap-70*$^{-/-}$ mice, which was confirmed by absolute cell numbers. Compared to their WT counterparts, the average frequency of Foxp3$^+$ Treg cells increased from 9.6 to 12.3%. A similar trend could be observed in scLN (**Figures 3G, H** and **Supplementary Figure S3B**). As already indicated for CD8 and CD4 Tcon cells in the periphery, also the Treg cell population in *Swap-70*$^{-/-}$ mice shifted from naive to memory phenotype (**Figures 3G, H**, **Supplementary Figure S3B**). We expanded the flow cytometric analysis to a large panel of markers related to Treg cell activation, migration, homing and suppressor function. MFI values of electronically gated Foxp3$^+$ Treg cells from *Swap-70*$^{-/-}$ mice were normalized to MFI values of electronically gated Foxp3$^+$ Treg cells from age-matched *Swap-70*$^{+/+}$ littermates and **Figure 3I** summarizes the differential protein expression of the distinct Treg cell markers. The data revealed marked upregulation of cell adhesion molecules (ICAM-1, CD62L, CD103) and molecules involved in Treg cell activation and effector function (Foxp3, Helios, Nrp-1, CD38, ICOS) in *Swap-70*$^{-/-}$ mice. However, the overall expression of CD25 appeared to be downregulated *Swap-70*$^{-/-}$ Treg cells.

Increased Frequency of Pre-Activated CD25$^-$ Effector-Memory-Like Treg Cells in *Swap-70*$^{-/-}$ Mice

To address whether the shift in CD25 expression results from downregulation of CD25 surface expression or reflects an increase in the CD25$^-$ Treg cell compartment, the frequency and MFI of CD25$^-$, CD25$^+$ and CD25^{int} Treg cell populations was analyzed. A significant increase in the frequency and number of CD25$^-$ Treg cells was detected in the spleen of *Swap-70*$^{-/-}$ mice. Even though the difference did not meet statistical significance in mesLN and scLN, at least a trend of increased CD25$^-$ Treg cell

frequencies could be established in these organs. In *Swap-70*$^{+/+}$ mice, the average proportion of CD25$^-$ Treg cells among the Foxp3$^+$ population accounted for 28.2 ± 2.6% in the spleen, 20.2 ± 3.8% in the mesLN and 18.9 ± 2.6% in the scLN. In *Swap-70*$^{-/-}$ mice, the CD25$^-$ compartment comprised 33.6 ± 1.2% in the spleen, 22.0 ± 2.8% in the mesLN and 21.7 ± 1.1% in the scLN. The most remarkable difference was manifested in the spleen, probably due to the overall increased presence of CD25$^-$ Treg cells in this organ (**Figures 3J, K**). However, MFI values of the CD25$^+$ and CD25$^-$ Treg cell subset were similar in WT and KO mice in all organs analyzed (mesLN, scLN, and spleen, data not shown). In summary, these data show that the reduced CD25 MFI detected in splenic Treg cells of *Swap-70*$^{-/-}$ mice results from an enrichment of a distinct CD25$^-$ Treg cell subset and is not a consequence of CD25 downregulation.

Next, we addressed whether there is a correlation between the observed decreased CD25 expression levels and increased activation marker expression in SWAP-70-deficient Treg cells. For this aim, activation marker versus CD25 expression was systematically analyzed by flow cytometry in *Swap-70*$^{+/+}$ and *Swap-70*$^{-/-}$ mice. Our data revealed that the largest part of CD44$^-$ Foxp3$^+$ Treg cells co-expressed CD25 in both, *Swap-70*$^{+/+}$ and *Swap-70*$^{-/-}$ mice, while CD44$^+$ Treg cells can acquire a CD25$^+$ or CD25$^-$ phenotype. Importantly, the population clearly shifted towards CD44$^+$CD25$^-$ in the spleen of *Swap-70*$^{-/-}$ mice. The vast majority of CD62L$^+$ Treg cells displayed a CD25$^+$ phenotype. CD62L$^-$ Treg cells were either CD25$^+$ or CD25$^-$. Compared to WT, the splenic Treg cell compartment of *Swap-70*$^{-/-}$ mice comprised an increased proportion of CD62L$^-$CD25$^-$ cells. ICOS$^+$ Treg cells were either CD25$^+$ or CD25$^-$, with a bias of the ICOS$^+$ population towards a CD25$^-$ phenotype in *Swap-70*$^{-/-}$ mice. (**Figure 3J**) Overall, these results describe an enriched CD25$^-$ Treg population in the spleen of *Swap-70*$^{-/-}$ mice, co-expressing high levels of CD44, ICOS, and low levels of CD62L, which is reminiscent of antigen-experienced T cells.

Suppressor Function of *Swap-70*$^{-/-}$ Treg Cells *In Vitro*

To determine the suppressive capacity of *Swap-70*$^{-/-}$ Treg cells, titrating numbers of FACS-purified CD4$^+$Foxp3$^+$ Treg cells (including CD25$^+$ and CD25$^-$ cells) from *Swap-70*$^{+/+}$ or *Swap-70*$^{-/-}$ mice were co-cultured with naïve polyclonal CD4$^+$ Tresp cells in the presence of irradiated APCs and soluble α-CD3ε. As shown by upregulation of CD25 expression and cell proliferation assessed by the progressive dilution of the dye ef670, CD4$^+$ Tresp cells were efficiently activated in the absence of Treg cells. At day 3 of *in vitro* stimulation, more than 90% of Tresp cells had undergone at least one cell division (**Figure 3L**, left and **N**). Co-culture with *Swap-70*$^{+/+}$ Treg cells efficiently suppressed Tresp cell activation, as revealed by the suppression of cell proliferation and expression of the early activation marker CD25 on Tresp cells in a dose-dependent manner (**Figures 3L**, middle and **M, N**). In some experiments, *Swap-70*$^{-/-}$ Treg cells appeared somewhat less potent in abrogating proliferation and upregulation of CD25 expression on Tresp cells (**Figures 3L**, right and **M, N**). The reduced ability to suppress the upregulation of CD25 was detectable as early as at day 1 of co-culture, i.e. at the time when undivided Tresp initiated TCR stimulation-induced upregulation of CD25 prior to proliferation (data not shown). At day 3, a slightly elevated frequency of divided Tresp cells, accompanied by a diminished proportion of undivided Tresp cells indicated a reduced suppressive capacity of *Swap-70*$^{-/-}$ Treg cells (**Figures 3L–M**).

Inefficient Suppression of Osteoclastogenesis by *Swap-70*$^{-/-}$ Treg Cells *In Vitro*

To assess the capacity of *Swap-70*$^{-/-}$ Treg cells to suppress osteoclastogenesis *in vitro*, pre-activated Foxp3$^+$CD25$^+$ Treg cells from *Swap-70*$^{+/+}$ or *Swap-70*$^{-/-}$ mice were co-cultured with pre-osteoclast under osteoclastogenic conditions. Consistent with previous reports (9), WT Treg cells efficiently suppressed osteoclast differentiation in a dose-dependent manner, as revealed by decreasing numbers of mature multinucleated TRAP-expressing osteoclasts cultured in the presence of increasing numbers of Treg cells. In some experiments, *Swap-70*$^{-/-}$ Treg cells appeared slightly less potent in suppressing osteoclastogenesis than SWAP-70-proficient Treg cells (**Figures 4A, B**). To determine the impact of Treg cells on the resorptive function of the osteoclasts, the co-culture was performed on bone slices using different Treg cell: monocyte ratios. In line with the observed reduced capacity of *Swap-70*$^{-/-}$ Treg cells to suppress osteoclastogenesis, the analysis of the bone resorption marker CTX revealed moderately elevated CTX levels in the supernatants of co-cultures of osteoclast precursors and *Swap-70*$^{-/-}$ Treg cells compared to co-cultures with *Swap-70*$^{+/+}$ Treg cells in all ratios analyzed (**Figure 4C**). Although the observed trend was statistically not significant, and the CTX assay replicates are reflected by the titration steps, the diminished ability to suppress osteoclast differentiation and function is reminiscent of and in line with the moderate differences we observed in standard suppression assays (**Figures 3L–N**). Overall, we soughed to address our question with multiple approaches, and found that different analyses converged on the same result, proposing that *Swap-70*$^{-/-}$ Treg cells are compromised with regard to their suppressor function. Representative SEM images of Treg cell and osteoclast interactions on bone slices demonstrated direct cell-cell interactions of giant bone-resorptive mature osteoclasts with the much smaller Treg cells (**Figure 4D** right). Importantly, we found less cell clusters in co-cultures of osteclasts with *Swap-70*$^{-/-}$ Treg cells (**Figure 4D** middle) than with *Swap-70*$^{+/+}$ Treg cells (**Figure 4D** left).

Inefficient *Swap-70*$^{-/-}$ Treg Cell-Mediated Downregulation of CD80/CD86 on Osteoclast Precursor Cells

Since SWAP-70 has been shown to be required for endocytosis in DCs (27), we assessed whether *Swap-70*$^{-/-}$ Treg cells are capable of efficient CD80 and CD86 down-modulation on osteoclast precursors. Flow cytometric analysis revealed progressive upregulation of CD80, CD86, the M-CSF receptor cfms, and

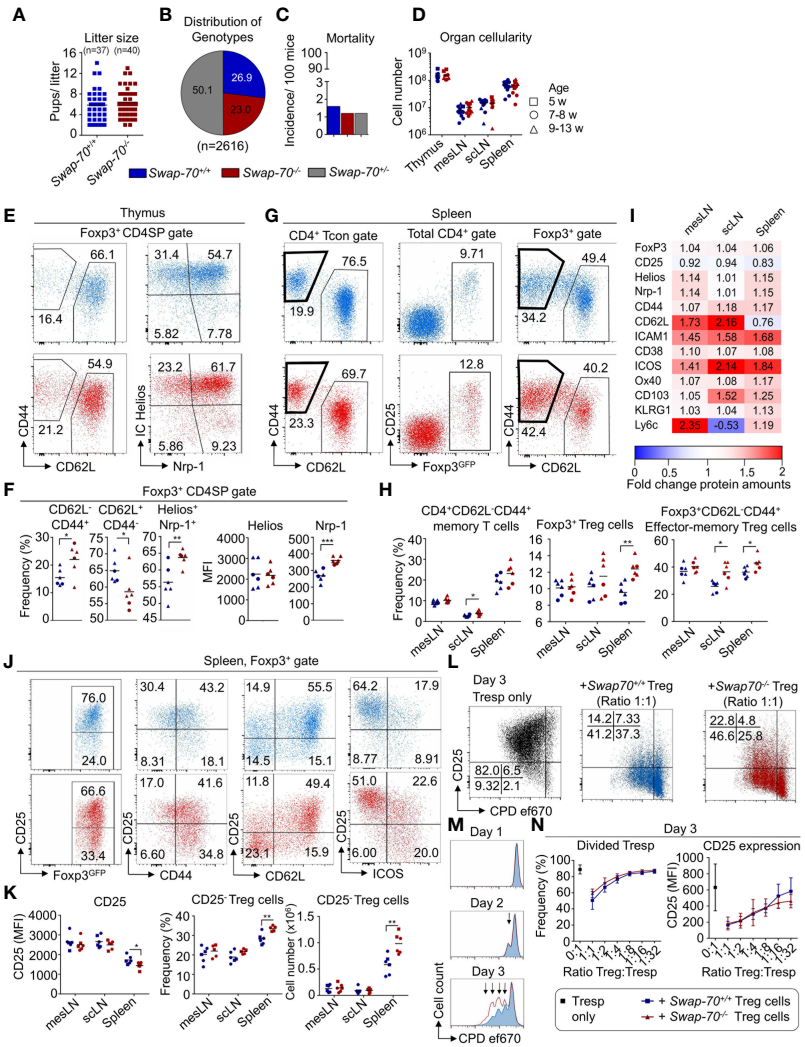

FIGURE 3 | Impact of SWAP-70 on immune homeostasis. **(A–D)** *Swap-70* deficiency does not affect fertility, mortality or organ cellularity. **(A)** Number of litters and litter sizes of 8 *Swap-70*$^{+/+}$ (blue) and 6 *Swap-70*$^{-/-}$ (red) mating trios (2♀ x 1♂) within a period of 15 months. Symbols and horizontal lines indicate individual mice and mean values, respectively. **(B)** Distribution of genotypes and **(C)** mortality rate of live born *Swap-70* x Foxp3^{GFP} pups. Pie and bar chart display data from 2616 mice monitored over a period of 36 months (*Swap-70*$^{+/+}$: blue; *Swap-70*$^{-/-}$: red; *Swap-70*$^{+/-}$: grey). **(D)** Total organ cellularity of *Swap-70*$^{+/+}$ and *Swap-70*$^{-/-}$ mice as indicator for multi-organ autoimmunity. Symbols and horizontal lines indicate individual mice and mean values, respectively (squares: 5-week-old, circles: 7-8-week-old; triangles: 9-13-week-old mice, n= 12 per genotype). **(E)** Representative flow cytometry of CD44, CD62L, IC Helios and Nrp-1 expression of electronically gated Foxp3^{GFP+} CD4SP thymocytes from *Swap-70*$^{+/+}$ (blue) and *Swap-70*$^{-/-}$ (red) Foxp3^{GFP} mice. **(F)** Graphs depict frequencies of the respective cell populations among electronically gated Foxp3^{GFP+} CD4SP thymocytes and Helios/Nrp-1 protein expression levels (MFI) of electronically gated Foxp3^{GFP+} CD4SP thymocytes. **(G)** Representative flow cytometry of CD44 and CD62L expression among gated CD4^{+} Foxp3^{GFP-}CD25^{-} Tcon, Foxp3^{GFP} and CD25 expression among total CD4^{+} and CD44 and CD62L expression among CD4^{+}Foxp3^{GFP+} Treg cells in the spleen of *Swap-70*$^{+/+}$ (blue) and *Swap-70*$^{-/-}$ (red) mice. **(H)** Graphs illustrate frequencies of memory T cells, Treg cells and effector-memory Treg cells in mesLN, scLN, and spleen. **(I)** Normalized protein expression levels in *Swap-70*$^{-/-}$ Foxp3^{GFP+} Treg cells from mesLN, scLN and spleen determined by surface and/or intracellular flow cytometry staining of the indicated proteins. MFIs of 4-6 individual mice were normalized to *Swap-70*$^{+/+}$ Foxp3^{GFP+} controls (set to 1). Mean values are shown as heatmap displaying *Swap-70*$^{-/-}$ to *Swap-70*$^{+/+}$ fold-change values. The differential expression is shown as up-regulation (red) or downregulation (blue). **(J)** Representative flow cytometry of electronically gated CD4^{+}Foxp3^{GFP+} Treg cells in the spleen of *Swap-70*$^{+/+}$ (blue) and *Swap-70*$^{-/-}$ (red) mice costained with CD25 and CD44, CD62L and ICOS. **(K)** Graphs depict CD25 expression levels (MFI) on electronically gated CD4^{+}Foxp3^{GFP+}CD25^{+}Treg cells, frequency and cell numbers of CD4^{+}Foxp3^{GFP+}CD25^{-} Treg cells. **(L–N)** Treg cell-mediated suppression of responder T cells (Tresp) *in vitro*: FACS-purified CD4^{+}CD62L^{+}Foxp3^{GFP-}CD25^{-} Tresp cells were co-cultured in different ratios with FACS-purified *Swap-70*$^{+/+}$ (blue) or *Swap-70*$^{-/-}$ (red) Foxp3^{GFP+} Treg cells - or as control alone (black) - in the presence of irradiated antigen presenting cells (APCs) and 1 µg/ml α-CD3ε. Cells were harvested and analyzed by flow cytometry at the indicated time points. **(L)** Representative flow cytometry of CD25 expression and cell proliferation dye (CPD) ef670 dilution of electronically gated Foxp3^{GFP-} Tresp cells. **(M)** Representative histogram overlays to determine CPD ef670 dilution of electronically gated Tresp cells that were co-cultured with *Swap-70*$^{+/+}$ (blue) or *Swap-70*$^{-/-}$ (red) Foxp3^{GFP+} Treg cells at a Treg : Tresp ratio of 1:1. Arrows mark proliferation dye dilution peaks (each peak represents one cell division). **(N)** Graphs depict frequencies of divided Tresp cells (left) and CD25 expression levels (MFI, right) at day 3 of culture for indicated Treg : Tresp ratios (n= 8 from 3 independent experiments). See also **Supplementary Figure S3**. *P ≤ 0.05; **P≤ 0.01; ***P ≤ 0.001; or ****P ≤ 0.0001.

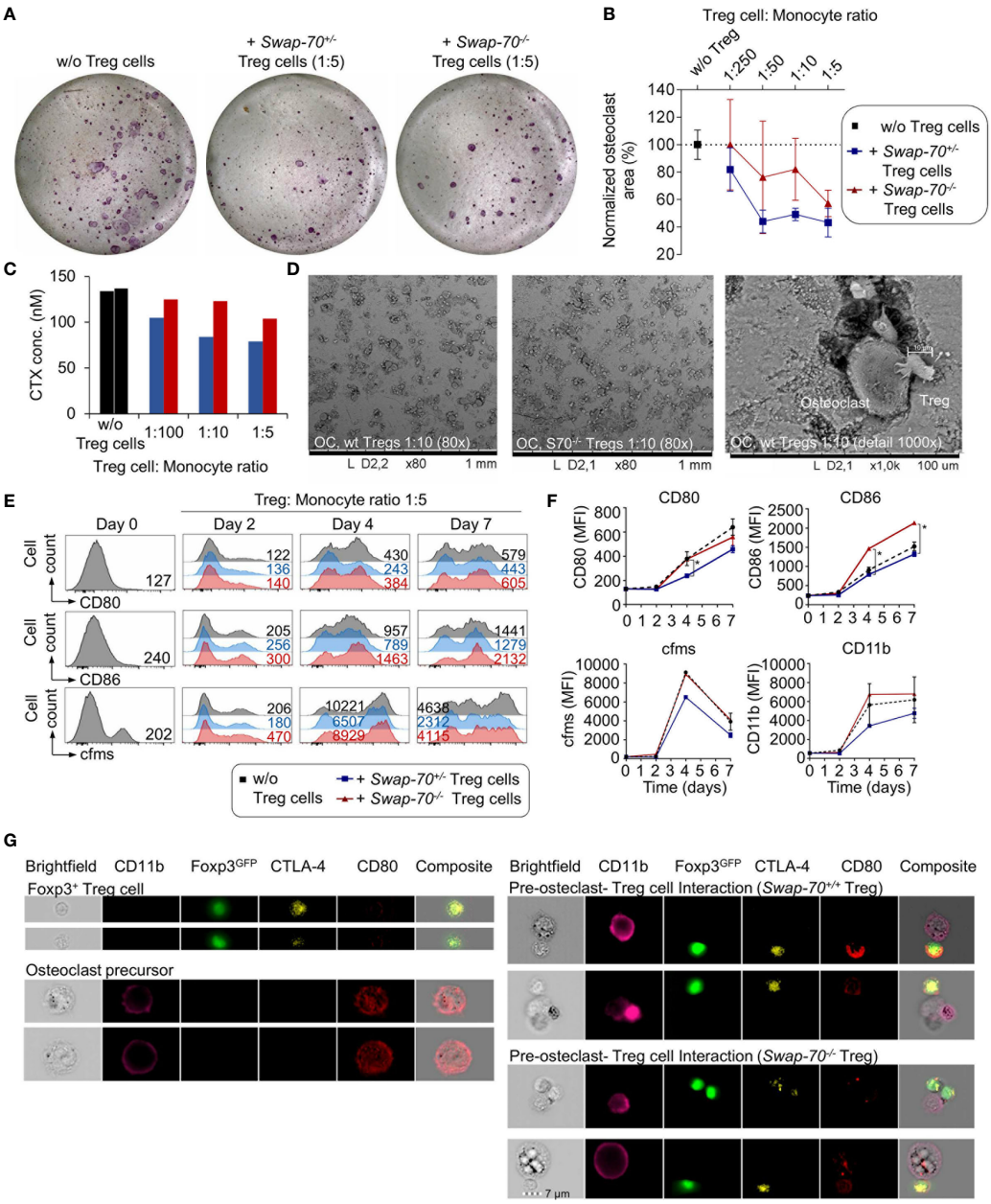

FIGURE 4 | Treg-cell-mediated suppression of osteoclastogenesis *in vitro*. Bone marrow-derived macrophages (BMMs) were cultured in the absence or presence of FACS-purified *Swap-70*$^{+/-}$ or *Swap-70*$^{-/-}$ Treg cells. **(A)** Representative images of tartrate-resistant acid-phosphatase (TRAP) stained osteoclast differentiation cultures without (left) or with Treg cells (middle: *Swap-70*$^{+/-}$, right: *Swap-70*$^{-/-}$ Treg cells) at day 6. **(B)**. Graph illustrates the impact of Treg cells on osteoclast formation assessed by the analysis of osteoclast areas (the number of TRAP-positive multinucleated cells) from co-cultures with *Swap-70*$^{+/+}$ (blue) or *Swap-70*$^{-/-}$ (red) Treg cells normalized to control cultures without Treg cells (black) (n= 3, mean values with SD shown). **(C)** Bone resorption *in vitro* assay: Pre-osteoclast-Treg cell co-culture was seeded on bone slices at different ratios, and carboxy-terminal collagen crosslinks (CTX) in the day 5 supernatant from one sample of each titration step were measured by ELISA. **(D)** The bone slices of the co-culture shown in **(C)** were harvested at day 7, dried, coated and analyzed by SEM. **(E–G)** Treg-cell-mediated downregulation of CD80/86 on pre-osteoclasts. BMMs were co-cultured with *Swap-70*$^{+/-}$ or *Swap-70*$^{-/-}$ Treg cells, harvested and analyzed by flow cytometry at the indicated time points. **(E)** Representative histogram overlays of CD80 (top), CD86 (middle) and MCSF receptor (cfms, bottom) expression on electronically gated CD4^{-}Foxp3^{GFP-}CD11b^{+} cells from osteoclast differentiation cultures cultured without (grey) or with Treg cells (*Swap-70*$^{+/-}$ blue; *Swap-70*$^{-/-}$ red) at indicated time points. Numbers in histograms indicate representative MFIs of gated cells. **(F)** Graphs show expression levels of CD80, CD86, cfms and CD11b (MFI) for indicated culture conditions and timepoints (one or two data points per condition from continuous co-culture). **(G)** Representative imaging flow cytometry of osteoclast-Treg cells co-culture derived cell suspensions that were analyzed for CD11b, Foxp3^{GFP}, CTLA-4 and CD80 expression, showing single cell (top left: Foxp3^{+} Treg cell, bottom left: pre-osteoclast) and cluster images (top right: pre-osteoclast - *Swap-70*$^{+/+}$ Treg cell interaction, bottom right: pre-osteoclast - *Swap-70*$^{-/-}$ Treg cell interaction).

CD11b during osteoclast maturation *in vitro*. Co-culture of osteoclast progenitors and SWAP-70-proficient Treg cells resulted in diminished upregulation of CD80 (day 7: 70 ± 3%, compared to culture without Treg cells) and CD86 (day 7: 87 ± 2%), with a more efficient down-modulation of CD80, and a concomitant limited expression of cfms (day 7: 65 ± 6%) and CD11b (day 7: 81 ± 16%) (**Figures 4E, F**). In contrast, *Swap-70*$^{-/-}$ Treg cells failed to efficiently downregulate CD80 (day 7: 86 ± 3%) and CD86 (day 7: 140 ± 7%), which is significantly different from *Swap-70*$^{+/+}$ Treg cells and moreover had no impact on cfms (day 7: 108 ± 18%) and CD11b (day 7: 119 ± 33%) expression during osteoclastogenesis. These observations are in line with the reduced suppressive capacity of *Swap-70*$^{-/-}$ Treg we described above (**Figures 3L–N** and **4A–C**).

To determine whether *Swap-70*$^{-/-}$ Treg cells are able to interact directly with osteoclast precursors, osteoclast-Treg cell co-culture were analyzed at day 2 by imaging flow cytometry, allowing the visualization of cell-cell interactions and subcellular protein localization. As we have shown previously (9), imaging analysis of CD11b/Foxp3^{GFP}-gated cell clusters indicated physical interaction of Foxp3^{+}CTLA4^{+} Treg cells with CD11b^{+} osteoclast precursor cells. CD11b^{+} cells that were detected in co-existence with Foxp3^{+} Treg cells displayed an overall reduced surface expression of CD80, as compared to CD11b^{+} single cells, while CD80 expression was clearly detectable in Foxp3^{+}CTLA4^{+} Treg cells, suggesting CD80 uptake by direct interaction between the two cell types and trans-endocytosis. (**Figure 4G**). However, we detected no difference between Foxp3^{GFP+}*Swap-70*$^{+/+}$ and Foxp3^{GFP+}*Swap-70*$^{-/-}$ Treg cells with regard to the up-take of CD80, proposing that trans-endocytosis is not, or only moderately compromised in Treg cells that lack SWAP-70.

DISCUSSION

Dynamic rearrangements of the actin cytoskeleton in antigen-specific T cells represent a prerequisite for the effective polarization, migration and exertion of specific functions such as the formation of an immunological synapse. Since SWAP-70 modulates F-actin rearrangements, regulates integrin activity, and thus cell migration and adhesion in a variety of cells of hematopoietic origin (26, 28–31, 33, 35), it seems tempting to speculate that the selective constitutive expression of SWAP-70 in the Foxp3^{+} Treg cell subset of the CD4^{+} T cell lineage (37) might represent a direct consequence of Foxp3-dependent transcriptional regulation and that SWAP-70 participates in the regulation of actin dynamics in Treg cells. Here, we follow up on this initial observation and perform detailed studies on the role of SWAP-70 in Foxp3^{+} Treg cell biology, identifying SWAP-70 as an important regulator of Treg cell homeostasis and suppressor function involved the interaction of Treg cells with osteoclasts. We found that *Swap-70* is constitutively expressed in Foxp3^{+} Treg cells, which is in line with initial studies (37), and that *Swap-70* expression is upregulated upon TCR-mediated stimulation in initially naïve *Swap-70*$^{-}$ CD4^{+} Tcon. We further established that *Swap-70* mRNA expression is under the direct control of Foxp3/NF-AT. These findings are consistent with the notion that Foxp3 controls Treg cell function through cooperation with NF-AT (52) and propose *Swap-70* as a member of the canonical Treg cell signature (37, 44).

When we analyzed the spatial localization of SWAP-70 upon TCR engagement, we observed that cytosolic SWAP-70 is recruited to the immunological synapse (IS) exclusively in Foxp3^{+} Treg cells, which was in contrast to CD4^{+} Tcon cells. The localization of SWAP-70 at the Treg-APC interface provides first evidence for an F-actin-dependent function of SWAP-70 selectively in primary Treg cells and suggest that SWAP-70 has a critical role in the formation of a stable IS between Treg cells and APCs. In contrast, SWAP-70`s only homolog DEF6 is constitutively expressed and involved in TCR-mediated cytoskeletal dynamics and recruitment in CD4^{+} Tcon cells (53, 54), emphasizing the distinct function of SWAP-70 in Treg cells.

The overall mature Foxp3^{+} Treg cell compartment has been shown to exhibit a remarkable phenotypic heterogeneity and comprises several subsets, as defined by their developmental origin, anatomical location, activation status and functional properties. The differential transgenic expression of GFP in RFP^{+} Treg cells of Foxp3$^{RFP/GFP}$ mice has been shown to faithfully discriminate tTreg and pTreg cells (40, 47). At least in some experimental settings, this can also be achieved by the expression analysis of the Ikaros transcription factor Helios (Ikzf2) (51) and the surface marker Nrp-1 (55, 56), but endogenous (i.e. non-transgenic) markers to unambiguously discriminate tTreg and pTreg cell subsets have yet to be defined (57). The concomitant induction of SWAP-70 expression with CD25, Helios and Nrp-1 in the instructive phase of tTreg cell lineage commitment (stage I) and progressive up-regulation to high levels during developmental progression and tTreg lineage consolidation (stage II and III) suggests a mechanism of TCR-mediated induction and subsequent Foxp3-mediated amplification/stabilization of SWAP-70 expression during tTreg cell development and supports the assumption that SWAP-70 is a Foxp3 target gene. Together with the observed correlation of SWAP-70 expression with the expression of CD44, Helios and Nrp-1 in mature Treg cells, our data suggest that - similar to Helios and Nrp-1 - SWAP-70 cannot be considered as a tTreg cell lineage marker, but rather propose SWAP-70 to be a putative marker for Helios^{hi}Nrp-1^{hi}Treg cells. In summary, the results demonstrate that SWAP-70 is differentially expressed during Foxp3^{+} Treg cell development and activation (**Supplementary Figure S2E**).

A role of SWAP-70 in T cells during thymic development and peripheral homeostasis is supported by the marked upregulation of cell adhesion molecules and molecules involved in their activation and effector function (ICAM-1, CD103 and Helios, Nrp-1, CD38, ICOS), in conjunction with increased proportions of effector/memory-type CD4^{+} and CD8^{+} T cells and an enriched CD25^{-} Treg population in the spleen of *Swap-70*$^{-/-}$ mice. *Swap-70*$^{-/-}$ CD25^{-} Treg co-express high levels of CD44, ICOS and low levels of CD62L, which is reminiscent of activation-experienced Treg cells (58).

Increased numbers of Foxp3^{+}CD25^{low}CD4^{+} Treg cells were detected in peripheral blood of patients with autoimmune diseases such as systemic lupus erythematosus, multiple sclerosis, type 1 diabetes and rheumatoid arthritis (59–63), and it was suggested that this may reflect an attempt to regulate an overt autoimmune response of pathogenic T cells and might

contribute to the perpetuation of chronic inflammation (61, 64). Furthermore, it has recently been reported that mice with diminished CD25 expression harbor decreased numbers of $CD62L^{+}CD44^{-}$ Treg cells indicating an impact of impaired IL-2R signaling on Treg cell stability (65). Efficient IL-2/IL-2R signaling is essential for Treg cell homeostasis and function, and competition for IL-2 has been suggested as one basic mechanism of immune suppression by Treg cells (66, 67). When we analyzed the *in vitro* function of *Swap-70*$^{-/-}$ Treg cells, we found that the suppression of proliferation and upregulation of CD25 expression on Tresp cells was somewhat less effective compared to SWAP-70-proficient Treg cells. As the reduced suppression of CD25 upregulation on Tresp cells was already apparent at day 1 of co-culture, we hypothesize that *Swap-70*$^{-/-}$ Treg cells suppress less effective due to their - at least initially - lower IL-2R expression and then upregulate IL-2R through local IL-2 secretion by Tresp and consequently could suppress more efficient.

To elucidate the role of SWAP-70 in osteoimmunology and in particular the interplay of Treg cells and osteoclasts, we performed co-cultures of Treg cells and osteoclast precursor cells. These experiments revealed an inefficient suppression of osteoclastogenesis and resorptive function by *Swap-70*$^{-/-}$ Treg cells *in vitro* correlating with diminished Treg cell-adhesion to osteoclasts and most importantly that *Swap-70*$^{-/-}$ Treg cells failed to efficiently downregulate CD80 and CD86 expression during osteoclastogenesis (**Figure 5**). Although *Swap-70*$^{-/-}$ Treg cells trans-endocytosed CD80 as efficiently as SWAP-70-proficient Treg cells, these findings suggest that SWAP-70 might represent a novel link between the immune and the skeletal system. Considering previously reported roles of SWAP-70 in integrin-mediated adhesion, we suggest that SWAP-70 is required for efficient Treg cell-mediated regulation of osteoclastogenesis through regulating integrin-mediated adhesion and cytoskeletal re-arrangements.

Together, our analysis of the suppressive capacity of *Swap-70*$^{-/-}$ Treg cells indicate a general but modest defect in Treg suppressor function in *Swap-70*$^{-/-}$ mice. However, *Swap-70*$^{-/-}$ mice did not show obvious clinical signs of a severe systemic autoimmune disease. Since we found *Swap-70* to be expressed in activated Teff cells, our data suggest a scenario in which the function of SWAP-70 in Teff is crucial for the establishment of autoimmunity in the context of SWAP-70-deficient Treg cells. On the other hand, it has been described that mice deficient in both SWAP-70 and its homolog DEF6 develop systemic lupus erythematosus (68), indicating that DEF6 expression might at least partially compensate for defects in *Swap-70*$^{-/-}$ mice. It is a limitation of our present study that we did not address this hypothesis, and it will be important to determine in future studies how these two proteins control and balance Treg cell function in the context of osteoimmunology.

In summary, our study uncovers a previously unrecognized role of the F-actin binding protein SWAP-70. We propose Swap-70 as a member of the so called canonical Treg cell signature and provide first evidence for a crucial role of SWAP-70 in Treg cell homeostasis and suppressor function. Collectively, our data define a novel role of SWAP-70 in osteoimmunology and may thus have future

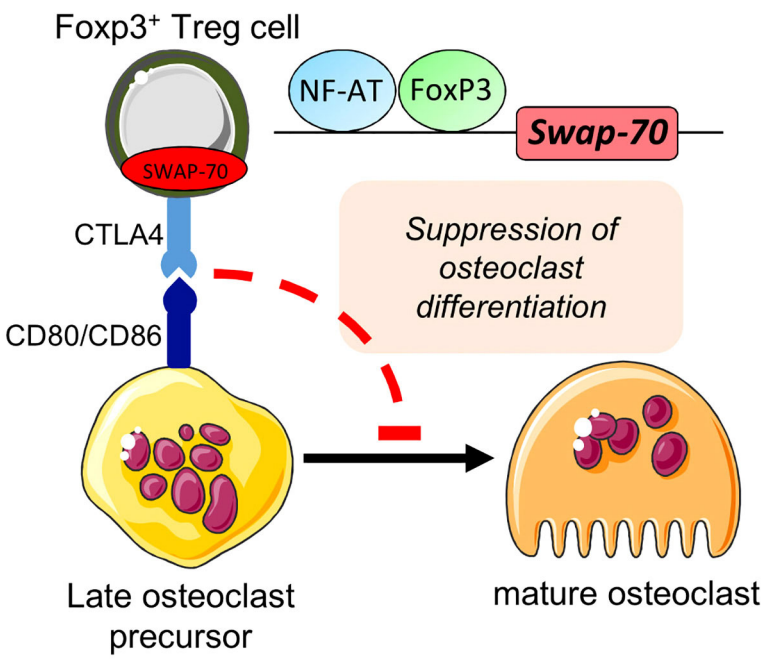

FIGURE 5 | Proposed role for SWAP-70 in the direct interplay between Foxp3⁺Treg cells and osteoclast precursors. Bone homeostasis mediated through Foxp3⁺ Treg cells (*via* CTLA-4 interacting with CD80/CD86) underlies SWAP-70-dependent mechanisms. Adapted from 9. This figure was in part created with modified Servier Medical Art templates, licensed under a Creative Commons Attribution 3.0 Unported license: http://smart.servier.com.

implications for studies on bone disorders associated with functional defects of Treg cells, including rheumatoid arthritis.

DATA AVAILABILITY STATEMENT

The original contributions presented in the study are included in the article/**Supplementary Material**. Further inquiries can be directed to the corresponding author.

ETHICS STATEMENT

The animal study was reviewed and approved by Regierungs präsidium Dresden.

AUTHOR CONTRIBUTIONS

SD designed, conducted, and analyzed the experiments, contributed to data interpretation and manuscript writing. SM and AS performed experiments. TK analyzed experiments and contributed to data interpretation. AG, RJ, and KK conceived the research. AG and KK guided its design, analysis and interpretation, and wrote the manuscript. All authors contributed to the article and approved the submitted version.

FUNDING

AG was supported by a DFG grant (GA1576/1-2) within the SPP1468 IMMUNOBONE and two intramural grants from the Technische Universität Dresden (MeDDrive Program of the Medical Faculty and Maria Reiche Program). In addition, AG and KK received funds from the FZT 111 (DFG, Center for Regenerative Therapies Dresden, Cluster of Excellence).

ACKNOWLEDGMENTS

The authors would like to thank Elena Kombarov, Marie Boernert and Denise Bärhold for excellent technical assistance, and Sonja Schallenberg and Anne Gompf (CMCB Flow Cytometry Core Facility) for expert help in flow cytometry, cell sorting and image stream analysis.

SUPPLEMENTARY MATERIAL

The Supplementary Material for this article can be found online at: https://www.frontiersin.org/articles/10.3389/fimmu.2022.836646/full#supplementary-material

Supplementary Figure 1 | SWAP-70 is expressed in $CD4^+Foxp3^+$ Treg cells. Flow cytometric analysis of SWAP-70 expression in indicated T cell subsets. Representative dot plots with gating strategy (arrows) and representative histograms of intracellularly (IC) stained SWAP-70 of indicated populations in thymus (left) and periphery (scLN, right). SWAP-70 expression in naïve ($CD62L^+CD44^-$) and memory-type ($CD62L^-CD44^+$) $CD4^+Foxp3^+$ Treg cells is shown at the bottom right. Numbers in dot plots and representative histograms indicate representative frequencies and MFIs of gated cells within the respective gates, respectively. Data are representative of 4 independent experiments.

Supplementary Figure 2 | FACS-purification of CD4SP $CD25^+$ Treg precursor stages according to the differential expression of $Foxp3^{RFP}$ and $Foxp3^{GFP}$ and co-expression of SWAP-70, Helios and Nrp-1. **(A)** Representative dot plots of presort gating strategy with (bottom) and without (top) CD25-bead enrichment. Lines with arrowheads in dot plots illustrate the gating strategy. **(B)** Representative flow cytometric analysis of FACS-purified $Foxp3^{RFP-}Foxp3^{GFP-}$ $CD25^+$ CD4SP (stage I), $Foxp3^{RFP+}Foxp3^{GFP-}$ $CD25^+$ CD4SP (stage II) and $Foxp3^{RFP+}Foxp3^{GFP+}CD25^{hi}$ CD4SP (stage III) thymocytes for IC Helios, Nrp-1 and IC SWAP-70 co-expression. **(C)** Representative dot plots of presort gating strategy with (bottom) and without (top) CD25-bead enrichment for pTreg and tTreg sorts (scLN shown). **(D)** Representative flow cytometric analysis of FACS-purified pTreg ($Foxp3^{RFP+}Foxp3^{GFP-}$ $CD25^+CD4^+$) and tTreg cells ($Foxp3^{RFP+}Foxp3^{GFP+}$ $CD25^+CD4^+$) for IC Helios, Nrp-1 and IC SWAP-70 co-expression. Numbers in representative dot plots indicate frequencies of the gated population. **(E)** Schematic summary of SWAP-70 protein expression during Treg cell development. SWAP-70 expression pattern based on flow cytometric analysis of thymocytes from $Foxp3^{RFP/GFP}$ mice and extrathymic $Foxp3^+$ Treg cells from $Foxp3^{GFP}$ x *Swap70*$^{+/+}$ mice. SWAP-70 expression was already detectable in the instructive phase of Treg cell lineage commitment (stage I) in the thymus and was highly expressed during consolidation phases (stage II and III), concomitant with Foxp3, indicating a TCR mediated induction of SWAP-70 *via* NF-AT. Constitutive expression of SWAP-70 in Treg cells in the periphery is stabilized by Foxp3.

Supplementary Figure 3 | Impact of SWAP-70 on immune homeostasis. **(A)** Graphs depict frequencies and cell numbers of the indicated populations in the thymus of *Swap-70*$^{+/+}$ (blue) and *Swap-70*$^{-/-}$ (red) x $Foxp3^{GFP}$ mice. **(B)** Frequencies and cell numbers of the indicated populations in scLN, mesLN and spleen of *Swap-70*$^{+/+}$ (blue) and *Swap-70*$^{-/-}$ (red) x $Foxp3^{GFP}$ mice. Symbols and horizontal lines indicate individual mice and mean values, respectively (circles: 8-9-week-old; triangles: 10-13-week-old mice; n= 6 per genotype).

REFERENCES

1. Curotto de Lafaille MA, Lafaille JJ. Natural and Adaptive Foxp3+ Regulatory T Cells: More of the Same or a Division of Labor? *Immunity* (2009) 30 (5):626–35. doi: 10.1016/j.immuni.2009.05.002
2. Rudensky AY. Regulatory T Cells and Foxp3. *Immunol Rev* (2011) 241 (1):260–8. doi: 10.1111/j.1600-065X.2011.01018.x
3. Sakaguchi S. Naturally Arising CD4+ Regulatory T Cells for Immunologic Self-Tolerance and Negative Control of Immune Responses. *Annu Rev Immunol* (2004) 22:531–62. doi: 10.1146/annurev.immunol.21.120601.141122
4. Miyara M, Sakaguchi S. Natural Regulatory T Cells: Mechanisms of Suppression. *Trends Mol Med* (2007) 13(3):108–16. doi: 10.1016/j.molmed.2007.01.003
5. Sakaguchi S. Naturally Arising Foxp3-Expressing CD25+CD4+ Regulatory T Cells in Immunological Tolerance to Self and non-Self. *Nat Immunol* (2005) 6 (4):345–52. doi: 10.1038/ni1178
6. Shevach EM. Mechanisms of Foxp3+ T Regulatory Cell-Mediated Suppression. *Immunity* (2009) 30(5):636–45. doi: 10.1016/j.immuni.2009.04.010
7. von Boehmer H. Mechanisms of Suppression by Suppressor T Cells. *Nat Immunol* (2005) 6(4):338–44. doi: 10.1038/ni1180
8. Campbell C, Rudensky A. Roles of Regulatory T Cells in Tissue Pathophysiology and Metabolism. *Cell Metab* (2020) 31(1):18–25. doi: 10.1016/j.cmet.2019.09.010
9. Fischer L, Herkner C, Kitte R, Dohnke S, Riewaldt J, Kretschmer K, et al. Foxp3+ Regulatory T Cells in Bone and Hematopoietic Homeostasis. *Front Endocrinol* (2019) 10(578). doi: 10.3389/fendo.2019.00578
10. Sharma A, Rudra D. Emerging Functions of Regulatory T Cells in Tissue Homeostasis. *Front Immunol* (2018) 9(883):883. doi: 10.3389/fimmu.2018.00883
11. Teitelbaum SL. Bone Resorption by Osteoclasts. *Science* (2000) 289 (5484):1504–8. doi: 10.1126/science.289.5484.1504

12. Sakaguchi S, Wing K, Onishi Y, Prieto-Martin P, Yamaguchi T. Regulatory T Cells: How do They Suppress Immune Responses? *Int Immunol* (2009) 21 (10):1105–11. doi: 10.1093/intimm/dxp095
13. Kelchtermans H, Geboes L, Mitera T, Huskens D, Leclercq G, Matthys P. Activated CD4+CD25+ Regulatory T Cells Inhibit Osteoclastogenesis and Collagen-Induced Arthritis. *Ann Rheumatic Dis* (2009) 68(5):744–50. doi: 10.1136/ard.2007.086066
14. Kim YG, Lee CK, Nah SS, Mun SH, Yoo B, Moon HB. Human CD4+CD25+ Regulatory T Cells Inhibit the Differentiation of Osteoclasts From Peripheral Blood Mononuclear Cells. *Biochem Biophys Res Commun* (2007) 357 (4):1046–52. doi: 10.1016/j.bbrc.2007.04.042
15. Luo CY, Wang L, Sun C, Li DJ. Estrogen Enhances the Functions of CD4(+) CD25(+)Foxp3(+) Regulatory T Cells That Suppress Osteoclast Differentiation and Bone Resorption *In Vitro*. *Cell Mol Immunol* (2011) 8 (1):50–8. doi: 10.1038/cmi.2010.54
16. Axmann R, Herman S, Zaiss M, Franz S, Polzer K, Zwerina J, et al. CTLA-4 Directly Inhibits Osteoclast Formation. *Ann Rheum Dis* (2008) 67(11):1603–9. doi: 10.1136/ard.2007.080713
17. Zaiss MM, Axmann R, Zwerina J, Polzer K, Guckel E, Skapenko A, et al. Treg Cells Suppress Osteoclast Formation: A New Link Between the Immune System and Bone. *Arthritis Rheum* (2007) 56(12):4104–12. doi: 10.1002/art.23138
18. Zaiss MM, Frey B, Hess A, Zwerina J, Luther J, Nimmerjahn F, et al. Regulatory T Cells Protect From Local and Systemic Bone Destruction in Arthritis. *J Immunol* (2010) 184(12):7238–46. doi: 10.4049/jimmunol.0903841
19. Laperine O, Blin-Wakkach C, Guicheux J, Beck-Cormier S, Lesclous P. Dendritic-Cell-Derived Osteoclasts: A New Game Changer in Bone-Resorption-Associated Diseases. *Drug Discovery Today* (2016) 21(9):1345–54. doi: 10.1016/j.drudis.2016.04.022
20. Madel MB, Ibanez L, Wakkach A, de Vries TJ, Teti A, Apparailly F, et al. Immune Function and Diversity of Osteoclasts in Normal and Pathological Conditions. *Front Immunol* (2019) 10:1408. doi: 10.3389/fimmu.2019.01408
21. Xiao Y, Zijl S, Wang L, de Groot DC, van Tol MJ, Lankester AC, et al. Identification of the Common Origins of Osteoclasts, Macrophages, and Dendritic Cells in Human Hematopoiesis. *Stem Cell Rep* (2015) 4(6):984–94. doi: 10.1016/j.stemcr.2015.04.012
22. Bozec A, Zaiss MM, Kagwiria R, Voll R, Rauh M, Chen Z, et al. T Cell Costimulation Molecules CD80/86 Inhibit Osteoclast Differentiation by Inducing the IDO/tryptophan Pathway. *Sci Transl Med* (2014) 6 (235):235ra60. doi: 10.1126/scitranslmed.3007764
23. Niedergang F, Di Bartolo V, Alcover A. Comparative Anatomy of Phagocytic and Immunological Synapses. *Front Immunol* (2016) 7:18. doi: 10.3389/fimmu.2016.00018
24. Siegmund K, Feuerer M, Siewert C, Ghani S, Haubold U, Dankof A, et al. Migration Matters: Regulatory T-Cell Compartmentalization Determines Suppressive Activity *In Vivo*. *Blood* (2005) 106(9):3097–104. doi: 10.1182/blood-2005-05-1864
25. Betaneli V, Jessberger R. Mechanism of Control of F-Actin Cortex Architecture by SWAP-70. *J Cell Sci* (2020) 133(2). doi: 10.1242/jcs.233064
26. Pearce G, Angeli V, Randolph GJ, Junt T, von Andrian U, Schnittler HJ, et al. Signaling Protein SWAP-70 is Required for Efficient B Cell Homing to Lymphoid Organs. *Nat Immunol* (2006) 7(8):827–34. doi: 10.1038/ni1365
27. Ocana-Morgner C, Reichardt P, Chopin M, Braungart S, Wahren C, Gunzer M, et al. Sphingosine 1-Phosphate-Induced Motility and Endocytosis of Dendritic Cells is Regulated by SWAP-70 Through RhoA. *J Immunol* (2011) 186(9):5345–55. doi: 10.4049/jimmunol.1003461
28. Ripich T, Jessberger R. SWAP-70 Regulates Erythropoiesis by Controlling Alpha4 Integrin. *Haematologica* (2011) 96(12):1743–52. doi: 10.3324/haematol.2011.050468
29. Sivalenka RR, Jessberger R. SWAP-70 Regulates C-Kit-Induced Mast Cell Activation, Cell-Cell Adhesion, and Migration. *Mol Cell Biol* (2004) 24 (23):10277–88. doi: 10.1128/MCB.24.23.10277-10288.2004
30. Chopin M, Quemeneur L, Ripich T, Jessberger R. SWAP-70 Controls Formation of the Splenic Marginal Zone Through Regulating T1B-Cell Differentiation. *Eur J Immunol* (2010) 40(12):3544–56. doi: 10.1002/eji.201040556
31. Garbe AI, Roscher A, Schuler C, Lutter AH, Glosmann M, Bernhardt R, et al. Regulation of Bone Mass and Osteoclast Function Depend on the F-Actin Modulator SWAP-70. *J Bone Miner Res* (2012) 27(10):2085–96. doi: 10.1002/jbmr.1670
32. Kriplani N, Duncan RR, Leslie NR. SWAP70 Undergoes Dynamic Conformational Regulation at the Leading Edge of Migrating Cells. *FEBS Lett* (2019) 593(4):395–405. doi: 10.1002/1873-3468.13326
33. Ocana-Morgner C, Wahren C, Jessberger R. SWAP-70 Regulates RhoA/RhoB-Dependent MHCII Surface Localization in Dendritic Cells. *Blood* (2009) 113(7):1474–82. doi: 10.1182/blood-2008-04-152587
34. Pearce G, Audzevich T, Jessberger R. SYK Regulates B-Cell Migration by Phosphorylation of the F-Actin Interacting Protein SWAP-70. *Blood* (2011) 117(5):1574–84. doi: 10.1182/blood-2010-07-295659
35. Roscher A, Hasegawa T, Dohnke S, Ocana-Morgner C, Amizuka N, Jessberger R, et al. The F-Actin Modulator SWAP-70 Controls Podosome Patterning in Osteoclasts. *Bone Rep* (2016) 5:214–21. doi: 10.1016/j.bonr.2016.07.002
36. Shinohara M, Terada Y, Iwamatsu A, Shinohara A, Mochizuki N, Higuchi M, et al. SWAP-70 is a Guanine-Nucleotide-Exchange Factor That Mediates Signalling of Membrane Ruffling. *Nature* (2002) 416(6882):759–63. doi: 10.1038/416759a
37. Marson A, Kretschmer K, Frampton GM, Jacobsen ES, Polansky JK, MacIsaac KD, et al. Foxp3 Occupancy and Regulation of Key Target Genes During T-Cell Stimulation. *Nature* (2007) 445(7130):931–5. doi: 10.1038/nature05478
38. Fontenot JD, Rasmussen JP, Williams LM, Dooley JL, Farr AG, Rudensky AY. Regulatory T Cell Lineage Specification by the Forkhead Transcription Factor Foxp3. *Immunity* (2005) 22(3):329–41. doi: 10.1016/j.immuni.2005.01.016
39. Borggrefe T, Keshavarzi S, Gross B, Wabl M, Jessberger R. Impaired IgE Response in SWAP-70-Deficient Mice. *Eur J Immunol* (2001) 31(8):2467–75. doi: 10.1002/1521-4141(200108)31:8<2467::AID-IMMU2467>3.0.CO;2-P
40. Petzold C, Steinbronn N, Gereke M, Strasser RH, Sparwasser T, Bruder D, et al. Fluorochrome-Based Definition of Naturally Occurring Foxp3(+) Regulatory T Cells of Intra- and Extrathymic Origin. *Eur J Immunol* (2014) 44(12):3632–45. doi: 10.1002/eji.201444750
41. Bettelli E, Pagany M, Weiner HL, Linington C, Sobel RA, Kuchroo VA, et al. Myelin Oligodendrocyte Glycoprotein-Specific T Cell Receptor Transgenic Mice Develop Spontaneous Autoimmune Optic Neuritis. *J Exp Med* (2003) 197(9):1073–81. doi: 10.1084/jem.20021603
42. Weischenfeldt J, Porse B. Bone Marrow-Derived Macrophages (BMM): Isolation and Applications. *CSH Protoc* (2008) 2008, pdb prot5080. doi: 10.1101/pdb.prot5080
43. Borggrefe T, Masat L, Wabl M, Riwar B, Cattoretti G, Jessberger R. Cellular, Intracellular, and Developmental Expression Patterns of Murine SWAP-70. *Eur J Immunol* (1999) 29(6):1812–22. doi: 10.1002/(SICI)1521-4141(199906)29:06<1812::AID-IMMU1812>3.0.CO;2-J
44. Hill JA, Feuerer M, Tash K, Haxhinasto S, Perez J, Melamed R, et al. Foxp3 Transcription-Factor-Dependent and -Independent Regulation of the Regulatory T Cell Transcriptional Signature. *Immunity* (2007) 27(5):786–800. doi: 10.1016/j.immuni.2007.09.010
45. Gavin MA, Rasmussen JP, Fontenot JD, Vasta V, Manganiello VC, Beavo JA, et al. Foxp3-Dependent Programme of Regulatory T-Cell Differentiation. *Nature* (2007) 445(7129):771–5. doi: 10.1038/nature05543
46. Lin W, Haribhai D, Relland LM, Truong N, Carlson MR, Williams CB, et al. Regulatory T Cell Development in the Absence of Functional Foxp3. *Nat Immunol* (2007) 8(4):359–68. doi: 10.1038/ni1445
47. Dohnke S, Schreiber M, Schallenberg S, Simonetti M, Fischer L, Garbe AI, et al. Approaches to Discriminate Naturally Induced Foxp3+ Treg Cells of Intra-And Extrathymic Origin: Helios, Neuropilin-1, and Foxp3RFP/GFP. *J Clin Cell Immunol* (2018) 9(1). doi: 10.4172/2155-9899.1000540
48. Schallenberg S, Petzold C, Tsai PY, Sparwasser T, Kretschmer K. Vagaries of Fluorochrome Reporter Gene Expression in Foxp3+ Regulatory T Cells. *PloS One* (2012) 7(8):e41971. doi: 10.1371/journal.pone.0041971
49. Singh K, Hjort M, Thorvaldson L, Sandler S. Concomitant Analysis of Helios and Neuropilin-1 as a Marker to Detect Thymic Derived Regulatory T Cells in Naïve Mice. *Sci Rep* (2015) 5:7767. doi: 10.1038/srep07767
50. Szurek E, Cebula A, Wojciech L, Pietrzak M, Rempala G, Kisielow P, et al. Differences in Expression Level of Helios and Neuropilin-1 Do Not Distinguish Thymus-Derived From Extrathymically-Induced CD4+Foxp3+ Regulatory T Cells. *PloS One* (2015) 10(10):e0141161. doi: 10.1371/journal.pone.0141161
51. Thornton AM, Korty PE, Tran DQ, Wohlfert EA, Murray PE, Belkaid Y, et al. Expression of Helios, an Ikaros Transcription Factor Family Member, Differentiates Thymic-Derived From Peripherally Induced Foxp3+ T Regulatory Cells. *J Immunol* (2010) 184(7):3433–41. doi: 10.4049/jimmunol.0904028
52. Wu Y, Borde M, Heissmeyer V, Feuerer M, Lapan AD, Stroud JC, et al. FOXP3 Controls Regulatory T Cell Function Through Cooperation With NFAT. *Cell* (2006) 126(2):375–87. doi: 10.1016/j.cell.2006.05.042

53. Gupta S, Lee A, Hu C, Fanzo J, Goldberg I, Cattoretti G, et al. Molecular Cloning of IBP, a SWAP-70 Homologous GEF, Which is Highly Expressed in the Immune System. *Hum Immunol* (2003) 64(4):389–401. doi: 10.1016/S0198-8859(03)00024-7
54. Tanaka Y, Bi K, Kitamura R, Hong S, Altman Y, Matsumoto A, et al. SWAP-70-Like Adapter of T Cells, an Adapter Protein That Regulates Early TCR-Initiated Signaling in Th2 Lineage Cells. *Immunity* (2003) 18(3):403–14. doi: 10.1016/S1074-7613(03)00054-2
55. Weiss JM, Bilate AM, Gobert M, Ding Y, Curotto de Lafaille MA, Parkhurst CN, et al. Neuropilin 1 is Expressed on Thymus-Derived Natural Regulatory T Cells, But Not Mucosa-Generated Induced Foxp3+ T Reg Cells. *J Exp Med* (2012) 209(10):1723–42. doi: 10.1084/jem.20120914
56. Yadav M, Louvet C, Davini D, Gardner JM, Martinez-Llordella M, Bailey-Bucktrout S, et al. Neuropilin-1 Distinguishes Natural and Inducible Regulatory T Cells Among Regulatory T Cell Subsets In Vivo. *J Exp Med* (2012) 209(10):1713–22, S1-19. doi: 10.1084/jem.20120822
57. Thornton AM, Shevach EM. Helios: Still Behind the Clouds. *Immunology* (2019) 158(3):161–70. doi: 10.1111/imm.13115
58. van der Veeken J, Gonzalez AJ, Cho H, Arvey A, Hemmers S, Leslie CS, et al. Memory of Inflammation in Regulatory T Cells. *Cell* (2016) 166(4):977–90. doi: 10.1016/j.cell.2016.07.006
59. Bonelli M, Savitskaya A, Steiner CW, Rath E, Smolen JS, Scheinecker C. Phenotypic and Functional Analysis of CD4+ CD25- Foxp3+ T Cells in Patients With Systemic Lupus Erythematosus. *J Immunol* (2009) 182(3):1689–95. doi: 10.4049/jimmunol.182.3.1689
60. de Paz B, Prado C, Alperi-Lopez M, Ballina-Garcia FJ, Rodriguez-Carrio J, Lopez P, et al. Effects of Glucocorticoid Treatment on CD25(-)FOXP3(+) Population and Cytokine-Producing Cells in Rheumatoid Arthritis. *Rheumatol (Oxford)* (2012) 51(7):1198–207. doi: 10.1093/rheumatology/kes039
61. Ferreira RC, Simons HZ, Thompson WS, Rainbow DB, Yang X, Cutler AJ, et al. Cells With Treg-Specific FOXP3 Demethylation But Low CD25 are Prevalent in Autoimmunity. *J Autoimmun* (2017) 84:75–86. doi: 10.1016/j.jaut.2017.07.009
62. Fransson M, Burman J, Lindqvist C, Atterby C, Fagius J, Loskog A. T Regulatory Cells Lacking CD25 are Increased in MS During Relapse. *Autoimmunity* (2010) 43(8):590–7. doi: 10.3109/08916930903541190
63. Zhang B, Zhang X, Tang FL, Zhu LP, Liu Y, Lipsky PE. Clinical Significance of Increased CD4+CD25-Foxp3+ T Cells in Patients With New-Onset Systemic Lupus Erythematosus. *Ann Rheum Dis* (2008) 67(7):1037–40. doi: 10.1136/ard.2007.083543
64. Wu H, Chen Y, Zhu H, Zhao M, Lu Q. The Pathogenic Role of Dysregulated Epigenetic Modifications in Autoimmune Diseases. *Front Immunol* (2019) 10:2305. doi: 10.3389/fimmu.2019.02305
65. Permanyer M, Bosnjak B, Glage S, Friedrichsen M, Floess S, Huehn J, et al. Efficient IL-2R Signaling Differentially Affects the Stability, Function, and Composition of the Regulatory T-Cell Pool. *Cell Mol Immunol* (2021) 18(2):398–414. doi: 10.1038/s41423-020-00599-z
66. de la Rosa M, Rutz S, Dorninger H, Scheffold A. Interleukin-2 is Essential for CD4+CD25+ Regulatory T Cell Function. *Eur J Immunol* (2004) 34(9):2480–8. doi: 10.1002/eji.200425274
67. Scheffold A, Murphy KM, Hofer T. Competition for Cytokines: T(reg) Cells Take All. *Nat Immunol* (2007) 8(12):1285–7. doi: 10.1038/ni1207-1285
68. Chandrasekaran U, Yi W, Gupta S, Weng CH, Giannopoulou E, Chinenov Y, et al. Regulation of Effector Treg Cells in Murine Lupus. *Arthritis Rheumatol* (2016) 68(6):1454–66. doi: 10.1002/art.39599

Conflict of Interest: The authors declare that the research was conducted in the absence of any commercial or financial relationships that could be construed as a potential conflict of interest.

Publisher's Note: All claims expressed in this article are solely those of the authors and do not necessarily represent those of their affiliated organizations, or those of the publisher, the editors and the reviewers. Any product that may be evaluated in this article, or claim that may be made by its manufacturer, is not guaranteed or endorsed by the publisher.

frontiers | Frontiers in Immunology

ORIGINAL RESEARCH
published: 04 May 2022
doi: 10.3389/fimmu.2022.817281

Modulation of Differentiation and Bone Resorbing Activity of Human (Pre-) Osteoclasts After X-Ray Exposure

Denise Eckert[1†§], Felicitas Rapp[1†‡§], Ayele Taddese Tsedeke[1†§], Daniela Kraft[1], Isabell Wente[1], Jessica Molendowska[1†], Sidra Basheer[1†], Markus Langhans[2†], Tobias Meckel[2†], Thomas Friedrich[1†], Anna-Jasmina Donaubauer[3,4], Ina Becker[3,4], Benjamin Frey[3,4†] and Claudia Fournier[1†]*

[1] Department of Biophysics, Gesellschaft für Schwerionenforschung (GSI) Helmholtzzentrum für Schwerionenforschung, Darmstadt, Germany, [2] Department of Macromolecular and Paper Chemistry and Membrane Dynamics, Technical University Darmstadt, Darmstadt, Germany, [3] Translational Radiobiology, Department of Radiation Oncology, Universitätsklinikum Erlangen, Friedrich-Alexander-Universität Erlangen-Nürnberg (FAU), Erlangen, Germany, [4] Department of Radiation Oncology, Universitätsklinikum Erlangen, Friedrich-Alexander-Universität Erlangen-Nürnberg (FAU), Erlangen, Germany

Low-dose radiotherapy (LD-RT) is a local treatment option for patients with chronic degenerative and inflammatory diseases, in particular musculoskeletal diseases. Despite reported analgesic and anti-inflammatory effects, cellular and molecular mechanisms related to osteoimmunological effects are still elusive. Here we test the hypothesis that X-irradiation inhibits the differentiation of precursor osteoclasts into mature osteoclasts (mOC) and their bone resorbing activity. Circulating monocytes from healthy donors were isolated and irradiated after attachment with single or fractionated X-ray doses, comparable to an LD-RT treatment scheme. Then monocytes underwent *ex vivo* differentiation into OC during cultivation up to 21 days, under conditions mimicking the physiological microenvironment of OC on bone. After irradiation, apoptotic frequencies were low, but the total number of OC precursors and mOC decreased up to the end of the cultivation period. On top, we observed an impairment of terminal differentiation, i.e. a smaller fraction of mOC, reduced resorbing activity on bone, and release of collagen fragments. We further analyzed the effect of X-irradiation on multinucleation, resulting from the fusion of precursor OC, which occurs late during OC differentiation. At 21 days after exposure, the observation of smaller cellular areas and a reduced number of nuclei per mOC suggest an impaired fusion of OC precursors to form mOC. Before, at 14 days, the nuclear translocation of Nuclear Factor Of Activated T Cells 1 (NFATc1), a master regulator of osteoclast differentiation and fusion, was decreased. In first results, obtained in the frame of a longitudinal LD-RT study, we previously reported a pain-relieving effect in patients. However, in a subgroup of patients suffering from Calcaneodynia or Achillodynia, we did not observe a consistent decrease of established blood markers for resorption and formation of bone, or modified T cell subtypes involved in regulating these processes. To assess the relevance of changes in bone metabolism for other diseases treated with LD-

OPEN ACCESS

Edited by:
Michal Tomcik, Institute of Rheumatology, Prague, Czechia

Reviewed by:
Elena Ambrogini, United States Department of Veterans Affairs, United States
Alexander Rühle, Freiburg University Medical Center, Germany
Meike Julia Saul, Darmstadt University of Technology, Germany

***Correspondence:**
Claudia Fournier
c.fournier@gsi.de

‡Present address:
Felicitas Rapp, Department of Hematology and Oncology, Medical Faculty Mannheim, Heidelberg University, Mannheim, Germany

§These authors have contributed equally to this work

Specialty section:
This article was submitted to Autoimmune and Autoinflammatory Disorders, a section of the journal Frontiers in Immunology

Received: *17 November 2021*
Accepted: *08 April 2022*
Published: *04 May 2022*

Citation:
Eckert D, Rapp F, Tsedeke AT, Kraft D, Wente I, Molendowska J, Basheer S, Langhans M, Meckel T, Friedrich T, Donaubauer A-J, Becker I, Frey B and Fournier C (2022) Modulation of Differentiation and Bone Resorbing Activity of Human (Pre-) Osteoclasts After X-Ray Exposure. Front. Immunol. 13:817281. doi: 10.3389/fimmu.2022.817281

RT will be subject of further studies. Taken together, we observed that *in vitro* X-irradiation of monocytes results in an inhibition of the differentiation into bone-resorbing OC and a concomitant reduction of resorbing activity. The detected reduced NFATc1 signaling could be one underlying mechanism.

Keywords: osteoclastogenesis, inflammation, musculo– skeletal disorders, low-dose radiotherapy, x-ray, NFATc-1, chronic degenerative and inflammatory diseases

INTRODUCTION

In chronic degenerative and inflammatory diseases such as Rheumatoid arthritis or Osteoarthritis, one hallmark is bone degradation and destruction of joint structures (1, 2), and in others, i.e. Calcaneodynia or Achillodynia, both degradation and neo-formation of bone can occur (3). This leads to significant pain, often to inflammation (4) and a reduction in quality of life of the patients. Standard treatments often involve non-steroidal anti-inflammatory drugs (NSAIDs), glucocorticoids, non-steroidal antirheumatics (NSARs) or biologicals like antibodies blocking inflammatory pathways. These drugs are important treatment modalities but can have severe side effects, especially when there is a need for taking them over longer periods (5, 6). As an alternative, patients with chronic degenerative and inflammatory diseases have been undergoing low-dose radiation therapy (LD-RT) for decades and report amelioration of their symptoms (7, 8). The molecular mechanisms which are responsible for this pain reduction are not yet fully unraveled, but, based on data obtained after radon exposure of patients, an influence on the immune system and bone metabolism is anticipated (9, 10).

In healthy bone tissue, a highly regulated homeostasis is maintained (11). The bone matrix is constantly remodeled by a tight interplay of bone-forming osteoblasts, sustaining osteocytes and bone resorbing osteoclasts (OC) (12). If this balance is disturbed and bone resorption is upregulated, as in chronic degenerative and inflammatory diseases, bone loss is the result, and the physiological function of joints is lost, leading to pain and movement restriction. Our hypothesis is that LD-RT has an impact on bone metabolism by restoring homeostasis transiently.

Unlike high-dose radiation therapy, as it is used in cancer therapy, for LD-RT, typically, a total dose of 3 to 5 Gy is administered locally in fractionated doses of 0.5 Gy each in 6 to 10 consecutive treatment sessions. Higher doses of X-irradiation have been reported to damage bone, such as growth disturbances in children (13, 14), radio-osteonecrosis (15) and resulting treatment-induced bone loss (CTIBL) (16) with a higher risk of fractures (17). As demonstrated for high doses in rodent models, damage to bone-forming cells, vasculature, or an impaired hormone balance can be responsible for the loss of bone mass. This is caused by inflammation, a restricted nutrient supply and a reduced bone neoformation (14, 18). For lower doses, no such harmful effects have been anticipated (19). In contrast, low-dose X-irradiation has been shown to promote osteoblast proliferation (20) and bone mineralization after fractures (21). The beneficial effect of LD-RT on inflamed joints and other parts of the musculoskeletal system is considered to be due to a modulation of anti-inflammatory signaling molecules such as iNOS (22) and a reduction of pro-inflammatory cytokines (23), which may act on a local and a systemic level of the body. To investigate the potential contribution of LD-RT to (24) modulations in bone metabolism, we aimed at investigating direct radiation induced effects on bone resorbing osteoclasts and their progenitor cells.

Mature OC (mOC) are multinucleated cells which are formed by the fusion of mononuclear progenitors of the monocyte/macrophage family and have distinct morphological features and functions (25). During this process, monocytes first differentiate under the influence of macrophage colony stimulating factor (M-CSF) into pro-osteoclasts (proOC), and then into OC precursors through receptor activator of nuclear factor 'kappa-light-chain-enhancer' of activated B-cells ligand (RANKL) signaling. Established markers for the differentiation stages are specific morphological features, Tartrate Resistant Acid Phosphatase (TRAP 5b) activity and fusion of three or more precursor OC, resulting in multinucleated (three or more nuclei), bone resorbing mOC. An additional marker for OC activity is the formation of a cytosolic actin ring (24, 26–28). Bone resorption as a functional marker is detectable by the formation of resorption pits on bone and the release of collagen fragments (CTX) by mOC. On a molecular level, multiple factors tightly regulate OC differentiation. Nuclear factor of activated T cells cytoplasmic-1 (NFATc1) is a master regulator of osteoclast differentiation (27, 29), regulating the expression of genes involved in cell fusion and activation of mOC (30, 31).

In most *in vitro/ex vivo* studies on OC, monocytes are isolated from blood (murine or human) and differentiated into OC by adding bone-specific growth factors, RANKL and M-CSF to the culture medium (25). Monocytic cell lines (RAW 264.7) are often used, which have some limitations because of their tumor component (32). A straightforward approach is to seed the monocytes on a conventional plastic substrate (24, 33). Then, the monocytes adhere to plastic, while other blood cells are removed by washing. The differentiated OC can then be analyzed *via* microscopy. However, for an analysis of the resorbing activity, the cultivation on plastic is not suitable. Therefore, in this study, we decided to cultivate, irradiate and differentiate OC precursors on bone slices, their physiological substrate, allowing the straightforward assessment of common markers of OC activity (e.g. CTX release and resorption pits formation). In addition, we established a method to evaluate nuclear translocation of NFATc1 in OC grown on bone by confocal microscopy. To characterize OC activity after irradiation, we

quantified OC precursor and mOC according to (26), as well as the formation of resorption pits on bone and the release of collagen fragments. Furthermore, we evaluated specific cellular and molecular markers, i.e. the number of nuclei and the size of the cellular area, TRAP 5b activity and nuclear translocation of the key transcription factor NFATc1 (24, 34, 35).

We set out to verify these findings *in vivo*. Patients with musculoskeletal diseases (mostly Calcaneodynia, Achillodynia and others) underwent LD-RT at the University Hospital Erlangen, Germany and in the frame of the prospective IMMO-LDRT01 study (NCT02653079), blood was drawn and analyzed at several time points before and after therapy.

We have reported in an interim analysis of this study that after local LD-RT, pain perception of the patients, evaluated with the VAS scale (1–10), significantly decreased over time, starting from a general pain level indicating medium to severe initial stages (36) and suggesting that inflammation might be involved in the course of the diseases (3). In addition to pain reduction, some immune cell types were modulated and their activation was downregulated (36).

As in an arthritic mouse model, it has been demonstrated that local LD-RT ameliorates bone resorption in arthritic joints (37), we tested a broader spectrum of markers of bone metabolism in blood samples of a subgroup of the patients, i.e. Calcaneodynia and Achillodynia patients, enrolled in the IMMO-LDRT01 study. Although bone degradation, but also bone formation and inflammation can occur in the course of these diseases, we could not consistently confirm the involvement of changes in bone resorption and formation *in vivo* for all markers tested. We speculate that this is related to the specific diseases of the patients of this subgroup.

MATERIAL AND METHODS

The supplement includes a graph to illustrate the flow of the *in vitro* experiments (**Figure S1**).

Isolation and Cultivation of OC Precursors and Differentiation Into mOC

For the isolation of human Peripheral Blood Mononuclear Cells (PBMC), buffy coats from healthy donors was either purchased from the blood donation service (Frankfurt/Main, Germany) or blood was drawn from healthy volunteers in Vacutainer tubes (BD Vacutainer® blood collection tubes, BD Biosciences, Heidelberg, Germany), both with Heparin as an anticoagulant. To isolate the PBMC from buffy coats, blood was diluted 1:1 with PBS (Sigma Aldrich Chemie GmbH, Steinheim, Germany) and carefully overlaid on Ficoll-Hypaque (Merck Millipore, Darmstadt, Germany) to avoid mixing of the phases. Vacutainer tubes with an integrated gel layer were directly used for centrifugation. The centrifugation followed at 1300 xg (buffy coat)/1500 xg (Vacutainer) for 30/20 min at room temperature (RT). Centrifugation resulted in separation into different phases, where the upper phase consisted of plasma and the second phase was the interphase containing the PBMC.

Plasma was removed for cultivation and heat-inactivated for 30 min at 56°C in a water bath (Grant SUB Aqua Pro, Fisher Scientific, Schwerte, Germany). Denatured proteins were removed by centrifugation (3360 xg, 5 min). The interphase with the PBMC was collected, washed with PBS/2 % FBS (Sigma Aldrich) and centrifuged (300 xg, 8 min). To remove the remaining erythrocytes, red blood cell lysis buffer (RBC, 8.29 g NH_4Cl, 1 g $KHCO_3$, 37.2 mg Na_2EDTA, 800 ml H_2O, pH 7.2-7.4 in 1 L H_20) was added (buffy coat: 5 ml, Vacutainer: 2 ml) and incubated at RT for 5 min. Then, PBS/2 % FBS (Sigma Aldrich) was added to stop the reaction (buffy coat: filled to 50 ml, vacutainer: filled to 15 ml), cells were collected (300 xg, 8 min) and suspended in X-Vivo-15 medium (Lonza/Biozym Scientific GmbH, Oldendorf, Germany) containing 3 % autologous plasma and 1 % Penicillin/ Streptomycin (Pen/ Strep) (PAN-BIOTECH, Aidenbach, Germany) (buffy coat: 50 ml, vacutainer: 5 ml).

Afterwards, PBMC were seeded on bone slices (ids immunodiagnostics, Boldon, UK) in X-Vivo-15 medium and incubated at 37°C/5 % CO_2 for 1-2 hours, allowing monocytes to adhere [modified after (24)]. For successful seeding on bone slices ($4x10^5$ cells in at least 100 µl), the slices were first placed in 96-well plates during the adhesion process, and at the same time, non-adherent lymphocytes were removed, and the remaining attached cells were transferred to 24-well plates, containing 500 µl of differentiation medium (Alpha-medium, Merck Millipore). The medium was supplemented with 1 % Pen/ Strep, 10 % autologous plasma and differentiation factors, i.e. RANK-L (40 ng/ml, EMD Millipore Corp., Billerica, MA, USA) and M-CSF (25 ng/ml, Miltenyi Biotec, Bergisch Gladbach, Germany), marking the onset of the differentiation process. Almost all attached cells displayed typical morphological features of the first OC differentiation stage (26) and were therefore classified as precursor OC from this time point on. For the following differentiation process, OC precursors were cultured for 21 days. Medium was changed twice a week, and supernatants were collected and stored at -80°C.

Irradiation of OC Precursors

After the adhesion step and in the presence of growth factors, attached cells were exposed to X-rays at single doses of 0.5 to 10 Gy with a dose rate of 1-2 Gy/min or at fractionated doses in 4 or 10 fractions (0.5 or 1 Gy each) in 24 h intervals to simulate a therapeutic setting. Irradiation was performed at RT with an X-ray tube with 250 kV and 16 mA (Seifert Isovolt DS1, Ahrensberg, Germany). Sham-irradiated cells were also transported to the X-ray tube and used as controls.

Analysis of Apoptotic Cells

Apoptotic cell death was evaluated *via* morphologic features of apoptosis (38–40) in osteoclast cells, such as nuclear condensation, nuclear fragmentation and membrane blebbing in the same microscopic pictures used for osteoclast characterization. The fraction of apoptotic cells was calculated in relation to the total cell number ranging from 150 to 250 cells per field of view at 6 and 12 hours and 3, 5, 7, 14 and 21 days after X-irradiation.

Identification of Precursor and mOC by Fluorescent Triple Staining

Morphological (cell size, number of nuclei) and functionality parameters of OC (TRAP, actin ring) were investigated according to standard criteria (24, 26, 28). However, additional molecular markers of OC differentiation have not been investigated because the choice of a bone matrix for cultivation brings along lower cell numbers than plastic, limiting the possibility of performing PCR analysis.

After fixation with 3.7 % PFA (Merck KGaA, Darmstadt, Germany) for 15 min at RT cells were incubated with TRAP staining solution for 10 min at 37°C. The staining solution consists of TRAP buffer (0.1 M acetate buffer: 35.2 ml 0.2 M Sodium Acetate solution, 14.8 ml 0.2 M acetic acid, 50 ml; Millipore, Burlington, USA) mixed with 0.3 M Sodium Tartrate (pH 5.5), 10 mg/ml Naphthol AS-MX phosphate, Triton X-100, 0.3 mg/ml Fast Red Violet LB Salt (all from Sigma Aldrich Chemie GmbH). After two washes with PBS, FITC-Phalloidin (0.66 µg/ml in PBS) (Sigma Aldrich Chemie GmbH) was added for 25 min in the dark at RT. Next, DAPI (1 µg/ml in PBS) (BD Biosciences) was added and incubated for another 7 minutes. After the last washing step, the cells were stored at 4°C in PBS in the dark.

Microscopic pictures were either taken on a confocal microscope (DMI4000B, Leica, Wetzlar, Germany; 5-10 images per bone slice) or with an epifluorescence microscope (DMIRE2, Leica, 20x) (**Figure 1A**). For evaluation, ImageJ (Wayne Rasband, NIH, Bethesda, USA) was used. Cells were classified into three subgroups according to established criteria (24, 26, 28): pro- (spindle-shaped with a single nucleus, **Figure 1D**), pre- (round with one or two nuclei, **Figure 1C**) and mOC (TRAP-positive and with three or more nuclei, **Figure 1B**). Throughout the text, pro-and pre-OC are not distinguished and termed OC precursors, unless stated otherwise. We show the total number of OC (OC precursor and mOC) and the number of mOC (reported per total number of OC and as fold change compared to controls). Furthermore, mOC with at least three nuclei were morphologically evaluated with regard to the number of nuclei and the cell surface area. The mean value for the total number of OC (OC precursor plus mOC) and mOC per total number of OC, was evaluated from 5-10 images per bone slice and afterwards from the technical replicates (n=2-3) for each donor. Finally, the mean value was calculated from all donor samples (N=4-8). No monocytes or dead cells were identified on the bone slices after 21 days of cultivation.

Measurement of Cellular Area and Counting of Nuclei per mOC

For the measurement of the cellular area of mOC, ImageJ was used. Outlines of cells with respect to actin staining (**Figures 1A–D**) were traced with the freehand tool, and the enclosed area was measured. The number of nuclei were also determined using ImageJ. An enhanced number of nuclei (three or more nuclei) is an established differentiation marker of mOC (25).

Analysis of Bone Resorbing Activity

A functional analysis of bone resorbing activity was performed by staining with toluidine blue. Cells were first removed with ammonium hydroxide solution (0.25 M Ammonium hydroxide

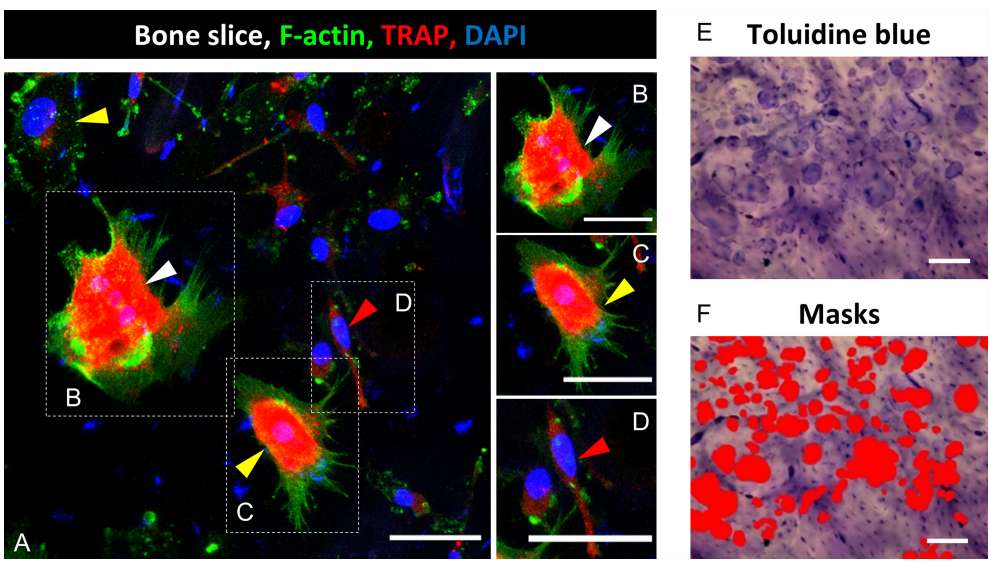

FIGURE 1 | Identification of mature osteoclasts (mOC) on bone slices and quantification of resorbing activity 21 days after onset of the differentiation process. A triple staining for OC markers was applied (TRAP, red; F-actin, green; nuclei: blue; **(A)**. A cell was classified as mOC when it TRAP-positive and had ≥ 3 nuclei (white arrowheads; all mOC showed an actin ring, **(B)**, precursor (preOC, round with one or two nuclei, yellow arrowheads, **(C)**, proOC (spindle-shaped with a single nucleus, red arrowhead, **(D)**. After microscopy, cells were removed, and resorption pits were visualized by Toluidine blue staining **(E)**. Semi-quantitative image analysis was performed using ImageJ and masks to measure the resorbed areas per field of view **(F)**. Scale bar: 50 µm **(A-D)**, 100 µm **(E, F)**.

solution, Sigma Aldrich Chemie GmbH, diluted with dist. water) for 5 min at RT and then wiped from the bone slice with a paper tissue. Toluidine blue staining solution (Toluidine blue staining solution in citric acid: 1 % Toluidine blue (Fluka/Sigma Aldrich Chemie GmbH) solved in 1 % sodium tetraborate (40°C, soluble in H_2O; Sigma Aldrich Chemie GmbH) was added to the bone slices for 10 min, and residues were washed away thoroughly with PBS. Images were taken with a light microscope (BX61, Olympus, Hamburg, Germany, 5-7 images per slice, 10x, **Figure 1E**) or a fluorescence microscope (Revolve 4M, Echo, San Diego, CA, USA). For analysis of the resorbed area, the color threshold function of ImageJ was used in order to mark the stained resorption pits (**Figure 1F**). Marked areas were measured and related to the total area per picture. In cases of weak staining or low contrast to the background, the ROI (Region of Interest) function was used to determine the resorbed area precisely. Per bone slice, six images were evaluated, and from this, the mean value was calculated. Subsequently, the mean value was calculated from the technical replicates of the respective healthy donors, and finally, the mean value was calculated from the respective healthy donors.

NFATc1 Immunofluorescent Staining

For immunofluorescent staining, 8 x 10^5 OC precursor cells were seeded on bone slices, fixed after 3, 5, 7 and 14 days of cultivation with 3.7 % PFA for 30 min at RT and washed with PBS. Then bone slices with cells were incubated with permeabilization solution (0.2 % Triton X-100, Sigma Aldrich Chemie GmbH) for 10 min at RT, followed by incubation in blocking buffer (5 % BSA, Sigma Aldrich and 5% Goat serum, Invitrogen) for 1 h. Afterwards, bone slices were incubated with anti-NFATc1 (Santa Cruz, Dallas, TX, USA, 1:200) overnight at 4°C. The next day, after washing three times with PBST (0.1 % Triton X-100, Sigma Aldrich Chemie GmbH), bone slices were incubated for 2 h with secondary antibody goat anti-mouse Alexa Fluor 488 or goat anti-mouse Alexa Fluor 647 (Thermo Fisher, Waltham, MA, USA, 1:500 in PBST) at RT. Subsequently, the bone slices were washed three times with PBS-T, TRAP staining buffer was added for 10 min at 37°C, and nuclei were counterstained with DAPI (Sigma Aldrich Chemie GmbH). Images were captured using a confocal microscope (DMIRE 4000B or TCS SP8, Leica) with a 20x or 40x oil-immersion objective. Fluorescent intensity of NFATc1was calculated using ImageJ from the integrated density of the entire cell, minus the integrated density of the nucleus. Subsequently, the values for nucleus or cytoplasm were divided by the total intensity of the cell.

Study Design of the IMMO-LDRT01 Trial

For details on the IMMO-LDRT01 trial (NCT02653079), see (36). Briefly, all patients enrolled were affected by chronic degenerative and inflammatory diseases. They have signed an informed consent, the trial was ethically approved by the 'Ethik Kommission der Friedrich-Alexander-Universität Erlangen-Nürnberg' (#289_15 B) and followed the 'Declaration of Helsinki' in its current form. Patients underwent a 1st series of irradiation with X-rays over 3 weeks, i.e. 6 fractions with a single dose of 0.5 Gy each. After 3 months, a 2nd series with the same scheme was administered if the patient stated that the therapeutic outcome was not satisfying. For the study presented here, blood samples have been drawn from a subgroup of 22 patients before (tp1) and after (tp2) the 1st series, before (tp3) and after (tp4) the 2nd series and 3 months later at the final follow-up appointment (tp5). The patients of this subgroup suffered mostly from Calcaneodynia and Achillodynia (see **Table 1**). According to their personal decision, all patients underwent in this study the 1st and the 2nd series. The pain perception of the patients, evaluated with the VAS scale (1–10), showed a significant decrease over time, starting from a general pain level of 6.5 and dropping to 3.8 (36). This mean pain level indicates advanced stages, suggesting that inflammation might be involved in the course of the treated diseases.

In the leukocyte fraction of the blood samples, the ratio of Th17/Treg was determined. In addition, in the plasma or serum fraction, resorption markers (CTX, TRAP 5b) and formation (OCN) of bone were quantified.

Analysis of Th17/Treg by Flow Cytometry

For the analysis of Th17/Treg ratio, isolated PBMC from LD-RT patients (see *Isolation and Cultivation of OC Precursors and Differentiation Into mOC*) were used. After isolation, 1x10^6 cells were fixed with 1x Human FoxP3 Buffer A (BD Pharmingen™, BD Pharmingen, Heidelberg, Germany) for 20 min at RT in the dark. Afterwards, they were centrifuged at 500 xg for 5 minutes and washed with PBS + 2 % FCS (500 xg, 5 min). Subsequently, cells were permeabilized by adding 0.5 ml of 1x working Human FoxP3 Buffer C (BD Pharmingen™) for 30 min at RT in the dark. Following, the cells were washed twice with PBS + 2 % FCS (500 xg, 5 min). Finally, fixed and permeabilized cells were stained with CD4 (PerCP-Cy5.5, clone SK3, #566923, BD), FoxP3 (Alexa Fluor 647, clone 259D/C7, #560045, BD), ROR-α (PE, clone #784652, #IC8924P-100, R&D Systems, Minneapolis, USA) for 40 min at RT in the dark. After two further washing steps, the expression of cell surface or

TABLE 1 | Characteristics of patients (IMMO-LDRT01 trial).

Total number		**22**	**patients**
Age at start	Mean	60	Years
	Range	38-77	Years
Gender	Male	4	patients
	Female	18	patients
Indications	Calcaneodynia	14 (64 %)	patients
	Achillodynia	4 (18 %)	patients
	Others	4 (18 %)	patients

intracellular markers was measured using a flow cytometer (CytoFLEX S, Beckman Coulter, Krefeld, Germany). The gating strategy is shown in **Figure 6A**. Using CytExpert software (Beckman Coulter), the frequency of cells related to the total number of $CD4^+$ cells was analyzed: $CD4^+FoxP3^+$ cells were classified as Treg cells and $CD4^+$ ROR-α^+ as Th17 cells.

Detection of CTX Fragments in Cell Culture Supernatants and Patient Samples

For the analysis of released collagen fragments, CTX ELISA [Serum CrossLaps® (CTX-I) ELISAs, ids immunodiagnostics, Boldon, UK] was used for cell culture supernatants and plasma from patients according to the manufacturer's protocol.

In brief, 50 µl of each standard, control and undiluted sample were pipetted on the Streptavidin-coated plate. Afterwards, 150 µl of the antibody solution AB SOLN were added and incubated for 120 min at RT on a microtiter plate mixer (300 rpm, Heidolph UNIMAX 1010, Schwabach, Germany). Subsequently, wells were washed 5 times with diluted wash solution. Then, 100 µl of substrate solution were added to each well and incubated for a further 15 min in the dark on a microtiter plate mixer (300 rpm). Subsequently, 100 µl of stopping solution (H_2SO_4) were added, and finally, the absorbance was measured with SpectraMax i3x (Molecular Devices, California, USA) at 450 nm with reference at 650 nm.

Detection of TRAP 5b Activity in Serum of Patients

For analysis of TRAP 5b activity in serum of patients, BoneTRAP® ELISA (ids immunodiagnostics, Boldon, UK) was used as described in the manufacturer's protocol. In brief, 100 µl of standard, control and patient serum were pipetted in duplicates. Afterwards, 50 µl of Releasing Reagent were added to each well and were incubated with constant shaking for 1 h at RT (with foil). Then, wells were washed four times with 300 µl Wash Buffer. Subsequently, 100 µl of Substrate were added and incubated for 1 h at 37°C (with foil). After the incubation step, 25 µl of Stop Solution were added. Finally, the absorbance was measured with SpectraMax i3x (Molecular Devices, California, USA) at 450 nm with reference at 650 nm.

Quantification of OCN in Plasma of Patients

For the analysis of Osteocalcin (OCN), Osteocalcin Human ELISA Kit (Thermo Fisher, Waltham, MA, USA) was used for plasma from patients according to the manufacturer's protocol.

In brief, 25 µl of each standard, control and undiluted sample were pipetted on the Streptavidin-coated plate. Afterwards, 100 µl of the Anti-OST-HRP conjugated Solution were added and incubated for 120 min at RT. Subsequently, wells were washed 3 times. Then, 100 µl of Stabilized Chromogen Solution were added to each well and incubated for a further 30 min at RT. Subsequently, 100 µl of Stop Solution were added, and finally, the absorbance was measured with SpectraMax i3x (Molecular Devices, California, USA) at 450 nm with reference at 650 nm.

Statistical Analysis and Graph Settings

Data and statistical analyses were calculated with GraphPad Prism 8 (GraphPad Software, Inc., La Jolla, CA, USA) and are displayed with mean ± SEM. Testing for normal distribution was done by performing the Shapiro-Wilk test. For unpaired and normal distributed data with more than two groups, one-way-ANOVA followed by a posthoc Tukey's multiple comparison test (**Figures 2C**, **3B, C**) was applied. For unpaired and non-normal distributed data with more than two groups, the Kruskal-Wallis test followed by Dunn's test (**Figures 2B**, **3A, E, F**, **4A, C**, **5E, F**) was applied. For unpaired and normal distributed data with two groups t-test was applied (**Figure 3D**). For analysis of patient samples (paired with more than two groups), repeated measures one-way ANOVA was used, followed by posthoc Tukey's multiple comparison tests (**Figures 6E, G**) for normal distributed data, or Friedman Test (**Figures 6B–D, F**) for non-normal distributed data. P-value ≤ 0.05 was considered as significant.

Histograms of data distribution are depicted for cell area and number of nuclei in **Figure 4**. Data were normalized to values of unirradiated cells, and a proper bin size was applied (for area bin = 2000 µm and nuclei bin = 1).

RESULTS

X-Ray Irradiation of Osteoclast Precursors Cultivated on Bone Slices Decreases Resorbed Area and CTX Fragment Release in a Dose-Dependent Manner

As shown earlier, LD-RT decreases pain in patients with chronic degenerative and inflammatory diseases, which is, at least for Rheumatoid arthritis (RA), thought to be related to reduced activation of OC (41). To investigate this, we examined the impact of single and therapy-relevant fractionated X-ray doses on the formation of resorption pits by OC, that underwent culture on bone slices during 21 days after exposure (exemplary images are shown in **Figure 2A**). Irradiation induced a decrease of resorbed area, dropping sharply with increasing dose (**Figure 2B**). The resorbed area decreased more than 3-fold after irradiation with 0.5 Gy compared to unirradiated samples. After irradiation with 2 Gy or more, resorbed area was clearly reduced to a very low level, for single as well as for fractionated doses.

To confirm the obtained results, an additional marker of bone resorption, the release of CTX into the supernatant was measured. A dose-dependent decrease in the CTX concentration was found (**Figure 2C**). After irradiation with 0.5 Gy, the CTX concentration was reduced by a factor of 2 compared to unirradiated samples; after exposure to single doses of 2 - 10 Gy and fractionated doses of 4 x 0.5 Gy, 10 x 0.5 Gy and 10 x 1 Gy, the concentration of CTX was significantly decreased, at least by ~7-fold. The results indicate that the bone-resorbing activity is already reduced after exposure to a single dose of 0.5 Gy.

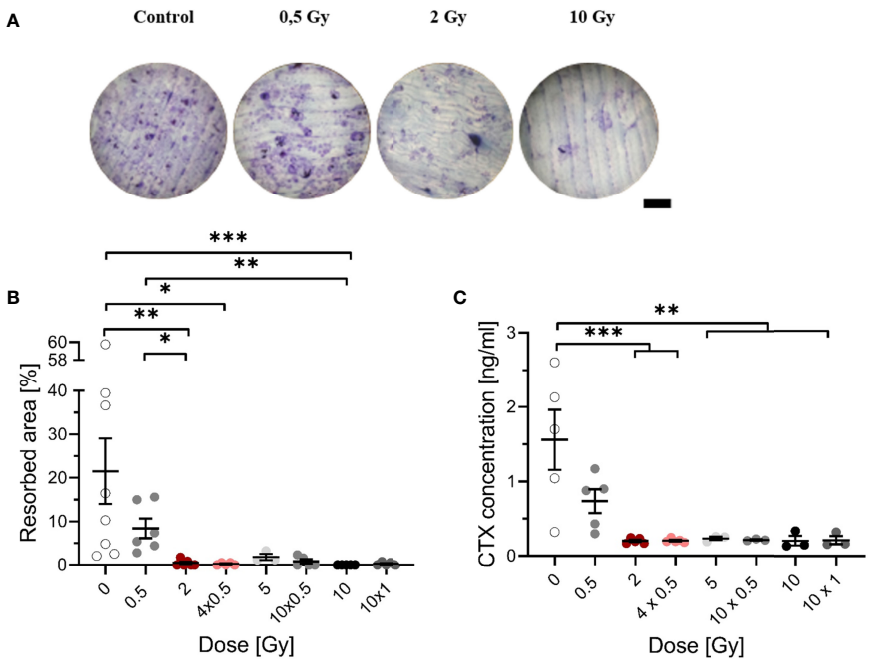

FIGURE 2 | Decreased resorbing activity of mOC on bone slices at 21 days after exposure to ionizing radiation (X-rays). Monocytes were attached on bone slices, then irradiated in the presence of growth and differentiation factors (M-CSF, RANKL) with single (0.5, 2 and 10 Gy) and fractionated doses (4 x 0.5, 10 x 0.5 and 10 x 1 Gy). Resorbing activity and release of collagen fragments (CTX) were investigated at 21 days. Resorbing activity of mOC was visualized by Toluidine blue, and the area of resorbed bone was measured by ImageJ [**(A)**, scale bar 100 µm]. Bone resorption was expressed as resorbed bone area in percent of total bone per field of view **(B)**. Soluble collagen fragments (CTX) were measured in culture supernatant as markers for OC resorbing activity **(C)**. Significance was tested with Kruskal-Wallis **(B)** for non-normal distributed data and with one-way ANOVA **(C)** for normal distributed data. P-values are indicated by asterisks with * for $p \leq 0.05$, ** for $p \leq 0.01$, and *** for $p \leq 0.001$. Error bars are reported as the mean ± SEM; N = 3-8.

The Fraction of mOC Is Decreased After X-Ray Irradiation on Bone Slices

To address whether a decreased cell number is responsible for the reduced bone resorbing activity of OC after irradiation, we next investigated 21 days after exposure the total OC number (OC precursor and mOC). In order to discriminate between cell loss over all differentiation stages and an inhibition of terminal differentiation, we report the respective fraction of mOC relative to the total number of OC and, in addition, the fold change of the number of mOC compared to controls. Monocytes were only sporadically observed and exclusively until 3 days after exposure.

The total number of OC, including proOC, preOC and mOC, was not significantly decreased at a single X-ray dose of 0.5 Gy, but decreased at single or fractionated doses of 2 Gy or higher (around 2.5-fold for 2, 4x 0.5, 5 and 10x 0.5 Gy, **Figure 3A**). A single dose of 10 Gy even lowered the cell number around 4-fold, whereas the fractionated dose of 10x 1 Gy resulted in a level comparable to the other doses.

Notably, on top of cell loss, the fraction of mOC, normalized on the respective total number of OC that was detectable for each sample, was strongly reduced after irradiating with X-ray in a dose-dependent manner. After 0.5 Gy, almost no change was detected, but after exposure to single or fractionated doses equal to or exceeding 2 Gy, a strong and significant reduction of mOC was visible (~5-fold for 2 and 4x 0.5 Gy, ~3-fold for 5 Gy, ~5-fold for 10 x 0.5 Gy, ~10-fold for 10 Gy and ~4-fold for 10x 1 Gy; **Figure 3B**). This indicates an impact of irradiation with single or fractionated doses on OC differentiation that is not detectable for a single dose of 0.5 Gy, but for all doses exceeding 0.5 Gy. The fold change of the number of mOC shows a clear decrease, significant for doses equal to or exceeding 0.5 Gy (**Figure 3C**).

To analyze the observed cell loss in more detail, we addressed apoptosis of OC precursor as a potential reason for our findings. For this, we analyzed microscopic pictures for morphological markers of apoptosis, like condensed or fragmented nuclei. At these earlier stages of differentiation (6 and 12 hours), there was a background level of cell death of around 4-8 % (**Figure 3D**). After 3 to 21 days, the level of apoptotic cells in irradiated samples did not exceed 5 %, while the level in unirradiated samples stayed at around 3 % (**Figures 3E, F**). Apoptosis did not increase after irradiation, most likely due to the protective effect of the differentiation factors (42). Therefore, apoptosis is unlikely to account for the drastic changes in mOC fractions reported above.

Directly after exposure, the induction of apoptosis in monocytes was assessed separately, without adding differentiation factors. The apoptotic frequency turned out to be low (see **Figure S2**) and was not further investigated in our study.

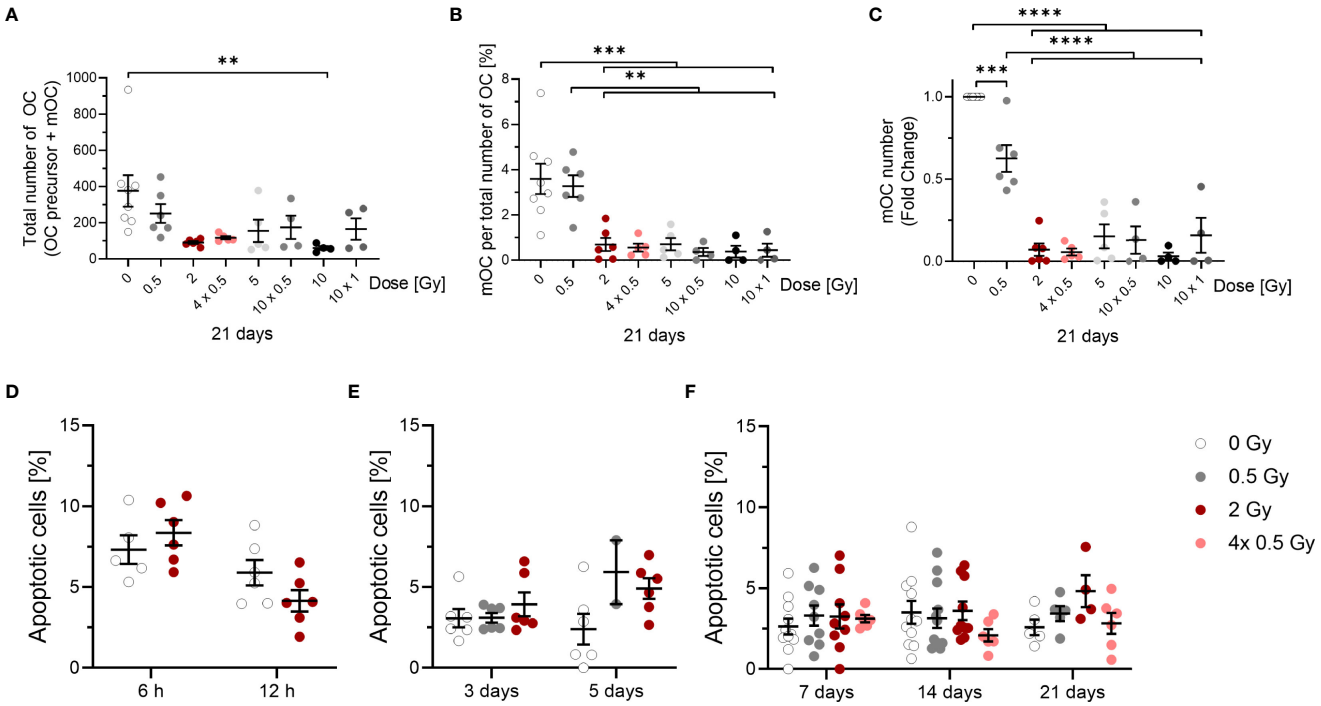

FIGURE 3 | Influence of irradiation (X-rays) on the survival of OC (OC precursors and mOC) and their differentiation into mOC (in relation to the respective OC number in each sample), following cultivation on bone slices for 21 days and apoptotic frequencies between 6h and 21 days after exposure. Monocytes were attached on bone slices, then irradiated in the presence of growth and differentiation factors (M-CSF, RANKL) with single doses (0. 0.5 and 2 Gy) and fractionated doses of X-rays (4× 0.5, 10x0.5 and 10x1 Gy). Differentiation into OC precursor and mOC was assessed at 21 days of cultivation. The total number of OC per field of view (OC precursor + mOC) is decreased in a dose-dependent manner **(A)**. On top of this reduction, mOC per total number of OC in each sample decreased after irradiation **(B)**. The fold change of mOC number compared to controls also shows a decrease **(C)**. mOC were identified based on morphological patterns (TRAP+, F-actin+ with ≥ three nuclei). Apoptotic frequencies were evaluated in cells 6 and 12 hours and after 3 to 21 days after exposure to the same doses as in **(A-C)** by morphological features **(D-F)**, indicating very low apoptotic frequencies at all time points investigated. Significance was tested with Kruskal-Wallis **(A, E, F)** for non-normal distributed data and with one-way ANOVA **(B, C)** for normal distributed data for more than two groups and with t-test **(D)** for normal distributed data for two groups. P-values are indicated by asterisks with *** for $p \leq 0.001$ and **** for $p \leq 0.0001$. Error bars are reported as mean ± SEM; N = 3-8.

Cell Fusion Is Inhibited After X-Ray Irradiation

Based on the finding that the fraction of mOC is strongly reduced after irradiation, we set out to identify the underlying mechanism. During differentiation, OC precursors fuse to form mOC, characterized by possessing three or more nuclei (43). As this was observed 21 days after irradiation and loss of OC cell explains only in part the massive reduction of resorbing activity, we analyzed next if the fusion of precursors is altered by X-ray irradiation. To this end, we analyzed the area covered by a single mOC and the average number of nuclei per mOC by fluorescent staining for OC markers TRAP, F-actin and nuclei (**Figure 4**).

X-ray irradiation reduced the area covered by mOC in a dose-dependent manner (**Figure 4A**). After irradiation with a single dose of 0.5 Gy, the mean cell area was only marginally changed, while it was decreased by a fold-change of ~1.5 after a single dose of 2 Gy. When this dose was delivered in fractions (4x 0.5 Gy), the mean cell area was only slightly changed compared to the single dose of 2 Gy. After single doses of 5 or 10 Gy, or fractionated doses of 10x 0.5 Gy or 10x 1 Gy, the area was strongly reduced by around 2.5- to 3-fold. This effect is even clearer when looking at the distribution of values in the histogram (**Figure 4B**). The distribution of the values for the area of unirradiated or 0.5 Gy-irradiated cells is wide and unimodal, whereas for higher doses, the distribution is more right-skewed, peaking at lower areas. Notably, the curve for the single dose of 2 Gy resembles those of higher doses, whereas the distribution of 4x 0.5 Gy is wider, bimodal and more comparable to the single dose of 0.5 Gy.

The mean number of nuclei per mOC did not change after a single dose of 0.5 Gy (**Figure 4C**), but was clearly reduced for single and fractionated delivery of doses exceeding 0.5 Gy. A strong reduction was measured after a single dose of 2, 5 and 10 Gy (~2-fold) and also after fractionated doses of 4x 0.5, 10x 0.5 and 10x 1 Gy (~2-fold). In the depiction of distributions, it becomes evident that after doses of 2 Gy or higher, a shift towards the minimum number of nuclei identifying an mOC occurs (**Figure 4D**). While histograms for all doses are right-skewed, the distribution is flatter for unirradiated or 0.5 Gy-irradiated cells, since a larger fraction of these cells has more than three nuclei, reaching up to 20 (after 0.5 Gy) or even 50 nuclei (unirradiated). These findings point to

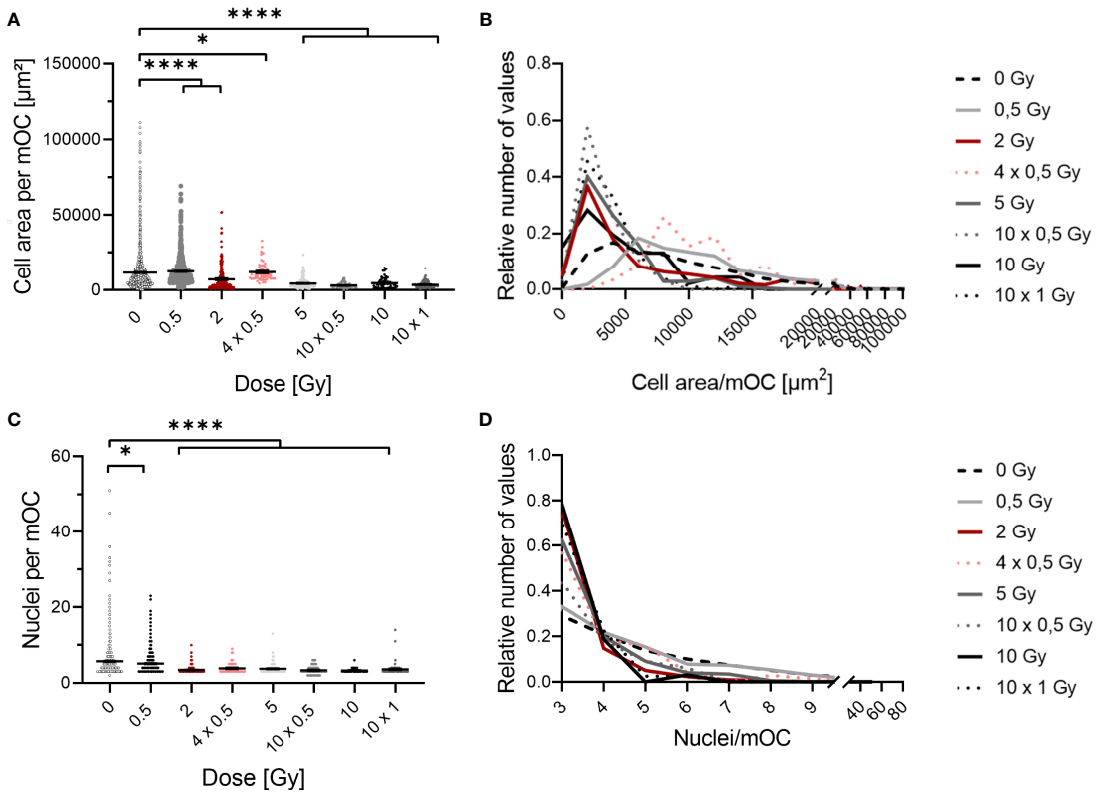

FIGURE 4 | Fusion of OC precursors is inhibited by irradiation with X-rays. At 21 days after exposure, mOC (21d in culture) exhibit a smaller area on bone slices after irradiation **(A)**. Depiction of the distribution of values demonstrates a shift from unirradiated cells and cells irradiated with 0.5 Gy with a higher area to cells with a smaller area irradiated with doses of 2 Gy or more **(B)**, bin size = 2000. mOC possess a smaller mean number of nuclei per cell after irradiation **(C)**, while the distribution of values shows the shift to the minimum number of three nuclei per mOC at doses higher than 2 or more Gy **(D)**, bin size = 1. Area measurements were performed by F-actin staining, nuclei were counterstained with DAPI (≥ three nuclei), and confocal microscopy pictures were evaluated using ImageJ. Significance was tested with Kruskal-Wallis for non-normal distributed data **(A, C)**. P-values are indicated by asterisks with * for $p \leq 0.05$ and **** for $p \leq 0.0001$. Error bars are reported as the mean ± SEM; N = 4-8.

radiation induced alterations occurring during fusion in the differentiation process.

X-Ray Irradiation Partially Inhibits Nuclear Translocation of NFATc1 Protein

Our data suggest that the fusion of OC precursor is affected by ionizing irradiation. So far, it is known that NFATc1 is a master regulator of osteoclast differentiation and fusion (27, 44), and dephosphorylation of cytosolic NFATc1 by the phosphatase calcineurin induces translocation of the protein into the nucleus. Therefore, we set out to investigate the nuclear translocation of NFATc1 protein in M-CSF and RANKL-stimulated OC populations, which were irradiated exemplarily for single doses of 0.5 and 2 Gy and a fractionated dose of 4×0.5 Gy and assessed after 3, 5, 7 and 14 days of cultivation on bone slices. As shown in **Figure 5**, at early stages (up to 7 days), immunofluorescence staining demonstrated that NFATc1 protein levels in the nucleus are not affected significantly upon ionizing irradiation (**Figures 5A, B, E**). However, at a later stage (14 days) of osteoclastogenesis, nuclear translocation of the NFATc1 protein still remains unchanged for 0.5 Gy, but is significantly reduced after a single dose of 2 Gy or fractionated delivery of the same dose (4×0.5 Gy) of X-ray irradiation (**Figures 5C, D, F**).

Markers for Changes in Bone Metabolism Are Not Modified *In Vivo* by LD-RT treat Calcaneodynia and Achillodynia Patients

In the frame of the IMMO-LDRT01 trial [details in (36)], blood samples were taken at several time points before and after therapy from a subgroup of patients, mostly suffering from Calcaneodynia and Achillodynia and further analyzed. In our analysis, we focused on the ratio of subtypes of T cells that impact bone metabolism, i.e. Th17 and Treg cells, the release of CTX in plasma samples, and the activity of the bone resorbing enzyme TRAP 5b, as well as a marker for bone formation OCN (**Figure 6**). As can be inferred from **Figures 6A–D**, the ratio of Th17 and Treg cells is not significantly changed after LD-RT, indicating no impact of these T cell subtypes on inflammation and/or bone metabolism after treatment. In **Figures 6E, F**, the results for bone resorption markers are shown, revealing a weak statistical significance for a decrease in CTX, but no detectable impact of LD-RT on TRAP 5b. The results for the marker of bone formation, **Figure 6G**, show a

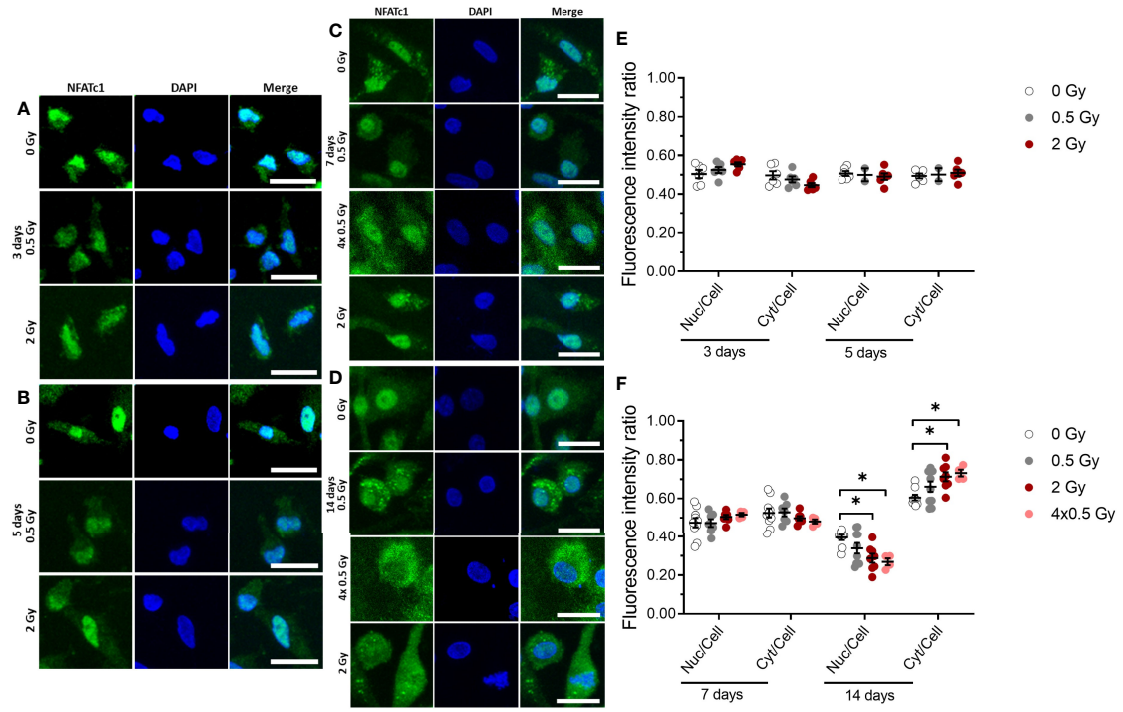

FIGURE 5 | NFATc1 translocation into the nucleus is partially inhibited by ionizing radiation (X-rays) at a later stage (14 days) of OC differentiation. Monocytes were attached on bone slices, then irradiated in the presence of growth and differentiation factors (M-CSF, RANKL) with single doses (0, 0.5 and 2 Gy) and fractionated doses of X-rays (4× 0.5 Gy). Immunostaining of NFATc1 protein (green) showing cytoplasmic and nuclear localization in osteoclast and counterstain with DAPI (blue) **(A-D)**. NFATc1 translocation into the nucleus was quantified using ImageJ software. The graph represents the fluorescent intensity ratio of the nucleus or cytoplasm to the cell at 3 and 5 days of cultivation **(E)** and 7 and 14 days of cultivation **(F)**. Activated NFATc1 is translocated from the cytoplasm into the nucleus **(E)**. Nuclear translocation is inhibited in the 4× 0.5 and 2 Gy irradiated samples at 14 days after exposure **(F)**. Significance was tested with Kruskal-Wallis for non-normal distributed data. P-values are indicated by asterisks with * for $p \leq 0.05$. N = 2-5. The values are given as mean ± SEM from at least 100-200 cells per donor. Scale bar: 20 µm **(A-D)**.

small but significant decrease between two time points. Taken together, at least for Calcaneodynia and Achillodynia and based on the markers tested after LD-RT, no clear and consistent impact can be inferred from our *in vivo* data.

DISCUSSION

The goal of the study presented here was to test the hypothesis, that one important mechanistic basis of pain relief and anti-inflammatory effects of local exposure to low X-ray doses in LD-RT is a transient inhibition of the terminal differentiation and activity of bone resorbing human OC. To investigate this, the experiment was designed to be as close as possible to the treatment situation in LD-RT by cultivating OC precursor on bone slices, which descended from monocytes that were isolated from peripheral blood from healthy donors and then cultivated with OC differentiation factors. In addition, X-ray irradiation schemes resembling those used in LD-RT for patients were applied. While in other studies the administration of low X-ray doses in LD-RT is not reflected, i.e. rodent cells or cell lines are used (33, 45), or mice were subjected to whole-body exposure (46, 47); our study is a new approach. After all, beside differences in the experimental design, the conflicting results may be reconciled by assuming a time effect, i.e. an enhanced osteoclastogenesis early after irradiation and reduced osteoclast activity at later times after exposure (37, 46).

Using established markers for bone resorption, such as the release of CTX or resorbed area (48, 49), we detected significant reductions for both markers after exposure (**Figure 2**). This is in line with the significant reduction of fractions of mOC as well as the fold change of number of OC related to the controls, which is not caused by apoptosis (**Figures 3** and **S2**).

Thus, we anticipate that X-irradiation inhibits the differentiation of OC precursors into mOC. This holds true also for repeated irradiations with 0.5 Gy fractions, which is similar to the LD-RT regimen. Hints for an inhibition of bone resorption by osteoclasts despite increasing cell numbers were obtained in murine mOC of healthy but not arthritic joints after X-irradiation in the dose range of 0.1-0.5 Gy (19). This interesting observation we cannot confirm, but our findings are in line with the observed decrease in the number of mOC from mouse arthritic joints, in spite of differences in the experimental approach, i.e. species, time points of analysis, and cultivation on bone versus plastic.

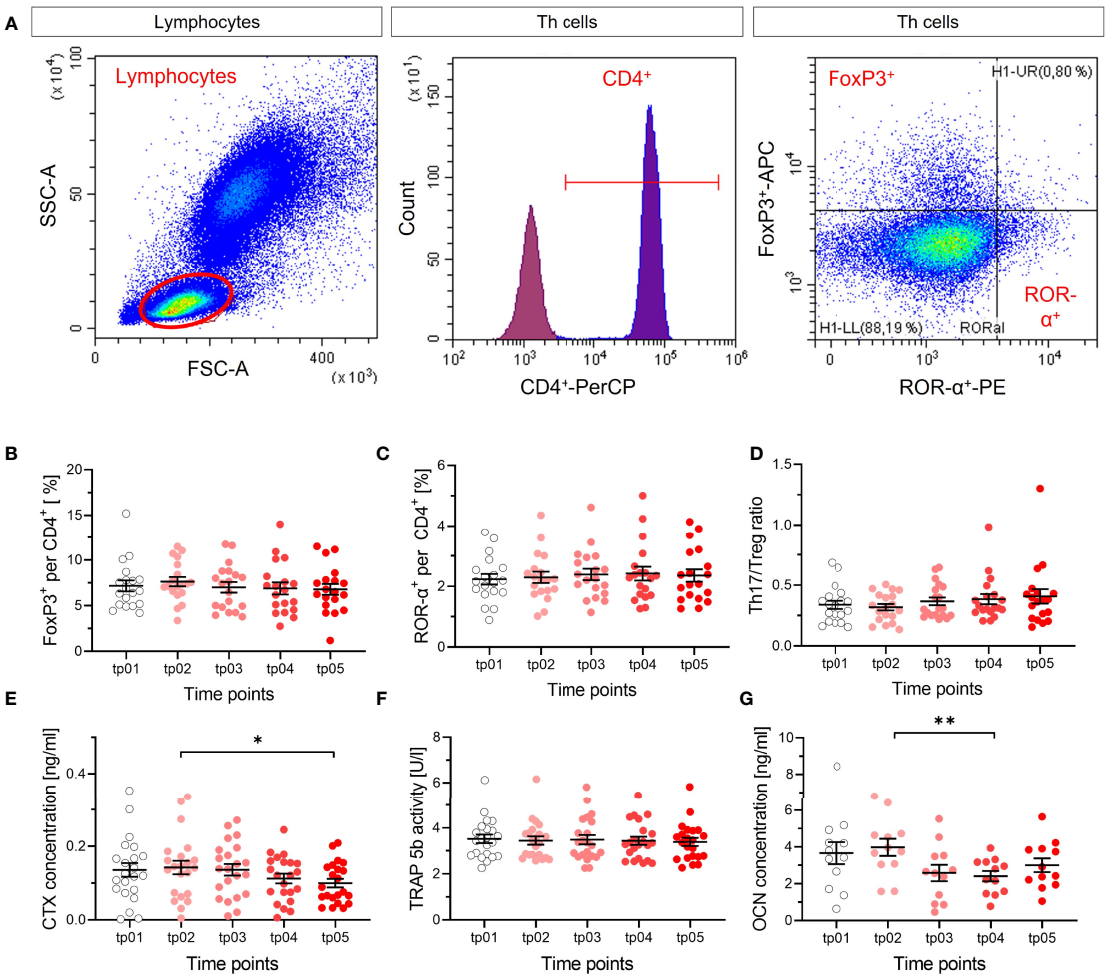

FIGURE 6 | No apparent modification of T cell subtypes and markers of resorption and formation of bone. The fractions of Treg (FoxP3$^+$) **(B)** and Th17 (ROR-α$^+$) **(C)** per and CD4$^+$ cells were measured in blood by flow cytometry before the start of LD-RT (tp01) and at several time points during and after therapy (tp02-tp05; N = 22). The ratio of both cell types **(D)** was calculated. Representative dot plots and gating strategy are shown in **(A)**. Lymphocytes were determined in the SSC/FSC dot plot. After exclusion of doublet's, CD4$^+$ (Per-CP) T helper cells were identified in the histogram. Subsequently, Treg cells were classified as FoxP3$^+$ (APC) and Th17 cells as ROR-α$^+$(PE) from CD4$^+$ cells. No changes in Treg cells, Th17 cells, nor Th17/Treg ratio are detectable after LD-RT, as for the markers of resorption and formation of bone, indicating no impact on T cell subtypes that are involved in the regulation of bone metabolism. CTX **(E)**, TRAP 5b **(F)** and OCN **(G)** were measured (tp01-tp05; N = 22). CTX concentration decreases slightly over time, which is not reflected by the activity of TRAP 5b, and OCN concentration decreases. Significance was tested with RM one-way ANOVA **(E, G)** for normal distributed data and Friedman Test **(B-D, F)** for not-normal distributed data. P-values are indicated by asterisks with * for $p \leq 0.05$ and ** for $p \leq 0.01$.

Interestingly, pharmacological downregulation of ROS leads to reduced numbers of mature osteoclasts as well as decreased resorbing activity in the remaining OC *via* RANKL/NFATc1 signaling without cytotoxicity (29, 50, 51). As the intracellular ROS level is reduced by exposure to low doses of X-rays (52), this reduced level of oxidative stress could be one cause for the reduced resorbing activity of irradiated OC precursors in our study. In line with this, results are reported in several preclinical rodent studies [(37, 53, 54), reviewed in (7)], which support radiation induced impairment of OC differentiation and resorbing activity. Moreover, this is in line with features of the radiation response of other cell types (55, 56).

In contrast, other studies show an enhancement of OC numbers and resorption activities. In this context, a differential impact of low versus higher doses on osteoclastogenesis is discussed, but published results are conflicting (reviewed in (7)), again likely due to the high variability in the study designs as discussed above. However, observation over longer times after irradiation may reconcile these opposed results. In mice exposed to 5 Gy, OC are initially activated, leading to bone loss, but a late onset of long-term depleted OC results in a non-physiological thickening of bone matrix (57), which is discussed as a result of the depletion of marrow-residing progenitors.

Our results suggest that radiation damage induced in an early stage of OC differentiation can lead to an impaired fusion process

during terminal differentiation. Scoring of established respective markers of mOC (43, 58), showed significantly decreased cell areas relatively late after exposure (**Figure 4A**) and a smaller average number of nuclei per mOC (**Figure 4C**), again for total doses equal or exceeding 2 Gy. Consistent with the observed late effects of radiation exposure in terms of impaired differentiation of mOC, is the nuclear translocation of NFATc1, which was impaired later, also for fractionated dose delivery, tested for 4x 0.5 Gy (**Figure 5**). This result and the key role in osteoclastogenesis (27) underlines the potential involvement of NFATc1 in the impairment of OC differentiation.

In our study, we have focused on the impact of irradiation of monocytes and the subsequent differentiation into OC. However, the cellular environment, i.e. the intercellular communication of OC progenitors, mOC and other cells, such as T-cells is most likely involved. This is known for osteoclastogenesis and the osteo-immunological cross-talk in inflammatory processes (25, 59, 60). Furthermore, it is in line with bone-forming activities in osteoblasts of *in vitro* and *in vivo* irradiated rodents reported for LD-RT (7, 19, 20, 37), and thus anti-inflammatory processes mediated by LD-RT could lead to a restored balance in bone homeostasis (61–63).

Important for osteoclastogenesis are other leukocytes, such as peripheral monocytes, which are relatively radioresistant (64). As different phenotypes of the monocytes determine the ability of OC to differentiate, the question about a potential radiation induced modulation of osteoclastogenesis by changing the phenotype (65) could be subject for further studies. Interestingly, a decreased activation of monocytes has been shown after LD-RT in the interim analysis of our study (36).

We assume that the reduced bone resorption observed *in vitro* after irradiation is relevant for part of the mechanistic basis of LD-RT. Reported data only provide indirect evidence for this assumption, i.e. the improved healing of bone fractures after low dose exposure (20, 21). To check for it, we collected blood and plasma of Calcaneodynia and Achillodynia patients before, during and after LD-RT, quantified immune cells involved in the regulation, and measured established markers of resorption and formation of bone. According to a rough estimation based on physiological and exposure parameters, less than a few percent of the circulating blood cells are irradiated with 0.5 Gy during a standard local, repeated LD-RT treatment (6 fractions à 0.5 Gy). Therefore, one cannot expect a direct impact on circulating blood cells, evoked by irradiation and relevant for bone metabolism. Hence, only an indirect response in peripheral blood cells is conceivable in this case, transmitted by irradiated cells located in the irradiation field and potentially amplified.

A local radiation treatment of bony structures implies the exposure of bone marrow, where bone precursor and immune cells cohabitate. During regulation of bone resorption and formation, both bone precursor and immune cells undergo complex interactions, with the potential to enhance or to shift immune responses (66). A potential indicator is a modified proportion of T helper and regulatory T cells in the peripheral blood (reduced Th17/Treg ratio), which is reported to correlate inversely with bone resorption markers (66, 67). We could not find such a modified proportion in the respective analysis (**Figures 6A–D**). Moreover, the markers indicating local changes in bone resorption were not consistently modified; a significant decrease of CTX (**Figure 6E**) faces an unchanged activity of the bone resorbing enzyme TRAP 5b (**Figure 6F**). In addition, bone resorption activities, assessed in *ex vivo* differentiated OC from LD-RT patients, did not show significant modifications after treatment (**Figure S3**). In view of the diseases of the patients enrolled in the study -Calcaneodynia and Achillodynia- where also bone formation can occur, we checked a respective marker for bone formation (OCN), which turned out to decrease significantly (**Figure 6G**). Taken together, the results do not provide consistent evidence for changes after treatment over time and we consider that the impact of local irradiation is somehow "diluted" in the circulation, in contrast to whole body exposure such as in Radon Spa therapy, where effects were measurable (9, 10).

Thus, our *in vivo* study performed with Calcaneodynia and Achillodynia patients, did not reveal clear indications for a radiation induced inhibition of bone degradation and resorption after LD-RT treatment. On this basis, we cannot infer a general relevance of the *in vitro* observed reduced differentiation and functionality of OC after irradiation for LD-RT. The pain relief reported by patients enrolled in the same study could at least for Calcaneodynia and tendinopathies be due to other modifications, i.e. the reported small but significant changes in the activation of immune cells (36). As for RA, reduced bone degradation after LD-RT has been shown in a preclinical model (37); the goal of further studies is to investigate the relevance of our *in vitro* observations in arthritic patients treated with LD-RT.

We conclude from our *in vitro* study that fractionated low-dose irradiation of human OC progenitors as administered in LD-RT reduces resorbing activity and impairs the terminal differentiation of OC. NFATc1 might be involved in this process. However, additional mechanisms most likely play a role in the cellular environment in bones and joints. The *in vivo* relevance of these results remains to be clearly shown in future studies.

DATA AVAILABILITY STATEMENT

The raw data supporting the conclusions of this article will be made available by the authors, without undue reservation.

ETHICS STATEMENT

The studies involving human participants were reviewed and approved by Institutional Review Board of the Friedrich-Alexander Universität Erlangen-Nürnberg. The patients/participants provided their written informed consent to participate in this study.

AUTHOR CONTRIBUTIONS

CF designed the experiments and contributed to the writing of the paper and the analysis of the data; FR, DE, and AT contributed to the design of the experiments, performed the experiments, analyzed the data, and contributed to writing the article; DK, IW, JM, SB, TF, ML, and TM contributed to performing experiments and data analysis, TF advised on statistical analyses; A-JD, IB, and BF contributed to designing and performing the patient study. All authors read and agreed to the manuscript.

FUNDING

This work was in part funded by the Bundesministerium für Bildung und Forschung (BMBF; GREWIS-alpha, 02NUK050A and 02NUK050E). The IMMO-LDRT01 trial is funded by Department of Radiation Oncology at Universitätsklinikum Erlangen.

ACKNOWLEDGMENTS

We are very grateful to Liliana Davkova for excellent technical support, Svetlana Ktitareva and Prof. Dr. Eva Hermann for valuable advice concerning statistical analyses, and Dr. Aljona Cucu for establishing OC cultures on bone slices. In addition, we are thankful to Maike Isbruch, Melissa Er, Lena Vollmer and Karola Bahrami for the support in performing the experiments and Svetlana Ktitareva for finalizing the manuscript. For the inclusion of the patients in the IMMO-LDRT study at the University Hospital Erlangen we thank Dr. med. Thomas Gryc and Dr. med. Thomas Weissmann. We acknowledge the support of BMBF for funding and GSI for covering publication costs.

SUPPLEMENTARY MATERIAL

The Supplementary Material for this article can be found online at: https://www.frontiersin.org/articles/10.3389/fimmu.2022.817281/full#supplementary-material

REFERENCES

1. Schett G. Erosive Arthritis. *Arthritis Res Ther* (2007) 9 Suppl 1:S2. doi: 10.1186/ar2166
2. Florencio-Silva R, Sasso GR, Sasso-Cerri E, Simoes MJ, Cerri PS. Biology of Bone Tissue: Structure, Function, and Factors That Influence Bone Cells. *BioMed Res Int* (2015) 2015:421746. doi: 10.1155/2015/421746
3. Kirkpatrick J, Yassaie O, Mirjalili SA. The Plantar Calcaneal Spur: A Review of Anatomy, Histology, Etiology and Key Associations. *J Anat* (2017) 230 (6):743–51. doi: 10.1111/joa.12607
4. Marchev AS, Dimitrova PA, Burns AJ, Kostov RV, Dinkova-Kostova AT, Georgiev MI. Oxidative Stress and Chronic Inflammation in Osteoarthritis: Can NRF2 Counteract These Partners in Crime? *Ann N Y Acad Sci* (2017) 1401(1):114–35. doi: 10.1111/nyas.13407
5. Bindu S, Mazumder S, Bandyopadhyay U. Non-Steroidal Anti-Inflammatory Drugs (NSAIDs) and Organ Damage: A Current Perspective. *Biochem Pharmacol* (2020) 180:114147. doi: 10.1016/j.bcp.2020.114147
6. Singh JA, Cameron C, Noorbaloochi S, Cullis T, Tucker M, Christensen R, et al. Risk of Serious Infection in Biological Treatment of Patients With Rheumatoid Arthritis: A Systematic Review and Meta-Analysis. *Lancet* (2015) 386(9990):258–65. doi: 10.1016/S0140-6736(14)61704-9
7. Donaubauer AJ, Zhou JG, Ott OJ, Putz F, Fietkau R, Keilholz L, et al. Low Dose Radiation Therapy, Particularly With 0.5 Gy, Improves Pain in Degenerative Joint Disease of the Fingers: Results of a Retrospective Analysis. *Int J Mol Sci* (2020) 21(16). doi: 10.3390/ijms21165854
8. Seegenschmiedt MH, Micke O, Willich N. Radiation Therapy for Nonmalignant Diseases in Germany. Current Concepts and Future Perspectives. *Strahlenther Onkol* (2004) 180(11):718–30. doi: 10.1007/s00066-004-9197-9
9. Cucu A, Shreder K, Kraft D, Ruhle PF, Klein G, Thiel G, et al. Decrease of Markers Related to Bone Erosion in Serum of Patients With Musculoskeletal Disorders After Serial Low-Dose Radon Spa Therapy. *Front Immunol* (2017) 8:882. doi: 10.3389/fimmu.2017.00882
10. Ruhle PF, Wunderlich R, Deloch L, Fournier C, Maier A, Klein G, et al. Modulation of the Peripheral Immune System After Low-Dose Radon Spa Therapy: Detailed Longitudinal Immune Monitoring of Patients Within the RAD-ON01 Study. *Autoimmunity* (2017) 50(2):133–40. doi: 10.1080/08916934.2017.1284819
11. Feng X, McDonald JM. Disorders of Bone Remodeling. *Annu Rev Pathol* (2011) 6:121–45. doi: 10.1146/annurev-pathol-011110-130203
12. Ginaldi L, De Martinis M. Osteoimmunology and Beyond. *Curr Med Chem* (2016) 23(33):3754–74. doi: 10.2174/0929867323666160907162546
13. Gevorgyan A, La Scala GC, Neligan PC, Pang CY, Forrest CR. Radiation-Induced Craniofacial Bone Growth Disturbances. *J Craniofac Surg* (2007) 18 (5):1001–7. doi: 10.1097/scs.0b013e31812f7584
14. Hopewell JW. Radiation-Therapy Effects on Bone Density. *Med Pediatr Oncol* (2003) 41(3):208–11. doi: 10.1002/mpo.10338
15. Rajpura A, Wright AC, Board TN. Medical Management of Osteonecrosis of the Hip: A Review. *Hip Int* (2011) 21(4):385–92. doi: 10.5301/HIP.2011.8538
16. Handforth C, D'Oronzo S, Coleman R, Brown J. Cancer Treatment and Bone Health. *Calcif Tissue Int* (2018) 102(2):251–64. doi: 10.1007/s00223-017-0369-x
17. D'Oronzo S, Stucci S, Tucci M, Silvestris F. Cancer Treatment-Induced Bone Loss (CTIBL): Pathogenesis and Clinical Implications. *Cancer Treat Rev* (2015) 41(9):798–808. doi: 10.1016/j.ctrv.2015.09.003
18. Lucatto SC, Guilherme A, Dib LL, Segreto HR, Alves MT, Gumieiro EH, et al. Effects of Ionizing Radiation on Bone Neoformation: Histometric Study in Wistar Rats Tibiae. *Acta Cir Bras* (2011) 26(6):475–80. doi: 10.1590/S0102-86502011000600012
19. Deloch L, Ruckert M, Fietkau R, Frey B, Gaipl US. Low-Dose Radiotherapy Has No Harmful Effects on Key Cells of Healthy Non-Inflamed Joints. *Int J Mol Sci* (2018) 19(10). doi: 10.3390/ijms19103197
20. Chen M, Huang Q, Xu W, She C, Xie ZG, Mao YT, et al. Low-Dose X-Ray Irradiation Promotes Osteoblast Proliferation, Differentiation and Fracture Healing. *PLoS One* (2014) 9(8):e104016. doi: 10.1371/journal.pone.0104016
21. Zhou XZ, Zhang G, Dong QR, Chan CW, Liu CF, Qin L. Low-Dose X-Irradiation Promotes Mineralization of Fracture Callus in a Rat Model. *Arch Orthop Trauma Surg* (2009) 129(1):125–32. doi: 10.1007/s00402-008-0634-6
22. Hildebrandt G, Radlingmayr A, Rosenthal S, Rothe R, Jahns J, Hindemith M, et al. Low-Dose Radiotherapy (LD-RT) and the Modulation of iNOS Expression in Adjuvant-Induced Arthritis in Rats. *Int J Radiat Biol* (2003) 79(12):993–1001. doi: 10.1080/09553000310001636639
23. Nakatsukasa H, Tsukimoto M, Ohshima Y, Tago F, Masada A, Kojima S. Suppressing Effect of Low-Dose Gamma-Ray Irradiation on Collagen-Induced Arthritis. *J Radiat Res* (2008) 49(4):381–9. doi: 10.1269/jrr.08002
24. Kleinhans C, Schmid FF, Schmid FV, Kluger PJ. Comparison of Osteoclastogenesis and Resorption Activity of Human Osteoclasts on Tissue Culture Polystyrene and on Natural Extracellular Bone Matrix in 2D and 3D. *J Biotechnol* (2015) 205:101–10. doi: 10.1016/j.jbiotec.2014.11.039
25. Feng X, Teitelbaum SL. Osteoclasts: New Insights. *Bone Res* (2013) 1(1):11–26. doi: 10.4248/BR201301003
26. Takeshita S, Kaji K, Kudo A. Identification and Characterization of the New Osteoclast Progenitor With Macrophage Phenotypes Being Able to

Differentiate Into Mature Osteoclasts. *J Bone Miner Res* (2000) 15(8):1477–88. doi: 10.1359/jbmr.2000.15.8.1477
27. Miyamoto T. Regulators of Osteoclast Differentiation and Cell-Cell Fusion. *Keio J Med* (2011) 60(4):101–5. doi: 10.2302/kjm.60.101
28. Wang Q, Xie Y, Du QS, Wu XJ, Feng X, Mei L, et al. Regulation of the Formation of Osteoclastic Actin Rings by Proline-Rich Tyrosine Kinase 2 Interacting With Gelsolin. *J Cell Biol* (2003) 160(4):565–75. doi: 10.1083/jcb.200207036
29. Xian Y, Su Y, Liang J, Long F, Feng X, Xiao Y, et al. Oroxylin A Reduces Osteoclast Formation and Bone Resorption *via* Suppressing RANKL-Induced ROS and NFATc1 Activation. *Biochem Pharmacol* (2021) 193:114761. doi: 10.1016/j.bcp.2021.114761
30. Takayanagi H. Osteoimmunology and the Effects of the Immune System on Bone. *Nat Rev Rheumatol* (2009) 5(12):667–76. doi: 10.1038/nrrheum.2009.217
31. Nakamura H, Nakashima T, Hayashi M, Izawa N, Yasui T, Aburatani H, et al. Global Epigenomic Analysis Indicates Protocadherin-7 Activates Osteoclastogenesis by Promoting Cell-Cell Fusion. *Biochem Biophys Res Commun* (2014) 455(3-4):305–11. doi: 10.1016/j.bbrc.2014.11.009
32. Raschke WC, Baird S, Ralph P, Nakoinz I. Functional Macrophage Cell Lines Transformed by Abelson Leukemia Virus. *Cell* (1978) 15(1):261–7. doi: 10.1016/0092-8674(78)90101-0
33. Zhang J, Wang Z, Wu A, Nie J, Pei H, Hu W, et al. Differences in Responses to X-Ray Exposure Between Osteoclast and Osteoblast Cells. *J Radiat Res* (2017) 58(6):791–802. doi: 10.1093/jrr/rrx026
34. Garnero P, Ferreras M, Karsdal MA, Nicamhlaoibh R, Risteli J, Borel O, et al. The Type I Collagen Fragments ICTP and CTX Reveal Distinct Enzymatic Pathways of Bone Collagen Degradation. *J Bone Miner Res* (2003) 18(5):859–67. doi: 10.1359/jbmr.2003.18.5.859
35. Vesprey A, Yang W. Pit Assay to Measure the Bone Resorptive Activity of Bone Marrow-Derived Osteoclasts. *Bio Protoc* (2016) 6(12). doi: 10.21769/BioProtoc.1836
36. Donaubauer AJ, Becker I, Weissmann T, Frohlich BM, Munoz LE, Gryc T, et al. Low Dose Radiation Therapy Induces Long-Lasting Reduction of Pain and Immune Modulations in the Peripheral Blood - Interim Analysis of the IMMO-LDRT01 Trial. *Front Immunol* (2021) 12:740742. doi: 10.3389/fimmu.2021.740742
37. Deloch L, Derer A, Hueber AJ, Herrmann M, Schett GA, Wolfelschneider J, et al. Low-Dose Radiotherapy Ameliorates Advanced Arthritis in hTNF-Alpha Tg Mice by Particularly Positively Impacting on Bone Metabolism. *Front Immunol* (2018) 9:1834. doi: 10.3389/fimmu.2018.01834
38. Cummings BS, Schnellmann RG. Measurement of Cell Death in Mammalian Cells. *Curr Protoc Pharmacol* (2004); Chapter 12::Unit 12 8. doi: 10.1002/0471141755.ph1208s56
39. Wu X, Ahn EY, McKenna MA, Yeo H, McDonald JM. Fas Binding to Calmodulin Regulates Apoptosis in Osteoclasts. *J Biol Chem* (2005) 280 (33):29964–70. doi: 10.1074/jbc.M500710200
40. Ma Q, Liang M, Wu Y, Luo F, Ma Z, Dong S, et al. Osteoclast-Derived Apoptotic Bodies Couple Bone Resorption and Formation in Bone Remodeling. *Bone Res* (2021) 9(1):5. doi: 10.1038/s41413-020-00121-1
41. Schett G, Gravallese E. Bone Erosion in Rheumatoid Arthritis: Mechanisms, Diagnosis and Treatment. *Nat Rev Rheumatol* (2012) 8(11):656–64. doi: 10.1038/nrrheum.2012.153
42. Yavropoulou MP, Yovos JG. Osteoclastogenesis–current Knowledge and Future Perspectives. *J Musculoskelet Neuronal Interact* (2008) 8(3):204–16.
43. Teitelbaum SL. Bone Resorption by Osteoclasts. *Science* (2000) 289 (5484):1504–8. doi: 10.1126/science.289.5484.1504
44. Kim K, Lee SH, Ha Kim J, Choi Y, Kim N. NFATc1 Induces Osteoclast Fusion *via* Up-Regulation of Atp6v0d2 and the Dendritic Cell-Specific Transmembrane Protein (DC-STAMP). *Mol Endocrinol* (2008) 22(1):176–85. doi: 10.1210/me.2007-0237
45. Song C, Yang X, Lei Y, Zhang Z, Smith W, Yan J, et al. Evaluation of Efficacy on RANKL Induced Osteoclast From RAW264. *7 Cells J Cell Physiol* (2019) 234(7):11969–75. doi: 10.1002/jcp.27852
46. Lima F, Swift JM, Greene ES, Allen MR, Cunningham DA, Braby LA, et al. Exposure to Low-Dose X-Ray Radiation Alters Bone Progenitor Cells and Bone Microarchitecture. *Radiat Res* (2017) 188(4):433–42. doi: 10.1667/RR14414.1
47. Willey JS, Lloyd SA, Robbins ME, Bourland JD, Smith-Sielicki H, Bowman LC, et al. Early Increase in Osteoclast Number in Mice After Whole-Body Irradiation With 2 Gy X Rays. *Radiat Res* (2008) 170(3):388–92. doi: 10.1667/RR1388.1
48. Fardellone P, Sejourne A, Paccou J, Goeb V. Bone Remodelling Markers in Rheumatoid Arthritis. *Mediators Inflamm* (2014) 2014:484280. doi: 10.1155/2014/484280
49. Vlot MC, den Heijer M, de Jongh RT, Vervloet MG, Lems WF, de Jonge R, et al. Clinical Utility of Bone Markers in Various Diseases. *Bone* (2018) 114:215–25. doi: 10.1016/j.bone.2018.06.011
50. Jiang C, Ma Q, Wang S, Shen Y, Qin A, Fan S, et al. Oxymatrine Attenuates Osteoclastogenesis *via* Modulation of ROS-Mediated SREBP2 Signaling and Counteracts Ovariectomy-Induced Osteoporosis. *Front Cell Dev Biol* (2021) 9:684007. doi: 10.3389/fcell.2021.684007
51. Mei L, Zheng Y, Ma T, Xia B, Gao X, Hao Y, et al. The Novel Antioxidant Compound JSH-23 Prevents Osteolysis by Scavenging ROS During Both Osteoclastogenesis and Osteoblastogenesis. *Front Pharmacol* (2021) 12:734774. doi: 10.3389/fphar.2021.734774
52. Large M, Reichert S, Hehlgans S, Fournier C, Rodel C, Rodel F. A non-Linear Detection of Phospho-Histone H2AX in EA.hy926 Endothelial Cells Following Low-Dose X-Irradiation is Modulated by Reactive Oxygen Species. *Radiat Oncol* (2014) 9:80. doi: 10.1186/1748-717X-9-80
53. Zhai J, He F, Wang J, Chen J, Tong L, Zhu G. Influence of Radiation Exposure Pattern on the Bone Injury and Osteoclastogenesis in a Rat Model. *Int J Mol Med* (2019) 44(6):2265–75. doi: 10.3892/ijmm.2019.4369
54. Sawajiri M, Mizoe J, Tanimoto K. Changes in Osteoclasts After Irradiation With Carbon Ion Particles. *Radiat Environ Biophys* (2003) 42(3):219–23. doi: 10.1007/s00411-003-0204-9
55. Becker D, Elsasser T, Tonn T, Seifried E, Durante M, Ritter S, et al. Response of Human Hematopoietic Stem and Progenitor Cells to Energetic Carbon Ions. *Int J Radiat Biol* (2009) 85(11):1051–9. doi: 10.3109/09553000903232850
56. Simoniello P, Wiedemann J, Zink J, Thoennes E, Stange M, Layer PG, et al. Exposure to Carbon Ions Triggers Proinflammatory Signals and Changes in Homeostasis and Epidermal Tissue Organization to a Similar Extent as Photons. *Front Oncol* (2015) 5:294. doi: 10.3389/fonc.2015.00294
57. Oest ME, Franken V, Kuchera T, Strauss J, Damron TA. Long-Term Loss of Osteoclasts and Unopposed Cortical Mineral Apposition Following Limited Field Irradiation. *J Orthop Res* (2015) 33(3):334–42. doi: 10.1002/jor.22761
58. Lees RL, Sabharwal VK, Heersche JN. Resorptive State and Cell Size Influence Intracellular pH Regulation in Rabbit Osteoclasts Cultured on Collagen-Hydroxyapatite Films. *Bone* (2001) 28(2):187–94. doi: 10.1016/S8756-3282(00)00433-6
59. Schett G. Cells of the Synovium in Rheumatoid Arthritis. *Osteoclasts Arthritis Res Ther* (2007) 9(1):203. doi: 10.1186/ar2110
60. Okamoto K, Takayanagi H. Regulation of Bone by the Adaptive Immune System in Arthritis. *Arthritis Res Ther* (2011) 13(3):219. doi: 10.1186/ar3323
61. Frey B, Hehlgans S, Rodel F, Gaipl US. Modulation of Inflammation by Low and High Doses of Ionizing Radiation: Implications for Benign and Malign Diseases. *Cancer Lett* (2015) 368(2):230–7. doi: 10.1016/j.canlet.2015.04.010
62. Ott OJ, Micke O, Mucke R, Niewald M, Rodel F, Schafer U, et al. Low-Dose Radiotherapy: Mayday, Mayday. *We've Been Hit! Strahlenther Onkol* (2019) 195(4):285–8. doi: 10.1007/s00066-018-1412-1
63. Rodel F, Keilholz L, Herrmann M, Sauer R, Hildebrandt G. Radiobiological Mechanisms in Inflammatory Diseases of Low-Dose Radiation Therapy. *Int J Radiat Biol* (2007) 83(6):357–66. doi: 10.1080/09553000701317358
64. Falcke SE, Ruhle PF, Deloch L, Fietkau R, Frey B, Gaipl US. Clinically Relevant Radiation Exposure Differentially Impacts Forms of Cell Death in Human Cells of the Innate and Adaptive Immune System. *Int J Mol Sci* (2018) 19(11). doi: 10.3390/ijms19113574
65. de Vries TJ, El Bakkali I, Kamradt T, Schett G, Jansen IDC, D'Amelio P. What Are the Peripheral Blood Determinants for Increased Osteoclast Formation in the Various Inflammatory Diseases Associated With Bone Loss? *Front Immunol* (2019) 10:505. doi: 10.3389/fimmu.2019.00505
66. Ehnert S, Relja B, Schmidt-Bleek K, Fischer V, Ignatius A, Linnemann C, et al. Effects of Immune Cells on Mesenchymal Stem Cells During Fracture

Healing. *World J Stem Cells* (2021) 13(11):1667–95. doi: 10.4252/wjsc.v13.i11.1667

67. Zaiss MM, Axmann R, Zwerina J, Polzer K, Guckel E, Skapenko A, et al. Treg Cells Suppress Osteoclast Formation: A New Link Between the Immune System and Bone. *Arthritis Rheumatol* (2007) 56(12):4104–12. doi: 10.1002/art.23138

Conflict of Interest: The authors declare that the research was conducted in the absence of any commercial or financial relationships that could be construed as a potential conflict of interest.

The reviewer MS declared a shared affiliation with the authors ML and TM to the handling editor at the time of review.

Publisher's Note: All claims expressed in this article are solely those of the authors and do not necessarily represent those of their affiliated organizations, or those of the publisher, the editors and the reviewers. Any product that may be evaluated in this article, or claim that may be made by its manufacturer, is not guaranteed or endorsed by the publisher.

†***ORCID:*** *Felicitas Rapp, orcid.org/0000-0003-0968-1546; Claudia Fournier, orcid.org/0000-0002-1007-9934; Denise Eckert, orcid.org/0000-0002-7304-8799; Ayele Taddese Tsedeke, orcid.org/0000-0001-7493-2511; Benjamin Frey, orcid.org/0000-0001-6743-3351; Anna-Jasmina Donaubauer, orcid.org/0000-0002-1655-373X; Sidra Basheer, orcid.org/0000-0001-9122-7558; Jessica Molendowska, orcid.org/0000-0003-3252-5031; Thomas Friedrich, orcid.org/ 0000-0003-0074-6390; Markus Langhans, orcid.org/0000-0002-1117-5645; Tobias Meckel, orcid.org/0000-0003-0759-2072*

frontiers | Frontiers in Immunology

ORIGINAL RESEARCH
published: 26 May 2022
doi: 10.3389/fimmu.2022.893301

Identification of SCRG1 as a Potential Therapeutic Target for Human Synovial Inflammation

Guoqiang Liu[1†], *Guisong He*[2†], *Jie Zhang*[1], *Zhongmin Zhang*[1,3*] *and Liang Wang*[1*]

[1] Department of Orthopedics, Academy of Orthopedics, The Third Affiliated Hospital, Southern Medical University, Guangzhou, China, [2] Department of Orthopedics, The Second Affiliated Hospital, Guangzhou Medical University, Guangzhou, China, [3] Division of Spine Surgery, Department of Orthopedics, Nanfang Hospital, Southern Medical University, Guangzhou, China

Synovial inflammation of joint tissue is the most important cause of tissue damage, joint destruction, and disability and is associated with higher morbidity or mortality. Therefore, this study aims to identify key genes in osteoarthritis synovitis tissue to increase our understanding of the underlying mechanisms of osteoarthritis and identify new therapeutic targets. Five GEO datasets with a total of 41 normal synovial membrane tissues and 45 osteoarthritis synovial membrane samples were used for analysis, and seven common differential genes were identified. The classification model constructed by LASSO analysis showed that six genes including CDKN1A, FOSB, STMN2, SLC2A3, TAC, and SCRG1 can be used as biomarkers of osteoarthritis, and the SCRG1 gene shows importance in osteoarthritis. Furthermore, drug database enrichment found that these six DEGs may be the drug targets of synovitis in osteoarthritis, and Valproic Acid CTD 00006977 may be a potential targeted therapeutic drug of SCRG1. Spearman correlation analysis was performed on the SCRG1 gene, and 27 genes with consistent expression were obtained. Functional analysis showed that 27 genes were mainly involved in metabolism, complement, antigen presentation, apoptosis, and regulation of immune pathways. The co-regulatory network of TFs-miRNA suggested that the SCRG1 gene may be regulated by hsa-miR-363-3p miRNA. In conclusion, SCRG1, as a diagnostic marker of osteoarthritis, co-regulates immune-related pathways through the interaction of related proteins, playing an important role in the occurrence and development of osteoarthritis, which may be a novel drug target.

Keywords: osteoarthritis, synovium, SCRG1, LASSO, pharmaceutical therapy

OPEN ACCESS

Edited by:
Maria Filkova,
Institute of Rheumatology, Prague, Czechia

Reviewed by:
Liam O'Neil,
University of Manitoba, Canada
Naoyuki Chosa,
Iwate Medical University, Japan

***Correspondence:**
Zhongmin Zhang
nfzzm@163.com
Liang Wang
liang091@aliyun.com

[†]*These authors have contributed equally to this work*

Specialty section:
This article was submitted to Autoimmune and Autoinflammatory Disorders, a section of the journal Frontiers in Immunology

Received: *10 March 2022*
Accepted: *26 April 2022*
Published: *26 May 2022*

Citation:
Liu G, He G, Zhang J, Zhang Z and Wang L (2022) Identification of SCRG1 as a Potential Therapeutic Target for Human Synovial Inflammation. Front. Immunol. 13:893301. doi: 10.3389/fimmu.2022.893301

INTRODUCTION

Osteoarthritis (OA) is one of the most common joint diseases and the main cause of disability in the elderly, accounting for 30% to 50% of people over 65 years old. The occurrence of OA is related to aging, obesity, inflammation, trauma, overuse of joints, metabolic disorders, and genetic factors (1, 2). OA is characterized by articular cartilage injury and degeneration, accompanied by subchondral bone

sclerosis, hyperplasia, and cystic degeneration, followed by joint space narrowing, meniscus, and synovitis. The typical symptoms of OA include pain, swelling, and stiffness, often accompanied by dysfunction and limited movement. Its clinical treatment includes pain relief and slowing tissue degradation (3–5). However, currently, there is no effective drug for treatment that can slow down the progression of the disease, as the exact pathogenesis of OA is still unclear (6–11).

Synovium is the boundary between an internal structure of the joint and the adjacent soft tissue, which is very important to maintain the stability of the internal environment. Although the main histopathological changes in osteoarthritic joints are cartilage destruction and chondrocyte proliferative differentiation, synovial lesions are also clinically found in many joint diseases and may play an important role in promoting the development and progression of the disease (12). In previous studies, it has been found that OA-related synovitis is a cartilage matrix degradation product caused by the secondary change. Synovitis is not a bystander in the occurrence of OA, but a participant in the destruction of joint structure, which promotes the progression of OA. Therefore, synovium may be a potential target for the treatment of OA (13, 14).

The pathogenesis of OA is complicated. It has been reported that a variety of inflammatory factors, including adipokine, interleukin, nerve growth factor, and tumor necrosis factor, can affect the progression of OA (14–16). In recent years, high-throughput chip technology has made great progress in molecular diagnosis and classification, prognosis prediction, target drug discovery, and other fields of OA research. Some gene expression profile studies on OA have revealed several key genes, diagnostic gene biomarkers, and related signaling pathways. Recent studies have implicated that secreted damage-associated molecular patterns (DAMPs) can act as ligands of Toll-like receptors (TLRs) or receptors for advanced glycation end-products (RAGEs) influencing synovial inflammation (17, 18). Impact injury stimulates the release of reactive oxygen species (ROS) that induce cell death in OA and activation of stress-induced kinases that upregulate MMP-13, ADAMTS-5, and TNF-α (19, 20). Other research reports that NOS-2, COX-2, MMPs, and ADAM were also associated with OA (21). In MicroRNAs, Tegner J et al. found in the OA FLS that the increased levels of miR-625 and miR-124 are related to the decreased expression of their target genes, while the expression levels of miR-155b and miR-203 are lower and the expression of their target genes is higher (22). Wang Q et al. found that NEAT1/miR-181c can regulate the proliferation of synovial inflammatory cells in OA (23). Similarly, inflammatory activation of the synovium can lead to the release of various proinflammatory mediators that not only cause widespread changes in the structure and function of synovial tissue but also promote articular cartilage damage and accelerate OA development (13). As several studies have shown, the release of inflammatory cytokine IL-1 β can induce and activate multiple immune signaling pathways including NF-κB, PI3K/AKT and MAPK, and then collagenase such as matrix metalloproteinase-13 (MMP-13) degradation of the extracellular matrix (24, 25). The disruption of the wnt signaling pathway is also associated with the pathogenesis of OA (26). Although there have been several studies on OA and new therapies that may help maintain joint homeostasis, little effect has been achieved (7, 11). Therefore, the biological treatment of inflammatory factors or intracellular inflammatory signal molecules is still the research direction of OA treatment. The research on the pathogenesis of OA and related genes still needs to be further studied. If potential diagnostic molecular markers of OA can be screened out before the onset, the quality of life of patients can be improved. In addition, biomarkers can help identify the early degradation of OA and may be applied to clinical practice decisions.

In view of this, in order to describe OA at the molecular level and reveal its pathogenesis and find suitable targets, we attempted to find differentially expressed genes (DEGs) in osteoarthritis by obtaining similar synovitis data for integrated analysis. We made use of the LASSO machine learning method to identify the key biomarkers and used the drug database and function enrichment method to obtain the ideal drug targets for osteoarthritis.

MATERIALS AND METHODS

Collection of the Dataset

The dataset GSE1919, GSE12021, GSE55235, GSE55457, GSE82107, which is based on the Affymetrix Human Genome Array platform, and dataset GSE89408, GSE143514, which is based on Illumina HiSeq 2000 were downloaded from the Gene Expression Omnibus (GEO) database (http://www.ncbi.nlm.nih.gov/geo/). All selected datasets were genome-wide expression data in joint synovial membrane tissues of OA or normal synovial membrane tissues. For all samples used in this study, the disease group included synovial membrane samples from patients who had undergone open synovectomy, arthroplasty, or joint replacement, and the normal control group included synovial membrane samples from patients who had undergone fatal accidents or joint trauma surgery, postmortem, or traumatic joint injury. Healthy subjects were defined as those who had no evidence of any form of arthritis on history or examination and had no cartilage damage or synovitis on knee arthroscopy. OA patients according to the respective criteria for OA and all patients suffered from synovitis. All the samples used above were obtained with the informed consent of patients or their families, and the study of each GEO dataset was approved by their respective Ethics Committee. In total, we obtained 41 normal and 45 OA human synovial membrane tissues in Array data and obtained 27 normal and 31 synovial membrane tissues in RNA-seq data. All datasets were generated by different laboratories. Because of the different sources of data production, we only used chip Array data for further analysis and used RNA-seq data to verify whether the expression of biomarkers in different tissues is consistent.

Common Gene Identification Between Synovial and Normal Tissues

Identification of DEGs for Array datasets is the primary task of this research. For microarray data, "GEOquery" and "limma" R software package was used to perform the differential gene expression analysis of each dataset between synovial and normal

knee cartilage tissues, and P-value were adjusted using the Benjamini and Hochberg method. In brief, the microarray matrix data were quartile data normalization and probe summarization was performed by the Robust Multi-array Average (RMA) algorithm. For RNA-Seq data, differential expression analysis was performed using Deseq2. In this study, genes with |log2fold change (FC)| > 2 and P-value < 0.05 between two groups were considered significantly different. The DEGs of each data set were annotated with Entrez IDs, official gene symbols, and gene names, and the intersection of DEGs between the synovial membrane and blood samples was shown by the Venn diagram and upset plot. During validation with microRNA GEO dataset, expression profiles obtained from the GEO dataset were analyzed with DEseq2, and the genes with a P-value less than 0.05 were considered differential expression in the GEO dataset. For Spearman correlation analysis, datasets from different research of synovial tissue were using limma and sva R software packages to remove batch effect and normalization, the associations between DEGs were evaluated by the Pearson correlation coefficient and Kruskal-Wallis test. All the analyses were performed in R (v4.0.2) using various bioconductor packages.

Identification of the Optimal Diagnostic Gene Biomarkers for OA

Least absolute shrinkage and selection operator (LASSO) has a strong predictive value and low correlation and is applied to select the best features for high-dimensional data. In order to identify optimal diagnostic gene biomarkers for OA, we utilized the seven key DEGs obtained between synovial and normal tissue from all microarray datasets as feature variables to construct the LASSO model. The LASSO algorithm analysis was performed by the 'glmnet' R software package to reduce data dimensions. A model index for each sample was created using the regression coefficients from the LASSO analysis to weight the expression value of the selected genes with the following formula: Index = ExpGene1*Coef1 + ExpGene2*Coef2 + ExpGene3*Coef3+… The "Coef" is the regression coefficient of the gene and is derived from the LASSO Cox regression, and "Exp" indicates the expression values of the gene. Then, five microarray datasets were randomly assigned to the training set (70%) and test set (30%). In order to evaluate the diagnostic ability of the above models and each gene biomarker to identify OA, we evaluated the receiver operating characteristic (ROC) area under the curve (AUC), sensitivity and specificity.

Gene Ontology and Pathway Enrichment Analysis

For the interest gene sets, Goseq (version 2.0), Kobas (version 3.0), and clusterProfiler (version 4.0) were used for GO and KEGG pathway enrichment analysis. P-value less than 0.05 was set as the cut-off criterion for the significant functional enrichment. Fisher's exact test (two-side) was performed to classify the pathway category. The false discovery rate (FDR) was used for the P-value correction. "Cluogo" plug-in based on Cytoscape software was used for network visualization of the enriched pathways. Gene set enrichment analyses (GSVA) were performed by the "gsva" R software package to identify enriched immune-related signaling pathways in OA. Spearman correlation analyses and linear regression analyses were performed for the correlation between genes or pathways. For the Gene Set Overrepresentation test, pathways with a false discovery rate less than 0.05 were considered significantly enriched.

Candidate Drugs Identification

Drug molecule identification is the key component of the ongoing research and molecular analysis of the key target gene can reveal the pathway of drug targeting. To better assist researchers in drug design, we perform drug analysis of DEGs using EnrichR (https://amp.pharm.mssm.edu/Enrichr/) analysis platform and DsigDB database. Each drug molecule in the platform contains the P-value and binding capacity of targeted genes, and the threshold value of adjusted P-value less than 0.05 as a significant result. The EnrichR platform also contains numerous analysis modules, including functional analysis, miRNA targeting analysis, and more.

Protein-Protein Interaction Network Construction and Module Analysis

In order to understand the associations between proteins of related genes, we used STRING database (version 11.0) integrating functional interactions from known and predicted protein-protein association data to predict the protein interaction network and function. For sub-network analysis, the Molecular Complex Detection (MCODE) plugin tool under the Cytoscape software package was used to cluster the large PPI network into smaller networks. Then Cytoscape software was used to visualize the network. The interactions between gene sets with a combined score > 0.9 were considered to be a key gene.

TF-miRNA Co-Regulatory Network

TFs-miRNA co-regulatory network can better understand the development mechanism of disease. In this research. NetworkAnalyst (https://www.networkanalyst.ca/) analysis platform is used to identify TF-miRNA interaction with identified common genes. NetworkAnalyst is a comprehensive web platform for performing gene expression network analysis, and the interaction network is obtained from the ENCODE (https://www.encodeproject.org/) database. Cytoscape was used to visualize the NetworkAnalyst analysis results.

Statistical Analysis

All statistical tests performed were two-sided using the R software by version 4.0.2 (http://www.R-project.org/). For two groups, unpaired Wilcox-test was used to measure the difference of continuous variables between normal groups and OA groups.

RESULTS

Identification of DEGs in OA Synovial Membrane

The purpose of this study was to use relevant differentially expressed genes (DEGs) in synovial membrane samples to

identify dysregulated genes and pathways and to better explain the pathogenesis of OA disease. To achieve this purpose, five GEO datasets (GSE1919, GSE12021, GSE55235, GSE55457, GSE82107) were included in our study as shown in **Table 1**. Then we performed differential analysis, a total of 3118 DEGs were identified in the OA datasets compared with normal tissues, including 293, 188, 287, 191, 289 up-regulated and 270, 419, 218, 375, 1146 down-regulated DEGs in five GEO datasets, respectively. To identify common DEGs in OA, we performed an integrative analysis, a total of 176 DEGs overlapped in 3/5 datasets, a total of 55 DEGs overlapped in 4/5 datasets, and a total of seven DEGs were obtained in five datasets (**Figure 1A**, **Table S1**). Furthermore, we used KEGG to analyze the functions of each gene set; the analysis results showed that both 176 and 56 DEGs were enriched immune-related pathways, such as Rheumatoid arthritis pathway, IL-17 signaling pathway, TNF signaling pathway, NF-kappa B signaling pathway, MAPK signaling pathway (**Figure 1B**). On the other hand, we also analyzed these seven DEGs, and the results showed that seven genes were significantly expressed in normal and synovial samples (**Figure 1C**), hierarchical clustering analysis of the seven DEGs was presented in **Figure 1D** and gene description with gene functions is shown in **Table S1**. These genes and related pathways analyzed above may be associated with the pathogenesis of OA.

Identification of the Optimal Diagnostic Gene Biomarkers for OA

In order to determine the best diagnostic gene biomarkers for OA, we extracted the expression profile of seven DEGs that are commonly differentially expressed from five GEO datasets to construct the LASSO model (**Figure 2A**). First, we divided the five GEO dataset samples into training sets and test sets in a ratio of 7:3, and then performed LASSO regression analysis. Using the LASSO method, seven DEGs were identified with non-zero regression coefficients, and the value of lambda.min was 0.00154252, according the threshold value, gene Nell1 excluded (**Figure 2B**). The six DEGs-based model index was created as the following formula: Index=TAC*(0.0051) + CDKN1A*(-0.002) + FOSB*(-0.001) + STMN2*(0.0052) + SLC2A3*(-0.0014) + SCRG1*(0.0004). Therefore, we selected these six DEGs as the optimal potential diagnostic gene biomarkers for OA. ROC curve analysis showed that the AUC of the six DEGs-based model was 0.8896 (95% CI: 78.29%-96.07%) in the training set and 0.9394 (95% CI: 76.03%-95.67%) in the test set; this result indicated the LASSO model has a high AUC value and may serve as a better biomarker of OA (**Figure 2C**). In addition, two RNA-seq GEO datasets (GSE89408 and GSE143514) associated with synovial membrane were used as validation sets to verify the accuracy (**Figure 2C**); the validated AUC value is 0.8713 (95% CI: 72.19%-95.15%). This is also a high accuracy to predict the occurrence of OA. Furthermore, we examined the six DEGs expression in two RNA-seq datasets and we found that SCRG1, CDKN1A, and SLC2A3 are significantly differentially expressed in OA which has the same expression trend with five microarray data (P-value<0.05), and indicated that these three DEGs were highly associated with OA, and they could play an important role in disease (**Figures 2D–I**).

TABLE 1 | Datasets of gene expression profiles.

ID	GEO	Sample source	OA samplessamples	Healthy samplessamp	Seq Type	Platform	year	country	author
1	GSE1919	Synovial tissue	5	5	Array	[HG_U95A] Affymetrix Human Genome U95A Array	2004	Germany	Ute Ungethuem
2	GSE12021	Synovial tissue	10	9	Array	GPL96[HG-U133A] Affymetrix Human Genome U133A Array	2008	Germany	Huber R
3	GSE55235	Synovial tissue	10	10	Array	GPL96[HG-U133A] Affymetrix Human Genome U133A Array	2014	Germany	Woetzel D
4	GSE55457	Synovial tissue	10	10	Array	GPL96[HG-U133A] Affymetrix Human Genome U133A Array	2014	Germany	Woetzel D
5	GSE82107	Synovial tissue	10	7	Array	GPL570 [HG-U133_Plus_2] Affymetrix Human Genome U133 Plus 2.0 Array	2019	Netherlands	de Vries M
6	GSE89408	Synovial tissue	22	28	RNA-Seq	Illumina HiSeq 2000 (Homo sapiens)	2016	USA	Alice Walsh
7	GSE143514	Synovial tissue	5	3	RNA-Seq	Illumina HiSeq X Ten (Homo sapiens)	2020	China	Zhou Y

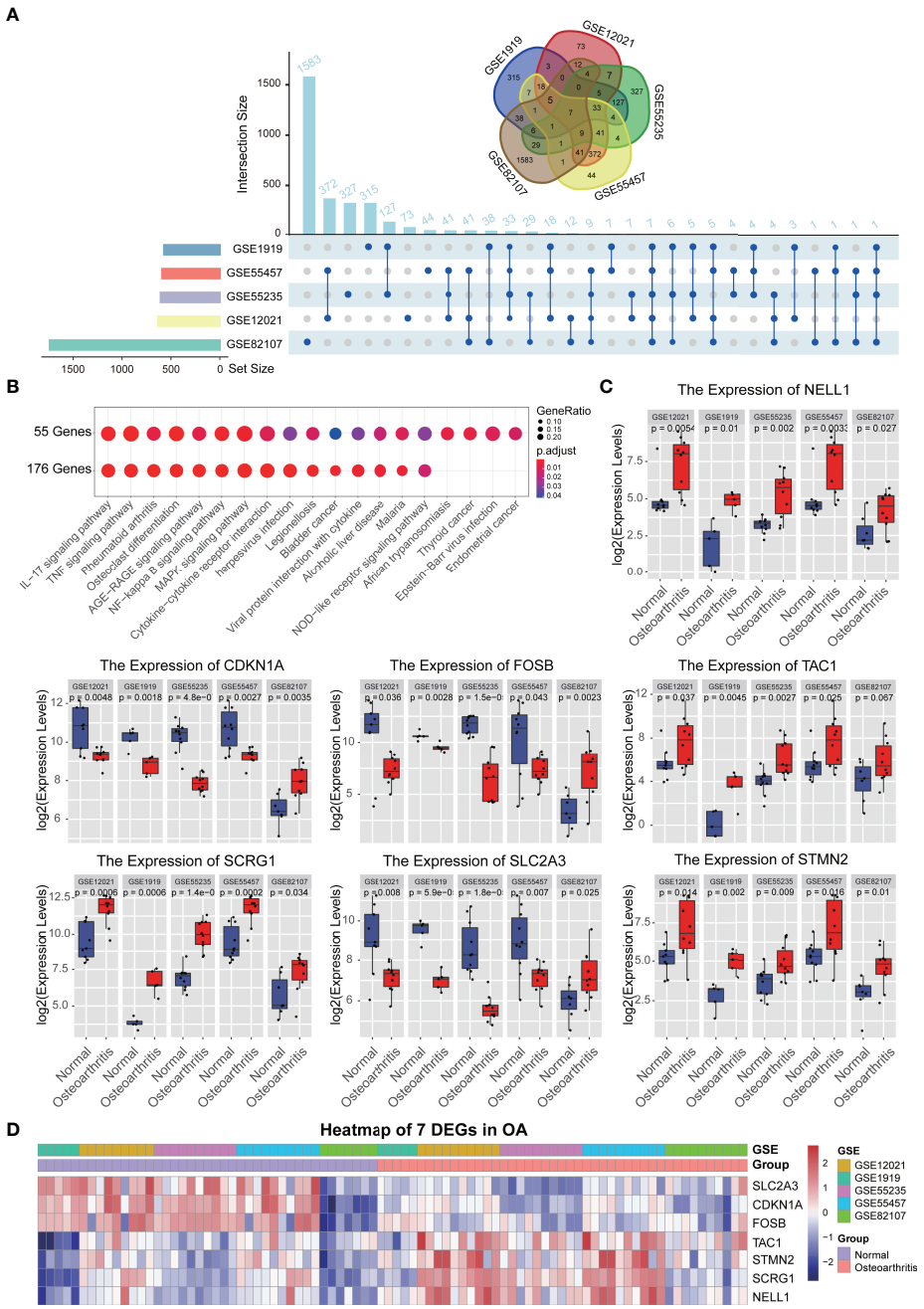

FIGURE 1 | Differential expression gene analysis. **(A)** The different analysis results of 5 synovium-related GEO data sets, upset and Venn diagram showed the relationship between the number of different genes in different GEO datasets. **(B)** KEGG function analysis of each gene sets. **(C)** Boxplot showed the expression levels of 7 genes which are commonly differentially expressed between synovial tissues and normal tissues in 5 GEO datasets. **(D)** A heatmap plot of 7 common differentially expressed genes in all synovial tissues and normal tissues.

Identification of Candidate Drugs for Six DEGs

Previous differential analysis and biomarker studies showed that six DEGs (TAC, CDKN1A, FOSB, STMN2, SLC2A3, SCRG1) play an important role in OA and may serve as disease targets, so we used EnrichR platform to analyze drug molecules that may be involved in the six genes. The drug data were collected from the DSigDB database. According to the adjusted P-value, the results from the candidate drugs were generated (**Table S2**). The drug result showed that there were 100 possible drug molecules targeting six DEGs, of

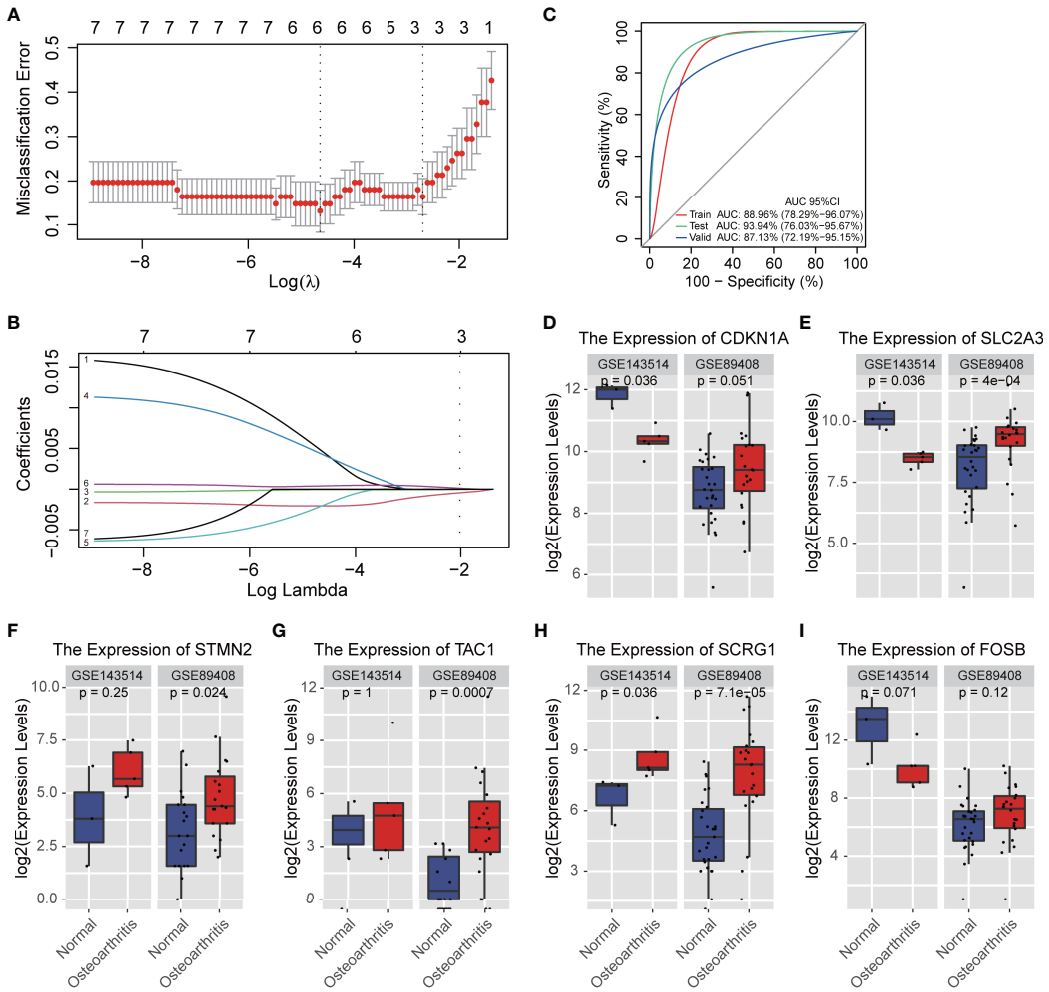

FIGURE 2 | A model for predicting OA and verification of gene differential expression. **(A)** CV statistical graph during the construction of the LASSO regression model, which shows that the minimum lambda at model construction is 0.00154252 (dotted line on the left). **(B)** the model regression coefficient diagram shows the change trend of the coefficient corresponding to each gene variable with the change of lambda value. The results showed that there were 6 prediction genes corresponding to the minimum lambda. **(C)** ROC curve predicts the identification effect of the above models in different datasets. The closer AUC value is to 1, the better of prediction effect on the model. The figure is shown that the AUC in the training set is 0.8896 and that in the test set is 0.9394, indicating that the model has good prediction accuracy. In RNA-seq validation data set, the AUC is 0.8713, which shows that the models constructed by the 6 genes can also have good accuracy in different types of data sets. **(D–I)** The expression levels of 6 genes affecting disease occurrence in the model are verified. The figure shows that 6 genes are also significantly differentially expressed in the RNA-SEQ data set.

which VALPROIC ACID CTD 00006977 was the common drug molecule associated with six DEGs, Tetradioxin CTD 00006848, Retinoic acid CTD 00006918, estradiol CTD 00005920, benzo pyrene CTD 00005488, and Silica CTD 00006678 were also significant drug molecules that interacted with other DEGs. Interestingly, we found that Retinoic acid-related orphan receptor (RORα) is a protein family that expressed in a variety of tissues such as retina, skeletal muscle, brain, thymus, liver, lung, kidney, and adipose tissue, and may mediate the process of OA by alterations in cholesterol metabolism (27). The inverse agonist of the retinoic acid-related orphan receptor has shown the potential to modify the progression of OA with minimal adverse effects (28). Combined with the results obtained in this study, it is suggested that the four DEGs (CDKN1A, FOSB, SLC2A3, SCRG1) may be the target of retinoic acid drugs, and other drugs in the list may also be targets for drug design in OA disease.

Spearman Correlation Analysis Suggested the Function of the SCRG1 Gene

For the six marker genes previously identified, we found that SCRG1, CDKN1A, SLC2A3 genes were significantly expressed in all microarray and RNA-seq datasets, and only SCRG1 gene showed an increased expression trend in all datasets. SCRG1 has also been observed to be specifically expressed in human articular cartilage (29–31), so we considered that SCRG1 might be a key regulatory factor in the development of synovial inflammation.

In order to understand the role of SCRG1 in OA, we performed gene expression correlation analysis to predict SCRG1 gene function by protein-protein interaction. First, we removed the batch effect and normalized it from the gene expression matrix after merging five microarray datasets, and PCA analysis was used to show the effect (**Figures 3A, B**). The PCA result showed that the cluster of each dataset sample was more concentrated, indicating that the batch difference has been removed and the sample matrix was reliable. Then, Spearman correlation analysis was performed to estimate the correlation of the SCRG1 gene with other genes at the expression level in the normalized data. The Spearman analysis results showed that 27 correlation genes were obtained, and these genes expressions were also differential in each microarray dataset (**Figures 3C, D**).

To ascertain the possible mechanisms of SCRG1 gene affecting OA progression, GO function and KEGG pathway analysis were used. The most significantly enriched GO terms based on the 27 genes in the biological process category were signal transduction, in the cellular component category was MHC protein complex, and in the molecular function category was receptor activity (**Figures S1A–C**). These results are consistent with previous research. For example, Mohammadi et al. found that aberrant signaling contributes to the maldevelopment of joints and the onset and progression of OA (32), and TLRs receptors or ligands also affect synovial membrane inflammation (17, 19).

The KEGG pathway analysis result showed some pathways like complement and coagulation cascades, antigen processing and presentation, cell cycle, rheumatoid arthritis, cell adhesion molecules (CAMs), metabolic pathways, FoxO signaling pathway, PI3K-Akt signaling pathway, Jak-STAT signaling pathway, TGF-beta signaling pathway, Wnt signaling pathway, Notch signaling pathway, NF-kappa B signaling pathway, apoptosis, and other signaling pathways were all quite significant in key cascades in the basic biology of OA, such as initiation, growth, maintenance, and development of OA (**Figure 3E**). Interestingly, "MAPK signaling pathway," "PI3K-Akt signaling pathway," "NF-kB signaling pathway," "TGF-beta signaling pathway," and "Wnt signaling pathway" have been reported to be essential for OA-immune evasion in human cartilage tissue (33–37), but these pathways were rarely reported in synovium with OA, and these pathways are also involved in other specific immuno-associated disease, such as in RA, SLE, and AS, many of which have shown optimistic response on therapy. Moreover, many other pathways were also found to be associated with OA in our results, such as cell adhesion molecules (CAMs), metabolic pathways, complement and coagulation cascades, antigen processing and presentation, apoptosis, and cell cycle.

PPIs Network Analysis of Correlation Genes to Identify Potential Molecular Signatures in Osteoarthritis Synovium

To improve the biological understanding of the correlation between 27 gene functions identified in this study, we conducted protein-protein interaction analysis. As shown in **Figure 4**, the protein-protein interactions result shows that 27 protein interaction network was divided into five subnetworks, molecular functions of the five subnetworks are mainly related to metabolic pathways, complement and coagulation cascades, antigen processing and presentation, apoptosis, and immune-related signaling pathway, respectively. Those subnetwork results suggest that the similar functional proteins may be protein complexes serving important biological functions in OA, which are closely associated not only with the growth process of OA but also with the synovial membrane environment. Furthermore, in this part of the result, we found that

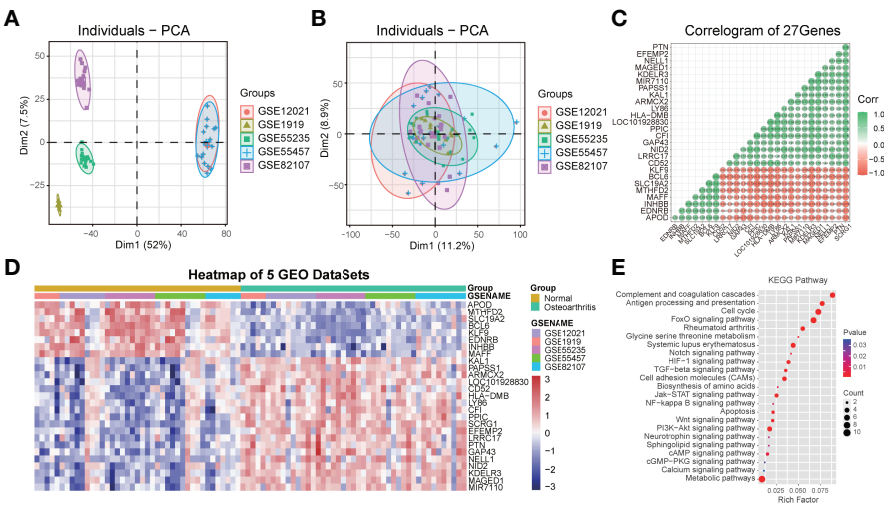

FIGURE 3 | PCA cluster plot before and after sample correction and protein-protein interaction analysis of spearman correlation genes with SCRG1. **(A, B)** Two-dimensional PCA cluster plot of the 5 microarray datasets before and after sample correction, the colors represent each osteoarthritis datasets. **(C)** The Spearman's correlation coefficients of gene expression with SCRG1, 27 genes were found. **(D)** Heatmap plot of 27 associated genes, and showed 27 genes also differentially expressed in all synovial tissues and normal tissues. **(E)** KEGG pathway analysis of the 27 genes, and the enriched immune-related pathways were shown.

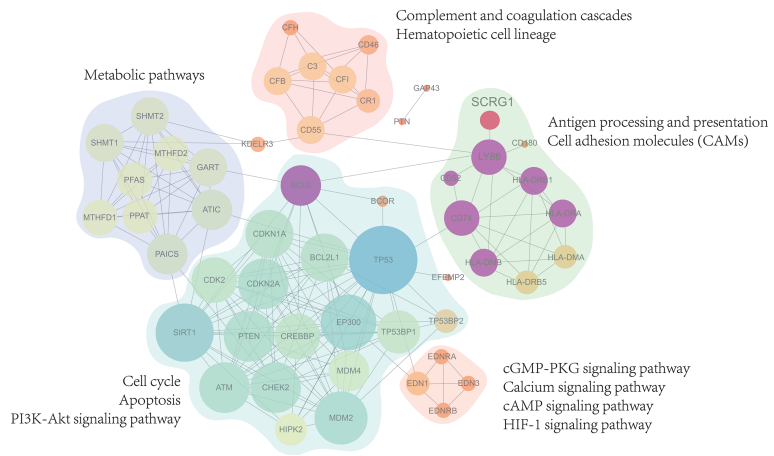

FIGURE 4 | Protein-Protein interactions analysis with 27 genes associated expression with SCRG1. The PPI network showed 5 sub-functional clusters were identified and suggest that SCRG1 may be a protein complexes service with important biological function in OA. And the biological function is mainly related to metabolic pathways, complement and coagulation cascades, Antigen processing and presentation, Apoptosis, and immune-related signaling pathway.

SCRG1 gene only participates in one subnetwork and serves immune-related biological functions such as antigen processing and presentation. On the other hand, SCRG1 only interacts with Ly86 gene, which may be due to the lack of research on the SCRG1 gene. For other functions in the PPIs network, we have reason to suspect that SCRG1 may interact with LY68 and form protein complexes with other proteins to perform corresponding functions. Therefore, SCRG1 as a potential predictive marker needs to be further investigated.

Co-Regulatory Network Mapping and Dysregulated Targets of Regulated miRNA

The analysis of the TF-miRNA co-regulatory network delivers miRNAs and TFs interaction with the common DEGs. This interaction can be the reason for regulating the expression of the DEGs. The regulatory network between 27 correlated genes and TFs, miRNAs were constructed using NetworkAnalyst that consisted of 657 edges and 432 nodes between 142 TFs, 261 miRNAs with 27 correlation genes in the context of OA (**Figure 5A**). The constructed regulatory network showed that four genes (BCL6, MTHFD2, GAP43, EDNRB) were high TFs and miRNAs interactions. In addition, multiple TFs that regulate these four genes representing differential expression in OA were identified as crucial TFs: JUN, SATA2, FOS, TP53, and MYC, which are associated with the development of OA. These TF-genes regulate more than one common correlation gene of the network, which indicates high interaction of the TF-genes with common genes. Interestingly, we found that six miRNAs regulate SCRG1 gene, and no TFs associated with SCRG1 gene in the regulatory network. To confirm the regulatory results of miRNA, miRNA sequencing data from GSE143514 were used to validate the miRNA expression level between the synovial membrane and normal tissue. We use DEseq2 method for miRNA differential expression analysis, and the volcano plot showed the differential expression of six miRNAs. The results showed hsa-miR-363-3p was significantly expressed and P-value of 0.00095 (**Figure 5C**), and heatmap showed six miRNAs were changed by a different expression level, indicating that six miRNAs, especially hsa-miR-363-3p, may play an important role in OA (**Figures 5B, D**). The SCRG1 gene may be regulated by multiple TFs in OA, affect the expression of targeted miRNA, and regulate the functions of other disease genes, which may play a critical role in the pathogenesis of OA and be a potential therapeutic target.

DISCUSSION

Osteoarthritis is a chronic joint disease with an increasing prevalence and burden of cartilage degeneration. The disease will cause cartilage degeneration, synovial inflammation, subchondral bone remodeling, and osteophyte formation (11, 38). Due to the lack of early diagnostic indicators, OA patients often lose the best treatment opportunities, resulting in poor prognosis. Chronic inflammation of the synovial membrane of joint tissue is considered to be the most important cause of tissue damage, joint destruction, and disability (39). Therefore, identifying biomarker genes and their activation status in OA synovitis tissues is crucial to increasing our understanding of the underlying mechanisms and the identification of new therapeutic targets. With the rapid development of science and technology and the deepening understanding of the pathophysiology of OA, bioinformatics provides a powerful strategy for screening molecular markers and found a variety of therapeutic targets that may participate in the structural progress of OA, some of which are promising and under clinical investigation in randomized controlled trials (7). In this study, we attempted to identify diagnostic markers in synovitis of OA and their possible drug targets, and further explore the role and function of diagnostic markers in OA.

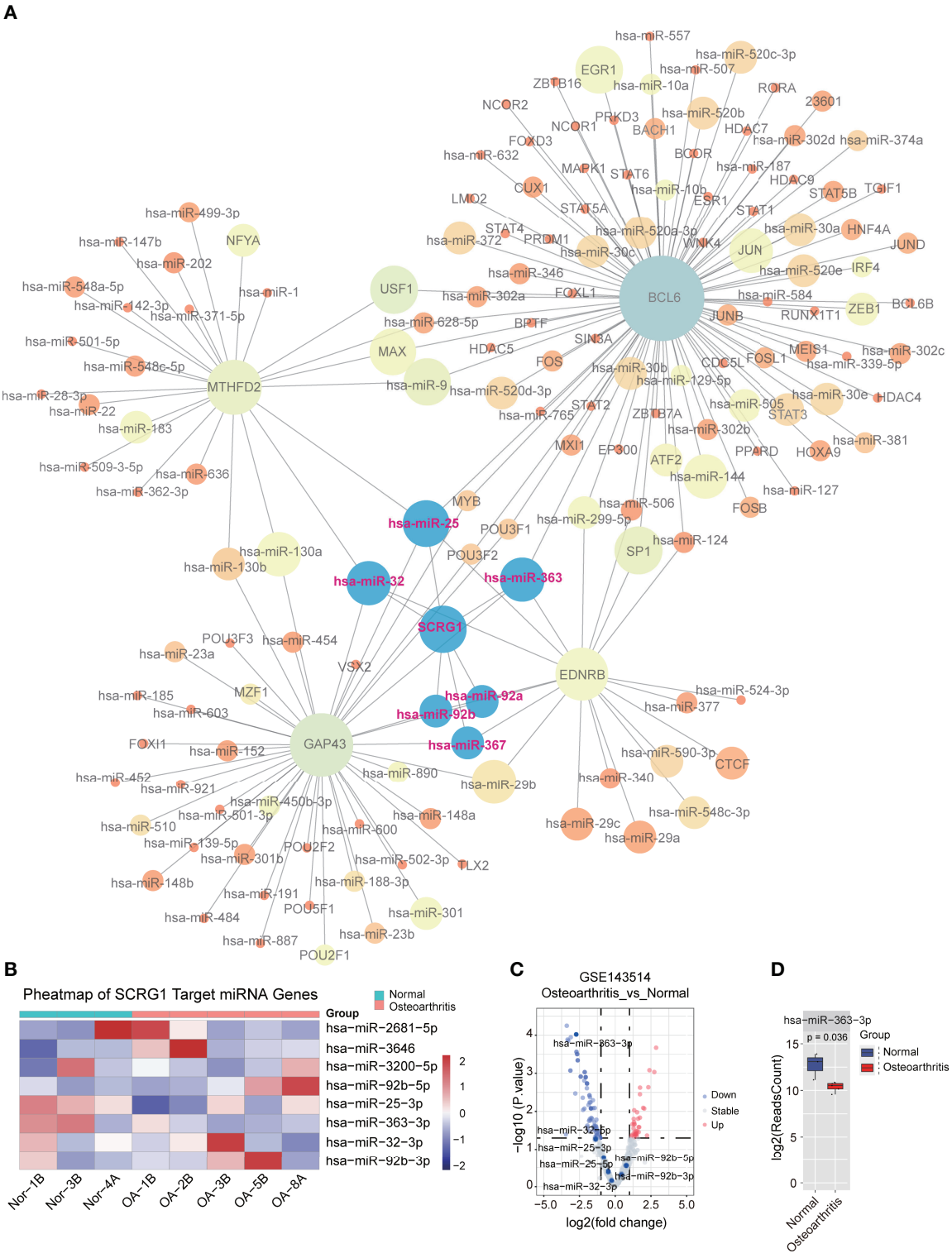

FIGURE 5 | TF-miRNA co-regulatory network of 27 genes associated with SCRG1. **(A)** The TF-miRNA co-regulatory network for 27 genes, SCRG1 was not found as the corresponding transcript factor in network, but 6 miRNAs can regulate SCRG1 gene expression. **(B,C)** volcano and heatmap plot of the miRNA expression in GSE143514 dataset, which represents the differential expression of values in synovium and normal tissues. Red color dot in Volcano plot represents up-regulated expression in synovium tissue. **(D)** hsa-miRA-363-3p was significantly differentially expressed in synovium tissues.

First, we downloaded the microarray expression profile data of 5 OA synovitis from GEO, and identified 3118 differentially expressed genes, among which seven overlapping genes coexist in five data sets. In order to exclude part of the false-positive markers, we used a LASSO machine learning method to build models and obtain biomarkers with higher accuracy. LASSO logistic regression determines variables by minimizing the classification error, which is mainly used to screen characteristic variables and build the optimal classification model. In this study, a total of six genes, TAC, CDKN1A, FOSB, STMN2, SLC2A3, and SCRG1, were identified as diagnostic markers of OA by feature selection using LASSO method, and a classification model of OA was constructed, whose validation set AUC was 0.9394. To further verify the reliability of the model's classification and identification, two synovium-related RNA-SEQ datasets were used for validation. The results showed that the AUC of the validation set was 0.8713, indicating that the model is a very reliable diagnostic classifier; that six genes are feasible as biomarkers in OA. In this study, we found that the expression trend of three DEGs (CDKN1A, FOSB, SLC2A3) in the GSE82107 data set were inconsistent with other data sets from the common difference DEG analysis step. We considered that these three DEGs may have multiple regulatory functions in synovial inflammation, such as involvement in multiple cell reprogramming processes. We also observed different expression trends of these three DEGs in the validation RNA-seq datasets, therefore, more consideration is needed in the function research of these three DEGs. Similarly, we found that only three DEGs (SCRG1, CDKN1A, SLC2A3) had a significant P-value in the RNA-seq data validation step, and only the SCRG1 gene showed a consistent expression trend, which was increased in the OA synovitis samples, so SCRG1 may be a reliable biomarker and therapeutic target for OA diseases.

For the six marker genes previously identified, we found that CDKN1A, FOSB, STMN2, and SLC2A3 genes were reported to be associated with cartilage inflammation in OA (40–51). For example, the expression level of CDKN1A will increase correspondingly during cartilage degeneration (44), IL-17 and IL-1beta induced collagenase-3 production through AP-1 occurred with differential protein complex, and stimulation resulted in FOSB activation (52), STMN2 has significant differences between preserved and subchondral bone (48). SCRG1 has also been observed to be specifically expressed in human articular cartilage and is involved in human mesenchymal stem cell (hMSC) growth suppression and differentiation during dexamethasone dependent chondrogenesis (31). Ochi et al. found that overexpression of SCRG1 can inhibit the proliferation of hMSCs, stimulate cartilage formation in C3H10T1 cells, play a role in mesenchymal chondrogenesis *in vitro*, and may have an important function in cartilage development (31). So, we suggest that these six DEGs may be the key genes of OA. Moreover, related drug molecules were identified from six biomarkers according to DSigDB database in this study. Among all candidate drugs, VALPROIC ACID CTD 00006977, Tetradioxin CTD 00006848, estradiol CTD 00005920, benzopyrene CTD 00005488, and Retinoic acid CTD 00006918 ranked in the top five with targeting multiple DEGs (P-value<0.05). Previous studies have found that the Retinoic acid-related orphan receptor (RORα) has potential in mediating OA and changing the progression of OA (11, 28). The screened drug, VALPROIC ACID CTD 00006977, was a reverse agonist of RORα, suggesting that this drug may be a targeted therapy for OA disease. The efficacy of other proposed drugs is also speculated, and these drugs may be considered for further validation by chemical experiments.

Although all six genes are associated with cartilage, they are rarely reported in OA synovitis. In order to further explore the role of the six genes in OA synovitis, we used STRING database to construct the protein interaction network, but the results showed that SCRG1 did not exist in the constructed network. Combined with the above difference analysis results and the basic research results of SCRG1 gene in the literature, SCRG1 gene was significantly different in all microarray and RNA-seq data sets, and was upregulated in all analysis data sets, and the role and function of SCRG1 gene in OA synovitis was not clear; therefore, it is very important to study the function and possible mechanism of SCRG1 in OA synovitis. SCRG1 is a small protein with a length of 98 amino acids, rich in cysteine, is mainly distributed in the central nervous system (31), and was discovered through the identification of the genes associated with the neurodegenerative changes observed in transmissible spongiform encephalopathies (53). SCRG1 was originally named "Scrapie responsive gene-1" by Dr. Dron (32), and HGNC was later named "Stimulator of chondrogenesis 1". The protein targets the Golgi apparatus and large dense-core vesicles and secretory granules of neurons (33). Recent studies have shown that SCRG1 is an important regulator during hMSC self-renewal, migration, and osteogenic differentiation along with its receptor BST1 (54), and has been found to be widely induced in neurons of scrapie-infected mice, suggesting that SCRG1 is involved in the host response to stress and neuronal death (33).

In order to explore the function of SCRG1 gene in OA, we obtained 27 genes consistent with the expression trend of SCRG1 gene by Spearman analysis in this study. When we annotated 27 gene functions using GO and KEGG databases, metabolism, complement, antigen presentation, apoptosis, and immune-related pathways were the most important functional category. Several studies have shown that dysfunctional synovial cell bioenergetics alter the distribution of OA synovial cells and promote inflammatory development. The protein network of 27 genes was constructed and the analysis network showed that the function of these genes was enriched in four aspects: immune response, cytokine production, migration, and osteoclast development. Immune response and cytokine production are directly related to inflammation. Interestingly, SCRG1 has been shown to be involved in immune regulation pathways in mouse cell lines (55), but the possible functional relationships between SCRG1 and neurons were not found, which might be a pitfall of bioinformatics or AI learning. Analyses by Dron's group revealed

colocalization of SCRG1 with SCG2, TAC2 (34), GM130, and protein disulfide isomerase (33). We suggest that SCRG1 may be involved in neuro-related biological functions, although colocalizations of SCRG1 with other molecules were detected by immunohistochemical analyses and may not be interpreted as evidence of protein-protein interactions, but there is still reason to believe that SCRG1 may be involved in neurobiological function (35). On the other hand, when we analyzed the genes interacting with SCRG1, we did not find the expression of the BST1 gene associated with the SCRG1 ligand. We suggest that BST1 might be communicating with specific cell types in OA synovitis by cell communication. While the data used in the analysis were not representative of BST1 gene expression in specific cell types of OA synovitis, the single-cell sequencing may help us to understand the role of SCRG1 in cell communication. Meanwhile, since forced expression of SCRG1 in hMSCs will be suppressed cell proliferation and stimulated chondrogenesis (31), and combined with the previous results obtained from synovial data we used, we believe that the role of the SCRG1 gene in OA synovitis may be related to the pathogenesis of disease, rather than the result of enhanced chondrogenesis to compensate for primary abnormalities such as degeneration of cartilages.

Further studies on the TFs-miRNA co-regulatory network found that hsa-mir-363-3p may be significantly regulated by SCRG1, which results in the miRNA dataset (39), indicating that the function of SCRG1 in OA may be regulated by miRNA hsa-mir-363-3p. It also revealed the important contribution of miRNA to transcriptome changes in OA synovial cells and explained the complexity of mutual regulation between miRNA and mRNA. Although several miRNA targets (hsa-mir-92b-5p, hsa-mir-32-3p, hsa-mir-92b-3p, and hsa-mir-25b-3p) were not validated with published data, important evidence of interactions between these targets and corresponding miRNAs was found from mirTarBase, and these targets should be followed up in future studies. Furthermore, considering the therapeutic potential of miRNAs in preclinical studies of OA, miRNA interaction for this dysfunction may be promising for OA.

The absence of experimental validation of biological samples is a significant limitation of this study, although the microarray and RNA-seq methods were combined to reduce the deviation introduced by using a single method, and RNA-seq data were also used to validate the conclusions. However, the sample data used still do not fully reflect all aspects of the transcriptome characteristics of OA synovitis. On the other hand, it should be mentioned that the validation RNA-seq datasets are weighted heavily towards GSE89408 because of clinical sample sizes. In this study, GSE89408 dataset contained 22 OA and 28 normal samples while GSE143514 contained only five OA and three normal samples were included in the validation RNA-seq datasets. In general, enlarging the sample size, adding tissue-specific data, and verifying the biological function will effectively prove the conclusion of the analysis.

In summary, this study combined bioinformatics and machine learning methods to analyze the transcriptional expression characteristics of OA synovitis and screened six biomarkers related to OA. Drug database enrichment found that these six DEGs may be the drug targets of synovitis in osteoarthritis, and Valproic Acid CTD 00006977 may be a potential targeted therapeutic drug of SCRG1. SCRG1 is upregulated in OA synovitis and is manifested by the increased immune response, suggesting that SCRG1 is involved in cell growth suppression and differentiation. miRNA hsa-miR-363-3p plays an important role in regulating SCRG1 in OA synovitis. The six genes identified in this study can provide potential targets for the diagnosis and treatment of OA. As a reliable biomarker and therapeutic target for OA synovitis, the extent to which SCRG1 upregulated promotes the development of OA in synovitis and the corresponding function remains to be studied.

CONCLUSIONS

SCRG1, as a diagnostic marker of OA, may be significantly up-regulated by hsa-miR-363-3p in synovitis of OA, and co-regulate immune-related pathways through the interaction of related proteins, playing an important role in the occurrence and development of OA, which may be a new drug target.

DATA AVAILABILITY STATEMENT

Publicly available datasets (GSE1919, GSE12021, GSE55235, GSE55457, GSE82107, GSE89408 and GSE143514) were analyzed in this study. All the datasets were obtained from the GEO (http://www.ncbi.nlm.nih.gov/geo) database.

AUTHOR CONTRIBUTIONS

GL analyzed and wrote the manuscript. GH designed the experiments and analyzed the data. ZZ devised the concept and supervised the study. All authors contributed to the article and approved the submitted version.

ACKNOWLEDGMENTS

The authors thank GEO Database for providing the data and thank Mr. He for his technical assistance.

SUPPLEMENTARY MATERIAL

The Supplementary Material for this article can be found online at: https://www.frontiersin.org/articles/10.3389/fimmu.2022.893301/full#supplementary-material

Supplementary Figure 1 | GO functional analysis of 27 related genes associated with SCRG1. **(A-C)** The Go analysis result showed by biology process, cellular component, molecular function. The results showed that 27 genes function was associated with immune signaling pathway, may be involved in synovial inflammation.

REFERENCES

1. Vina ER, Kwoh CK. Epidemiology of Osteoarthritis: Literature Update. *Curr Opin Rheumatol* (2018) 30(2):160. doi: 10.1097/BOR.0000000000000479
2. Collaborators G. B. D. R. F. Global, Regional, and National Comparative Risk Assessment of 84 Behavioural, Environmental and Occupational, and Metabolic Risks or Clusters of Risks for 195 Countries and Territories, 1990-2017: A Systematic Analysis for the Global Burden of Disease Study 2017. *Lancet* (2018) 392(10159):1923. doi: 10.1016/S0140-6736(18)32225-6
3. Kroon FPB, Carmona L, Schoones JW, Kloppenburg M. Efficacy and Safety of non-Pharmacological, Pharmacological and Surgical Treatment for Hand Osteoarthritis: A Systematic Literature Review Informing the 2018 Update of the EULAR Recommendations for the Management of Hand Osteoarthritis. *RMD Open* (2018) 4(2):e000734. doi: 10.1136/rmdopen-2018-000734
4. Bannuru RR, Osani MC, Vaysbrot EE, Arden NK, Bennell K, Bierma-Zeinstra SMA, et al. OARSI Guidelines for the Non-Surgical Management of Knee, Hip, and Polyarticular Osteoarthritis. *Osteoarthritis Cartilage* (2019) 27 (11):1578. doi: 10.1016/j.joca.2019.06.011
5. Kloppenburg M, Berenbaum F. Osteoarthritis Year in Review 2019: Epidemiology and Therapy. *Osteoarthritis Cartilage* (2020) 28(3):242. doi: 10.1016/j.joca.2020.01.002
6. Reynard LN, Barter MJ. Osteoarthritis Year in Review 2019: Genetics, Genomics and Epigenetics. *Osteoarthritis Cartilage* (2020) 28(3):275. doi: 10.1016/j.joca.2019.11.010
7. Coryell PR, Diekman BO, Loeser RF. Mechanisms and Therapeutic Implications of Cellular Senescence in Osteoarthritis. *Nat Rev Rheumatol* (2021) 17(1):47. doi: 10.1038/s41584-020-00533-7
8. Xie J, Wang Y, Lu L, Liu L, Yu X, Pei F. Cellular Senescence in Knee Osteoarthritis: Molecular Mechanisms and Therapeutic Implications. *Ageing Res Rev* (2021) 70:101413. doi: 10.1016/j.arr.2021.101413
9. Pelletier JP, Martel-Pelletier J, Rannou F, Cooper C. Efficacy and Safety of Oral NSAIDs and Analgesics in the Management of Osteoarthritis: Evidence From Real-Life Setting Trials and Surveys. *Semin Arthritis Rheu* (2016) 45(4): S22. doi: 10.1016/j.semarthrit.2015.11.009
10. Savvidou O, Milonaki M, Goumenos S, Flevas D, Papagelopoulos P, Moutsatsou P. Glucocorticoid Signaling and Osteoarthritis. *Mol Cell Endocrinol* (2019) 480:153. doi: 10.1016/j.mce.2018.11.001
11. Latourte A, Kloppenburg M, Richette P. Emerging Pharmaceutical Therapies for Osteoarthritis. *Nat Rev Rheumatol* (2020) 16(12):673. doi: 10.1038/s41584-020-00518-6
12. Loeser RF, Goldring SR, Scanzello CR, Goldring MB. Osteoarthritis: A Disease of the Joint as an Organ. *Arthritis Rheum-Us* (2012) 64(6):1697. doi: 10.1002/art.34453
13. Mathiessen A, Conaghan PG. Synovitis in Osteoarthritis: Current Understanding With Therapeutic Implications. *Arthritis Res Ther* (2017) 19 (1):18. doi: 10.1186/s13075-017-1229-9
14. Scanzello CR, Goldring SR. The Role of Synovitis in Osteoarthritis Pathogenesis. *Bone* (2012) 51(2):249. doi: 10.1016/j.bone.2012.02.012
15. Tavallaee G, Rockel JS, Lively S, Kapoor M. MicroRNAs in Synovial Pathology Associated With Osteoarthritis. *Front Med* (2020) 7:376. doi: 10.3389/fmed.2020.00376
16. Berenbaum F. Osteoarthritis as an Inflammatory Disease (Osteoarthritis is Not Osteoarthrosis!). *Osteoarthritis Cartilage* (2013) 21(1):16. doi: 10.1016/j.joca.2012.11.012
17. van den Berg WB. Osteoarthritis Year 2010 in Review: Pathomechanisms. *Osteoarthritis Cartilage* (2011) 19(4):338. doi: 10.1016/j.joca.2011.01.022
18. Sellam J, Berenbaum F. The Role of Synovitis in Pathophysiology and Clinical Symptoms of Osteoarthritis. *Nat Rev Rheumatol* (2010) 6(11):625. doi: 10.1038/nrrheum.2010.159
19. Ding L, Heying E, Nicholson N, Stroud NJ, Homandberg GA, Buckwalter JA, et al. Mechanical Impact Induces Cartilage Degradation *via* Mitogen Activated Protein Kinases. *Osteoarthritis Cartilage* (2010) 18(11):1509. doi: 10.1016/j.joca.2010.08.014
20. Goodwin W, McCabe D, Sauter E, Reese E, Walter M, Buckwalter JA, et al. Rotenone Prevents Impact-Induced Chondrocyte Death. *J Orthop Res* (2010) 28(8):1057. doi: 10.1002/jor.21091
21. Goldring MB, Otero M. Inflammation in Osteoarthritis. *Curr Opin Rheumatol* (2011) 23(5):471. doi: 10.1097/BOR.0b013e328349c2b1
22. de la Rica L, Urquiza JM, Gomez-Cabrero D, Islam AB, Lopez-Bigas N, Tegner J, et al. Identification of Novel Markers in Rheumatoid Arthritis Through Integrated Analysis of DNA Methylation and microRNA Expression. *J Autoimmun* (2013) 41:6. doi: 10.1016/j.jaut.2012.12.005
23. Wang Q, Wang W, Zhang F, Deng Y, Long Z. NEAT1/miR-181c Regulates Osteopontin (OPN)-Mediated Synoviocyte Proliferation in Osteoarthritis. *J Cell Biochem* (2017) 118(11):3775. doi: 10.1002/jcb.26025
24. Chow YY, Chin KY. The Role of Inflammation in the Pathogenesis of Osteoarthritis. *Mediat Inflammation* (2020) 2020:8293921. doi: 10.1155/2020/8293921
25. Tecchio C, Micheletti A, Cassatella MA. Neutrophil-Derived Cytokines: Facts Beyond Expression. *Front Immunol* (2014) 5:508. doi: 10.3389/Fimmu.2014.00508
26. Stampella A, Monteagudo S, Lories R. Wnt Signaling as Target for the Treatment of Osteoarthritis. *Best Pract Res Cl Rh* (2017) 31(5):721. doi: 10.1016/j.berh.2018.03.004
27. Choi WS, Lee G, Song WH, Koh JT, Yang J, Kwak JS, et al. The CH25H-CYP7B1-RORalpha Axis of Cholesterol Metabolism Regulates Osteoarthritis. *Nature* (2019) 566(7743):254. doi: 10.1038/s41586-019-0920-1
28. Zhang W, Robertson WB, Zhao J, Chen W, Xu J. Emerging Trend in the Pharmacotherapy of Osteoarthritis. *Front Endocrinol* (2019) 10:431. doi: 10.3389/fendo.2019.00431
29. Zuo B, Zhu JF, Xiao F, Wang CL, Shen Y, Chen XD. Identification of Novel Biomarkers and Candidate Small Molecule Drugs in Rheumatoid Arthritis and Osteoarthritis Based on Bioinformatics Analysis of High-Throughput Data. *Biosci Rep* (2020) 40:BSR20193823. doi: 10.1042/Bsr20193823
30. Chang HZ, Yang XL, You KM, Jiang MW, Cai F, Zhang Y, et al. Integrating Multiple Microarray Dataset Analysis and Machine Learning Methods to Reveal the Key Genes and Regulatory Mechanisms Underlying Human Intervertebral Disc Degeneration. *Peerj* (2020) 8:e10120. doi: 10.7717/peerj.10120
31. Ochi K, Derfoul A, Tuan RS. A Predominantly Articular Cartilage-Associated Gene, SCRG1, Is Induced by Glucocorticoid and Stimulates Chondrogenesis *In Vitro*. *Osteoarthritis Cartilage* (2006) 14(1):30. doi: 10.1016/j.joca.2005.07.015
32. Dron M, Bailly Y, Beringue V, Haeberle AM, Griffond B, Risold PY, et al. SCRG1, a Potential Marker of Autophagy in Transmissible Spongiform Encephalopathies. *Autophagy* (2006) 2(1):58. doi: 10.4161/auto.2228
33. Dandoy-Dron F, Griffond B, Mishal Z, Tovey MG, Dron M. Scrg1, a Novel Protein of the CNS is Targeted to the Large Dense-Core Vesicles in Neuronal Cells. *Eur J Neurosci* (2003) 18(9):2449. doi: 10.1046/j.1460-9568.2003.03009.x
34. Dron M, Bailly Y, Beringue V, Haeberle AM, Griffond B, Risold PY, et al. Scrg1 is Induced in TSE and Brain Injuries, and Associated With Autophagy. *Eur J Neurosci* (2005) 22(1):133. doi: 10.1111/j.1460-9568.2005.04172.x
35. Dron M, Tartare X, Guillo F, Haik S, Barbin G, Maury C, et al. Mouse Scrapie Responsive Gene 1 (Scrg1): Genomic Organization, Physical Linkage to Sap30, Genetic Mapping on Chromosome 8, and Expression in Neuronal Primary Cell Cultures. *Genomics* (2000) 70(1):140. doi: 10.1006/geno.2000.6358
36. Zhou F, Mei J, Han X, Li H, Yang S, Wang M, et al. Kinsenoside Attenuates Osteoarthritis by Repolarizing Macrophages Through Inactivating NF-Kappab/MAPK Signaling and Protecting Chondrocytes. *Acta Pharm Sin B* (2019) 9(5):973. doi: 10.1016/j.apsb.2019.01.015
37. Monteagudo S, Lories RJ. A Notch in the Joint That Exacerbates Osteoarthritis. *Nat Rev Rheumatol* (2018) 14(10):563. doi: 10.1038/s41584-018-0076-7
38. Murphy CA, Garg AK, Silva-Correia J, Reis RL, Oliveira JM, Collins MN. The Meniscus in Normal and Osteoarthritic Tissues: Facing the Structure Property Challenges and Current Treatment Trends. *Annu Rev Biomed Eng* (2019) 21:495. doi: 10.1146/annurev-bioeng-060418-052547
39. Zhao Y, Lv J, Zhang H, Xie J, Dai H, Zhang X. Gene Expression Profiles Analyzed Using Integrating RNA Sequencing, and Microarray Reveals Increased Inflammatory Response, Proliferation, and Osteoclastogenesis in Pigmented Villonodular Synovitis. *Front Immunol* (2021) 12:665442. doi: 10.3389/fimmu.2021.665442
40. Kim G, Han MS, Nam E, Shin D, Cho HJ, Lee EJ, et al. Endogenously Expressed Cxc Chemokine Receptor Type 7 Is Involved In Inflammation Of Chondrocyte From Mice. *Osteoarthritis Cartilage* (2020) 28:S123. doi: 10.1016/j.joca.2020.02.205

41. Tanideh N, Borzooeian G, Lotfi M, Sani M, Irajie C, Ghaemmaghami P, et al. Novel Strategy of Cartilage Repairing *via* Application of P. Atlantica With Stem Cells and Collagen. *Artif Organs* (2021) 45(11):1405. doi: 10.1111/aor.14026
42. Xie JX, Deng ZQ, Alahdal M, Liu JQ, Zhao Z, Chen XQ, et al. Screening and Verification of Hub Genes Involved in Osteoarthritis Using Bioinformatics. *Exp Ther Med* (2021) 21(4). doi: 10.3892/Etm.2021.9761
43. Yang H, Chen C, Chen H, Duan XJ, Li J, Zhou Y, et al. Navitoclax (ABT263) Reduces Inflammation and Promotes Chondrogenic Phenotype by Clearing Senescent Osteoarthritic Chondrocytes in Osteoarthritis. *Aging-Us* (2020) 12 (13):12750. doi: 10.18632/Aging.103177
44. Faust HJ, Zhang H, Han J, Wolf MT, Jeon OH, Sadtler K, et al. IL-17 and Immunologically Induced Senescence Regulate Response to Injury in Osteoarthritis. *J Clin Invest* (2020) 130(10):5493. doi: 10.1172/Jci134091
45. Nishimura H, Kawasaki M, Suzuki H, Matsuura T, Baba K, Motojima Y, et al. The Neurohypophysial Oxytocin and Arginine Vasopressin System is Activated in a Knee Osteoarthritis Rat Model. *J Neuroendocrinol* (2020) 32 (8):e12892. doi: 10.1111/jne.12892
46. Zhang R, Yang X, Wang J, Han L, Yang A, Zhang J, et al. Identification of Potential Biomarkers for Differential Diagnosis Between Rheumatoid Arthritis and Osteoarthritis *via* Integrative Genomewide Gene Expression Profiling Analysis. *Mol Med Rep* (2019) 19(1):30. doi: 10.3892/mmr.2018.9677
47. Jiang L, Sun X, Kong H. microRNA-9 Might be a Novel Protective Factor for Osteoarthritis Patients. *Hereditas* (2020) 157(1):15. doi: 10.1186/s41065-020-00128-y
48. Tuerlings M, van Hoolwerff M, Houtman E, Suchiman EHED, Lakenberg N, Mei HL, et al. RNA Sequencing Reveals Interacting Key Determinants of Osteoarthritis Acting in Subchondral Bone and Articular Cartilage: Identification of IL11 and CHADL as Attractive Treatment Targets. *Arthritis Rheumatol* (2021) 73(5):789. doi: 10.1002/art.41600
49. Naot D, Watson M, Choi AJ, Musson DS, Callon KE, Zhu MR, et al. The Effect of Age on the Microarchitecture and Profile of Gene Expression in Femoral Head and Neck Bone From Patients With Osteoarthritis. *Bone Rep* (2020) 13:100287. doi: 10.1016/J.Bonr.2020.100287
50. Li CS, Zheng Z. Males and Females Have Distinct Molecular Events in the Articular Cartilage During Knee Osteoarthritis. *Int J Mol Sci* (2021) 22 (15):7876. doi: 10.3390/Ijms22157876
51. Lee BC, Kang KS. Functional Enhancement Strategies for Immunomodulation of Mesenchymal Stem Cells and Their Therapeutic Application. *Stem Cell Res Ther* (2020) 11(1). doi: 10.1186/s13287-020-01920-3
52. Benderdour M, Tardif G, Pelletier JP, Di Battista JA, Reboul P, Ranger P, et al. Interleukin 17 (IL-17) Induces Collagenase-3 Production in Human Osteoarthritic Chondrocytes *via* AP-1 Dependent Activation: Differential Activation of AP-1 Members by IL-17 and IL-1beta. *J Rheumatol* (2002) 29 (6):1262.
53. Dandoy-Dron F, Guillo F, Benboudjema L, Deslys JP, Lasmezas C, Dormont D, et al. Gene Expression in Scrapie - Cloning a New Scrapie-Responsive Gene and the Identification of Increased Levels of Seven Other mRNA Transcripts. *J Biol Chem* (1998) 273(13):7691. doi: 10.1074/jbc.273.13.7691
54. Aomatsu E, Takahashi N, Sawada S, Okubo N, Hasegawa T, Taira M, et al. Novel SCRG1/BST1 Axis Regulates Self-Renewal, Migration, and Osteogenic Differentiation Potential in Mesenchymal Stem Cells. *Sci Rep* (2014) 4. doi: 10.1038/Srep03652
55. Inoue M, Yamada J, Aomatsu-Kikuchi E, Satoh K, Kondo H, Ishisaki A, et al. SCRG1 Suppresses LPS-Induced CCL22 Production Through ERK1/2 Activation in Mouse Macrophage Raw264.7 Cells. *Mol Med Rep* (2017) 15 (6):4069. doi: 10.3892/mmr.2017.6492

Conflict of Interest: The authors declare that the research was conducted in the absence of any commercial or financial relationships that could be construed as a potential conflict of interest.

Publisher's Note: All claims expressed in this article are solely those of the authors and do not necessarily represent those of their affiliated organizations, or those of the publisher, the editors and the reviewers. Any product that may be evaluated in this article, or claim that may be made by its manufacturer, is not guaranteed or endorsed by the publisher.

frontiers | Frontiers in Immunology

ORIGINAL RESEARCH
published: 25 July 2022
doi: 10.3389/fimmu.2022.909783

Bidirectional Relationship Between Osteoarthritis and Periodontitis: A Population-Based Cohort Study Over a 15-year Follow-Up

Kevin Sheng-Kai Ma[1,2,3], *Jung-Nien Lai*[4,5], *Eshwar Thota*[3], *Hei-Tung Yip*[6,7], *Ning-Chien Chin*[8,9*], *James Cheng-Chung Wei*[10,11,12*] *and Thomas E. Van Dyke*[13,14*]

[1] *Department of Epidemiology, Harvard T.H. Chan School of Public Health, Boston, MA, United States,* [2] *Center for Global Health, Perelman School of Medicine, University of Pennsylvania, Philadelphia, PA, United States,* [3] *Graduate Institute of Biomedical Electronics and Bioinformatics, National Taiwan University, Taipei, Taiwan,* [4] *School of Chinese Medicine, College of Chinese Medicine, China Medical University, Taichung, Taiwan,* [5] *Department of Chinese Medicine, China Medical University Hospital, Taichung, Taiwan,* [6] *Management office for Health Data, China Medical University Hospital, Taichung, Taiwan,* [7] *College of Medicine, China Medical University, Taichung, Taiwan,* [8] *Department of Orthopedics, Taichung Veterans General Hospital, Taichung, Taiwan,* [9] *Department of Orthopedics, Antai Tian-Sheng Memorial Hospital, Pingtung, Taiwan,* [10] *Division of Allergy, Immunology and Rheumatology, Chung Shan Medical University Hospital, Taichung, Taiwan,* [11] *Institute of Medicine, Chung Shan Medical University, Taichung, Taiwan,* [12] *Graduate Institute of Integrated Medicine, China Medical University, Taichung, Taiwan,* [13] *Center for Clinical and Translational Research, Forsyth Institute, Cambridge, MA, United States,* [14] *Department of Oral Medicine, Infection, and Immunity, Harvard School of Dental Medicine, Boston, MA, United States*

OPEN ACCESS

Edited by:
Michal Tomcik, Institute of Rheumatology, Prague, Czechia

Reviewed by:
Petr Fulin, Charles University, Czechia
Eija Könönen, University of Turku, Finland

***Correspondence:**
Ning-Chien Chin
orthobutterfly@gmail.com
James Cheng-Chung Wei
wei3228@gmail.com
Thomas E. Van Dyke
tvandyke@forsyth.org

Specialty section:
This article was submitted to Autoimmune and Autoinflammatory Disorders, a section of the journal Frontiers in Immunology

Received: *31 March 2022*
Accepted: *10 June 2022*
Published: *25 July 2022*

Citation:
Ma KS-K, Lai J-N, Thota E, Yip H-T, Chin N-C, Wei JC-C and Van Dyke TE (2022) Bidirectional Relationship Between Osteoarthritis and Periodontitis: A Population-Based Cohort Study Over a 15-year Follow-Up. Front. Immunol. 13:909783. doi: 10.3389/fimmu.2022.909783

Objective: To identify the relationship between osteoarthritis and periodontitis.

Methods: 144,788 periodontitis patients and 144,788 propensity score-matched controls without history of periodontitis were enrolled in this cohort study. A Cox proportional hazard model was used to estimate the risk of osteoarthritis. Survival analysis was utilized to assess the time-dependent effect of periodontitis on osteoarthritis. Age and gender were stratified to identify subgroups at risk. A symmetrical case-control analysis was designed to determine the relationship between present periodontitis and history of osteoarthritis.

Results: Patients with periodontitis had higher risk of osteoarthritis (hazard ratio, HR =1.15, 95% CI =1.12–1.17, $p < 0.001$) and severe osteoarthritis that led to total knee replacement or total hip replacement (TKR/THR) (HR =1.12, 95% CI =1.03–1.21, $p < 0.01$) than controls, which was time-dependent (log-rank test $p < 0.01$). The effect of periodontitis on osteoarthritis was significant in both genders and age subgroups over 30 years-old (all $p < 0.001$). Among them, females (HR=1.27, 95% CI = 1.13–1.42, $p < 0.001$) and patients aged over 51 (HR= 1.21, 95% CI =1.10-1.33, $p < 0.001$) with periodontitis were predisposed to severe osteoarthritis. In addition, periodontitis patients were more likely to have a history of osteoarthritis (odds ratio = 1.11, 95% CI = 1.06 - 1.17, $p < 0.001$).

Conclusions: These findings suggest an association between periodontitis and a higher risk of osteoarthritis, including severe osteoarthritis that led to TKR/THR. Likewise, periodontitis is more likely to develop following osteoarthritis. A bidirectional relationship between osteoarthritis and periodontitis was observed.

Keywords: cohort study, periodontitis, osteoarthritis, total knee replacement, total hip replacement, inflammation

KEY MESSAGES

1. Periodontitis was independently associated with a significantly higher risk of osteoarthritis than did controls.
2. Females and those aged over 50 with periodontitis were predisposed to severe osteoarthritis that needed surgery.
3. An independent bidirectional relationship between osteoarthritis and periodontitis was observed.

INTRODUCTION

Osteoarthritis is characterized by progressive deterioration of articular cartilage with remodelling and proliferation of the bone beneath it (1–3), which serves as one of the leading causes of disability (1). Following the deterioration of articular cartilage, worsening osteoarthritis is one major indication for total joint replacement, with other indications including rheumatoid arthritis (RA) (2, 3). Among well-known etiological factors of osteoarthritis, primary osteoarthritis is caused by the malfunctioning synthetic function of hyaline cartilage, for which obesity and overloading contribute to its progression (1). Osteoarthritis can as well be secondary to causes such as instability of joint due to ligamentous laxity, neuropathies following diabetes mellitus (DM) (4, 5), inflammatory conditions following RA (6) or gout (3, 7), and aseptic necrosis (8). Mechanical insults in the form of trauma also fall into the secondary form of post-traumatic osteoarthritis, in which mechanical overload is then associated with a failure of the axis in the sense of valgosity and varosity of the knee joint (1). Apart from these recognized etiologies, it has been recently proposed that complement-mediated inflammatory cascades play a central role in osteoarthritis progression (9). That is, in addition to the conventional degenerative model (1), our knowledge of osteoarthritis pathogenesis has been expanded with an inflammation-dependent theory (9).

Periodontitis is an oral disease characterized by progressive inflammatory destruction of the periodontium and alveolar bone caused by biofilm-forming micro-organisms (10, 11). Such destructive inflammation is driven by complement-dependent mechanisms following oral microbial dysbiosis (12), and may translocate out of the oral cavity (10, 13–15). Clinical signs of periodontitis include gingival inflammation, alveolar bone loss, tooth mobility and eventually tooth loss (16). Periodontitis has been suggested to be a risk factor for systemic inflammatory conditions such as RA, even after considering known comorbidities (17); the underlying mechanism of which involve anti–citrullinated protein antibody (ACPA) formation by the periodontitis-associated pathogen *Porphyromonas gingivalis* (11). Likewise, periodontitis has been demonstrated to predispose to type 2 diabetes (14, 18–20), through mechanisms including metastatic inflammation in response to periodontal bacteria invasion (10, 18). These findings suggest a role for periodontal micro-organisms in systemic inflammation (17, 18) that may serve as the etiology of osteoarthritis acting through both complement cascades and periodontitis-associated systemic inflammation.

Failure of knee joint prosthesis may result from bacterial infection (2, 3), including oral bacteria that exist in the joint synovial samples from both natural and artificial joint tissues (13, 15). That is, there is an association between periodontitis and worse prognosis of total knee replacement (TKR) surgery (13, 15, 21, 22). Moreover, mechanical debridement to reduce oral bacteria has been proposed to reduce TKR failure (21, 22). This is consistent with our knowledge that periodontitis is associated with high risk of peri-prosthetic infection of alveolar bone implants, also known as peri-implantitis; as well as our knowledge of the proven efficacy of mechanical debridement for peri-implantitis management (23). Although the effect of periodontitis on risk of RA (24) and worse prognosis of TKR (13, 15, 21, 22) has been suggested, so far no studies have reported whether periodontitis as an chronic low-grade inflammatory event may be an independent risk factor of osteoarthritis in the general population. Given both the fact that bacterial invasion to the synovium could trigger complement cascades, and that periodontitis may exacerbate systemic inflammatory diseases that may drive osteoarthritis (11, 17, 25, 26), we conducted this population-based cohort study to identify whether periodontitis is a risk factor for osteoarthritis.

MATERIALS AND METHODS

Study Design and Data Sources

This retrospective cohort study used data from the Longitudinal Health Insurance Database (LHID), a registry that includes all claimed diagnoses and treatments from outpatient visits, as well as emergency and hospitalization medical records. From LHID, one million randomly sampled eligible patients with periodontitis diagnosed between 1997-2013 were enrolled.

To select non-periodontitis controls without bias, propensity score matching was applied. The propensity score match using strata was performed by adjusting for age, gender, socioeconomic variables, including income, occupation, and healthcare accessibility in the residential area, underlying comorbidities, including systemic lupus erythematosus (SLE), RA, obesity, DM,

hypertension, hyperlipidaemia, chronic liver disease, osteonecrosis, Paget's disease, and hypothyroidism, and the year of periodontitis onset or matched-year for controls, to control for confounding factors between the periodontitis and non-periodontitis groups. The propensity score is a probability estimated through logistic regression (27–30), with which the cases and controls were matched on a 1:1 basis. To ensure the selection of the matched periodontitis and non-periodontitis cases was not biased, standard mean difference (SMD) was derived for the comparison between the cases and the controls. When the SMDs were equal to or less than 0.05, the characteristics of both groups were considered similar (25).

To assure the validity and consistency of the diagnosis used in the cohort, both osteoarthritis and periodontitis were confirmed in at least two outpatient visits or at least one inpatient discharge note within one year; all medical records, along with the diagnoses, were peer-reviewed for quality control by rheumatologists and dentists, respectively. Moreover, the validity of diagnoses has been confirmed in previous studies (31–33).The database was de-identified, and the current study was approved by the Institutional Review Board of Chung Shan Medical University Hospital (approval number CS15134).

Case Definition for the Periodontitis Cohort

To determine whether periodontitis was associated with higher risks of osteoarthritis, medical records of patients diagnosed with periodontitis during 1997 to 2013 were retrieved from LHID. The occurrence of osteoarthritis after periodontitis onset was compared with that of propensity score-matched controls without periodontitis. The diagnosis of periodontitis was made following periodontal examinations that evaluated: (1) probing depth ≥ 5 mm in at least 4 teeth with each ≥ 1 site, (2) clinical attachment level (CAL) loss ≥5 mm at the same site, and (3) observed bleeding upon stimulus. The periodontal evaluations and diagnoses of periodontal diseases were made by dentists from medical centres, community hospitals and private dental clinics; the diagnosis of chronic periodontitis was confirmed in at least two outpatient visits within two years and peer-reviewed by other dentists to ensure its validity and consistency. The enrolled participants were followed up until the occurrence of osteoarthritis, December, 2013, or withdrawal, whichever occurred first.

To ensure each observed osteoarthritis case developed after periodontitis, we excluded the following patients: (1) patients with missing data throughout the period, including demographic information, comorbidity covariates, and death or loss to follow-up, (2) edentulous patients, (3) patients with tobacco addiction or alcoholism, (4) patients who throughout the study period had been diagnosed with osteoarthritis before periodontitis onset, (5) those whose diagnoses were made before 2000 or after 2012.

Outcome Measurement for the Periodontitis Cohort

The diagnosis of osteoarthritis, which was the primary outcome of the periodontitis cohort, was made following the American College of Rheumatology (ACR) diagnostic criteria for osteoarthritis of the hand (26), hip (27), and knee (28, 29). A sensitivity analysis restricting the outcome of interest to only severe osteoarthritis that resulted in TKR or total hip replacement (THR) was conducted, for which osteoarthritis had to be the main diagnosis in the discharge notes of TKR/THR. Accordingly, the subsequent risks of receiving TKR/THR for osteoarthritis following periodontitis throughout the study period, as parameterized by adjusted hazard ratios (aHRs), was derived.

To identify the subgroups at risk of developing osteoarthritis and severe osteoarthritis following periodontitis, stratification of the analyses based on age and sex were carried out.

The Osteoarthritis Case-Control Analysis and Follow-Up For Periodontitis Development

To identify whether the relationship between osteoarthritis and periodontitis was bidirectional or unidirectional, a symmetrical case-control analysis was designed parallel to the periodontitis cohort. Cases eligible for osteoarthritis case-control analysis were patients with periodontitis, for which their past history of osteoarthritis was retrieved from LHID. Propensity score-matched controls in the case-control analysis were selected based on demographic characteristics and comorbidities at baseline of periodontitis onset. Adjusted variables in propensity score matching were identical to those matched in the above-mentioned cohort design, and in the above-mentioned sensitivity analysis. The primary outcome, set as the history of osteoarthritis before periodontitis onset, was compared with that of propensity score-matched non-periodontitis controls, for which the odds ratios (ORs) were derived. Patients who had been diagnosed with periodontitis prior to osteoarthritis onset were excluded.

Statistical Analysis

Baseline demographics and comorbidities at periodontitis onset were compared through chi-square tests for categorical variables and t-tests for continuous variables. Kaplan-Meier survival analysis (34) was used to compute the cumulative incidence of osteoarthritis, and a log-rank test was used to test the significance of differences between cases of periodontitis and propensity score-matched controls. Cox proportional hazard regression with time-dependent periodontitis and comorbidity information using the counting process was used to produce the HRs of osteoarthritis between periodontitis cases and propensity score-matched non-periodontitis controls. All analyses were conducted using SPSS version 18.0 (SPSS Inc., Chicago, IL, USA).

RESULTS

Basic Demographics of the Study Subjects

For the periodontitis cohort, a total of 148,224 eligible patients who were newly diagnosed with periodontitis were identified from LHID (**Figure 1**). After propensity score matching, 144,788

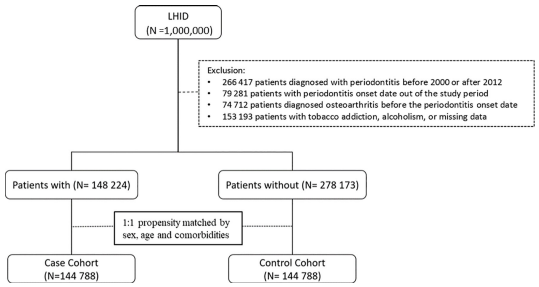

FIGURE 1 | Patient selection flowchart for the periodontitis cohort.

subjects from periodontitis and the non-periodontitis group were selected (**Figure 1**) with a matched mean age of 39 ± 15 years for the final cohort (**Table 1**). There was no statistically significant difference for demographic variables and incidence of comorbidities between the periodontitis group and the non-periodontitis group (all SMDs>0.05) (**Table 1**).

Risk of Osteoarthritis in Patients With Periodontitis

Among the 144,788 periodontitis cases enrolled in this study, 21,021 cases developed osteoarthritis after the onset of periodontitis, which was identified over 1,218,644 observed person-years. The incidence rate (IR) of osteoarthritis in patients who had periodontitis was significantly higher than the non-periodontitis cohort (1.72 v.s. 1.48 per 1,000 person-years) ($p < 0.001$). Patients who had periodontitis had a significantly higher risk of osteoarthritis when compared to the non-periodontitis controls (adjusted HR=1.15, 95%CI=1.12-1.17) (**Table 2**). To sum up, the cumulative incidence of osteoarthritis in the periodontitis group was significantly higher than that of the non-periodontitis group, which was statistically significant (log-rank test $p < 0.01$) (**Figure 2**).

Subgroup Analysis for the Risk of Osteoarthritis in Patients with Periodontitis, Stratified by Age and Gender

Findings of the subgroup analysis suggested that the association between periodontitis and the risk of developing osteoarthritis was significant for both genders. Among them, the risk of osteoarthritis for 9,626 male periodontitis patients (aHR=1.18, 95% CI=1.15-1.22, $p < 0.001$) was higher than that for 11,395 female periodontitis patients (aHR=1.11, 95% CI = 1.09-1.15, $p < 0.001$) (**Table 3**).

Likewise, subgroup analysis based on age stratification showed that the risk of osteoarthritis in the periodontitis group was particularly high among patients aged over 30. Specifically, periodontitis patients aged between 31-40 (n=2,803, aHR=1.14, 95% CI = 1.08-1.21, $p < 0.001$), aged between 41-50 (n=5,766, aHR=1.17, 95% CI=1.12-1.21, $p < 0.001$), and aged over 51 (n=10,700, aHR = 1.15, 95% CI = 1.12-1.18, $p < 0.001$) had significantly higher risk of developing osteoarthritis. In comparison, the association between periodontitis and risk of osteoarthritis in those aged 18-30 (n = 1,752, aHR = 1.07, 95% CI = 1-1.14) was not significant (**Table 3**).

TABLE 1 | Baseline characteristics for the periodontitis and the non-periodontitis cohorts after propensity score matching.

Variables	Periodontitis				SMD
	No (N = 144 788)		Yes (N = 144 788)		
	n	%	n	%	
Gender					0.01
Female	66756	46%	67304	46%	
Male	78032	54%	77484	54%	
Age, year					
18-30	51354	35%	50052	35%	0.02
31-40	31955	22%	31145	22%	0.01
41-50	29552	20%	31247	22%	0.03
>=51	31927	22%	32344	22%	0.01
mean, (SD)*	38.6	(15.0)	38.7	(14.8)	0.01
Comorbidities					
obesity	100	0.07%	155	0.11%	0.01
SLE	7	0.00%	12	0.01%	0.004
Septic arthritis	0	0%	0	0%	
Rheumatoid arthritis	739	1%	921	1%	0.02
Hypertension	19153	13%	18944	13%	0.004
diabetes mellitus	8926	6%	9090	6%	0.01
Hyperlipidemia	11026	8%	10888	8%	0.004
CLD	19979	14%	20125	14%	0.003
Osteonecrosis	3	0.002%	5	0.003%	0.003
Paget's disease of bone	9	0.01%	10	0.01%	0.001
Underactive thyroid	206	0.14%	300	0.21%	0.02

*, examined by Student's t-test; SMD, standard mean difference; SMDs ≤ 0.05 were considered similar. SLE, systemic lupus erythematosus; CLD, chronic liver disease.

TABLE 2 | Multiple Cox proportional model for risks of osteoarthritis (OA) in the periodontitis cohort.

	OA					OA with TKR/THR				
Variables	**n**	**PY**	**IR**	**aHR†**	**(95% CI)**	**n**	**PY**	**IR**	**aHR†**	**(95% CI)**
Non-periodontitis	17598	1191717	1.48	1.00	–	1069	1192884	0.90	1.00	–
Periodontitis	21021	1218644	1.72	1.15	(1.12,1.17)***	1199	1219829	0.98	1.12	(1.03,1.21)**
Gender										
Female	21169	1111895	1.90	1.00	–	1264	1112910	1.14	1.00	–
Male	17450	1298465	1.34	0.66	(0.65,0.67)***	1004	1299803	0.77	0.58	(0.53,0.62)***
Age, year										
18-30	3411	904164	0.38	1.00	–	71	904303	0.08	1.00	–
31-40	5253	575982	0.91	2.32	(2.23,2.43)***	189	576353	0.33	4.18	(3.18,5.49)***
41-50	10342	506429	2.04	4.84	(4.66,5.03)***	376	506934	0.74	8.89	(6.90,11.5)***
>=51	19613	423785	4.63	9.59	(9.23,9.97)***	1632	425122	3.84	39.6	(31.1,50.5)***
Comorbidities										
Obesity										
No	38587	2409187	1.60	1.00	–	2268	2411539	0.94		
Yes	32	1174	2.73	1.18	(0.83,1.66)	0	1174	0.00		
SLE										
No	38617	2410215	1.60			2268	2412568	0.94		
Yes	2	145	1.38			0	145	0.00		
Rheumatoid arthritis										
No	38112	2399522	1.59	1.00	–	2209	2401773	0.92	1.00	–
Yes	507	10838	4.68	1.56	(1.43,1.71)***	59	10940	5.39	2.69	(2.07,3.48)***
Hypertension										
No	26935	2164469	1.24	1.00	–	1283	2166031	0.59	1.00	–
Yes	11684	245892	4.75	1.46	(1.43,1.50)***	985	246682	3.99	1.97	(1.79,2.16)***
Diabetes mellitus										
No	33361	2295345	1.45	1.00	–	1868	2297335	0.81	1.00	–
Yes	5258	115015	4.57	1.09	(1.06,1.13)***	400	115378	3.47	1.05	(0.93,1.18)
Hyperlipidemia										
No	32699	2271556	1.44	1.00	–	1832	2273566	0.81	1.00	–
Yes	5920	138804	4.26	1.10	(1.06,1.13)***	436	139147	3.13	1.00	(0.89,1.13)
CLD										
No	29683	2113086	1.40	1.00	–	1709	2114974	0.81	1.00	–
Yes	8936	297275	3.01	1.39	(1.36,1.43)***	559	297739	1.88	1.32	(1.19,1.46)***
Osteonecrosis										
No	38615	2410325	1.60	1.00	–	2265	2412677	0.94	1.00	–
Yes	4	35	11.3	4.43	(1.66,11.81)**	3	35	84.8	39.1	(12.6,122)***
Paget's disease of bone										
No	38613	2410246	1.60	1.00	–	2267	2412599	0.94	1.00	–
Yes	6	114	5.27	1.63	(0.73,3.62)	1	114	8.78	3.01	(0.43,21.3)
Underactive thyroid										
No	38519	2407116	1.60	1.00	–	2266	2409468	0.94		
Yes	100	3245	3.08	1.07	(0.88,1.30)	2	3245	0.62		

n, number of events; PY, person-years; IR, incidence rate per 1,000 person-years; cHR, crude hazard ratio; aHR, adjusted hazard ratio; SLE, systemic lupus erythematosus; CLD, chronic liver disease; TKR, total knee replacement; THR, total hip replacement.

**: p-value <0.05; **: p-value <0.01; ***: p-value <0.001; †: adjusted by gender, age, and all comorbidities.*

Sensitivity Analysis on the Risk of TKR/THR for Severe Osteoarthritis Following Periodontitis

Among the 21,021 cases that developed osteoarthritis following periodontitis onset, 1,199 patients received TKR/THR. The risk of osteoarthritis-associated TKR/THR in periodontitis patients was significantly higher than the non-periodontitis controls (aHR = 1.12, 95% CI = 1.03-1.21, p < 0.01) (**Table 2**). Likewise, the incidence rate (IR) of severe osteoarthritis that needed TKR/THR in patients who had periodontitis was significantly higher than the non-periodontitis controls (0.98 v.s. 0.90 per 1,000 person years) (p <0.01) (**Table 2**).

The subgroup analysis suggested that the association between periodontitis and the risk of severe osteoarthritis that needed TKR/THR was particularly significant for females (aHR = 1.27; 95% CI = 1.13 – 1.42) (**Table 4**). Likewise, subgroup analysis based on age stratification showed that the risk of osteoarthritis in the periodontitis group was significantly higher among patients aged over 51 (n = 878, aHR = 1.21, 95% CI = 1.10-1.33, p < 0.001). In comparison, the association between periodontitis and risks of osteoarthritis for those aged below 50 and males was not significant (**Table 4**).

Current Periodontitis and the History of Osteoarthritis

Patients with periodontitis were more likely to have a history of osteoarthritis (adjusted OR, aOR = 1.11, 95% CI = 1.06 - 1.17, p < 0.001), compared to non-periodontitis controls. This was identified in the symmetrical case-control analysis consisting of 51,551 periodontitis patients (**Supplementary Table S1**), in

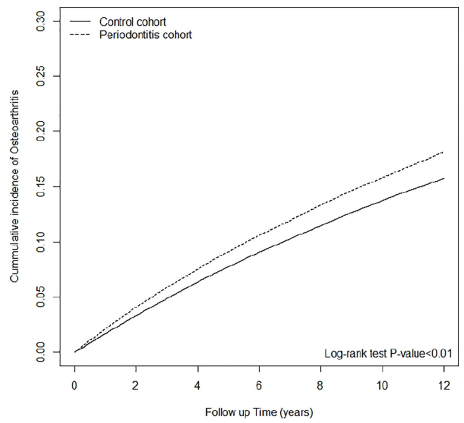

FIGURE 2 | Cumulative incidence of osteoarthritis in patients with and without periodontitis.

which 4,783 cases (9.3%) had osteoarthritis before periodontitis onset. The OR of osteoarthritis history was significantly higher among periodontitis patients than that of non-periodontitis controls (9.3% v.s. 8.0%) (**Table 5**).

Among all enrolled patients, 330 patients (1.0%) below the age of 30 had osteoarthritis before periodontitis onset. Compared with those aged below 30, patients with periodontitis aged between 31-40 (n=396, aOR=2.11, 95% CI = 1.82-2.45), patients aged between 41-50 (n=979, aOR=3.59, 95% CI = 3.16-4.08), and aged over 51 (n=7,202, aOR=12.2, 95% CI = 10.9-13.7) were associated with higher incidence of osteoarthritis history (**Table 5**). Moreover, females were associated with higher incidence of osteoarthritis history (n=5,425, 11%), compared to males (n=3,482, aOR= 0.56, 95% CI =0.53-0.59) (**Table 5**). Both the age and sex distribution of osteoarthritis were in line with previous studies (1, 4).

DISCUSSION

The findings of this cohort study suggest that periodontitis and osteoarthritis are linked in a bidirectional pattern. After propensity score matching for potential confounding factors including common risk factors for osteoarthritis, the Cox proportional hazard model revealed that the risk of osteoarthritis was significantly higher for patients who had periodontitis than that for the non-periodontitis controls. These findings were time-dependent, as suggested by the log-rank test of the Kaplan–Meier curve, and persisted in the sensitivity analysis, in which the criteria of osteoarthritis was confined to surgically treated osteoarthritis with TKR/THR. Patients of both genders and all age groups aged over 30 had higher risks for osteoarthritis following periodontitis; among them, women and those aged over 51 had higher risks for severe osteoarthritis that led to TKR/THR. In line with the epidemiology of osteoarthritis (1–4), the incidence rates of osteoarthritis were higher among females and the elders in our study. To the contrary, the association between periodontitis and the risk for osteoarthritis in males was higher following periodontitis. This is interesting as periodontitis is also more frequent and severe in males as opposed to females (35, 36). In the symmetrical case-control analysis, where the incidences of osteoarthritis history among periodontitis versus non-periodontitis participants were compared, periodontitis patients were more likely to have a history of osteoarthritis. Overall, increased risks of osteoarthritis and periodontitis were observed for patients with either disease.

Based on its etiologies, osteoarthritis could be classified into primary and secondary osteoarthritis. Primary osteoarthritis, caused by a disorder in the synthetic function of hyaline cartilage, comprises most of the cases. Although conventionally considered as a non-inflammatory arthritis (1), osteoarthritis has lately been suggested to be driven by complement-mediated inflammatory processes (9, 37) and has been managed as an inflammatory disease with medications including nonsteroidal antiinflammatory drugs (NSAIDs) (38). Hence, a paradigm shift of osteoarthritis pathogenesis has occurred towards an inflammatory-associated progression, which expands our understanding of the wear-and-tear theory (1). At the same time, infections originating in the oral cavity, with pathogens being isolated from the synovial fluid of patients operated for peri-prosthetic joint infection (PJI), have been suggested to contribute to a worse prognosis for TKR/THR (13, 22). These concepts (13, 15) have been applied to promote prophylactic management of periodontal diseases prior to joint replacement surgeries (21, 22). Given the fact that periodontopathic bacteria have been identified in joint synovium (10, 13–15), and that inflammatory complement cascades may be

TABLE 3 | Subgroup analyses on risks of osteoarthritis following periodontitis, based on sex and age stratification.

	Non-periodontitis			Periodontitis						
Variables	**n**	**PY**	**IR**	**n**	**PY**	**IR**	**cHR**	**(95% CI)**	**aHR†**	**(95% CI)**
Gender										
Female	9774	549242	1.78	11395	562654	2.03	1.14	(1.11,1.17)***	1.11	(1.09,1.15)***
Male	7824	642475	1.22	9626	655990	1.47	1.21	(1.17,1.24)***	1.18	(1.15,1.22)***
Age, year										
18-30	1659	453385	0.37	1752	450779	0.39	1.06	(0.99,1.14)	1.07	(1,1.14)
31-40	2450	288011	0.85	2803	287971	0.97	1.14	(1.08,1.21)***	1.14	(1.08,1.21)***
41-50	4576	243394	1.88	5766	263035	2.19	1.17	(1.12,1.21)***	1.17	(1.12,1.21)***
>=51	8913	206927	4.31	10700	216859	4.93	1.15	(1.12,1.18)***	1.15	(1.12,1.18)***

n, number of events; PY, person-years; IR, incidence rate per 1,000 person-years; cHR, crude hazard ratio; aHR, adjusted hazard ratio.

**: p-value <0.05; **: p-value <0.01; ***: p-value <0.001.*

†: adjusted by gender, age, and comorbidities.

TABLE 4 | Subgroup analyses on risks of severe osteoarthritis that led to total knee or total hip replacement following periodontitis, based on sex and age stratification.

	Non-periodontitis			Periodontitis						
Variables	**n**	**PY**	**IR**	**n**	**PY**	**IR**	**cHR**	**(95% CI)**	**aHR†**	**(95% CI)**
Gender										
Female	577	549721	1.05	687	563189	1.22	1.19	(1.06, 1.32)**	1.27	(1.13, 1.42)***
Male	492	643163	0.76	512	656640	0.78	1.04	(0.92, 1.18)	1.05	(0.93, 1.19)
Age, year										
18-30	36	453458	0.08	35	450845	0.08	0.98	(0.62, 1.56)	0.96	(0.60, 1.54)
31-40	94	288208	0.33	95	288146	0.33	1.02	(0.77, 1.36)	0.99	(0.75, 1.32)
41-50	185	243654	0.76	191	263280	0.73	0.98	(0.80, 1.20)	0.98	(0.80, 1.20)
>=51	754	207564	3.63	878	217558	4.04	1.17	(1.06, 1.29)**	1.21	(1.10, 1.33)***

n, number of events; PY, person-years; IR, incidence rate per 1,000 person-years; cHR, crude hazard ratio; aHR, adjusted hazard ratio.

**: p-value <0.05; **: p-value <0.01; ***: p-value <0.001.*

†: adjusted by gender, age, rheumatoid arthritis, hypertension, diabetes mellitus, hyperlipidemia, CLD, osteonecrosis and Paget's disease of bone.

TABLE 5 | Odds ratios of osteoarthritis developed within 5 year before periodontitis.

	Osteoarthritis						
Variables	**N**	**n**	**%**	**cOR**	**(95% CI)**	**aOR**	**(95% CI)**
Non-periodontitis	51551	4124	8.0%	1.00	–	1.00	–
Periodontitis	51551	4783	9.3%	1.18	(1.13,1.23)***	1.11	(1.06,1.17)***
Gender							
Female	48229	5425	11%	1.00	–	1.00	–
Male	54873	3482	6%	0.53	(0.51,0.56)***	0.56	(0.53,0.59)***
Age, year							
18-30	33421	330	1.0%	1.00	–	1.00	–
31-40	16974	396	2.3%	2.40	(2.07,2.78)***	2.11	(1.82,2.45)***
41-50	19738	979	5.0%	5.23	(4.61,5.94)***	3.59	(3.16,4.08)***
≥51	32969	7202	21.8%	28.0	(25.1,31.3)***	12.2	(10.9,13.7)***
Comorbidities							
Obesity							
No	102742	8845	9%	1.00	–	1.00	–
Yes	360	62	17%	2.21	(1.68,2.91)***	1.07	(0.78,1.47)
SLE							
No	103081	8904	9%	1.00	–		
Yes	21	3	14%	1.78	(0.53,6.01)		
Rheumatoid arthritis							
No	101430	8180	8%	1.00	–	1.00	–
Yes	1672	727	43%	8.77	(7.94,9.69)***	3.69	(3.3,4.14)***
Hypertension							
No	83457	3643	4%	1.00	–	1.00	–
Yes	19645	5264	27%	8.02	(7.66,8.4)***	2.12	(2,2.24)***
Diabetes mellitus							
No	92999	6046	7%	1.00	–	1.00	–
Yes	10103	2861	28%	5.68	(5.4,5.98)***	1.25	(1.17,1.33)***
Hyperlipidemia							
No	89035	5045	6%	1.00	–	1.00	–
Yes	14067	3862	27%	6.30	(6.01,6.6)***	1.64	(1.55,1.74)***
CLD							
No	85613	5398	6%	1.00	–	1.00	–
Yes	17489	3509	20%	3.73	(3.56,3.91)***	1.64	(1.55,1.73)***
Osteonecrosis							
No	103090	8901	9%	1.00	–	1.00	–
Yes	12	6	50%	10.5	(3.41,32.82)***	7.65	(2.07,28.2)**
Paget's disease of bone							
No	103087	8902	9%	1.00	–	1.00	–
Yes	15	5	33%	5.29	(1.81,15.48)**	2.80	(0.85,9.21)
Underactive thyroid							
No	102646	8804	9%	1.00	–	1.00	–
Yes	456	103	23%	3.11	(2.5,3.88)***	1.23	(0.96,1.58)

*N, number of participants; n, number of events; cOR, crude odds ratio; aOR, adjusted odds ratio; SLE, systemic lupus erythematosus; CLD, chronic liver disease. *: p-value < 0.05; **: p-value < 0.01; ***: p-value < 0.001.*

initiated by bacterial infection (39–41), it is possible that periodontitis could lead to or exacerbate the progression of osteoarthritis. In this first hypothesis, instead of obvious infection and inflammation that develops into septic arthritis (42), periodontal pathogens may cause or aggravate the inflammatory process in the joints, finally developing into osteoarthritis, or even severe osteoarthritis that requires surgical treatment.

Apart from being involved in idiopathic or primary osteoarthritis, periodontitis and periodontopathic bacterial invasion (43) have been shown to increase the risk of RA (7, 11, 17) and DM (5, 10, 14, 18, 20, 44, 45). These clinically evident correlations provide a plausible causal interpretation that may connect periodontitis to secondary osteoarthritis. Periodontal pathogens may trigger osteoarthritis indirectly through mechanisms including autoantibodies such as ACPA (11, 46), or humoral immunity (47–50) that involves ANCA and B cell activation upon bacterial infection (25).

Osteoarthritis could develop following periodontal pathogen invasion, which may further indicate an infection-associated model for osteoarthritis progression. The underlying mechanism of this relationship could be similar to odontogenic infections that lead to metastatic infection, metastatic inflammation, or endotoxin-driven metastatic injury (10, 14, 51). In this sense, our findings could be interpreted that periodontitis is an etiologic factor for osteoarthritis, which may trigger joint degeneration once metastatic injury is initiated. To further explore this potential relationship, intervention studies are required to determine whether mechanical debridement and surgical management for periodontal diseases leads to the primary prevention of osteoarthritis, the clinical improvement of osteoarthritis, the prevention of PJI in patients who had received TKR/THR.

Periodontitis has been suggested to be a comorbidity with knee osteoarthritis in a cross-sectional study (52). Although the underlying mechanisms are yet to be studied, potential common denominators might include underlying inflammatory traits that made those individuals susceptible to both osteoarthritis and periodontitis, with the two diseases being regarded as inflammatory diseases. Our findings may be interpreted as periodontitis serving as an early sign, or a predictor of osteoarthritis, which may be clinically identified prior to osteoarthritis onset.

Findings in the present study supported that osteoarthritis also increased the risk for future periodontitis. Whether this is a direct common susceptibility of related to impaired motor function is unknown. Osteoarthritis of the hands, knees, and hip has been suggested to result in impaired functional ability (40) that may result in poor oral hygiene due to a lack of daily activity and patient education (53), with excess biofilm formation on teeth and the periodontium, followed by increased risks of dental caries (54, 55) and periodontal diseases. This may explain our findings in the case-control analysis of the correlation between present periodontitis and a history of osteoarthritis. Prospective studies including more parameters for osteoarthritis measurement, such as the Kellgren-Lawrence (K&L) grading scale (56), is warranted, to precisely depict the observed association between osteoarthritis and periodontitis.

Some limitations of this study include the lack of periodontal charting data, including probing depth measurments, clinical attachment level measurments, or relevant local inflammatory biomarker measurments. These parameters may be of interest as they represent the degree of periodontal destruction underlying periodontitis (57), through which their simultaneous correlation with K&L scores would be reflective of the above-propsed reciprocal or bidirectional model. Additionally, even though we have observed the temporal association between periodontitis and risk of osteoarthritis through time-dependent survival analysis, we cannot infer causation as bacterial cultures based on synovial samples and inflammatory biomarkers in pateints with osteoarthritis were not available in our database. Accordingly, we advocate studies with both K&L scores and synovial samples from osteoarthritis-involved joints to validate our findings. Despite these potential limitations, in relation to the previous studies, which were mainly cross-sectional, our major strengths include a fairly large sample size in a real-world setting (58, 59). Also, propensity score matching was adopted in this longitudinal study to minimize the effect of potential confounding factors (60) on associations.

To our knowledge, this is the first study suggesting a long-term association between periodontitis and osteoarthritis. After adjusting for known comorbidities and covariates, the association between periodontitis and risk of osteoarthritis was significant, for both sexes, and all periodontitis patients aged over 30 years. Females with periodontitis and those aged over 50 with periodontitis were predisposed to severe osteoarthritis that led to TKR/THR. We advocate for more research on infection-associated osteoarthritis pathogenesis and clinical studies.

DATA AVAILABILITY STATEMENT

The raw data supporting the conclusions of this article will be made available by the authors, without undue reservation.

ETHICS STATEMENT

The studies involving human participants were reviewed and approved by The institutional review board, chung shan medical university hospital. The ethics committee waived the requirement of written informed consent for participation.

AUTHOR CONTRIBUTIONS

KM , JW, and TD conceived and designed the study. KM and H-TY contributed to data analysis and interpretation. KM, J-NL, ET, and N-CC wrote the manuscript. All authors approved the final version of the manuscript to be published.

FUNDING

This work was supported by a research grant from International Team for Implantology (fund no. 1577_2021 to KSM).

SUPPLEMENTARY MATERIAL

The Supplementary Material for this article can be found online at: https://www.frontiersin.org/articles/10.3389/fimmu.2022.909783/full#supplementary-material

REFERENCES

1. Hunter DJ, Bierma-Zeinstra S. Osteoarthritis. *Lancet* (2019) 393:1745–59. doi: 10.1016/S0140-6736(19)30417-9
2. Lenguerrand E, Whitehouse MR, Beswick AD, Kunutsor SK, Foguet P, Porter M, et al. Risk Factors Associated With Revision for Prosthetic Joint Infection Following Knee Replacement: An Observational Cohort Study From England and Wales. *Lancet Infect Dis* (2019) 19:589–600. doi: 10.1016/S1473-3099(18)30755-2
3. Sodhi N, Mont MA. Survival of Total Hip Replacements. *Lancet* (2019) 393:613. doi: 10.1016/S0140-6736(18)31859-2
4. Swain S, Sarmanova A, Mallen C, Kuo CF, Coupland C, Doherty M, et al. Trends in Incidence and Prevalence of Osteoarthritis in the United Kingdom: Findings From the Clinical Practice Research Datalink (CPRD). *Osteoarthr Cartilage* (2020) 28:792–801. doi: 10.1016/j.joca.2020.03.004
5. Berenbaum F. Diabetes-Induced Osteoarthritis: From a New Paradigm to a New Phenotype. *Postgrad Med J* (2012) 88:240–2. doi: 10.1136/pgmj.2010.146399rep
6. Ma KS, Wang LT, Tsai SY. Correspondence to: 'Combination of Human Umbilical Cord Mesenchymal (Stromal) Stem Cell Transplantation With IFN-Gamma Treatment Synergistically Improves the Clinical Outcomes of Patients With Rheumatoid Arthritis'. *Ann Rheum Dis* (2020). doi: 10.1136/annrheumdis-2020-218704
7. Figueiredo CP, Simon D, Englbrecht M, Haschka J, Kleyer A, Bayat S, et al. Q.uantification and Impact of Secondary Osteoarthritis in Patients With Anti-Citrullinated Protein Antibody-Positive Rheumatoid Arthritis. *Arthritis Rheumatol* (2016) 68:2114–21. doi: 10.1002/art.39698
8. Bullough PG, DiCarlo EF. Subchondral Avascular Necrosis: A Common Cause of Arthritis. *Ann Rheum Dis* (1990) 49:412–20. doi: 10.1136/ard.49.6.412
9. Wang Q, Rozelle AL, Lepus CM, Scanzello CR, Song JJ, Larsen DM, et al. Identification of a Central Role for Complement in Osteoarthritis. *Nat Med* (2011) 17:1674–9. doi: 10.1038/nm.2543
10. Van Dyke TE, Starr JR. Unraveling the Link Between Periodontitis and Cardiovascular Disease. *J Am Heart Assoc* (2013) 2:e000657. doi: 10.1161/JAHA.113.000657
11. Ma KS, Chiang CH, Chen YW, Wang LT. Correspondence to 'Bacterial Citrullinated Epitopes Generated by Porphyromonas Gingivalis Infection-A Missing Link for ACPA Production'. *Ann Rheum Dis* (2021), 219255. doi: 10.1136/annrheumdis-2020-219255
12. Hajishengallis G, Kajikawa T, Hajishengallis E, Maekawa T, Reis ES, Mastellos DC, et al. Complement-Dependent Mechanisms and Interventions in Periodontal Disease. *Front Immunol* (2019) 10:406. doi: 10.3389/fimmu.2019.00406
13. Temoin S, Chakaki A, Askari A, El-Halaby A, Fitzgerald S, Marcus RE, et al. Identification of Oral Bacterial DNA in Synovial Fluid of Patients With Arthritis With Native and Failed Prosthetic Joints. *J Clin Rheumatol* (2012) 18:117–21. doi: 10.1097/RHU.0b013e3182500c95
14. Van Dyke TE, van Winkelhoff AJ. Infection and Inflammatory Mechanisms. *J Clin Periodontol* (2013) 40 Suppl 14:S1–7. doi; 10.1111/jcpe.12088
15. Adamkiewicz K, Platek AE, Legosz P, Czerniuk MR, Maldyk P, Szymanski FM. Evaluation of the Prevalence of Periodontal Disease as a non-Classical Risk Factor in the Group of Patients Undergoing Hip and/or Knee Arthroplasty. *Kardiol Pol* (2018) 76:633–36. doi: 10.5603/KP.a2017.0263
16. Wang CY, Lee BS, Jhang YT, Ma KS, Huang CP, Fu KL, et al. Er:YAG Laser Irradiation Enhances Bacterial and Lipopolysaccharide Clearance and Human Gingival Fibroblast Adhesion on Titanium Discs. *Sci Rep* (2021) 11:23954. doi: 10.1038/s41598-021-03434-1
17. Chen HH, Huang N, Chen YM, Chen TJ, Chou P, Lee YL, et al. Association Between a History of Periodontitis and the Risk of Rheumatoid Arthritis: A Nationwide, Population-Based, Case-Control Study. *Ann Rheum Dis* (2013) 72:1206–11. doi: 10.1136/annrheumdis-2012-201593
18. Preshaw PM, Alba AL, Herrera D, Jepsen S, Konstantinidis A, Makrilakis K, et al. Periodontitis and Diabetes: A Two-Way Relationship. *Diabetologia* (2012) 55:21–31. doi: 10.1007/s00125-011-2342-y
19. Chapple IL, Genco Rworking group 2 of the joint EFPAAPw. Diabetes and Periodontal Diseases: Consensus Report of the Joint EFP/AAP Workshop on Periodontitis and Systemic Diseases. *J Periodontol* (2013) 84:S106–12. doi: 10.1902/jop.2013.1340011
20. Engebretson SP, Hyman LG, Michalowicz BS, Schoenfeld ER, Gelato MC, Hou W, et al. The Effect of Nonsurgical Periodontal Therapy on Hemoglobin A1c Levels in Persons With Type 2 Diabetes and Chronic Periodontitis: A Randomized Clinical Trial. *JAMA* (2013) 310:2523–32. doi: 10.1001/jama.2013.282431
21. Tai TW, Lin TC, Ho CJ, Kao Yang YH, Yang CY. Frequent Dental Scaling Is Associated With a Reduced Risk of Periprosthetic Infection Following Total Knee Arthroplasty: A Nationwide Population-Based Nested Case-Control Study. *PloS One* (2016) 11:e0158096. doi: 10.1371/journal.pone.0158096
22. Frey C, Navarro SM, Blackwell T, Lidner C, Del Schutte HJr. Impact of Dental Clearance on Total Joint Arthroplasty: A Systematic Review. *World J Orthop* (2019) 10:416–23. doi: 10.5312/wjo.v10.i12.416
23. Ferreira SD, Martins CC, Amaral SA, Vieira TR, Albuquerque BN, Cota LOM, et al. Periodontitis as a Risk Factor for Peri-Implantitis: Systematic Review and Meta-Analysis of Observational Studies. *J Dent* (2018) 79:1–10. doi: 10.1016/j.jdent.2018.09.010
24. Luan YZ, Chen BS, Ma KS. Sequencing of the 16S Ribosomal DNA Gene and Virulence of the Oral Microbiome in Patients With Rheumatoid Arthritis. *Arthritis Rheumatol* (2022). doi: 10.1002/art.42106
25. Novo E, Garcia-MacGregor E, Viera N, Chaparro N, Crozzoli Y. Periodontitis and Anti-Neutrophil Cytoplasmic Antibodies in Systemic Lupus Erythematosus and Rheumatoid Arthritis: A Comparative Study. *J Periodontol* (1999) 70:185–8. doi: 10.1902/jop.1999.70.2.185
26. Wu YD, Lin CH, Chao WC, Liao TL, Chen DY, Chen HH. Association Between a History of Periodontitis and the Risk of Systemic Lupus Erythematosus in Taiwan: A Nationwide, Population-Based, Case-Control Study. *PloS One* (2017) 12:e0187075. doi: 10.1371/journal.pone.0187075
27. Ma KS, Thota E, Huang JY, Huang YF, Wei JC. Onset of Oral Lichen Planus Following Dental Treatments: A Nested Case-Control Study. *Oral Dis* (2021). doi: 10.1111/odi.14115
28. Ma KS, Illescas Ralda MM, Veeravalli JJ, Wang LT, Thota E, Huang JY, et al. Patients With Juvenile Idiopathic Arthritis are at Increased Risk for Obstructive Sleep Apnoea: A Population-Based Cohort Study. *Eur J Orthod* (2021) 44(2):226–31. doi: 10.1093/ejo/cjab050
29. Wu MC, Ma KS, Wang YH, Wei JC. Impact of Tonsillectomy on Irritable Bowel Syndrome: A Nationwide Population-Based Cohort Study. *PloS One* (2020) 15:e0238242. doi: 10.1371/journal.pone.0238242
30. Wu MC, Ma KS, Chen HH, Huang JY, Wei JC. Relationship Between Helicobacter Pylori Infection and Psoriasis: A Nationwide Population-Based Longitudinal Cohort Study. *Med (Baltimore)* (2020) 99:e20632. doi: 10.1097/MD.0000000000020632
31. Ma KS, Lai JN, Veeravalli JJ, Chiu LT, Van Dyke TE, Wei JC. Fibromyalgia and Periodontitis: Bidirectional Associations in Population-Based 15-Year Retrospective Cohorts. *J Periodontol* (2021) 93(6):877–87. doi: 10.1002/JPER.21-0256
32. Ma KS, Wu MC, Thota E, Wang YH, Alqaderi HE, Wei JC. Tonsillectomy as a Risk Factor of Periodontitis: A Population-Based Cohort Study. *J Periodontol* (2021) 93(5):721–31. doi: 10.1002/JPER.21-0215
33. Ma KS, Hasturk H, Carreras I, Dedeoglu A, Veeravalli JJ, Huang JY, et al. Dementia and the Risk of Periodontitis: A Population-Based Cohort Study. *J Dent Res* (2021) 101(3):270–7. doi: 10.1177/00220345211037220
34. Ma KS. Screening programs incorporating big data analytics. In: P Keikhosrokiani, editor. *Big Data Analytics for Healthcare: Datasets, Techniques, Life Cycles, Management, and Applications*. Academic Press: Elsevier (2022). p. (pp. 313–327). doi: 10.1016/B978-0-323-91907-4.00023-6
35. Shiau HJ, Reynolds MA. Sex Differences in Destructive Periodontal Disease: A Systematic Review. *J Periodontol* (2010) 81:1379–89. doi: 10.1902/jop.2010.100044
36. Eke PI, Dye BA, Wei L, Slade GD, Thornton-Evans GO, Borgnakke WS, et al. Update on Prevalence of Periodontitis in Adults in the United States: NHANES 2009 to 2012. *J Periodontol* (2015) 86:611–22. doi: 10.1902/jop.2015.140520
37. Wang LT, Ma KS. Correspondence to 'Normal Human Enthesis Harbours Conventional CD4+ and CD8+ T Cells With Regulatory Features and Inducible IL-17A and TNF Expression'. *Ann Rheum Dis* (2020). doi: 10.1136/annrheumdis-2020-217309

38. Haile Z, Khatua S. Beyond Osteoarthritis: Recognizing and Treating Infectious and Other Inflammatory Arthropathies in Your Practice. *Prim Care* (2010) 37:713–27. doi: 10.1016/j.pop.2010.07.004
39. Walport MJ. Complement. First of Two Parts. *N Engl J Med* (2001) 344:1058–66. doi: 10.1056/NEJM200104053441406
40. Kemper C, Mitchell LM, Zhang L, Hourcade DE. The Complement Protein Properdin Binds Apoptotic T Cells and Promotes Complement Activation and Phagocytosis. *Proc Natl Acad Sci U.S.A.* (2008) 105:9023–8. doi: 10.1073/pnas.0801015105
41. Ricklin D, Hajishengallis G, Yang K, Lambris JD. Complement: A Key System for Immune Surveillance and Homeostasis. *Nat Immunol* (2010) 11:785–97. doi: 10.1038/ni.1923
42. Mathews CJ, Weston VC, Jones A, Field M, Coakley G. Bacterial Septic Arthritis in Adults. *Lancet* (2010) 375:846–55. doi: 10.1016/S0140-6736(09)61595-6
43. Ma KS, Chiang C, Lopez AAV, Wang L, Tsai S. Identifying Mechanisms Underlying the Association Between Cardiovascular Diseases and Periodontitis Using in Silico Analysis of Canonical Pathways. *Am Heart J* (2020) 229:172–3. doi: 10.1016/j.ahj.2020.10.038
44. Thota E, Veeravalli JJ, Manchala SK, Lakkepuram BP, Kodapaneni J, Chen YW, et al. Age-Dependent Oral Manifestations of Neurofibromatosis Type 1: A Case-Control Study. *Orphanet J Rare Dis* (2022) 17:93. doi: 10.1186/s13023-022-02223-x
45. Ma KSK, Liou YJ, Huang PH, Lin PS, Chen YW, Chang RF. (2021). Identifying Medically-Compromised Patients With Periodontitis-Associated Cardiovascular Diseases Using Convolutional Neural Network-Facilitated Multilabel Classification of Panoramic Radiographs. in: *International Conference on Applied Artificial Intelligence (ICAPAI)*, (2021). pp. 1–4. doi: 10.1109/ICAPAI49758.2021.9462069
46. Wu KJ, Tu CC, Hu JX, Chu PH, Ma KS, Chiu HY, et al. Severity of Periodontitis and Salivary Interleukin-1beta Are Associated With Psoriasis Involvement. *J Formos Med Assoc* (2022) 29:S0929-6646(22)00037-7. doi: 10.1016/j.jfma.2022.01.017
47. Ma KS, Lee CC, Liu KJ, Wei JC, Lee YT, Wang LT. Safety and Seroconversion of Immunotherapies against SARS-CoV-2 Infection: A Systematic Review and Meta-Analysis of Clinical Trials. *Pathogens* (2021) 10(12):1537. doi: 10.3390/pathogens10121537
48. Ma KS, Saeed HN, Chodosh J, Wang CW, Chung YC, Wei LC, et al. Ocular manifestations of anti-neoplastic immune checkpoint inhibitor-associated Stevens-Johnson syndrome/toxic epidermal necrolysis in cancer patients. *Ocul Surf.* (2021) 22:47–50. doi: 10.1016/j.jtos.2021.06.010
49. Huang JW, Kuo CL, Wang LT, Ma KS, Huang WY, Liu FC, et al. Case Report: *In Situ* Vaccination by Autologous CD16+ Dendritic Cells and Anti-PD-L 1 Antibody Synergized With Radiotherapy To Boost T Cells-Mediated Antitumor Efficacy In A Psoriatic Patient With Cutaneous Squamous Cell Carcinoma. *Front Immunol* (2021) 12:752563. doi: 10.3389/fimmu.2021.752563
50. Ma KS. (2021). Deep neural networks for prediction and detection of ocular sequelae among survivors of Stevens-Johnson syndrome/toxic epidermal necrolysis, in: *2021 IEEE 17th International Conference on Intelligent Computer Communication and Processing (ICCP)*, . pp. 463–7. doi: 10.1109/ICCP53602.2021.9733636
51. Li X, Kolltveit KM, Tronstad L, Olsen I. Systemic Diseases Caused by Oral Infection. *Clin Microbiol Rev* (2000) 13:547–58. doi: 10.1128/CMR.13.4.547
52. Kim JW, Chung MK, Lee J, Kwok SK, Kim WU, Park SH, et al. Association of Periodontitis With Radiographic Knee Osteoarthritis. *J Periodontol* (2020) 91:369–76. doi: 10.1002/JPER.19-0068
53. Ma KS, Chang HC, Krupat E. Teaching Evidence-Based Medicine With Electronic Databases for Preclinical Education. *Adv Physiol Educ* (2021) 45:849–55. doi: 10.1152/advan.00057.2021
54. Ma KS, Wang LT, Blatz MB. Efficacy of Adhesive Strategies for Restorative Dentistry: A Systematic Review and Network Meta-analysis of Double-blind Randomized Controlled Trials Over 12 Months of Follow-up. *J Prosthodont Res* (2022). doi: 10.2186/jpr.JPR_D_21_00279
55. Ma KSK. Dose-dependent relationship between history of dental caries and increased risk of newly-onset systemic lupus erythematosus: a nationwide population-based cohort study. *Ann Rheumatic Dis* (2021) 80:648. doi: 10.1136/annrheumdis-2021-eular.3945
56. El-Sherif HE, Kamal R, Moawyah O. Hand Osteoarthritis and Bone Mineral Density in Postmenopausal Women; Clinical Relevance to Hand Function, Pain and Disability. *Osteoarthr Cartilage* (2008) 16:12–7. doi: 10.1016/j.joca.2007.05.011
57. Caton JG, Armitage G, Berglundh T, Chapple ILC, Jepsen S, Kornman KS, et al. A New Classification Scheme for Periodontal and Peri-Implant Diseases and Conditions - Introduction and Key Changes From the 1999 Classification. *J Clin Periodontol* (2018) 45 (Suppl 20):S1–8. doi: 10.1111/jcpe.12935
58. Ma KS, Tsai SY. Big Data-Driven Personal Protective Equipment Stockpiling Framework Under Universal Healthcare for Disease Control and Prevention in the COVID-19 Era. *Int J Surg* (2020) 79:290–1. doi: 10.1016/j.ijsu.2020.05.091
59. Ma KS. Integrating Travel History *via* Big Data Analytics Under Universal Healthcare Framework for Disease Control and Prevention in the COVID-19 Pandemic. *J Clin Epidemiol* (2021) 130:147–8. doi: 10.1016/j.jclinepi.2020.08.016
60. Juang SE, Ma KS, Kao PE, Wei JC, Yip HT, Chou MC, et al. Human Papillomavirus Infection and the Risk of Erectile Dysfunction: A Nationwide Population-Based Matched Cohort Study. *J Pers Med* (2022) 12 (5):699. doi: 10.3390/jpm12050699

Conflict of Interest: The authors declare that the research was conducted in the absence of any commercial or financial relationships that could be construed as a potential conflict of interest.

Advantages of publishing in Frontiers

OPEN ACCESS
Articles are free to read for greatest visibility and readership

FAST PUBLICATION
Around 90 days from submission to decision

HIGH QUALITY PEER-REVIEW
Rigorous, collaborative, and constructive peer-review

TRANSPARENT PEER-REVIEW
Editors and reviewers acknowledged by name on published articles

Frontiers
Avenue du Tribunal-Fédéral 34
1005 Lausanne | Switzerland

Visit us: www.frontiersin.org
Contact us: frontiersin.org/about/contact

REPRODUCIBILITY OF RESEARCH
Support open data and methods to enhance research reproducibility

DIGITAL PUBLISHING
Articles designed for optimal readership across devices

FOLLOW US
@frontiersin

IMPACT METRICS
Advanced article metrics track visibility across digital media

EXTENSIVE PROMOTION
Marketing and promotion of impactful research

LOOP RESEARCH NETWORK
Our network increases your article's readership